



HAL
open science

Structural and functional characterization of the human endosulfatases HSulfs, key editing enzymes of heparan sulfate

Nesrine El Omrani

► **To cite this version:**

Nesrine El Omrani. Structural and functional characterization of the human endosulfatases HSulfs, key editing enzymes of heparan sulfate. *Biochimie [q-bio.BM]*. Université Paris-Saclay, 2024. Français. NNT : 2024UPASL135 . tel-04951224

HAL Id: tel-04951224

<https://theses.hal.science/tel-04951224v1>

Submitted on 17 Feb 2025

HAL is a multi-disciplinary open access archive for the deposit and dissemination of scientific research documents, whether they are published or not. The documents may come from teaching and research institutions in France or abroad, or from public or private research centers.

L'archive ouverte pluridisciplinaire **HAL**, est destinée au dépôt et à la diffusion de documents scientifiques de niveau recherche, publiés ou non, émanant des établissements d'enseignement et de recherche français ou étrangers, des laboratoires publics ou privés.

Structural and functional characterization of the human endosulfatases HSulfs, key editing enzymes of heparan sulfate

*Caractérisation structurale et fonctionnelle des endosulfatases humaines
HSulf, enzymes clés de l'édition de l'héparane sulfate*

Thèse de doctorat de l'université Paris-Saclay

École doctorale n° 577, Structure et Dynamique des Systèmes Vivants (SDSV)
Spécialité de doctorat : Biochimie et biologie structurale
Graduate School: Sciences de la vie et santé. Référent : Université d'Évry Val d'Essonne

Thèse préparée dans le laboratoire LAMBE (**Université Paris-Saclay, Univ Evry, CNRS**), sous la direction de **Régis DANIEL**, Directeur de recherche et la codirection de **Florence GONNET**, Professeure.

Thèse soutenue à Paris-Saclay, le 18 décembre 2024, par

Nesrine EL OMRANI

Composition du Jury

Membres du Jury avec voix délibérative

Sarah CIANFERANI Directrice de recherche, Université de Strasbourg- IPHC (UMR 7178)	Présidente
Fabrice ALLAIN Professeur des universités, Université de Lille- UGSF (UMR 8576)	Rapporteur
Bernard PRIEM Maître de conférences, Université de Grenoble -CERMAV)	Rapporteur
Kenji UCHIMURA Directeur de recherche, Université de Lille- UGSF (UMR 8576)	Examineur

Table of contents

Chapter I: Introduction.....	1
1 Discovery: timeline and evolutionary conservation of SULF genes	4
1.1 From quail embryos to human Sulf enzymes: a comprehensive discovery timeline	4
1.2 Evolutionary conservation of SULF genes across species.....	4
1.3 Nature's rationale: the evolutionary divergence and regulatory convergence that govern the dual destiny of SULF genes.....	6
1.4 The secretory pathway of HSulfs from synthesis to extracellular secretion: a proposed model	8
2 Structural organization: main structural features and post-translational modifications (PTMs)	9
2.1 Structural organization: main structural features	9
2.2 Post-translational modifications.....	11
3 HSulf enzymes and their natural substrate: heparan sulfate S-domains and 6- <i>O</i> -sulfation specificity.....	18
3.1 Heparan sulfate: the natural substrate of HSulfs.....	18
3.2 HS S-domains: the importance of 6- <i>O</i> -sulfation.....	22
3.3 Substrate specificity and desulfation mechanisms of HSulf enzymes: molecular determinants of heparan sulfate 6- <i>O</i> -sulfate pattern.....	23
4 Role of the HD domain: the distinctive feature of Sulfs	25
4.1 Impact of the hydrophilic domain on Sulf enzymatic activity	26
4.2 The hydrophilic domain: key regulator of HSulf localization	26
4.3 HD: The engine behind substrate specificity and binding	27
4.4 HSulf-HS interactions: a delicate balance of binding, catalysis, and autoregulation.....	28
4.5 HD: insights on the structural and functional divergence of HSulf isoforms	30
5 Dynamic cellular distribution of HSulfs: from extracellular matrix to nuclear localization	31
5.1 Extracellular localization	31
5.2 Intracellular localization.....	31
5.3 Particular cellular localization.....	32
5.4 Organ-specific distribution and expression of HSulfs	32
6 Implication in cell biology and physiology	35
7 Implication in pathology and cancer biology	37
8 HSulfs as therapeutic targets: advances in inhibition strategies and regulatory mechanisms ..	39
8.1 Indirect inhibition of HSulf activity.....	39
8.2 Direct inhibition of HSulf activity	41
8.3 Innovative approaches and future directions.....	47
9 Current understanding and structural challenges.....	49
Aims of PhD.....	52
Chapter II: Characterization of the impact of post-translational modifications and domain structure on HSulf oligomerization and size	54
1 AFM analysis: impact of GAG chain on protein size	55
2 Structural features related to the oligomerization of HSulf-2	57
2.1 Impact of the GAG chain	58
2.2 Impact of the hydrophilic domain (HD).....	59
2.3 Impact of mutations within the hydrophilic domain (HD).....	62
2.4 Oligomerization tendencies of HSulf-1 <i>versus</i> HSulf-2	70
2.5 Oligomerization Tendency Upon Substrate Binding	72
Chapter III: Functional Characterization of HSulf Endosulfatase Activity: Substrate Preferences and Structure-functional Relationships.....	76

1	Methodological considerations.....	77
2	Comparative analysis of HSulf-1 and HSulf-2 activity on oligosaccharide substrates of defined sequence.....	79
3	Impact of structural variations on the endosulfatase activity of HSulf-2	89
3.1	Impact of the (CS/DS) GAG chain on HSulf-2 endosulfatase activity	89
3.2	Impact of mutations within the HD domain on HSulf-2 endosulfatase activity	95
3.3	Comparative ion mobility-mass spectrometry (IM-MS) analysis of HSulf-1 and HSulf-2 desulfation patterns on Fondaparinux substrate	99
Chapter IV: Inhibitory effect of synthetic oligosaccharides with defined structures and modifications on HSulf activity		103
1	Evaluation of sulfamate-modified oligosaccharides as inhibitors of HSulf activity	105
2	Effect of the length of heparin oligosaccharides as competitive inhibitors (dp2, dp5, dp6 and dp8).....	110
3	Inhibitory effect of the sulfamate dp9 on HSulf-2 SG mutant and wild-type arylsulfatase activity	112
4	Inhibitory effect of the sulfamate dp9 on HSulf-1 and HSulf-2 endosulfatase activity	115
Chapter V: Discussion and Perspectives.....		118
1	Impact of post-translational modifications (PTMs) and domain organization on HSulfs structure and function	119
2	6- <i>O</i> -endosulfatase assay for the functional characterization of HSulfs.....	125
3	Inhibitory effects of synthetic oligosaccharides on HSulf activity.....	128
Chapter VI: Materials and Methods.....		132
1	Endosulfatase activity assay	133
1.1	Hydrophilic Interaction Liquid Chromatography -MS analysis.....	133
1.2	Flow Injection-Ion mobility-MS analysis	136
2	Arylsulfatase activity assay	137
3	Atomic force microscopy analysis	139
4	Mass photometry analysis:	140
5	Size exclusion chromatography analysis.....	142
6	Protein sequencing	143
7	Sodium dodecyl-sulfate polyacrylamide gel electrophoresis (SDS -PAGE)	146
8	Carbohydrate Gel Electrophoresis (C-PAGE).....	148
9	Enzymatic treatments of HSulfs.....	149
Supplementary Information		154
Résumé en Français		172
Bibliography		179

List of Figures

Figure 1: Phylogenetic tree analysis of Sulf family members	5
Figure 2: Structural comparison of HSulf-1, HSulf-2, and human GlcN6Sase: domain organization and sequence homology.....	10
Figure 3: Catalytic mechanisms and active site architecture of sulfatases.	12
Figure 4: Structure and composition of GAGs: main constitutive disaccharide units.....	20
Figure 5: Schematic illustration of HS proteoglycan structure showing	22
Figure 6: Domain organization and key features of the hydrophilic domain (HD) of HSulf-1 and HSulf-2.....	25
Figure 7: Model of HD-mediated HSulf-HS interactions and substrate recognition.....	29
Figure 8: Tissue distribution and expression of HSulf-1 and HSulf-2 in the human body.....	34
Figure 9: Regulation of cell signaling pathways through HSulf-6-O-desulfation of cell surface HS chains	36
Figure 10: Proposed mechanisms of sulfamate-based inhibition of sulfatases.	42
Figure 11: AlphaFold model of HSulf-2 and HSulf-2/LG3BP complex and its impact on HSulf-2 activity.....	47
Figure 12: Proposed model for the impact of HSulf-2 monoclonal antibody 5D5 on the inhibition of the PDGFR β -YAP signaling pathway.....	48
Figure 13: Predicted structure of HSulf-1 (AF-Q8IWU6-F1) and HSulf-2 AF-Q8IWU5-F1)	50
Figure 14: AFM images of HSulf-2 wild-type and SG mutant.....	56
Figure 15: Histograms showing the lateral size distribution of wild-type HSulf-2 WT and HSulf-2-SG mutant	57
Figure 16: Mass photometry analysis of HSulf-2 wild-type and HSulf-2-SG mutant.....	58
Figure 17: Predicted structure and key features of HSulf-2 based on AlphaFold2 modeling..	60
Figure 18: MALDI-TOF mass spectrum of the isolated HD domain of HSulf-2	61
Figure 19: Analysis of the HD domain under native conditions.	62
Figure 20: AlphaFold2 predicted structure of HSulf-2, highlighting domains and mutation sites.....	63
Figure 21: Mass photometry analysis of HSulf-2 variants. HSulf-2-HDC, HSulf-2-DelC, and HSulf-2-N561Q.....	64
Figure 22: Electrophoretic analysis of HSulf-2 variants. (A) SDS-PAGE analysis (B) C-PAGE analysis.....	67
Figure 23: Mass photometry analysis of HSulf-2 wild-type and mutants (N561Q and DelC-T with and without hyaluronidase treatment.	69

Figure 24: Mass photometry analysis of HSulf-2 wild-type and HSulf-1 wild-type.....	70
Figure 25:C-PAGE analysis of HSulf-1-WT and HSulf-2-WT.....	71
Figure 26: Mass photometry analysis of HSulf-2-DelC with increasing ratios of heparin polysaccharide	73
Figure 27: Mass photometry analysis of HSulf-1/2-wild-type, and HSulf-2-HDC	74
Figure 28: Extracted ion chromatograms illustrating the reactivity of HSulf-1 and HSulf-2 with oligosaccharides of varying lengths after 24h reaction time:	81
Figure 29: Structures of the four heparan sulfate octasaccharides (dp8-3-O-S, dp8-C, dp8-B, and dp8-A, Iduron) tested for HSulf-1 and HSulf-2 activity.....	82
Figure 30: Endosulfatase activity of HSulf-1 and HSulf-2 measured by HILIC-MS on four octasaccharide substrates (dp8-C, dp8-3-O-S, dp8-A, and dp8-B) over 24 hours.....	83
Figure 31: Structures of the synthetic heparan sulfate octasaccharides tested for HSulf-1 and HSulf-2 activity.....	85
Figure 32: Endosulfatase activity of HSulf-1 and HSulf-2 measured by HILIC-MS on four octasaccharide substrates (I3III, II3II, III3I, and IIII3) over 32 hours.....	88
Figure 33: Impact of GAG chain on the endosulfatase activity of HSulf-2 measured by HILIC-MS on 3-O-sulfated oligosaccharide substrates (Fondaparinux: dp5 and dp8-3-O-S) over 48 hours..	90
Figure 34: Extracted ion chromatograms of the triply desulfated species $[M-10Na+8H-3SO_3]^{2-}$ m/z 632.52, showing the progression of HSulf-2 desulfation reaction on Fondaparinux (dp5) at t=0, 2, 8, and 48h.....	92
Figure 35: Extracted ion chromatograms of the triply desulfated species $[M-3H-3SO_3]^{3-}$ m/z 695.37 portraying the progression of HSulf-2 desulfation reaction on dp8-3-O-S and the present species at t=0, 2, 8, and 48h.	94
Figure 36: Impact of structural modifications on the endosulfatase activity of HSulf-2 measured by HILIC-MS on the dp8-C octasaccharide over 48 hours. (A) HSulf-2-WT, (B) HSulf-2-DelC mutant, (C) HSulf-2-WT+PNGaseF, and (D) HSulf-2-N561Q mutant.....	96
Figure 37: Impact of structural modifications on the endosulfatase activity of HSulf-2 measured by HILIC-MS on Fondaparinux over 24 hours.....	98
Figure 38: Time-course analysis of Fondaparinux desulfation by HSulf-1 and HSulf-2 using cyclic ion mobility mass spectrometry (cIMS-MS)	101
Figure 39: Schematic representation of the Arylsulfatase fluorogenic assay used to measure HSulf activity and inhibition.	106
Figure 40: Inhibitory effects of sulfamate-oligosaccharides on HSulf-2 WT and mutants.	107
Figure 41: Average initial rates (Relative Fluorescence Units (RFU/min) of HSulf-2 WT and	

mutant enzymes with 4-MUS.	108
Figure 42: Aryl-sulfatase Activity of HSulf-1 and HSulf-2 with 4-MUS.	109
Figure 43: Comparison of inhibitory effects of sulfamate-modified oligosaccharides (dp3, dp5, dp7, sulfamate-dp9) to unmodified heparin oligosaccharides (dp2, dp5, dp6, dp8) at 50 μ M concentration on HSulf-2 SG mutant activity.....	111
Figure 44: Inhibitory effects of sulfamate-dp9 oligosaccharide on the arylsulfatase activity of HSulf-2 SG mutant and wild-type (WT).....	112
Figure 45: Inhibition of SG Mutant by sulfamate-dp9 at Different 4-MUS Concentrations.....	114
Figure 46: Time-course analysis of sulfamate-dp9 desulfation by HSulf-1 and HSulf-2. over 30 hours.	115
Figure 47: Time-course analysis of HSulf-1 and HSulf-2 desulfation activity on dp8-C with and without sulfamate-dp9 inhibitor.	116
Figure 48: Schematic representation of key structural elements and residues within full-length HSulf-2 and its isolated hydrophilic domain (HD_HSulf-2).....	121
Figure 49: AFM analysis workflow.....	139
Figure 50: Calibration curve with protein standards for mass photometry analysis.....	141

List of Tables

Table 1: Main differences between heparin and heparan sulfate.....	21
Table 2: Impact of mutations within the HD domain on Sulf activity.....	26
Table 3: Competitive HSulf-1/2 inhibitors: structures and potencies.....	45
Table 4: Theoretical molecular masses of HSulf-2 with SNAP/His Tags.....	58
Table 5: Sequence coverage analysis of HSulf-2 wild-type and mutant constructs.	65
Table 6: Sequence coverage analysis of HSulf-1 and HSulf-2 by nanoLC-MS.....	72

Chapter I: Introduction

Pluricellular organisms are highly complex systems that rely on cellular communication and coordination between cells and their surrounding environment. The interactions within these organisms are orchestrated through signaling cascades mediated by effectors and their corresponding receptors. Such interactions are highly influenced by post-translational modifications (PTMs) that are generated post-synthesis by various editing enzymes. These post-translational modifications, including sulfation, serve as encoded information in the highly regulated systems of pluricellular organisms.

Sulfation, as PTM, plays a major role in defining the functional state of an organism by modulating cellular signaling pathways. This process involves finely tuning the "sulfation code" to achieve optimal signal/response levels necessary for proper cellular function. An imbalance in sulfation levels, particularly an excess, can lead to dysregulation and contribute to various diseases. This underscores the critical need for precise regulation within the organism. Sulfotransferases and sulfatases, two classes of enzymes, work in concert to maintain this delicate balance by dynamically adding and removing sulfate groups, highlighting their essential role in cellular homeostasis.

Sulfatases (EC 3.1.5.6) have emerged as crucial components in various biological processes; they catalyze the removal of sulfate groups through hydrolytic or oxidative mechanisms. They can be classified into sulfuric ester hydrolases (EC 3.1.6.-), which catalyze the hydrolytic removal of sulfate groups, sulfamidases (EC 3.10.1.-), which catalyze the hydrolytic removal of sulfate groups from sulfamides, and dioxygenases (EC 1.14.11.-), which catalyze the oxidative removal of sulfate groups (Stam et al., 2023). These enzymes act on substrates ranging from small cytosolic steroids, such as estrogen sulfate, to complex cell-surface carbohydrates like glycosaminoglycans (GAGs) (Sarah R. Hanson et al., 2004). The transformation of these molecules is linked to essential cellular functions, and disruptions in these processes can lead to several pathophysiological conditions, such as hormone-dependent cancers, lysosomal storage disorders, and developmental abnormalities (Diez-Roux and Ballabio, 2005). Seventeen human sulfatases have been identified so far (Mashima and Nakanishi, 2022); they are classified into two main categories based on their subcellular localization: lysosomal and non-lysosomal sulfatases. Non-lysosomal sulfatases can be located at the cell surface, in the Golgi apparatus, or within the endoplasmic reticulum, and they act at a neutral pH optimum.

In contrast, all lysosomal sulfatases have optimal activity in an acidic pH (Wiegmann et al., 2013). The discovery of the human endosulfatases, HSulfs, adds a new layer of complexity and intrigue to the understanding of sulfation dynamics and its regulation by these editing enzymes. HSulf-1 and HSulf-2 (EC 3.1.6.14) are divergent from the other 15 intracellular exosulfatases, which remove sulfate esters from the non-reducing end of sugars. HSulfs specifically modulate the sulfation patterns of heparan sulfate (HS) in the extracellular matrix by regioselectively removing the 6-O sulfate on the glucosamine residues within the sequences of highly sulfated regions of HS. By editing the "sulfation code" within these regions, HSulfs critically influence cellular processes such as growth, differentiation, and migration.

This introduction section focuses on HSulf-1 and HSulf-2, the subjects of this PhD research, detailing their distinct and significant characteristics. Current knowledge about their similarities and differences is examined, highlighting what differentiates them from the remaining 15 human sulfatases. Understanding how these unique enzymes are implicated in various biological and physiological processes will provide insights into their significant roles in disease mechanisms and therapeutic applications.

1 Discovery: timeline and evolutionary conservation of SULF genes

1.1 From quail embryos to human Sulf enzymes: a comprehensive discovery timeline

The discovery of the Sulfs can be traced back to 2001 when the Emerson group (Dhoot et al., 2001) conducted a pioneering study identifying QSulf-1 through a screen for Sonic hedgehog (Shh) response genes expressed in somites in the quail embryo. The study revealed that the expression of the QSulf-1 gene enhances canonical Wingless/Integrated signaling (Wnt) signaling pathways during the differentiation of somites to muscle tissue. The analysis of the predicted amino acid sequence of QSulf-1 showed that it belongs to the sulfatase family. This classification was based on QSulf-1 sharing a highly conserved N-terminal domain with the Glucosamine-6-sulfatase (G6S, EC 3.1.6.14), which is crucial for the formation of the active site for sulfatases. Subsequently, the mammalian orthologs of Sulf-1 were identified in rodents and humans (Morimoto-Tomita et al., 2002). During the process of cloning the human Sulf-1 gene, researchers analyzed public genomic sequences to identify mammalian orthologs in rodents and humans. This analysis simultaneously led to the discovery and cloning of the closely related Sulf-2 gene in both human and mice. The full-length cDNA sequences for human and murine (mouse) Sulf-1 and Sulf-2 were characterized by the group of Dr. Steven D. Rosen (Morimoto-Tomita et al., 2002). Subsequent studies of the murine model revealed that the Sulf genes, Sulf-1 and Sulf-2, exhibited a diverse range of expression patterns during various stages of development, with some overlapping and non-overlapping patterns suggesting unique roles for each gene in specific developmental processes (Langsdorf et al., 2007).

1.2 Evolutionary conservation of SULF genes across species

The genetic mapping of SULF-1 and SULF-2 in human and mice revealed syntenic relationships between these genes across species, indicating that their genomic locations and neighborhoods are conserved in various organisms. Further sequence analysis showed that the human Sulfs (HSulf-1 and HSulf-2) share significant sequence similarity with their counterparts QSulf-1 in quail and RSulfFP1 in rats.(Morimoto-Tomita et al., 2002). This evolutionary conservation of genomic context and protein sequences suggested that Sulf enzymes play crucial roles in regulating extracellular signaling pathways, such as the Wnt pathway, essential for various biological processes in mammals (Morimoto-Tomita et al., 2002). Following these initial discoveries, researchers identified SULF genes in a broad array of organisms, ranging from vertebrates like birds (chicken), amphibians (frog/Xenopus) (Freeman et al., 2008; Winterbottom and Pownall, 2009), and fish (zebrafish) (Gorsi et al., 2010) to invertebrates like echinoderms (sea urchin) (Fujita

et al., 2010) and insects (fruit fly/*Drosophila*) (Wojcinski et al., 2011). Fujita *et al.*, 2010 performed a phylogenetic analysis linking Sulf enzymes among various human and non-human species, using Human Glucosamine-6-sulfatase (HG6S) as an outgroup to correlate Sulfs to the well-established sulfatase family (Figure 1). The phylogenetic tree analysis of Sulf family members based on their sulfatase domain amino acid sequences clearly illustrates the division between invertebrate and vertebrate Sulfs, with HG6S serving as an outgroup. Notably, vertebrate Sulfs are further divided into distinct Sulf-1 and Sulf-2 clusters, reflecting their evolutionary divergence. The high bootstrap values throughout the tree indicate strong confidence in these relationships. This analysis provides valuable insights into the evolutionary history and relationships among Sulf enzymes, emphasizing their conservation and functional importance across various species. Their widespread presence likely indicates participation in fundamental signaling pathways and developmental mechanisms preserved throughout evolution.

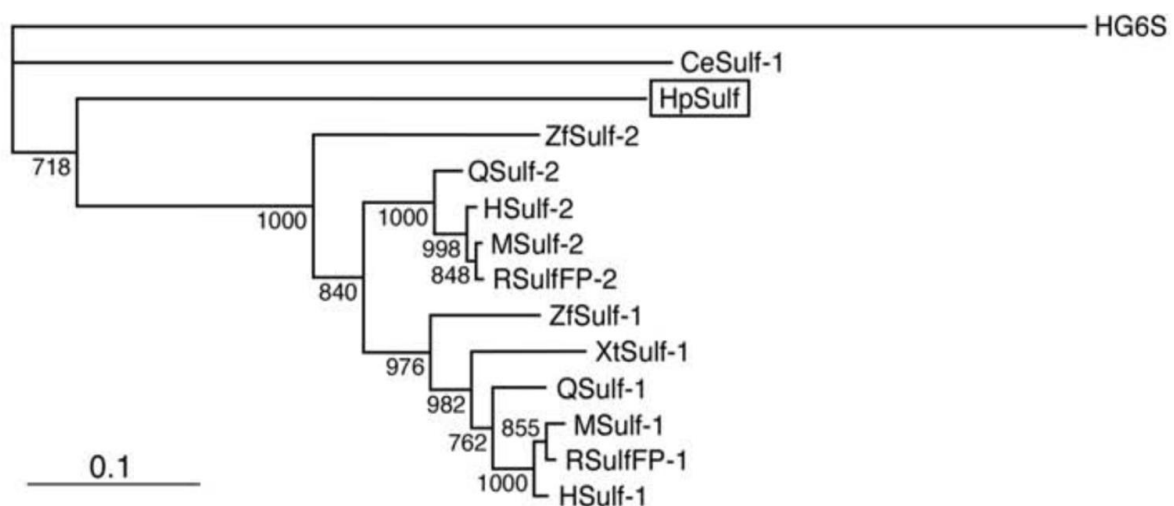


Figure 1: Phylogenetic tree analysis of Sulf family members based on the amino acid sequences of the sulfatase domain (Fujita et al., 2010).

1.3 Nature's rationale: the evolutionary divergence and regulatory convergence that govern the dual destiny of SULF genes

Despite sharing 64% sequence homology and targeting the same substrate, human Sulf-1 and Sulf-2 are encoded by genes located on two separate chromosomes. HSULF-1 is located on chromosome 8 at q13.2–13.3. It spans 194.3 kilobases and contains 22 exons. HSULF-2 is found on chromosome 20 at q13.12, covering 128.7 kilobases and comprising 21 exons (Morimoto-Tomita et al., 2002; Holmes, 2017).

One question that comes to mind here is what nature's rationale is behind having two homologous enzymes encoded by distinct genes and segregated into different loci. As described above, SULF genes show evolutionary conservation throughout the course of time and across several species. The syntenic relationships and the continuous presence of two homologous genes within these species suggest that there is a specific reason behind this duality. Evolutionary adaptability is likely a major factor, as gene duplication events can provide a foundation for functional divergence and innovation. As demonstrated through phylogenetic analyses of SULF genes, it is highly probable that the two distinct lines of vertebrate gene evolution for Sulf-1 and Sulf-2 paralogs originate from a gene duplication event of a higher ancestral invertebrate gene in *C. elegans*, for example (Holmes, 2017).

Dual-mode gene regulation mechanisms are well-conserved within eukaryotic organisms (Lee et al., 2021). This regulatory system is particularly relevant in higher eukaryotes, where various tissues and developmental stages require specific patterns of gene expression. The regulation of SULF genes can be examined within this framework, although multiple regulatory mechanisms likely contribute to their expression patterns. A notable feature of SULF genes is the presence of CpG islands (Cytosine-phosphate-Guanine islands) in their promoter regions, categorizing them as CGI+ hypomethylated of this regulatory model (Hur et al., 2012; Lee et al., 2021). This suggests that SULF genes generally maintain an euchromatic state, potentially allowing for broad expression across tissues and developmental stages. Research has shown that SULF genes exhibit dynamic expression in response to different cellular conditions, playing roles in diverse biological processes with functional specialization and tissue-specific expression (Nagamine et al., 2012; Wang and Beck, 2015). SULF1 and SULF2 have different promoter regions, which may contribute to their expression in distinct tissues and at specific times. For instance, SULF2 has been reported to have an estrogen receptor binding site in its promoter, which may influence its expression in female reproductive tissues, whereas SULF1 lacks this feature (Holmes, 2017). These differences potentially enable them to perform specialized functions in various parts of the body and respond

to changing conditions. The ability of SULF genes to be expressed differentially in a distinct spatiotemporal manner suggests the involvement of complex regulatory mechanisms. These mechanisms could potentially allow for differential responses to environmental and developmental cues.

Moreover, the distinct expression patterns of SULF1 and SULF2 may contribute to both specialized functions and potential functional overlap in important biological processes. Studies on SULF gene knockout mice evidence this. Notably, abnormalities were more pronounced in the double SULF gene null than in the single null mice, suggesting two possible explanations: first, indicating an overlapping distribution of the two enzymes in certain tissues as well as an ability to compensate for the absence of each other, second, the heightened severity in double mutants could indicate that the two Sulf enzymes work cooperatively. In this scenario, the presence of both enzymes is necessary for optimal function, and losing either one impairs their collective effectiveness (Gorsi et al., 2010; Lemjabbar-Alaoui et al., 2010). This duality thus provides a safeguard against complete loss of function, highlighting the importance of having two distinct but related genes.

Gene families with multiple related members that have coordinated functions often occur in gene clusters. Several relevant examples can be cited, such as the Hox gene clusters. The position of these genes within their cluster correlates with their collinear expression pattern along the anterior-posterior axis of the developing embryo (Tanzer et al., 2005; Gaunt, 2022). A question that comes to mind here is whether HSULF genes are part of any specific regulatory cluster of genes, even though they are localized within separated loci. Holmes et al. suggested that SULF1 and SULF2 are part of the human Group 4 arylsulfatase (ARS) genes (Holmes, 2017). This group also includes the Glucosamine 6-*O*-sulfatase (G6S), which is more closely related to Sulfs in sequence and substrate specificity compared to other human arylsulfatases. The G6S gene is located on a distinct chromosome from Sulfs, precisely on chromosome 12 at q14 (Robertson et al., 1988). Accordingly, HSulfs and G6S don't belong to a specific cluster of genes, as is the case for arylsulfatases (ARSD, ARSE, ARSF, ARSH, and ARSC), which cluster on the X-chromosome (Franco et al., 1995; Holmes, 2016).

Altogether, these observations can contribute to building a general hypothesis, being that the main reason behind loci divergence in HSULF genes is likely linked to an ancient gene duplication event. This duplication presumably allowed for the functional diversification of these enzymes. Additionally, the complex regulatory mechanisms involving HSulfs necessitate a balance of redundant and compensatory effects, enabling precise control over development and cellular processes.

1.4 The secretory pathway of HSulfs from synthesis to extracellular secretion: a proposed model

While the complete secretory pathway of HSulf-1 and HSulf-2 has not been fully elucidated in a single comprehensive study, we can propose a model based on available information from various sources. This model draws on knowledge of HSulf structure, post-translational modifications, and comparisons with other sulfatases. HSULF genes are transcribed into mRNA, which are then translated by ribosomes into prepro-protein forms of the enzymes. These prepro-proteins are initially synthesized in the endoplasmic reticulum (ER) with an N-terminal cleavable signal sequence (Tang and Rosen, 2009). Similar to lysosomal sulfatases, these signal peptides are then cleaved off within the ER by a signal peptidase, converting them into pro-proteins.

The ER provides an oxidizing environment that promotes the formation of disulfide bridges, which are crucial for protein structure and stability in many secretory and membrane proteins (Bulleid, 2012; Ellgaard et al., 2018). After synthesis, HSulf-1 and HSulf-2 undergo crucial post-translational modifications. These include the formation of C α -formylglycine, generated by the oxidation of a conserved cysteine in the active site (Cosma et al., 2003; Dierks et al., 2009), and N-linked glycosylation, which begins in the ER and continues in the Golgi apparatus. These modifications are essential for proper protein folding, stability, substrate binding, and overall functional activity (Ambasta et al., 2007; Morimoto-Tomita et al., 2002; Seffouh et al., 2023).

The single-chain pro-proteins are then transported to the Golgi apparatus, where they mature through cleavage by a furin-type proteinase into two fragments. The generated fragments subsequently form disulfide-linked heterodimers. While initial disulfide bonds likely form in the ER, the final configuration of these heterodimers may be achieved in the Golgi, where additional disulfide bond formation or rearrangement can occur (Reznik and Fass, 2022).

A portion of the mature heterodimers is packaged into secretory vesicles and transported to the plasma membrane, where they are secreted into the extracellular environment. Meanwhile, a significant fraction is retained on the cell membrane, contributing to their functional roles at the cell surface (Morimoto-Tomita et al., 2002; Tang and Rosen, 2009). All human sulfatases are processed through the secretory pathway and undergo extensive glycosylation in the ER and the Golgi apparatus during transport to their final subcellular destination (Wiegmann et al., 2013). Lysosomal sulfatases often undergo additional modifications, such as mannose-6-phosphate (M6P) tagging in the Golgi, which is crucial for their proper delivery to lysosomes (Sommerlade et al., 1994; Coutinho et al., 2012).

2 Structural organization: main structural features and post-translational modifications (PTMs)

2.1 Structural organization: main structural features

HSulfs are multi-domain proteins consisting of 870 amino acids in HSulf-2 and 871 amino acids in HSulf-1 (Figure 2). They exhibit a high overall sequence homology of 64% along their full length and demonstrate structural features that are highly similar to those of previously characterized orthologs in quail, murine, and rat species, displaying 93-94% sequence homology (Dhoot et al., 2001; Morimoto-Tomita et al., 2002; Nagamine et al., 2005). Initially synthesized as pre-proteins, HSulfs contain a 22-24 amino acid signal peptide sequence that directs their secretion to the extracellular environment (Ai et al., 2006). The signal peptide is further cleaved in the ER during the secretion process and is absent from HSulf's mature form. Beyond the signal peptide, HSulfs contain a highly conserved N-terminal domain, also known as the catalytic domain (CAT), consisting of 392 amino acids in HSulf-1 and 391 amino acids in HSulf-2, with 81% homology between the two enzymes. Significant sequence homology is shared between the N-terminal region of the human lysosomal Glucosamine-6-sulfatase and the CAT domain of Sulfs (Ai et al., 2006). Within its sequence, the CAT domain harbors two highly conserved consensus signature sequences: (P86-M-C-C-P-S-R-S-S-(M/I)-L-T-G98) and (G135-Y-R-T-A-F-F-G-K-Y-L-N-E145), characteristic of sulfatases (Nagamine et al., 2005). The first signature contains a conserved cysteine at position 89 in HSulf-1 and position 88 in HSulf-2, required to form the C α -formylglycine catalytic residue (Morimoto-Tomita et al., 2002; Dierks et al., 2005). Additionally, the CAT domain accommodates metal binding residues at the active site (51Asp, 52Asp, 316Asp, and 317His) responsible for coordinating the divalent Ca²⁺ ion (Holmes, 2017). It also contains two HS binding epitopes, V179-K-E-K182 and L401-K-K-K404, which contribute to the specific endosulfatase activity of Sulfs and are conserved within Sulf isoforms and orthologs (A. Seffouh et al., 2019). Immediately following the catalytic domain, HSulfs possess a second functional domain known as the hydrophilic domain (HD), consisting of 327 amino acids in HSulf-1 and 307 amino acids in HSulf-2. The HD is renowned for its abundance in hydrophilic amino acid residues and its involvement in high-affinity interactions with HS substrates (Ai et al., 2006). This domain is remarkably rich in basic amino acids, contributing to a theoretical pI of around 9.8, which makes HSulfs highly positively charged at neutral pH (Frese et al., 2009). Within this hydrophilic region, HSulfs exhibit a coiled-coil structural unit of 34-35 residues that can serve as multimerization elements and two furin cleavage sites, essential for protein maturation (Morimoto-Tomita et al., 2002; Tang and Rosen, 2009). The HD domain is a unique feature of Sulfs. It has no sequence

homology with other known proteins, making Sulfs significantly larger enzymes than their closest sulfatase relatives, which are approximately 550 amino acids in length (Frese et al., 2009). The N- and C-terminal sequences of the HD domain are highly conserved among orthologs, underscoring the functional relevance of these sequences. Notably, there is a well-conserved cluster of basic residues on the C-terminal side of the HD domain (Ai et al., 2006). Interestingly, the HD domains of HSulf-1 and HSulf-2 share only 43% sequence homology, suggesting potential isoform-specific functional divergences (Ai et al., 2005). In fact, all sequence divergence between Sulf-1 and Sulf-2 is related to the internal region of the HD domain (Ai et al., 2006). Finally, the C-terminal domains of HSulfs comprise 130 and 148 residues in HSulf-1 and HSulf-2, respectively, and share 71% sequence homology. This domain exhibits significant sequence identity with the C-terminal region of GlcNAc transferase from *Arabidopsis thaliana* and human lysosomal glucosamine-6-sulfatase (HG6S). This similarity suggests the involvement of the C-terminal domain in the recognition of glucosamine motifs (Morimoto-Tomita et al., 2002).

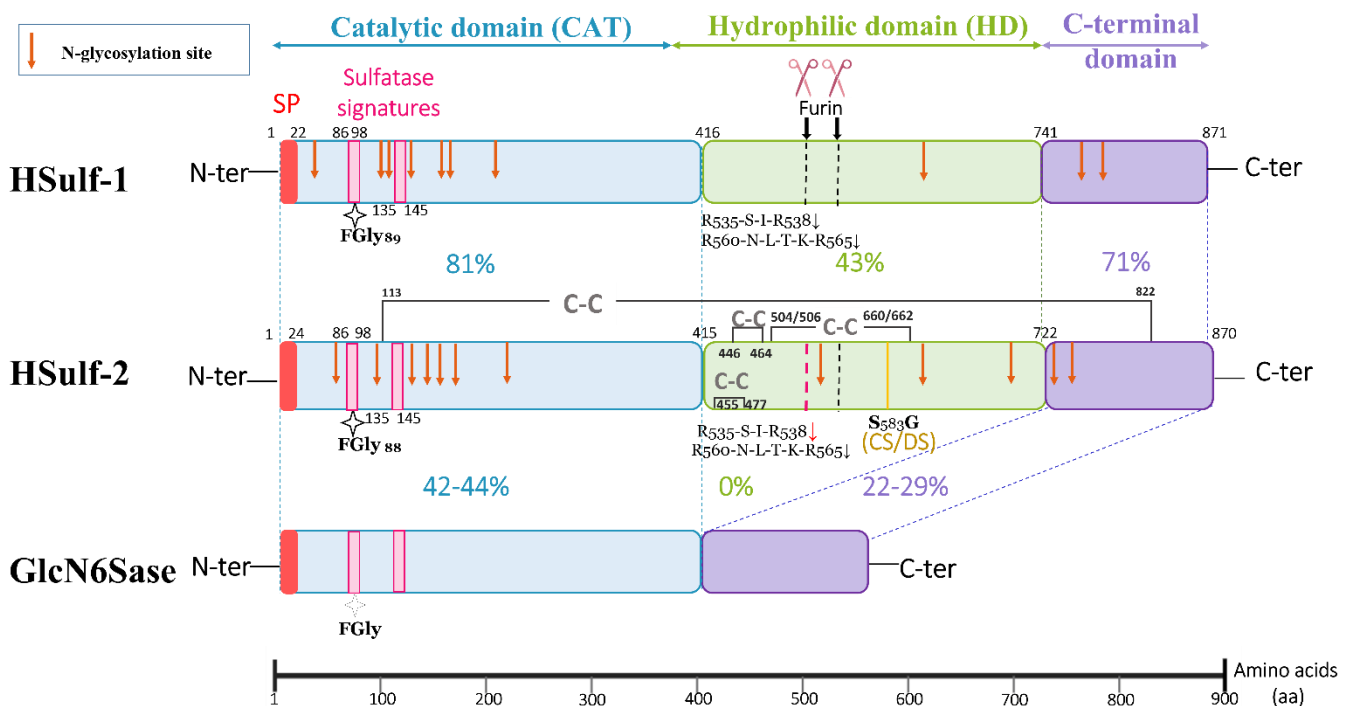


Figure 2: Structural comparison of HSulf-1, HSulf-2, and human GlcN6Sase: domain organization and sequence homology. Updated and expanded on (Nagamine et al., 2005). SP: signal peptide, %: percentage homology, CS: chondroitin sulfate, DS: dermatan sulfate, FGly: formylglycine.

2.2 Post-translational modifications

To become mature proteins, Sulfs undergo several post-translational modifications (PTMs). These modifications include the conversion of cysteine to formylglycine (FGly) at the active site, which is essential for their arylsulfatase activity. Additionally, Sulf pro-proteins mature through furin cleavage. These modifications, along with glycosylation and the formation of disulfide bridges, are crucial for the proper function and stability of HSulfs. This section introduces the various post-translational modifications that HSulfs undergo, setting the stage for a more detailed description of each modification.

2.2.1 Formylglycine

The formylglycine post-translational modification is, in fact, a defining feature of sulfatases; without this crucial modification, the protein remains enzymatically inert, lacking the essential sulfatase catalytic function. More specifically, formylglycine (FGly) is a catalytic residue primarily found in the active sites of type I sulfatases. These sulfatases, also known as hydro-FGly-sulfatases, account for the largest family registered in the UniProt database (Barbeyron et al., 2016) and possess a highly efficient catalytic mechanism for sulfate ester hydrolysis (Appel and Bertozzi, 2015). This mechanism depends on the C α -formylglycine (FGly) residue, also referred to as 3-oxoalanine. The catalytic mechanism involves a complex interplay between FGly and highly conserved active site residues, where two potential pathways have been proposed: an addition-hydrolysis (AH) mechanism and a transesterification-elimination (TE) mechanism (Figure 3). These mechanisms are supported by a sophisticated active site architecture featuring essential metal coordination and an extensive hydrogen bonding network involving conserved amino acid residues (Sarah R. Hanson et al., 2004).

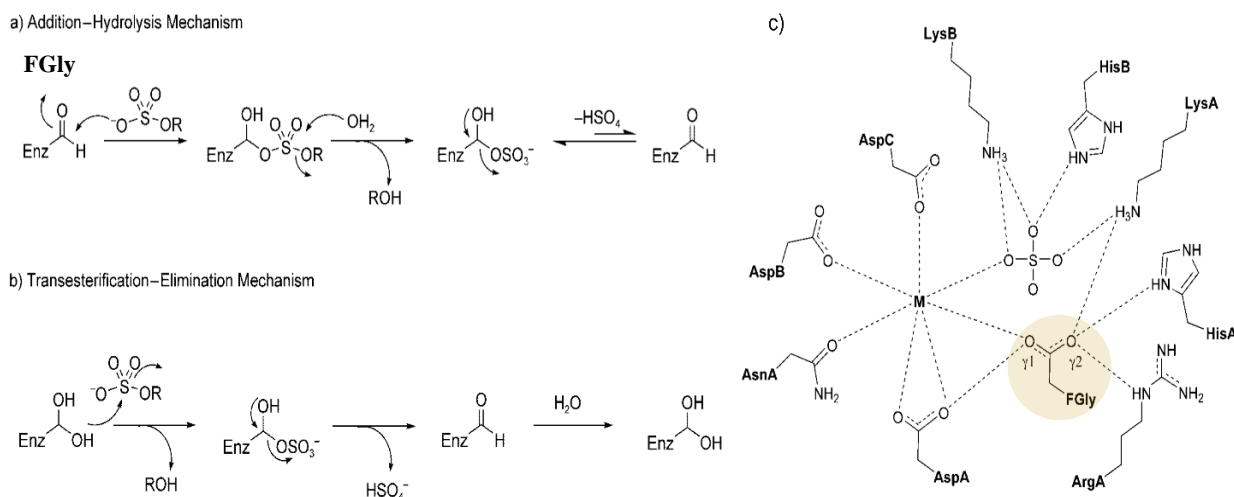


Figure 3: Catalytic mechanisms and active site architecture of sulfatases.

(A) Addition-Hydrolysis (AH) mechanism: The formylglycine (FGly) aldehyde within the catalytic site initiates the reaction by attacking the sulfate ester substrate, forming a sulfate hemiacetal intermediate (FGS). This intermediate undergoes hydrolysis, releasing the alcohol product (ROH) and forming a covalent enzyme-sulfate complex, which subsequently decomposes to regenerate the FGly aldehyde and release inorganic sulfate.

(B) Transesterification-Elimination (TE) mechanism: The hydrated form of FGly (FGH) performs a nucleophilic attack on the sulfate ester substrate, leading to transesterification. This is followed by the elimination of sulfate (HSO_3^-) and the formation of the FGly aldehyde, which is then rehydrated to complete the catalytic cycle.

(C) Conserved active site architecture: schematic representation of the sulfatase active site showing key conserved residues and their interactions. A metal ion (M) is coordinated by residues such as AspA, AspB, AspC, and AsnA. The catalytic FGly residue (highlighted) is surrounded by essential amino acids (LysA, LysB, HisA, HisB, ArgA) that facilitate substrate binding and catalysis through a hydrogen bonding network (dotted lines). Figure adapted from Hanson *et al.* (2004).

As members of this family, the catalytic activity of HSulfs depends on the presence of the FGly in their active site (Morimoto-Tomita *et al.*, 2002). In fact, FGly is an aldehyde, functionalized by the post-translational oxidation of the side chain of a cysteine or serine within the highly conserved consensus motif (C/S)-X-P-X-R-X-X-X-L-T-G-R (where X is any amino acid) at the N-terminal region of the sulfatases. Proline and arginine at the third and fifth positions, respectively, are essential for FGly modification, while the subsequent sequence X-X-X-L-T-G-R aids in the proper presentation of the (C/S)-X-P-X-R core motif to the enzyme responsible for formylglycine generation (Dierks *et al.*, 2009).

This enzyme, known as Formylglycine-generating enzyme (FGE), exclusively activates type I sulfatase targets, making it a unique enzyme at the structural and mechanistic level (Appel and Bertozzi, 2015). FGE is encoded by SUMF1, the sulfatase modifying factor 1 gene. This gene is a key regulator for all known sulfatases in the organism. Coexpression of SUMF1 with sulfatases was found to enhance enzymatic activity significantly, emphasizing its role as a critical and limiting factor of the sulfatase family (Cosma *et al.*, 2003). SUMF1 has a paralog gene, SUMF2, that shares a 48% amino-acid identity and 62% similarity with it. The close levels of expression of SUMF1

and SUMF2 suggest that they are possibly coregulated on the transcription level (Ntenti et al., 2024).

Moreover, the conversion of formylglycine (FGly) has been remarkably conserved throughout evolution, from bacteria to humans, underscoring the critical role of this PTM in biological systems (Cosma et al., 2003). Indeed, failure to conduct this PTM results in inactive sulfatases and causes multiple sulfatase deficiency (MSD), a rare but fatal lysosomal storage disorder (Waldow et al., 1999; Ntenti et al., 2024). Beyond its primary catalytic function in sulfatases, FGly is gaining attention for its potential in biotechnological applications, particularly due to the unique reactivity of its aldehyde functional group. This opens horizons for site-specific protein modifications, including targeted diagnostic tools and therapeutic conjugates (Appel et al., 2019). Apart from this, and given the essential catalytic role of FGly, its presence at different levels could serve as an indirect indicator of sulfatase enzymatic potential. Quantifying FGly levels may provide an indirect method to estimate sulfatase activity.

2.2.2 Furin cleavage maturation

Proteolytic maturation is an intricate process that marshalls secretory pathway proteins to their endmost destinations, where their activity is most favorable. This process is ensured by specific proprotein convertases (PCs) that transform precursor proteins into their mature forms through precise cleavage at consensus motifs within their amino acid sequences (Steiner, 1998). Furin, a member of this family, is a serine endoprotease, active in several cellular compartments, including the cell surface, endosomes, and primarily in the trans-Golgi network (Nakayama, 1997). It functions by specifically cleaving multibasic motifs R-X(R/K/X)-R↓ (where X can be any amino acid and ↓ pinpoints the cleavage site) in precursor proteins, including those from pathogens, thereby converting them into fully functional proteins with biological roles (Remacle et al., 2008). The simplicity of this reaction contrasts with the widespread involvement of furin in homeostasis, diseases, and viral infections, including SARS-Cov-2, where it has been demonstrated to play a major role in the infection process of this deadly virus (Wu et al., 2020).

There are several consensus motifs for furin cleavage within the primary sequences of HSulfs, with five and seven predicted sites for HSulf-1 and HSulf-2, respectively. These sites are primarily located within the hydrophilic domain (Morimoto-Tomita et al., 2002). No specific lines of evidence are available about furin-mediated maturation for other sulfatases, making Sulfs unique in undergoing furin cleavage. Noteworthy, human lysosomal glucosamine-6-sulfatase (HG6S), which shares important structural and functional similarities with Sulfs, lacks furin cleavage sites in its mature protein sequence (Morimoto-Tomita et al., 2002). This supports the fact that HSulfs

are the only hydro-Fgly-sulfatases present in a hetero-dimeric form. The mature forms of HSulfs consist of disulfide-bond-linked chains of 75 and 50 kDa at the N-terminal and C-terminal regions, respectively (Morimoto-Tomita et al., 2002; Tang and Rosen, 2009).

Two principal furin-type proteinase cleavage sites were identified by Edman sequencing in both Sulf-1 and Sulf-2 and are highly conserved among human, mouse, and quail orthologs (Tang & Rosen, 2009). The identified cleavage sites, RNRSIR and RNLTKR, concord with the consensus sequence for cleavage by furin (Nagamine et al., 2010). Deletion mutations were conducted to define the paramount sites for furin's action on Sulfs; the results showed that it cleaves Sulf-1 equivalently at both sites but chiefly acts on the first site for Sulf-2 (Tang & Rosen, 2009). However, when both sites were mutated, furin's action was completely abolished (Nagamine et al., 2010). For HSulf-2, the first site is R535-S-I-R538↓, which coincides with the most common furin target sequences, as indicated in the literature. Meanwhile, the secondary site, R560-N-L-T-K-R565↓, appears to be less frequently targeted by furin.

As for functional relevance, astonishingly, the maturation process of Sulfs is not an absolute requirement for their enzymatic activity. Mutant proteins made resistant to furin-type proteinase cleavage maintained both arylsulfatase and endosulfatase activities *in vitro*. Neither the secretion nor the solubility of HSulfs were impacted by the abolishment of the cleavage sites *in vivo*. However, their tendency to multimerize was enhanced in the absence of proteolytic processing (Tang and Rosen, 2009; Nagamine et al., 2010). In contrast, mutations did impact the capacity of Sulfs to localize within specialized membrane microdomains and their involvement in the regulation of signaling cascades. Mutants failed to localize in lipid rafts and lost their capacity to promote Wnt signaling (Tang and Rosen, 2009; Rosen and Lemjabbar-Alaoui, 2010). This impact offers a potential therapeutic target for modulating HSulf activity, mainly in certain cancers.

2.2.3 Disulfide bonds

Disulfide bond formation is a crucial post-translational modification involving the oxidation of thiol groups in cysteine side chains. This process occurs within various folding domains across the proteome, playing a key role in stabilizing protein structures by forming covalent crosslinks that secure their folding (Robinson and Bulleid, 2020).

Western blot analysis of HSulfs under reducing and non-reducing conditions confirmed the presence of disulfide bridges in their mature forms. Following furin cleavage, they form heterodimers linked by disulfide bonds (Tang and Rosen, 2009). HSulfs are, thus, capable of forming at least one inter-chain disulfide bridge to link the two chains that form the heterodimer.

The amino acid sequences of HSulfs reveal the presence of 22 and 23 cysteine residues for HSulf-1 and HSulf-2, respectively, distributed across the N-terminal and C-terminal chains generated by furin cleavage. A recent study conducted MS analysis to identify the disulfide bonds within the sequence of HSulf-2. The results revealed four intra-domain disulfide bridges and two inter-domain disulfide bridges between the C-terminal and the catalytic domain (Bilong, 2022).

Two of the four intra-domain disulfide bridges identified within the hydrophilic domain (HD) were located prior to the furin cleavage site, presumably exerting little influence on the structuring of the HD domain or the overall protein. However, the other two bridges, linking the two parts of the cleaved HD domain, likely play a more significant role in the structuring of this domain and the enzyme as a whole. Circular dichroism analysis revealed that mutants lacking the HD were fully folded, while constructs containing the HD exhibited an unfolded region likely corresponding to this domain. NMR analysis confirmed the weak structural organization of the HD domain and identified secondary structures at its N- and C-terminal regions, where cysteines involved in disulfide bridge formation are located (Cretinon, 2022). The isolated HD domain produced in a bacterial expression system also exhibited disulfide bridges, suggesting that the formation of these bonds is an intrinsic property of the HD sequence and does not depend on eukaryotic machinery (Bilong, 2022). This can correspond to a specific script edited by the cells, dictating that disulfide bonding within intermediate misfolded domains could result in the generation of the native functional structure (Feige et al., 2018).

Regarding the inter-domain disulfide bridges, their presence strongly suggests folding interactions between the catalytic and C-terminal domains, potentially influencing their structural organization and relative positioning. This suggests that HSulf-2 belongs to the group of proteins that undergo oxidative folding during the secretory pathway, exhibiting a propensity for forming long-range disulfide bonds between non-adjacent cysteine residues. The oxidative folding process of several proteins featuring this group has been extensively studied. Examples include the HIV-1 envelope glycoprotein gp160 and the cytokine IL-12, which consists of an alpha and a beta subunit assembled into a covalent heterodimer. The alpha subunit contains three intramolecular disulfide bonds, with at least one disulfide bond formed between distant cysteines within the sequence, thus requiring significant conformational changes during folding. This long bond is likely formed post-folding of this category of proteins, thereby bending the native monomeric structures into a conformation suitable for multimerization and subsequent transport to the Golgi apparatus (Feige et al., 2018).

The identified cysteine residues that are involved in forming disulfide bridges are conserved within the amino acid sequence of HSulf-1, indicating that the positions of these disulfide bridges may be

similar to those observed in HSulf-2. Disulfide bridges have significant functional relevance beyond maintaining a protein's structure and function or stabilizing the substrate recognition site. Mutations in cysteine are one of the most impactful in terms of disease causality (Vitkup et al., 2003). In the case of iduronate-2-sulfatase, a member of the formylglycine-generating sulfatase family, disruption of these disulfide bonds due to mutations in the corresponding cysteine residues can lead to Hunter syndrome, also known as Mucopolysaccharidosis II, highlighting their functional importance and significance in preventing severe diseases like this syndrome (Demydchuk et al., 2017).

2.2.4 *N*-glycosylation

N-glycosylation can impact various aspects, such as proper folding and stability of nascent proteins in the ER, as well as their preservation from proteolysis. Moreover, it is involved in cell-cell communication by ensuring interactions with other molecules (Scott and Panin, 2014). Aberrant modification of *N*-glycans can lead to pathological conditions (Reily et al., 2019), underscoring the importance of this modification for the proper function of glycoproteins, including sulfatases.

As ascertained in studies on quail Sulf-1, *N*-glycosylation is required for Sulf activity and is necessary for appropriate cell surface localization and enzyme activity (Ambasta et al., 2007). *N*-linked glycosylation begins within the lumen of the endoplasmic reticulum (ER) with the transfer of a core *N*-linked glycosylation unit onto acceptor asparagine residues in the tripeptide consensus sequence (N-X-(S/T), X≠P) (Mohanty et al., 2020). Sulf-1s are glycosylated at multiple *N*-linked sites, and these modifications are pivotal for their substrate binding, membrane targeting, and secretion (Ambasta et al., 2007; Morimoto-Tomita et al., 2002). The sequence of human HSulf-1 contains 10 potential *N*-glycosylation sites, essentially located in the N-terminal region, with one located within the hydrophilic domain (HD). Experiments showed that deleting the (HD) domain does not significantly affect protein glycosylation, confirming that the HD itself is not glycosylated (Frese et al., 2009). For HSulf-2, mass spectrometry initially identified five out of twelve potential *N*-glycosylation sites. These sites are distributed over the two chains of the enzyme, with one located in close proximity to the furin cleavage site. (Seffouh et al., 2023). Further, similar studies revealed that 9 out of the 12 potential *N*-glycosylation sites were fully occupied, with variations in glycan types and site occupancy levels (Benicky et al., 2023).

Regarding the functional pertinence of this modification, *N*-glycosylation on HSulf-1 is presumed necessary for the proper localization and activity of HSulf-1, based on pioneering studies on quail Sulf-1. Recent research on HSulf-2 has yielded varying results regarding this modification's impact. Some studies suggest that removing *N*-glycans significantly reduces enzyme activity (Benicky et

al., 2023). However, other research indicates HSulf-2 can maintain its integrity even with reduced glycosylation (Seffouh et al., 2023). These findings collectively highlight the importance of *N*-glycans for enzyme activity and structural stability while also suggesting HSulf-2's resilience under varying glycosylation conditions.

These observations align with the broader understanding of *N*-glycosylation in the human sulfatase family. *N*-glycosylation contributes to enzymatic activity, structural stability, and proper folding across various sulfatases. For lysosomal sulfatases specifically, the presence of mannose-6-phosphate (M6P) tags on *N*-glycans is crucial for their recognition by M6P receptors and subsequent transport to lysosomes (Wiegmann et al., 2013)

2.2.5 *O*-glycosylation

Whilst *N*-glycosylation is the most common form of glycosylation, *O*-glycosylation also plays a key role in cell biology. It is indispensable for the biosynthesis of various vital proteins, including mucins and antibodies, and for the assembly of proteoglycans. Unlike *N*-glycosylation, which occurs within the ER during protein folding, *O*-glycosylation occurs in the Golgi after protein folding. A multitude of glycosyltransferases interfere in this process by sequentially adding monosaccharides to proteins through a glycosidic linkage between the terminal sugar residue and the hydroxyl group of Serine or Threonine residues. These monosaccharides can be *N*-acetylgalactosamine (GalNAc), xylose, glucose, fucose, or mannose (Thompson and Wakarchuk, 2022).

Presently, narrow specific information is available on the *O*-glycosylation of sulfatases. Most studies have focused on *N*-glycosylation and its role in enzymatic activity and stability. Previous leading studies indicated that there are no predicted sites for *O*-glycosylation on QSulf1 and its human ortholog (Ambasta et al., 2007; Frese et al., 2009). It was not until recently that HSulf-2 was shown to exhibit an unusual *O*-glycosylation consisting of a glycosaminoglycan (GAG) chain that belongs to the chondroitin/dermatan sulfate family of GAGs (El Masri et al., 2022). This GAG chain was found to be covalently attached to the hydrophilic domain (HD) of the short chain of HSulf-2 through a canonical glycosaminoglycan attachment sequence observed in proteoglycans, consisting of an SG dipeptide motif (Seffouh et al., 2023).

This unique feature makes HSulf-2 one of a kind and classifies it within the family of proteoglycans. Given the structural similarities between HSulf-1 and HSulf-2, it is plausible that *O*-glycosylation may also play a role in HSulf-1. However, the same major work (El Masri et al., 2022) reported that analysis of HSulf-1 showed an absence of any GAG chain in the HEK293

overexpressing system. This unique modification could thus account for the functional divergence reported between HSulf-1 and HSulf-2.

Structural Features and Post-Translational Modifications: potential interplay?

The structural features and post-translational modifications (PTMs) of HSulf-1 and HSulf-2 described herein provide clues for a comprehensive framework of their unique characteristics within the human sulfatase family. These structural details help explain the complex relationship between enzyme structure and function. However, it would be wise to consider the potential interplay between the different constitutive domains of Sulfs as well as the potential cross-talk between the described PTMs, which can contribute to their functional specificities. For instance, as described in previous studies, the furin secondary cleavage site in HSulf-2 is located in close proximity to an N-glycan site, and the dipeptide SG motif is necessary for the attachment of the GAG chain. Mutation of the SG dipeptide allowed the detection of secondary cleavage, potentially linked to the presence of the neighboring glycosaminoglycan (GAG) chain (El Masri, 2019; Bilong, 2022). This finding underscores the relevance of the proximate GAG chain and N-glycosylation on furin cleavage, supporting the hypothesis of cross-talk between modifications.

Furthermore, the presence of a GAG chain on HSulf-2 but not on HSulf-1 raises intriguing questions about the evolutionary divergence of these paralogs. This unique modification may represent an adaptive feature supporting HSulf-2-specific functions. Understanding how post-translational modifications co-evolve with catalytic mechanisms and substrate preferences can provide valuable insights into the molecular adaptations that shape these enzymes' roles in signaling pathways. This knowledge can enhance our comprehension of how structural features and modifications influence the diverse functions of HSulf-1 and HSulf-2 in heparan sulfate editing and related biological processes.

3 HSulf enzymes and their natural substrate: heparan sulfate S-domains and 6-O-sulfation specificity

3.1 Heparan sulfate: the natural substrate of HSulfs

Heparan sulfate (HS), the natural substrate of HSulfs, is a key component of the extracellular matrix (ECM) that plays a crucial role in numerous signaling pathways. Traditionally viewed as an extracellular molecule, HS has also been found in the nucleus, where it influences cell cycle regulation and gene expression (Stewart and Sanderson, 2014). As a member of the glycosaminoglycan (GAG) family, HS was initially seen as part of the ECM's structural framework,

acting like a biological "glue" around cells (Perez et al., 2023). The discovery of heparin (HP) in 1916 (Mclean, 1959) and the later identification of heparan sulfate (HS) as a separate entity in the 1950s by Jorpes and Gardell marked significant milestones in glycoscience research (Varki et al., 1999). These findings highlighted the critical role of structural specificity in these macromolecules, which are now known to regulate various biological processes.

Structurally, GAGs are long linear polysaccharides composed of repeating disaccharide units consisting of a hexosamine paired with uronic acid or galactose. The uronic acid component can be either iduronic acid (IdoA) or glucuronic acid (GlcA), and the hexosamine component can be either N-acetyl glucosamine (GlcNAc) or N-acetyl galactosamine (GalNAc) (Figure 4). Most GAGs are present as proteoglycans (PGs), where one or more polysaccharide chains are covalently attached to a core protein, which can be membrane-bound or located in the pericellular matrix (PCM). Hyaluronic acid (HA) is an exception among GAGs, as it is neither sulfated nor covalently attached to core proteins (Esko et al., 2009).

The complexity and diversity of GAG structures stem from modifications within their disaccharide units. These modifications include O-sulfation of hydroxyl groups at specific carbon positions in uronic acids and hexosamines and N-acetylation or N-sulfation of glucosamines. The unique properties of each GAG family member, including the highly complex heparan sulfate, are determined by the specific combination of sugar components, modification patterns, and types of glycosidic bonds between them. (Perez et al., 2023).

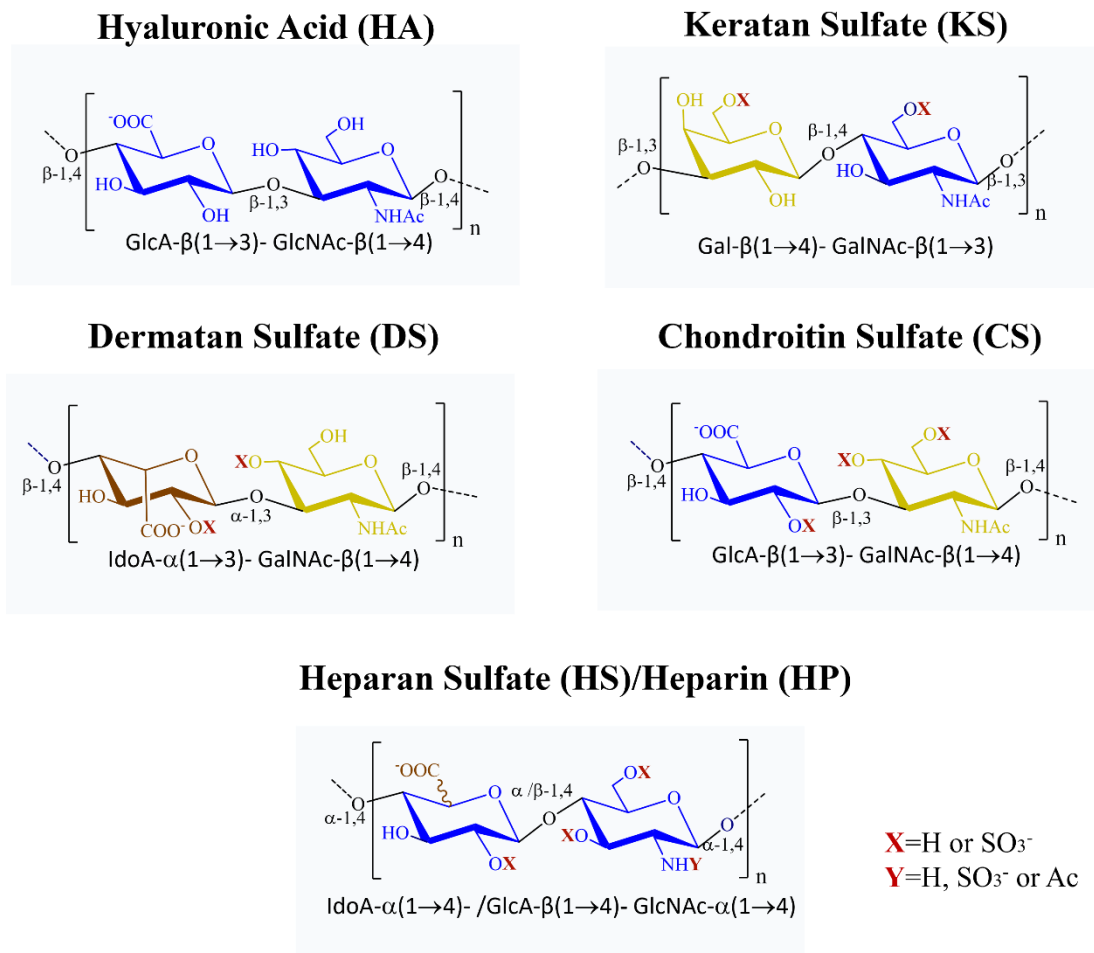


Figure 4: Structure and composition of GAGs: main constitutive disaccharide units. Color code: brown: iduronic acid; yellow: galactosamine. n: number of repetitive units.

The structural complexity of heparan sulfate arises from an intricate biosynthesis process involving a series of enzymatic modifications. This process is not genetically template-driven but relies on competent enzymatic complexes that cooperatively induce multiple modifications, including sulfation and epimerization, within the nascent macromolecule. These modifications form mature sulfated HS chains with diverse structural and functional properties. At the molecular level, HS comprises α 1–4-linked GlcNAc and β 1–4-linked GlcA residues. During biosynthesis, these components undergo various modifications, such as N-deacetylation of GlcNAc followed by N-sulfation to form GlcNS and epimerization of GlcA to IdoA. Additionally, O-sulfations can occur on C2 of the uronic acid, on C6, and rarely on C3 of the glucosamine. These modifications create specific domain distribution patterns within the HS chain, consisting of highly sulfated “NS domains” and unmodified “NAc domains” interspersed with partially sulfated “NS/NAc domains” (Esko and Selleck, 2002; Thacker et al., 2014).

Heparin is structurally similar to heparan sulfate, making it a suitable substrate for HSulfs. However, heparin exhibits a higher sulfation rate, primarily consisting of α 1–4-linked IdoA2S-GlcNS6S trisulfated disaccharide units, thereby resulting in a more homogeneous and extended NS domain-type organization compared to heparan sulfate (Khan et al., 2013). HS and HP have distinct cellular origins that contribute to their different characteristics. While HS is synthesized by virtually all cells and exists as various proteoglycans (with ~17 different core proteins), HP is specifically produced by mast cells in connective tissues as serglycin proteoglycan (Table 1).

Table 1: Main differences between heparin and heparan sulfate updated from (Xu & Esko, 2014).

Characteristics	Heparan sulfate	Heparin
Site of synthesis	Most, if not all, mammalian cells	Connective tissue-type mast cells
Core protein	Many (~17)	Serglycin
Cell membrane attached?	Yes	No
Size	20-100 kDa	7-20 kDa
Alternate NS/NAc domains	Yes	Minimal
Average sulfate/disaccharide	0.6-1.8	1.8-2.6
IdoA	20-50%	\geq 80%
N-Sulfate	30-60%	\geq 80%
2-O-Sulfate	10-40%	\geq 80%
6-O-Sulfate	10-40%	\geq 80%
Major disaccharide unit	IdoA/GlcA-GlcNAc6S and GlcA-GlcNS	IdoA2S-GlcNS6S
Binding to antithrombin	0-0.3%	~30%
Commercial availability	Milligrams	Kilograms

Once matured and expressed at the cell surface, heparan sulfate proteoglycans (HSPGs) undergo a highly regulated post-synthetic process, where HSulfs interfere to catalyze the 6-*O*-desulfation within the NS domains specifically (Figure 5). By finely modifying the 6-*O* sulfation pattern of HS chains, HSulfs cause minimal structural changes, reducing overall sulfation by approximately 4 to 5%. However, targeting the 6-*O*-sulfate groups significantly impacts HS binding properties, leading to substantial functional consequences (I. Seffouh et al., 2019). This highlights the importance of the 6-*O*-sulfation motifs within HS chains.

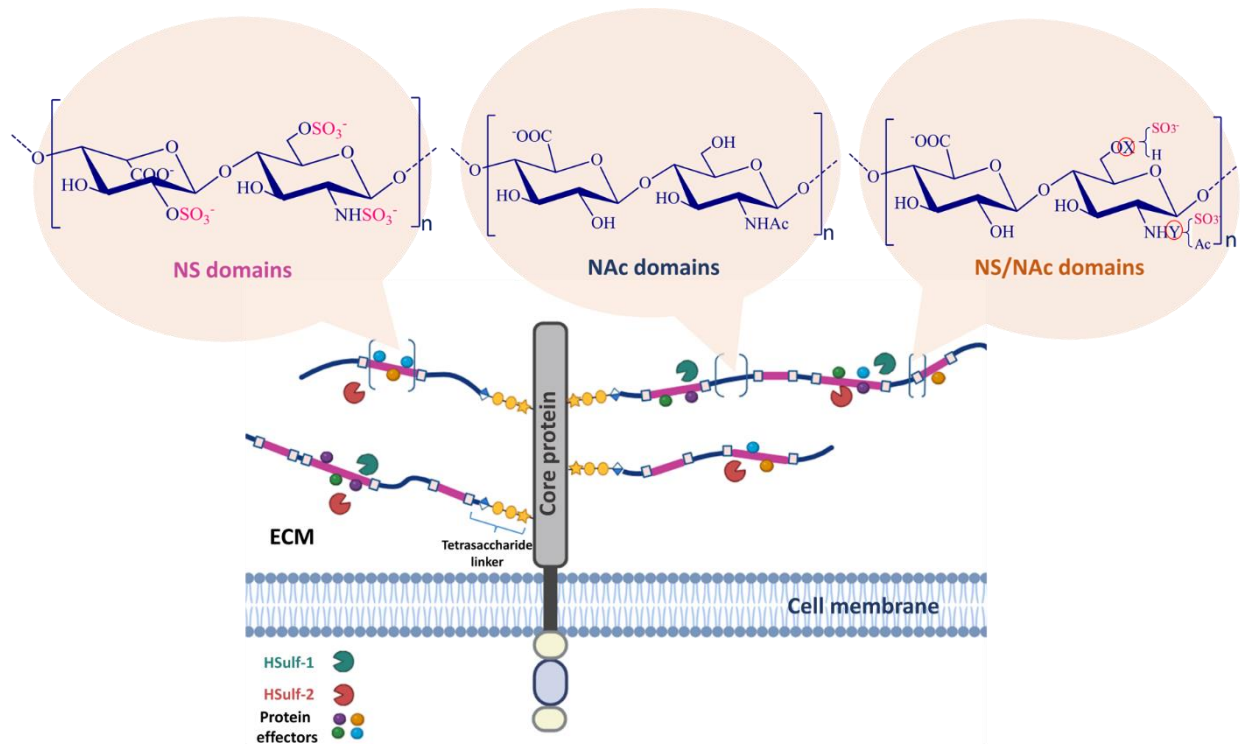


Figure 5: Schematic illustration of HS proteoglycan structure showing NS, NAc, and NS/NAc domains, and their interactions with HSulf-1 (green), HSulf-2 (red), and protein effectors (colored circles) in the extracellular matrix (ECM). Tetrasaccharide linker: star: U (Glucuronic acid - GlcA); circle: G (Galactose - Gal); diamond: X (Xylose - Xyl)

3.2 HS S-domains: the importance of 6-O-sulfation

The diverse and intricate sulfation patterns of heparan sulfate (HS), often referred to as the "heparanome," form the molecular basis for its multifunctional nature in physiological processes and developmental biology. The highly sulfated NS domains within HS chains, characterized by their unique structural features and sulfation patterns, serve as critical scaffolds for interactions with a diverse array of proteins (Lamanna et al., 2007; Nurcombe, 2024). These domains can adopt a rigid double-helical conformation, which helps optimize the positioning of binding motifs for proper protein interactions. Moreover, the conformational plasticity of the iduronate ring, coupled with the flexible NAc domains, contributes to the formation of specific spatial configurations of the carboxylate and 2-O-sulfate groups. This structural adaptability enables HS to accommodate various protein partners (Gallagher, 2015). These characteristics, combined with specific sulfation patterns enriched in the trisulfated disaccharides [IdoA(2S), GlcNS(6S)] within NS domains, facilitate HS-protein binding through both electrostatic and specific saccharide motif interactions (Xu and Esko, 2014; Matsuzaka and Yashiro, 2024).

The importance of 6-*O*-sulfation in HS is exemplified by its effective role in modulating interactions with various signaling molecules and protein effectors. For instance, 6-*O*-sulfation is essential for optimal binding and activity induction of fibroblast growth factors (FGFs) (Sugaya et al., 2008; Li and Kusche-Gullberg, 2016). Additionally, it plays a vital role in regulating morphogen signaling, such as Wnt, and in chemokine interactions, where it facilitates the formation of chemokine gradients (Ai et al., 2003; Uchimura et al., 2006). Furthermore, 6-*O*-sulfation mediates HS-antithrombin III interaction, which is crucial for heparin's anticoagulant properties (Chen et al., 2007). It also plays a vital role in modulating pro-inflammatory effectors (El Masri et al., 2020). The significance of 6-*O*-sulfation extends to interactions with various other partners, including viral particles (De Pascale et al., 2021). The versatility of 6-*O*-sulfation in HS underscores its potential as a therapeutic target, particularly in developing HS mimetics for regenerative medicine and inhibitors for viral entry (Matsuzaka and Yashiro, 2024; Nurcombe, 2024). These roles of 6-OS explain why, despite minimal Sulf impact on overall HS sulfation, it significantly affects HS binding properties for a wide array of effectors, modulating critical cellular functions such as growth, migration, and differentiation. This functional diversity underscores the role of Sulfs in various physiological processes and pathological conditions, including development, tissue repair, inflammation, and cancer (El Masri et al., 2016).

Given the significant effects of HSulfs on HS function, understanding the specific molecular mechanisms and substrate preferences that allow these enzymes to exert such influence is crucial. This leads us to consider two areas of inquiry: what are the specific molecular determinants that allow Sulfs to achieve this fine-tuned regulation of HS activity, and how do these mechanisms contribute to their diverse physiological roles?

3.3 Substrate specificity and desulfation mechanisms of HSulf enzymes: molecular determinants of heparan sulfate 6-*O*-sulfate pattern

HSulfs exhibit regioselective endo-6-*O*-sulfatase activity within heparan sulfate (HS) and heparin (HP) chains. They have specific substrate sequence preferences, particularly targeting 6-*O*-sulfate groups within highly sulfated NS domains. Their primary targets are the trisulfated disaccharide units [IdoA(2S) - GlcNS(6S)], which contain most protein binding sites (Saad et al., 2005; Frese et al., 2009). While Sulfs predominantly act on these trisulfated structures, they can also remove 6-*O*-sulfate groups from disulfated disaccharides, specifically [UA-GlcNS6S] motifs, where UA can be GlcA or IdoA (Ai et al., 2006; Staples et al., 2011; Pempe et al., 2012). Importantly, N-sulfation is crucial for substrate recognition, as no desulfation is observed on structures containing only *O*-sulfated N-acetylglucosamine (GlcNAc6S). Notably, HSulfs process GlcA, IdoA, or heparinase-

generated $\Delta 4,5$ uronic acid indiscriminately, and the presence of 3-*O*-sulfate groups does not impede their activity, allowing efficient 6-*O*-desulfation of structures like the antithrombin-III binding pentasaccharide (Seffouh et al., 2023).

The mechanism of HSulf-mediated 6-*O*-desulfation of HS is both oriented and processive. HSulf-2, in particular, employs a unique mechanism to desulfate HS chains, starting its action at the non-reducing end and progressively moving towards the reducing end. This process is governed by the HD domain, which is responsible for high-affinity binding, while low-affinity HS binding sites within the CAT domain ensure proper alignment of the HS chain with the enzyme's active site (Seffouh et al., 2013). The processive nature and specificity of HSulf-2 activity have been demonstrated *in vitro*, using synthetic heparin octasaccharides, and *in vivo*, using epithelial cell lines that naturally express HS. Various analytical techniques have confirmed these findings, including oligosaccharide sequencing, mass spectrometry, and NMR spectroscopy. Furthermore, phage display techniques have elegantly supported this identified directionality, with epitope loss occurring in a specific order from the non-reducing end toward the reducing end of the HS chain (Uchimura et al., 2010; A. Seffouh et al., 2013). Interestingly, in addition to targeting internal highly sulfated (NS) domains, HSulf-2 can also process the non-reducing terminus of HS and heparin chains, suggesting a broader substrate range than initially established (Staples et al., 2011; Huang et al., 2014). Recent studies have further elucidated that HSulf-1 and HSulf-2 employ a dual mechanism to regulate interactions between cell-surface HS and growth factors (GFs). This dual mechanism relies on their catalytic remodeling of HS sulfated regions, thereby altering its binding specificity and on their competitive binding to occupy and block GF binding sites (Timm et al., 2023).

While both Sulf paralogs are generally reported to share similar substrate sequence preferences, subtle differences in their specificity may exist due to variations in the internal region of the HD domain. Studies using engineered HS conjugates with defined sulfation compositions revealed distinct binding and catalytic preferences for each paralog. HSulf-1 tends to bind HS subsets with lower sulfation levels, while HSulf-2 prefers more highly sulfated HS. However, HSulf-1 demonstrates a greater ability to remodel highly sulfated HS chains, particularly those with 2-*O*-sulfation and 3-*O*-sulfation motifs. These motifs potentially contribute to enhancing its activity (Timm et al., 2023).

The discrepancy between the globally similar *in vitro* activities of HSulf-1 and HSulf-2 and their often antagonistic or redundant properties *in vivo* remains a subject of investigation. While *in vitro* assays have provided valuable insights into Sulf activity, they do not fully capture the complexity

of the natural extracellular matrix environment, which involves differential spatiotemporal expression patterns of these enzymes. Despite these limitations, these studies contribute significantly to our understanding of Sulf function. Understanding the complex interplay between HS biosynthesis, its post-synthetic modifications by Sulfs, and the various modulated effectors may explain the functional differences observed between HSulf-1 and HSulf-2 in biological systems. Nevertheless, further research into the molecular determinants of HSulf-1 and HSulf-2 activity in physiological contexts is necessary to elucidate their distinct roles *in vivo* and to reconcile the observed discrepancies.

4 Role of the HD domain: the distinctive feature of Sulfs

The hydrophilic domain (HD) is a distinctive feature of HSulfs that sets them apart from other members of the human sulfatase family. Composed of three subdomains (N-terminal, internal, and C-terminal), HD plays a crucial role in substrate recognition and enzymatic activity. Given its distinctive nature and importance in HSulf function, it is essential to explore the specific role of the hydrophilic domain and its related subdomains. Understanding how these features contribute to the unique properties that distinguish HSulfs from other human sulfatases or any known protein is important.

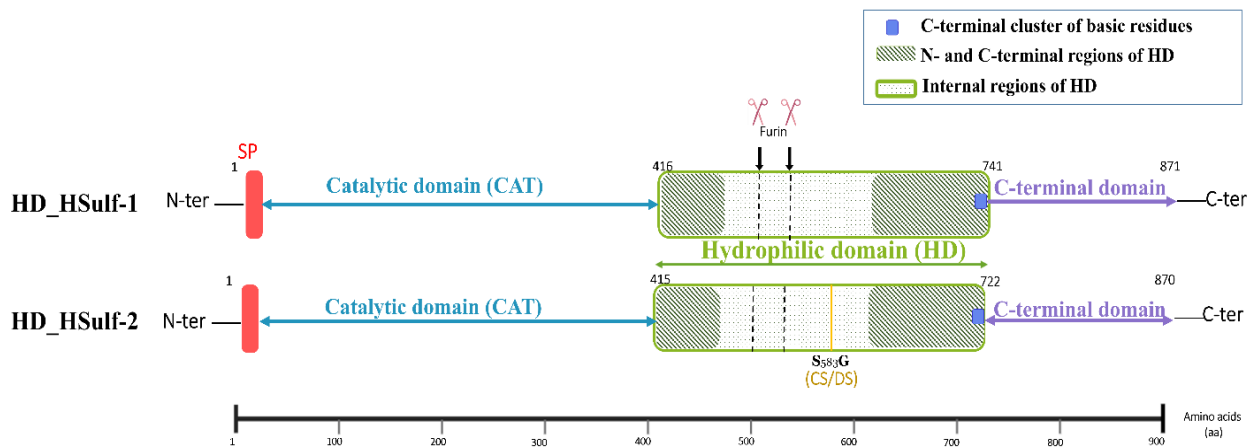


Figure 6: Domain organization and key features of the hydrophilic domain (HD) of HSulf-1 and HSulf-2.

4.1 Impact of the hydrophilic domain on Sulf enzymatic activity

The hydrophilic domain (HD) is a key feature that distinguishes Sulfs from lysosomal exosulfatases and likely confers endosulfatase activity. Domain deletion studies have revealed the critical role of HD and its distinct subdomains in mediating HSulf enzymatic activity. These investigations, mainly led by Frese *et al.*, (2009), Ai *et al.*, (2006), and Tang & Rosen (2009), used different approaches to assess Sulf activity. Ai *et al.* and Tang & Rosen measured endosulfatase activity using $^{35}\text{SO}_4$ -labeled HS with scintillation counting for QSulf-2 and HSulfs, respectively, while Frese *et al.* examined both arylsulfatase activity using the synthetic substrate 4-MUS and endosulfatase activity of HSulf-1 through HS disaccharide composition analysis by Strong Anion Exchange HPLC (SAX-HPLC). The impact of HD modifications on Sulf activity was evaluated by comparing various HD mutants to the wild-type enzyme, as summarized in Table 2.

Table 2: Impact of mutations within the HD domain on Sulf activity.

HD Region/Modification	Impact on Sulf Activity	Reference
Mutants lacking the complete HD	Reduced arylsulfatase activity Abolished endosulfatase activity	(Ai <i>et al.</i> , 2006; Frese <i>et al.</i> , 2009; Tang and Rosen, 2009)
Mutants lacking the internal region	Preserved aryl and endosulfatase activities	(Ai <i>et al.</i> , 2006; Frese <i>et al.</i> , 2009)
Mutants lacking the C-terminal basic cluster	Impaired substrate interaction and reduced enzymatic activity	(Frese <i>et al.</i> , 2009)
Mutants retaining only the C-terminal basic cluster	Retained arylsulfatase activity	(Frese <i>et al.</i> , 2009)

Collectively, these findings demonstrate that without the HD, HSulfs resemble other sulfatases in structure and function. The outer C-terminal and N-terminal subdomains of the HD, particularly its C-terminal basic cluster, are crucial for the catalytic process of HSulfs, affecting both their ability to process the synthetic substrate 4-MUS and their unique endosulfatase activity against HS polysaccharides.

4.2 The hydrophilic domain: key regulator of HSulf localization

Studies conducted by Frese *et al.* (2009) enabled the identification of HD as a crucial domain for HSulfs' ability to modulate various HS-dependent signaling pathways within the extracellular matrix (ECM). Through deletion mutants and GST-HD fusion proteins, they demonstrated that HD includes a conserved basic sequence within its C-terminal region that binds negatively charged heparan sulfate (HS) chains with nanomolar affinity, as confirmed by surface plasmon resonance

analysis. This binding enables the anchoring of HSulf proteins to the cell surface and facilitates their interaction with HS substrates for enzymatic catalysis, a process validated through heparinase-sensitive cell surface association studies. Thus, HD is essential not only for HSulf activity but also for cell surface localization. Consequently, the HD can be characterized as a novel high-affinity binding domain that efficiently localizes HSulfs in close proximity to their specific 6-*O*-sulfate substrate groups within heparan sulfate proteoglycans (HSPGs) at the cell surface.

Initial studies of HD subdomains showed that while the mutant lacking the C-terminal basic cluster loses enzymatic activity, cell surface anchoring can still be maintained through the N- and C-terminal conserved sequences of the HD. This finding suggests that although Sulfs require substrate binding for their action, this physical interaction alone is insufficient for enzymatic activity (Ai et al., 2006).

Subsequent research revealed that removing the entire HD significantly reduces cell surface localization while increasing secretion into the extracellular medium. In contrast, eliminating only the internal, less conserved region of the HD enhances HSulf secretion without affecting enzymatic activity or substrate specificity. These findings indicate that the internal region of HD is critical for regulating HSulf localization and secretion. In contrast, its outer regions are more important for maintaining enzymatic function and substrate recognition (Frese et al., 2009)

4.3 HD: The engine behind substrate specificity and binding

HD plays a crucial role in recognizing and binding to sulfated structures, primarily determining substrate specificity. Studies using various experimental approaches have highlighted the distinct binding characteristics of HD. Surface plasmon resonance showed stable complex formation between HD and heparin with nanomolar affinity, and heparinase treatment confirmed HD's specificity by causing loss of cell surface association (Frese et al., 2009). Further characterization using affinity chromatography analysis demonstrated that while full-length HSulf-1 can interact broadly with various sulfated glycosaminoglycans (GAGs), HD alone exhibits outstanding specificity toward HS, showing no interaction with chondroitin sulfate (CS), dermatan sulfate (DS), or 6-*O*-desulfated HS (Milz et al., 2013).

This specificity is achieved through at least two distinct binding sites found in the internal and C-terminal regions of HD, enabling precise interaction with the polysaccharide substrate. Each HD subdomain can independently interact with heparin, with their combined effect resulting in high avidity through multivalent HD/heparin interactions. Surface plasmon resonance experiments demonstrated stable complex formation with nanomolar affinity, reflecting the high avidity of these

multivalent interactions (Milz et al., 2013).

The cooperative action of these binding sites, working in conjunction with the catalytic domain, enables processive action of HSulf-1 along or across HS chains. This represents a novel and highly dynamic mode of protein-HS interaction mediated by the HD domain, a characteristic also observed in HSulf-2's heparin desulfation activity (Seffouh et al., 2013). The remarkable specificity of HD's interaction with heparan sulfate is further highlighted by its inability to bind to enzymatically 6-*O*-desulfated HS, demonstrating HD's crucial role in substrate recognition and specificity (Milz et al., 2013).

4.4 HSulf-HS interactions: a delicate balance of binding, catalysis, and autoregulation

A compelling model to define the unique 6-*O*-endosulfatase activity of Sulfs would be that the hydrophilic domain initially binds to heparan sulfate (HS) substrates before presenting them to the catalytic domain. On the one hand, it needs to specifically bind to its substrate groups, and on the other hand, it must also detach from these groups after hydrolysis to continue its function (Ai et al., 2006; Frese et al., 2009), suggesting a delicate balance in HSulf interactions with heparan sulfate chains (Figure 7). Moreover, treatment of HS with active HSulf abolishes the binding of HD to the latter, pointing to a self-regulatory mechanism governing the enzyme's interaction with its substrate (Frese et al., 2009; Milz et al., 2013). In this context, non-specific interactions of HSulf with non-substrate GAGs like CS or DS can serve an important purpose, as they may help maintain the enzyme tethered to the cell surface, preventing its release and keeping it present in the local cellular environment where it can continue to function (Milz et al., 2013). Deletion mutation of the internal region of HD induced higher affinity towards HS, leading to a hypothetical model suggesting that the N- and C-terminal regions of the HD contain at least two separate GAG-binding sites. When the inner region of the HD is deleted, these binding sites are brought closer to each other. This might explain the uniform binding efficiency with heparin that is evenly sulfated. The inner region of the HD may play a role in regulating HS affinity or allowing the outer regions of the HD to interact simultaneously with two different GAG chains in a tandem fashion (Frese et al., 2009). Atomic force microscopy-based single molecule force spectroscopy (AFM-SMFS) analyses of the interaction between HD and HS provided clear evidence of catch bond behavior. These studies further demonstrated that the system shifts through a simple slip bond regime between each dynamic HD/HS association and dissociation events, allowing for successive interactions between binding sites. The interplay between multiple cooperative binding sites and conformational changes suggests a directed allostery-driven mechanism that successively introduces 6-*O*-sulfate groups to the catalytic center and synchronously moves HSulfs along the GAG chain (Harder et al., 2015).

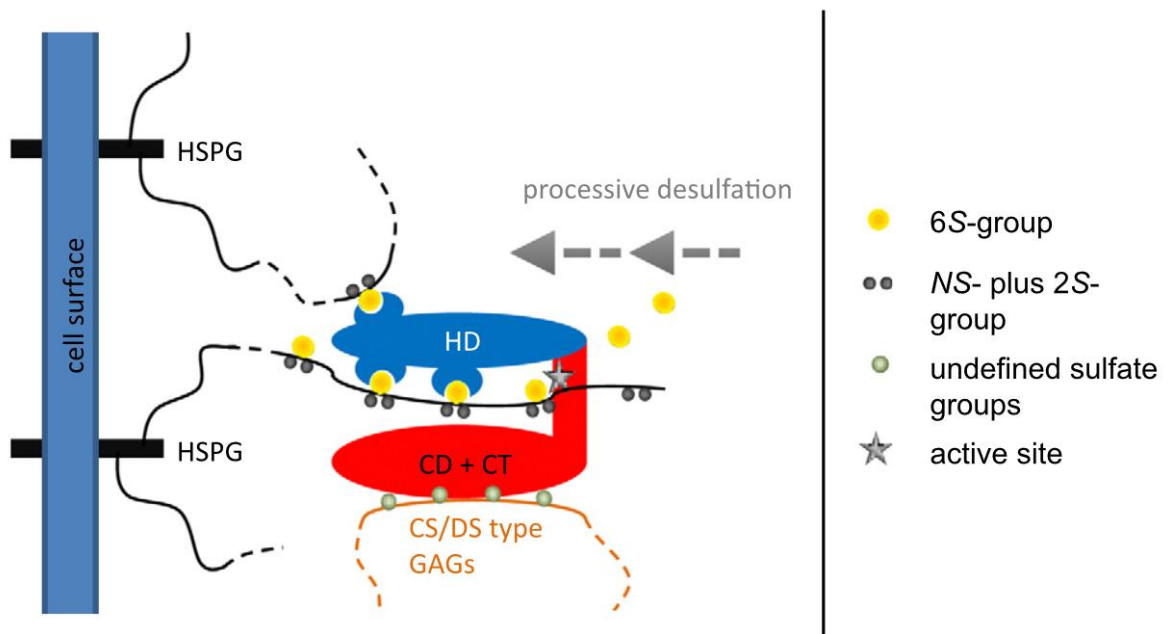


Figure 7: Model of HD-mediated HSulf-HS interactions and substrate recognition. The hydrophilic domain (HD, blue) extends from the catalytic (CD) and C-terminal (CT) domains (red) of HSulf. HD specifically recognizes and binds to 6-*O*-sulfate groups (yellow balls) on heparan sulfate chains, presenting them to the active site (gray star) in CD. N- and 2-*O*-sulfate groups (black dots) and undefined sulfate groups (green dots) are shown. The model illustrates potential non-specific interactions with CS/DS-type GAGs (orange dotted line) that may contribute to cell surface anchoring via HSPGs. Gray arrows indicate the directional nature of HSulf activity along the HS chain. Adapted from Milz *et al.*, 2013.

4.5 HD: insights on the structural and functional divergence of HSulf isoforms

The hydrophilic domain (HD) plays a crucial role in HSulf enzyme function, with most studies focusing on the HSulf-1 isoform. However, it is essential to consider the potential similarities and divergences between HSulf-1 and HSulf-2, particularly given the isoform-specific sequence in the internal regions of their hydrophilic domains. These structural variations may contribute to diverse functions and modulate interactions with cell surface components in an isoform-specific manner. Consequently, while insights gained from HSulf-1 studies are valuable, they may not fully represent the functional characteristics of both HSulf isoforms, especially concerning their hydrophilic domains.

Recent research has uncovered more complexity in the divergence between HSulf-1 and HSulf-2. Notably, HSulf-2 undergoes an unusual O-glycosylation in its hydrophilic domain, leading to the attachment of a glycosaminoglycan (GAG) chain. This modification impacts the enzyme's structure and catalytic properties by increasing its hydrodynamic volume and affecting substrate interactions (Seffouh et al., 2023).

The presence of a GAG chain on HSulf-2 but not on HSulf-1 suggests several hypotheses for their different localization and interactions within the extracellular matrix (ECM). Given the demonstrated HSulf-1 affinity for chondroitin sulfate (CS) and dermatan sulfate (DS) and the nature of the HSulf-2 GAG chain, consisting of a mixture of CS/DS chains, we can speculate on potential protein-protein interactions or even repulsive forces between the enzymes and ECM components. For instance, the GAG chain on HSulf-2 could promote the recruitment of GAG-binding proteins, potentially facilitating the formation of multi-protein complexes. Alternatively, it might create electrostatic repulsion with certain ECM components, influencing the spatial distribution and activity of HSulf-2.

These structural differences may account for the variations observed in the enzymes' localization patterns and substrate preferences. Additionally, they raise the possibility of direct interactions between HSulf-1 and HSulf-2 through GAG-protein binding, potentially leading to the formation of heterodimers with unique functional properties. These hypotheses highlight the need for further research into the specific roles of the GAG chain in HSulf-2's cellular interactions and how it contributes to the distinct functions of the two isoforms in different biological contexts.

5 Dynamic cellular distribution of HSulfs: from extracellular matrix to nuclear localization

5.1 Extracellular localization

Building upon the previously discussed structural features and enzymatic activities of HSulfs, we can reiterate several key pieces of information that can contribute to a comprehensive overview of their cellular distribution. The furin cleavage plays a crucial role by inducing their localization within lipid rafts, which serve as critical platforms for trafficking most cellular signaling events (Tang and Rosen, 2009). In the absence of such modification, HSulfs exhibit a non-homogeneous distribution on the cell membrane. Although primarily investigated in the Quail ortholog, N-glycosylations appear also as an essential PTM for appropriate cell surface localization and enzyme activity (Ambasta et al., 2007).

Besides these PTMs, several structural features of HSulfs are significantly involved in orienting their localization. Their molecular architecture includes a hydrophobic signal peptide for secretion and, most importantly, a hydrophilic domain ideally suited for docking to the cell surface through specific binding to HS. These interconnected aspects, along with acknowledged research, define a characteristic extracellular yet differential presence of the two paralogs, considering that secreted HSulfs show differential localization patterns within the cell surface and the extracellular matrix (ECM). HSulf-1 tends to bind and remain on the cell surface, whereas HSulf-2 is more readily released into the ECM (Lamanna et al., 2008; Hossain et al., 2010). This differential presence can be linked to the possible interaction of the GAG (CS/DS) chain of HSulf-2 with other protein partners present on the cell surface and in the extracellular matrix (ECM), thereby regulating its localization and diffusion. Lastly, enzymatically active forms have been detected in the conditioned medium and cell surface (Mark S. Singer et al., 2015). Their participation in cell signaling by mediating several pathways requiring a specific pattern of sulfated HSPGs directly links their extracellular localization to these critical cellular events.

5.2 Intracellular localization

Recent studies have unveiled a more complex picture than the traditional view of HSulfs as solely extracellular enzymes. Nuclear localization of HSulfs was demonstrated in neuronal cells through immunocytochemical staining and immunoblotting of isolated nuclear fractions from different neuronal cell types (Krishnakumar et al., 2018). The identified levels of HSulf expression were not static, and their localization varied markedly during different stages of growth, thus demonstrating highly dynamic spatial and temporal patterns during nuclear cell division for both enzymes.

Preferential nuclear or membrane, or both nuclear and membrane-associated enzyme expression, suggested potential coordination between extracellular cell signaling and nuclear events related to cell proliferation.

Furthermore, their high post-division cytoplasmic expression suggested involvement in cell size increase and commitment to cell division (Krishnakumar et al., 2018). However, while their role on the cell membrane is known to desulfate HSPGs to modulate cell signaling pathways, the precise mechanism of HSulfs' nuclear action is not well established. HSPGs are present in the nucleus in both sulfated and desulfated states, where they are believed to play regulatory roles in the cell cycle, transcription, and transport of nuclear cargo (Stewart and Sanderson, 2014). While the variation in nuclear HSPG sulfation during these processes, including the cell cycle, was previously attributed to sulfotransferase activities, the presence of HSulfs in the nucleus suggests they might also play a role in these processes, although their precise function remains to be determined.

5.3 Particular cellular localization

Both Sulf paralogs were detected in the acrosome of spermatids, suggesting an implication in the breakdown of the zona pellucida and HS degradation during fertilization (Langsdorf et al., 2011). Immunofluorescence microscopy has shown that HSulfs localize to the endoplasmic reticulum (ER), consistent with findings for QSulfs. While the significance of their presence in the ER is not fully understood, it adds depth to our understanding of Sulf distribution and activity (Lamanna et al., 2008).

HSulfs, therefore, demonstrate a remarkable ability to adapt their localization and activity based on cellular phase, environmental cues, and tissue-specific needs. Rather than functioning as static "gendarmes," HSulfs act as "special agents" capable of responding to various cellular stimuli. This dynamic behavior allows them to fine-tune HS modifications in response to changing conditions, highlighting their sophisticated role in cellular regulation and underscoring the importance of considering their diverse localizations when studying their functions and potential therapeutic applications.

5.4 Organ-specific distribution and expression of HSulfs

In addition to their dynamic and differential cellular distribution, HSulfs exhibit differential yet overlapping organ-specific expression patterns. This has been the subject of extensive research and can be traced back to pioneer studies conducted by Morimoto-Tomita *et al.* in 2002. This work revealed different expression patterns of the two enzymes using PCR techniques on a panel of cDNAs from various human tissues to detect their transcripts. HSulf-1 showed high expression in

the testes, skeletal muscle, stomach, lung, and kidney, while HSulf-2 showed prominent expression in the skeletal muscle, stomach, brain, heart, ovary, uterus, kidney, and placenta (Morimoto-Tomita et al., 2002).

Holmes et al. (2017) further supported the organ specific expression, identifying an Estrogen Receptor Gene (ESR1) in the promoter of HSulf-2, which potentially directs its expression in female reproductive tissues. HSulf-2 was shown to have an important role in both local tissue environments and systemic circulation, with detection of its release from cells and presence in blood plasma, while HSulf-1 was undetectable in blood leukocytes either before or after glucocorticoid therapy (Agrawal et al., 2021).

Further studies on mouse orthologs demonstrated a correlation between Sulf expression and organ-specific sulfation patterns of heparan sulfate. Disaccharide composition analysis of HS in Sulf1/2 knockout mice revealed significant increases in Δ UA2S-GlcNS6S in multiple organs. This result was correlated with the normal expression patterns of Sulfs in these organs. Moreover, *in situ* hybridization experiments revealed differential expression of Sulfs' mRNAs in specific cell types within various organs, such as lungs and kidneys. For instance, in the lungs, Sulf1 mRNA was detected in blood vessels, while Sulf2 mRNA was detected in bronchial walls. In the kidney, Sulf1 was expressed in the glomeruli, and Sulf2 was expressed in the distal renal tubules (Nagamine et al., 2012).

Furthermore, the Human Protein Atlas, based on data of HSulf-1 and HSulf-2 expression collected in various physiological and pathophysiological contexts, has provided a comprehensive schematic representation of their distribution in male as well as female organs (Uhlén et al., 2015). This data confirms and broadens the scope of previous findings, which all together underscore the tailored localization and activity of HSulf-1 and HSulf-2 to the specific needs of different tissues.

HSulf-1 and HSulf-2 show differential expression patterns across various tissues, suggesting their involvement in tissue-specific functions. This specificity indicates that their roles extend beyond a single tissue or system, contributing to context-dependent tissue homeostasis. Understanding this diversity and specificity in their expression is crucial for grasping their implications in cell biology and physiology, as well as their involvement in a wide range of diseases, particularly in cancer.

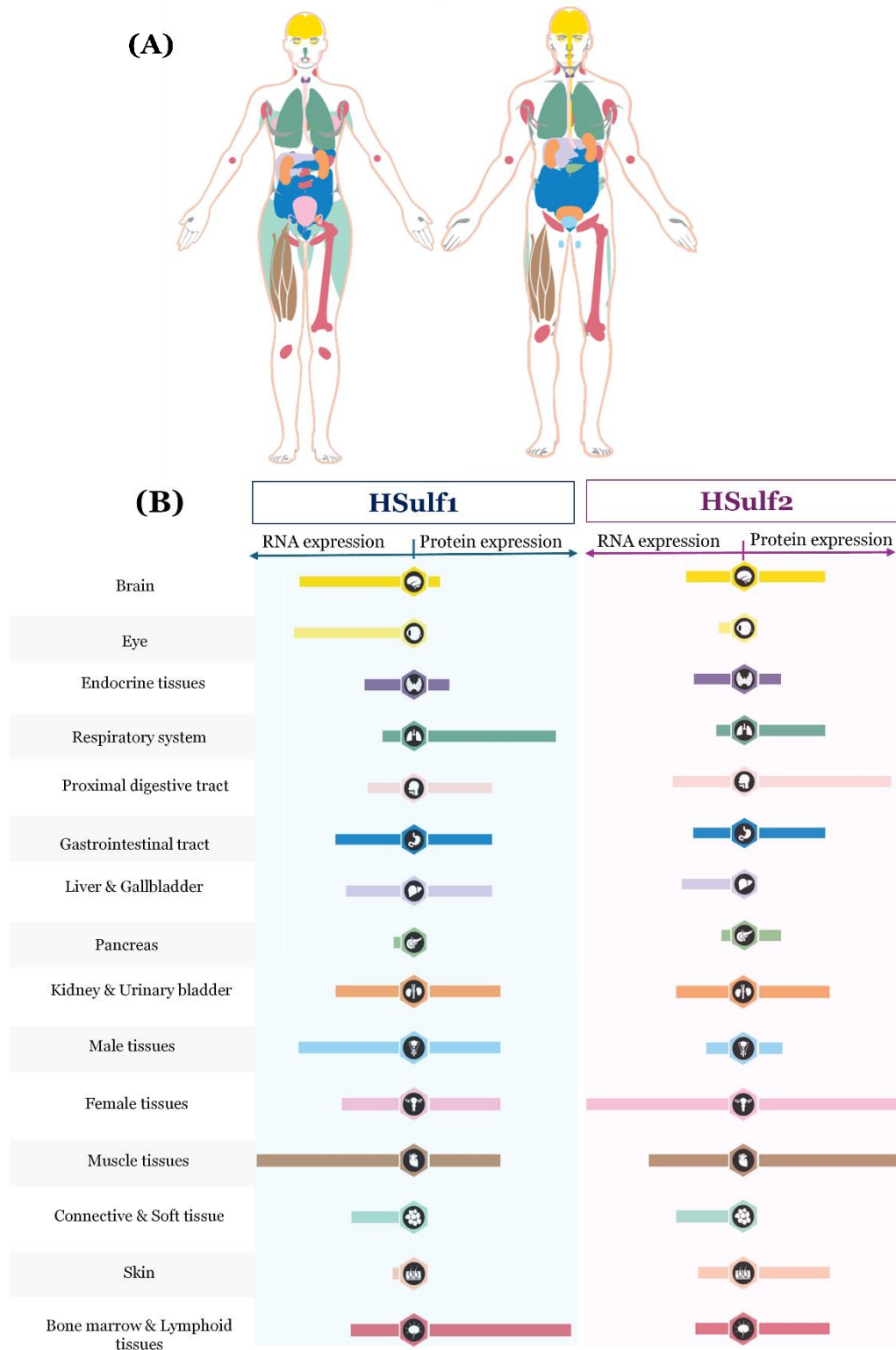


Figure 8: Tissue distribution and expression of HSulf-1 and HSulf-2 in the human body. (A) Merged tissue distribution of HSulf-1 and HSulf-2 in female and male human bodies. (B) RNA and protein expression of HSulf-1 and HSulf-2 in female and male body tissues. RNA expression summary shows consensus data based on normalized expression (nTPM) values from two sources: internally generated Human Protein Atlas (HPA) RNA-seq data and RNA-seq data from the Genotype-Tissue Expression (GTEx) project. Color coding is based on tissue groups with common functional features. Each bar represents the highest expression score found in a particular group of tissues. Data adapted and modified from the Human Protein Atlas (<https://www.proteinatlas.org>).

6 Implication in cell biology and physiology

HSulfs' targeted modification of HS 6-*O*-sulfation patterns exemplifies how subtle structural changes can lead to major biological consequences. Through their specific 6-*O*-desulfation mechanism, HSulfs regulate multiple signaling pathways critical for development and tissue homeostasis. HSulfs modulate two key categories of signaling molecules: growth factors and morphogens, thereby influencing a variety of cellular processes. In growth factor signaling, HSulfs play a regulatory role by repressing FGF pathway activity, influencing angiogenesis through Vascular Endothelial Growth Factor (VEGF) modulation, and modulating other growth factor pathways. They can either promote or inhibit signaling depending on the pathway (Rosen and Lemjabbar-Alaoui, 2010). For morphogen signaling, HSulfs impact key developmental pathways, particularly by promoting Wnt signaling through modifying HSPG sulfation patterns (Nawroth et al., 2007) and regulating BMP (Beta/Bone Morphogenetic Protein) activity through interactions with inhibitors like Noggin (Figure 9).

These molecular interactions translate into essential roles in development and tissue homeostasis. The broad biological functions of HSulfs and their orthologs have been demonstrated in models such as mouse, quail, *Xenopus*, chick, and *Drosophila*, using various experimental methods like knockout studies and genetic manipulation (detailed in Supplementary Table S1, page 160).

HSulfs exhibit both overlapping and distinct functions. Severe phenotypes observed in double-knockout mice highlight their critical roles in embryonic development, neuronal growth, and skeletal formation (Holst et al., 2007). However, their individual contributions differ in areas such as neural plasticity, growth factor responsiveness, and signaling pathway modulation (Kalus et al., 2009). Sulf1 and Sulf2 show distinct yet complementary expression patterns during development (Winterbottom and Pownall, 2009) and have context-dependent effects on key signaling pathways like Wnt and Shh (Kalus et al., 2015; Justo et al., 2022).

The ability of HSulfs to modulate growth factor signaling, particularly their inhibitory effects on certain growth factor responses, has sparked significant interest in their potential roles in cancer biology. In cancer, intensified growth factor signaling often leads to increased cell proliferation and reduced apoptosis (Parker and Kohler, 2010). This understanding has driven further research into the implications of HSulfs in various pathological conditions, especially tumor development and progression, opening avenues for potential therapeutic strategies targeting these enzymes (Rosen and Lemjabbar-Alaoui, 2010).

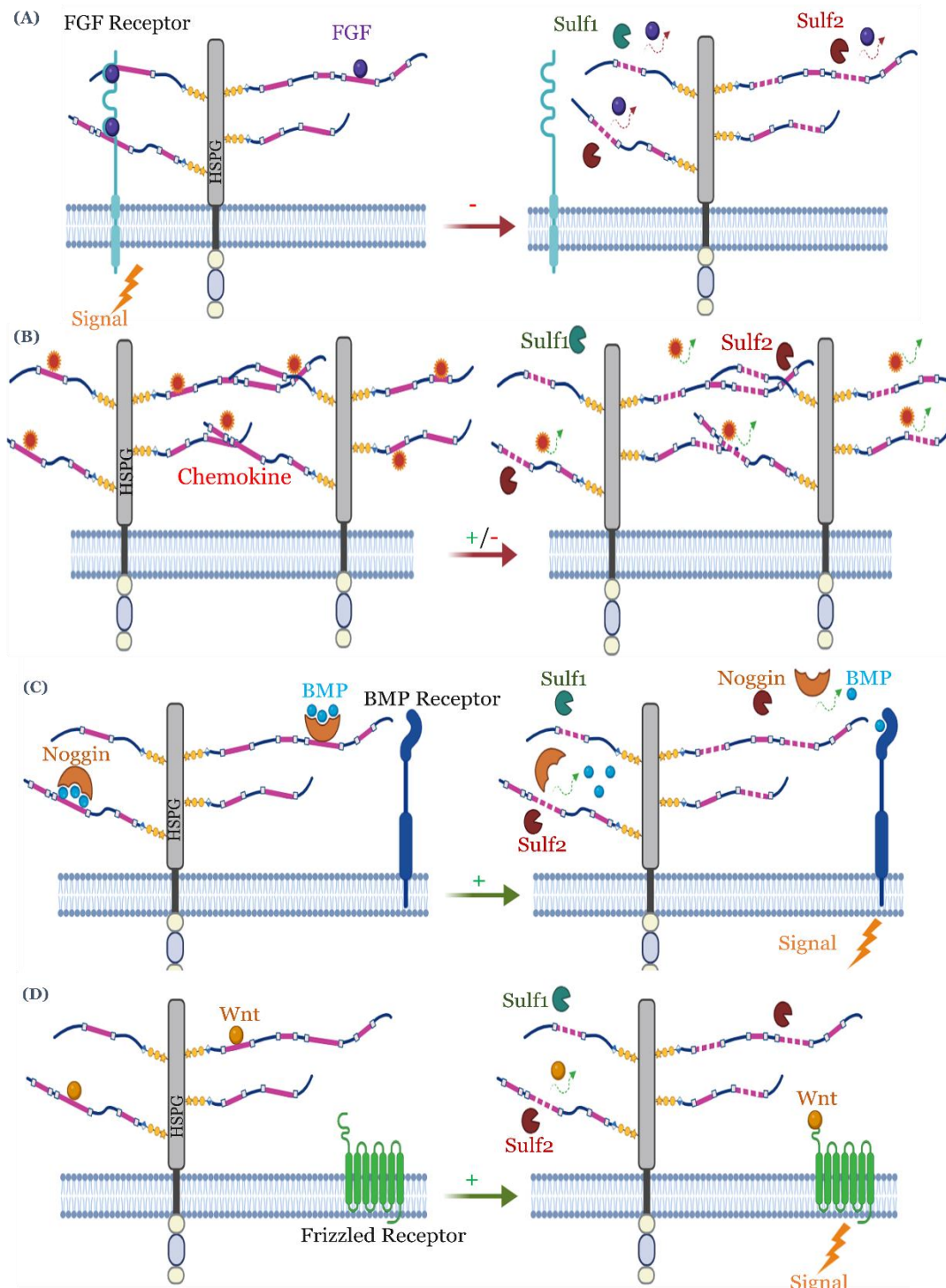


Figure 9: Regulation of cell signaling pathways through HSulf-6-*O*-desulfation of cell surface HS chains (shown as solid lines before and dashed lines after HSulf action). (A) FGF signaling: 6-*O*-sulfation is required for the formation of the functional FGF/FGF receptor/HS ternary complex. HSulf-mediated desulfation inhibits complex formation and subsequent signaling while maintaining FGF binding to HS. (B) Chemokine gradient formation: HSulfs modify chemokine distribution by altering their interaction with HS chains, potentially disrupting the formation of chemotactic gradients essential for cell migration. (C) BMP pathway: HSulf activity releases Noggin (BMP antagonist) from the cell surface by reducing its binding to HS, thereby enabling BMP to interact with its receptor (BMPR) and trigger signaling. (D) Wnt signaling: High-affinity binding of Wnt to 6-*O*-sulfated HS prevents its interaction with the Frizzled receptor. HSulf-mediated removal of 6-*O*-sulfates reduces this binding, facilitating Wnt-Frizzled interaction and subsequent signal activation. Updated from (Vives et al., 2014)

7 Implication in pathology and cancer biology

Over the past two decades, HSulf enzymes have raised interest in extensive biological research aiming to elucidate their roles in various pathological processes. Initially, the main attention was directed towards their potential involvement in cancer development. Dysregulation of HSulf activities and expression pattern was correlated to modulating tumor progression (Lemjabbar-Alaoui et al., 2010). In recent years, the scope of HSulf research has broadened significantly, with new evidence indicating their influence on a wide range of health conditions, particularly cardiovascular diseases and metabolic disorders associated with cardiovascular risk (Justo et al., 2021). This growing body of research underscores the extensive implications of HSulf activity throughout the human body, from the brain to the bones, highlighting their complex and sometimes conflicting roles across different tissues. A comprehensive "journey through the human body" detailing HSulfs' implications in both oncogenic and non-oncogenic pathologies across various organs and tissues is provided in Supplementary (Table S2, page 163).

The complex interplay between HSulf-1 and HSulf-2 in cancer biology dictates a delicate balance akin to the ancient Chinese Yin-Yang philosophy, a metaphor previously attributed to Sulfs by (Vives et al., 2014). This delicate balance highlights the complementary and sometimes opposing forces of these enzymes in maintaining cellular homeostasis, as well as in promoting cellular carcinogenesis. Throughout various organs and systems of the human body, HSulf-1 exhibits a dominating downregulation pattern of expression within cancer pathophysiology, whereas HSulf-2 presents an upregulation pattern. In fact, since the first pioneering studies (Lai et al., 2003), HSulf-1 was identified as a tumor suppressor, inhibiting angiogenesis and tumorigenesis across various cancers, while HSulf-2 was described as pro-angiogenic, often promoting cancer progression through enhanced cell signaling and angiogenesis (Morimoto-Tomita et al., 2005).

However, this dichotomy is not absolute and is still debated. HSulf-1, while most commonly acknowledged as tumor-suppressive, shows pro-tumoral effects in certain cancers, notably ovarian (Backen et al., 2007), gastric (Junnala et al., 2010; Hur et al., 2012), pancreatic (Li et al., 2005; Nawroth et al., 2007), and in leukemia (Bret et al., 2011). Its overexpression in pancreatic cancer is associated with decreased cell proliferation but increased invasive potential (Abiatari et al., 2006). Similarly, HSulf-2, generally considered pro-oncogenic, exhibits tumor-suppressive properties in myeloma (Dai et al., 2005) and renal carcinoma (Kumagai et al., 2016). In lung cancer, Sulf2 is expressed in all squamous cell carcinoma samples but not in adenocarcinoma samples (Lemjabbar-Alaoui et al., 2010). Conflicting results are also reported in breast cancer, where HSulf-2 both promotes (Zhu et al., 2016) and inhibits (Peterson et al., 2010) tumor growth. These overlapping

and sometimes conflicting aspects related to different types of cancer extend to stage-specific roles, as seen in head and neck squamous cell carcinoma. HSulf-1 correlates with poor survival in the early stages, and HSulf-2 significantly impacts survival in the later stages (Yang et al., 2022).

Despite sharing similar substrate specificities and molecular organization, HSulf-1 and HSulf-2 exhibit divergent actions in cancers and pathophysiology, challenging the initial view of their functional redundancy. As discussed in previous sections, a key distinguishing feature is the presence of a unique post-translational modification (PTM) in HSulf-2, consisting of a chondroitin sulfate/dermatan sulfate (CS/DS) glycosaminoglycan (GAG) chain, which is absent in HSulf-1. This structural difference can be one of the main specificities contributing to their complex interplay. In an attempt to understand the elusive mechanisms that lay behind, one should consider the complex composition of the extracellular matrix as well as the tumor microenvironment, which Sulfs modify through the editing of heparan sulfate proteoglycan (HSPG), thereby influencing cancer progression and metastasis. Hyaluronidase, a hydrolase that plays a crucial role in the extracellular matrix, specifically degrades hyaluronic acid and can also act on chondroitin sulfate chains (Honda et al., 2012; Bilong et al., 2021). Increased hyaluronidase activity has been linked to cancer progression and metastasis in various cancers, including pancreatic, lung, ovarian, breast, and colorectal cancers (Lokeshwar et al., 2005; McAtee et al., 2014). An overlap between the actions of HSulf-2 and hyaluronidase in these types of cancers is therefore possible. We can even speculate that hyaluronidase may act on the (CS/DS) glycosaminoglycan chain of HSulf-2, thereby modulating its localization and activity (El Masri et al., 2022). However, further research is needed to elucidate the specific interactions between hyaluronidase and Sulf2 across different cancer types and determine the extent of their interconnected roles in cancer progression.

Although most studies have focused on HSulf expression in cancer cells, their production by other cells within the tumor microenvironment significantly influences HSPG-mediated signaling. HSulf-1, for example, can inhibit growth factor signaling, suggesting a tumor suppressor role. However, its expression patterns in cancer are complex, being reduced in some tumors but overexpressed in others (Bret et al., 2011). Understanding HSulf functions and their therapeutic potential requires considering multiple factors: the type and stage of cancer, cellular context, HSulf expression levels, HSPG patterns, and growth factor levels. (Lemjabbar-Alaoui et al., 2015).

In non-oncologic pathologies, HSulf-1 and HSulf-2 show largely overlapping actions, unlike their opposing roles in cancer, making the Yin-Yang concept less applicable to these conditions without additional evidence. As we deepen our knowledge of HSulfs, their structure and function, and the relationships between these aspects, their complex roles in both oncologic and non-oncologic

conditions present significant challenges for therapeutic targeting.

8 HSulfs as therapeutic targets: advances in inhibition strategies and regulatory mechanisms

The extensive involvement of HSulfs in various physiological and pathological processes has sparked interest in understanding their molecular mechanisms, especially in developing strategies for inhibiting their pro-malignant activities. While most malignant conditions are associated with the upregulation of HSulf-2, HSulf-1 has also been implicated in certain cases. Targeting HSulf-2 with inhibitors could yield anti-cancer effects. However, the impact of modulating HSulf-1 is more complex and varies significantly depending on the specific type of cancer and the major signaling pathways involved.

The field of HSulf inhibition is still relatively recent, and the earliest studies demonstrating specific HSulf inhibitors and their potential therapeutic applications emerged in the late 2000s to early 2010s. These studies laid the groundwork for developing more potent and selective HSulf inhibitors. Over the past decade, interest in this area has grown, as evidenced by recent studies in the 2020s. Strategies developed so far can be divided into two main categories: direct inhibition and indirect regulation of HSulf activity.

8.1 Indirect inhibition of HSulf activity

Limited structural information about HSulfs initially led researchers to explore indirect regulation strategies to modulate their expression and activity, mainly in cancer. Early studies have identified epigenetic mechanisms, such as DNA methylation and histone modifications, as crucial regulators of Sulf expression. Hypermethylation of HSulfs promoters was found to lead to their inactivation in various cancers, including ovarian for (Staub et al., 2007) and gastric and lung cancers for HSulf-2 (Tessema et al., 2012; Wang et al., 2013). Targeting these epigenetic modifications through DNA methylase inhibitors, such as Zebularin (J.-P. Lai et al., 2008) and 5-aza-2'deoxyctidine (Staub et al., 2007), showed promise in reactivating HSulf-1 expression in ovarian cancer cells, thereby enhancing chemotherapy sensitivity and improving patient survival. Conversely, methylation of the HSulf-2 promoter was considered as potential strategy to promote its silencing (Tessema et al., 2012).

Parallel research has revealed significant roles of transcription factors and tumor suppressor genes in HSulf regulation. For instance, the p53 pathway directly activates HSulf-2 transcription in response to DNA damage, which, when suppressed, cells show decreased senescence under stress

(Chau et al., 2009). Similarly, the Von Hippel-Lindau (VHL) tumor suppressor positively regulates HSulf-2 expression by promoting the degradation of hypoxia-inducible factors (HIF) in response to hypoxic conditions (Khurana et al., 2012).

In 2012, Liu *et al.* introduced an innovative gene therapy approach using heparin/polyethyleneimine nanogels to deliver recombinant plasmid DNA containing HSulf-1 cDNA into cancer cells, aiming to restore HSulf-1 levels and its tumor suppressor function (Liu et al., 2012). This strategy was effective in ovarian cancer models without apparent systemic toxicity. The following year, Khurana *et al.* demonstrated that proteasome inhibitors, such as MG132, Lactacystin, and specifically Bortezomib, could reduce tumor size in breast cancer models by repressing HSulf-2 expression (Khurana et al., 2013). A notable finding came in the same year when Bao et al. identified miR-21, a microRNA that can target multiple genes and function as an oncogene, as a negative regulator of HSulf-1 and PTEN expression in hepatocellular carcinoma (HCC) cells (Bao et al., 2013). The suppression of HSulf-1 and PTEN, the latter being a crucial tumor suppressor that helps regulate cell division, by miR-21 leads to the activation of AKT/ERK pathways and epithelial-mesenchymal transition (EMT), promoting HCC cell proliferation and tumor growth. This discovery highlighted the potential of targeting miR-21 and its downstream effects on HSulf-1 as a therapeutic strategy for HCC.

Further research into HSulf targeting led to identifying 2,4-DiSulfophenyl-N-tert-butylNitron (OKN-007, formerly NXY-059) as a potential HSulf-2 inhibitor in hepatocellular carcinoma (HCC) cells (Zheng et al., 2013). OKN-007 effectively inhibits HSulf-2, particularly in cells with high HSulf-2 expression, leading to the suppression of TGF β 1/SMAD2 and Hedgehog/GLI1 signaling pathways. This inhibition reduces tumor growth and progression. Supported by both *in vitro* and *in vivo* studies, OKN-007's specificity for HSulf-2-expressing cells underscores HSulf-2's role as a tumoral protein and highlights its potential as a therapeutic target in HCC.

Later, in 2017, a connection between HSulf-1 loss and the dysregulation of autophagy and lipid metabolism in ovarian cancer cells was identified. This suggested that restoring HSulf-1 expression could serve as a potential therapeutic strategy for ovarian cancer (Roy et al., 2017). Subsequently, Yoon *et al.* revealed that invalidation of HSulf-2 significantly increases the susceptibility of liver cancer cells to sorafenib, which is a multikinase inhibitor anticancer drug, suggesting that combining HSulf-2 inhibitors with sorafenib could lead to improved therapeutic outcomes in liver cancer patients (Yoon et al., 2018).

More recently, Yang *et al.* developed an innovative triple-strategy drug delivery system to improve drug delivery and targeting in hepatocellular carcinoma (HCC) treatment. The developed system

consists of engineered *E. coli* bacteria (ASEc) with nanoparticles loaded with plasmids encoding for HSulf-1 anchored on their surface, enabling the release of drugs directly into tumor cells. The synergistic combination of ASEc and nanoparticles (PNPs) significantly suppresses HCC *in vivo* while reducing side effects. This multidimensional approach presented significant potential to enhance the efficacy of HCC therapy by targeting the tumor through multiple mechanisms (Yang et al., 2024).

8.2 Direct inhibition of HSulf activity

HSulfs, primarily located on the cell surface and within the extracellular matrix, are valuable targets for inhibition by small-molecule drugs. These inhibitors can regulate HSulf activity by targeting the active site or specific epitopes, offering potential therapeutic strategies for disorders associated with HSulfs, particularly in cancer. As research progresses, a variety of inhibitors have been identified and characterized, focusing on direct inhibition of HSulf activity. These inhibitors exploit the structural and chemical properties of the HSulf catalytic site, emphasizing the role of hydrophobic interactions, as shown by *in silico* studies (Hemakumar et al., 2023). Developing effective inhibitors involves creating molecules with high affinity for the enzyme's active site, often mimicking the binding strength of natural substrates. These inhibitors can be classified based on their mechanisms of action, including competitive inhibitors (Table 3, page 45) and non-competitive inhibitors. Collectively, these inhibitors hold significant promise for advancing our understanding of HSulfs' intricate mechanisms and developing targeted cancer therapies.

8.2.1 Competitive inhibitors

8.2.1.1 HS-Mimetics

Phosphomannopentaose polysulfate (PI-88), a mixture of highly sulfated, monophosphorylated mannose oligosaccharides, was initially developed as a heparanase inhibitor but was later found to inhibit HSulfs by mimicking the structure of heparan sulfate (Hossain et al., 2010). The key strategy behind using PI-88 is mimicking heparan sulfate, thus reducing and abolishing HSulfs enzymatic activity. PI-88 inhibits HSulfs with IC₅₀ values of 0.6–3.6 µg/mL, comparable to its heparanase inhibition (2 µg/mL) (Hossain et al., 2010). Phase III clinical trials demonstrated PI-88's efficacy as an adjuvant therapy in hepatocellular carcinoma, particularly benefiting patients with microvascular invasion and showing an acceptable safety profile (Liu, 2014). The use of PI-88 as an HSulf inhibitor demonstrates the potential of targeting heparan Sulfate-related pathways in cancer treatment.

8.2.1.2 Sulfamate Substrate Analogs

HSulfs have only recently emerged as therapeutic targets, resulting in a limited number of studies describing their chemical inhibitors compared to those for steroid sulfatases (STS), a well-established target in hormone-dependent cancers. STS inhibition strategies, which primarily involve replacing the substrate's sulfate moiety with a sulfamate group, have provided valuable insights for HSulf inhibitor design (Daško et al., 2020; Foster, 2021). The highly conserved structure and mechanism across the sulfatase family, including HSulfs, make them susceptible to inhibition by aryl sulfamates. These sulfamate-based inhibitors act as transition state analogs, forming a covalent bond with the catalytic formylglycine residue in the enzyme's active site, leading to irreversible inhibition (Figure 10). Building on these observations, researchers have hypothesized that introducing sulfamate-based motifs into molecules mimicking HSulfs' natural substrates could yield potent and specific inhibitors.

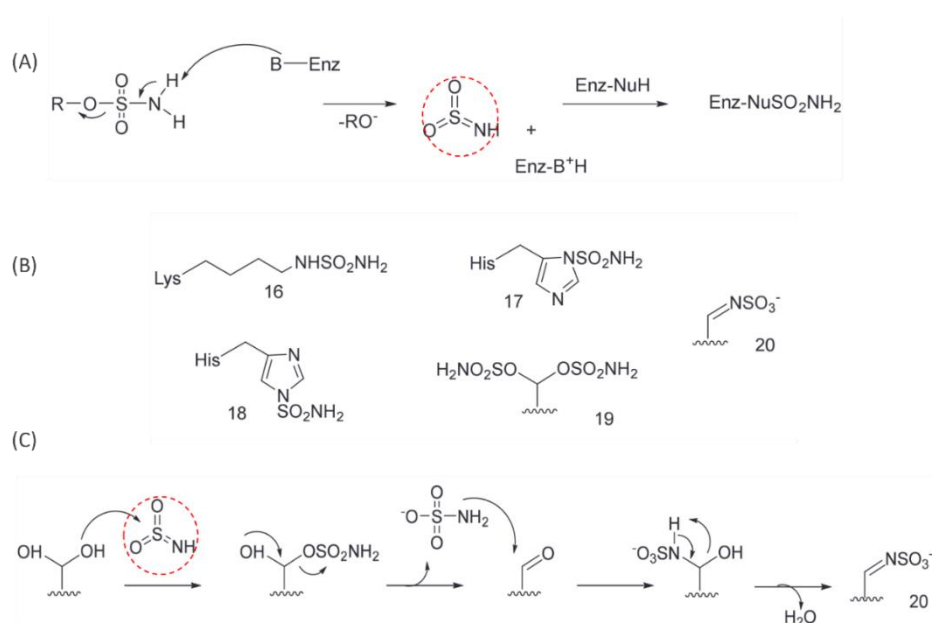


Figure 10: Proposed mechanisms of sulfamate-based inhibition of sulfatases. (A) Proposed E1cb mechanism for sulfatase inactivation by sulfamates. A basic residue in the enzyme's catalytic site deprotonates the sulfamate (pKa ~7-8), leading to oxygen-sulfur bond cleavage and formation of the SO_2NH intermediate. (B) Potential products formed by the reaction of SO_2NH intermediate with various catalytic site residues (compounds 16-20), including lysine and histidine modifications. (C) Proposed mechanism for formylglycine modification leading to irreversible enzyme inactivation, resulting in the formation of compound 20, which is believed to be responsible for permanent catalytic site disruption. Scheme adapted and updated from Quellier (2020).

➤ Biphenyl Trichloroethylsulfamate:

Molecular modeling studies by Reuillon *et al.* have led to the development and synthesis of a new pharmacophore from the trichloroethylsulfamate group for HSulf-2 inhibition. This discovery was made by developing two novel series of sulfatase inhibitors based on biphenyl and biphenyl ether templates, allowing for the synthesis of various sulfamates and amino sulfate compounds. The trichloroethylsulfamates exhibited HSulf-2 inhibition, with an IC₅₀ value of $167 \pm 5 \mu\text{M}$ (Reuillon *et al.*, 2016). These findings not only establish the trichloroethylsulfamate group as a new pharmacophore for Sulfatase inhibition but also represent a highly potent small molecule inhibitor of HSulf-2.

➤ Glucosamine-6-Sulfamate Analogs:

A leading study by Schelwies *et al.* introduced the development of glucosamine-based small molecule inhibitors by substituting the 6-*O*-Sulfate ($-\text{OSO}_3^-$) with the Sulfamate motif ($-\text{OSO}_2\text{NH}_2$) (Schelwies *et al.*, 2010). This study has initially confirmed that general phenyl sulfamates could eventually inhibit HSulfs before developing the first generation of carbohydrate-based sulfamate inhibitors. Structurally, these inhibitors consisted of the smallest, most relevant unit of HS, α -GlcNS(6S), with a sulfamate surrogate on the 6-*O* position. The biochemical characterization of this compound in a competition assay with fluorogenic substrate 4-methylumbelliferyl Sulfate (4-MUS) revealed IC₅₀ values of 95 μM for HSulf-1 and 130 μM for HSulf-2 and, importantly, was more selective for the HSulfs than other sulfatases investigated.

➤ Oligosaccharide-based Sulfamate Analogs:

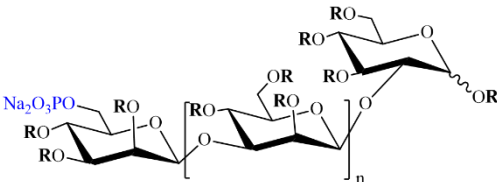
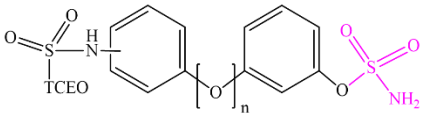
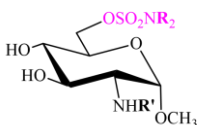
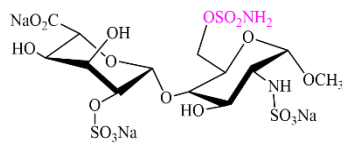
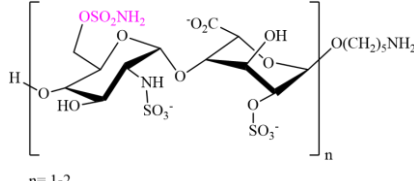
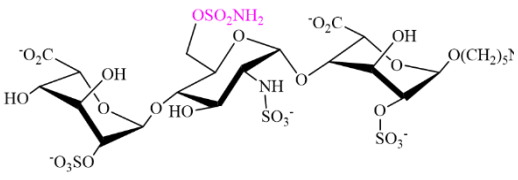
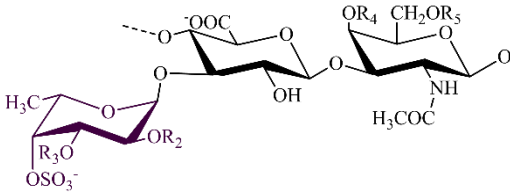
A recent study by Chiu *et al.* reported the design and synthesis of di-, tri-, and tetra-saccharide HS oligosaccharides with sulfamate modifications as inhibitors of HSulf-1 (Chiu *et al.*, 2020). Their findings first revealed the minimal-size substrate for HSulf-1, consisting of the trisaccharide IdoA2S-GlcNS6S-IdoA2S. Importantly, the substitution of the 6-*O*-Sulfate group on the D-glucosamine unit with a sulfonamide surrogate resulted in potent HSulf-1 inhibition. The biochemical characterization of this compound in a competition assay with fluorogenic substrate 4-methylumbelliferyl Sulfate (4-MUS) revealed an IC₅₀ of 0.53 μM . In comparison, the disaccharide GlcNS(6Sulfamate)-IdoA(2S) showed only 20% HSulf-1 inhibition at 0.7 mM, while the tetrasaccharide analog demonstrated an IC₅₀ of 29.6 μM . Subsequent to these findings, Kennett *et al.* reported the design, synthesis, and evaluation of modified minimal-size HS fragments as inhibitors of HSulf-2 (Kennett *et al.*, 2023). This study focused on designing and synthesizing sulfated disaccharide inhibitors based on the trisulfated disaccharide IdoA(2S)-GlcNS(6S), with

the introduction of a sulfamate group at the reducing end. The trisulfated disaccharide inhibitor, IdoA(2S)-GlcNS(6Sulfamate), showed potent inhibition of HSulf-2 in a 4-MUS competition assay, with an IC₅₀ value of 39.8± 18.3µM. Based on these results, the authors suggest that the trisulfated HS disaccharide unit constitutes the shortest fragment size required to effectively inhibit HSulfs.

➤ Polysaccharide-based inhibitors

Fucosylated Chondroitin Sulfate (HfFucCS) from the sea cucumber *Holothuria floridana* was recently identified as an effective inhibitor of HSulf-2. The related research was conducted in the context of the invasiveness of head and neck squamous cell carcinoma (HNSCC) (Mukherjee et al., 2023). The biochemical characterization of HfFucCS in both a competition assay with fluorogenic substrate 4-methylumbelliferyl Sulfate (4-MUS) and heparan-specific 6-*O*-desulfation assays, demonstrated significant inhibitory potential, with calculated IC₅₀ values of 0.18 and 0.14 ng per ng of HSulf-2, respectively. HfFucCS allowed for complete HSulf-2 inhibition at near equimolar concentrations, with inhibitor-to-substrate ratios as low as 1:100,000. HfFucCS treatment reduced the invasion of two separate cancer cell lines in a cancer-associated fibroblast (CAF) model mimicking the tumor microenvironment, and the observed effects were similar to those observed in HSulf-2 knock-out cancer cells. Based on these findings, the authors suggest that HfFucCS is a valuable tool for studying HSulf-2's function and developing potential therapeutic interventions, estimating that their results warrant further exploration of HSulfs and their inhibition in HNSCC and other cancers.

Table 3: Competitive HSulf-1/2 inhibitors: structures and potencies.

Inhibitor	Structure	HSulf-1/2 related	IC50	Reference
PI-88	 <p>R = SO₃Na or H, n = 0-4</p>	- HSulf-1 - HSulf-2	- [0.6–3.6] μg/mL	(Hossain et al., 2010)
Biphenyl Trichloroethylsulfamate		- HSulf-2	- 167 ± 5 μM	(Reuillon et al., 2016)
α-GlcNS (6Sulfamate)	 <p>R = CH₃ or H, R' = SO₃Na or Ac</p>	- HSulf-1 - HSulf-2	- 95 μM - 130 μM	(Schelwies et al., 2010)
IdoA(2S)-GlcNS (6Sulfamate)		- HSulf-2	- 39.8±18.3μM	(Kennett et al., 2023)
(IdoA(2S)-GlcNS (6Sulfamate))₁₋₂	 <p>n = 1-2</p>	- HSulf-1	- Disaccharide (20% at 0.7 mM) - Tetrasaccharide (29.6 μM)	(Chiu et al., 2020)
IdoA2S-GlcNS (6Sulfamate)-IdoA2S			- Trisaccharide (0.53 μM)	
HfFucCS	 <p>R₂=SO₃⁻, R₃=H (45%); R₂=H, R₃=SO₃⁻ (35%); R₂=R₃=H (20%); and R₄=R₆=SO₃⁻ as the major form.</p>	- HSulf-2	- 0.14-0.18 ng /ng	(Mukherjee et al., 2023)

8.2.2 Non-competitive inhibitors:

Galectin-3-binding protein (LG3BP) was recently identified as a highly specific binding partner of HSulf-2 in head and neck squamous cell carcinoma (HNSCC) cell lines. The interaction between LG3BP and HSulf-2 was validated *in vitro* using various methods, including monoclonal antibody affinity purification, reciprocal co-immunoprecipitation with both native and recombinant proteins, and mass spectrometry analysis. These techniques provided strong evidence of their direct interaction in cell culture and purified protein systems. The chondroitin sulfate (CS) chain on HSulf-2 was found to affect this interaction, with a significant increase in binding observed after treatment with chondroitinase ABC. Importantly, LG3BP showed significant inhibition of HSulf-2 activity *in vitro* in a concentration-dependent manner, with an IC₅₀ value of 4.3 µg/mL, as determined using a synthetic 2S2-6S4 oligosaccharide substrate and HPLC-UV assay (Benicky et al., 2023). Based on conducted kinetics analysis, this study revealed that LG3BP acts as a non-competitive inhibitor of HSulf-2 and reported functional consequences of this interaction/inhibition. Upon the addition of LG3BP to spheroid cell culture, the invasion of HNSCC cells into Matrigel was inhibited. These findings suggest that the interaction between HSulf-2 and LG3BP may represent a novel regulatory mechanism for HSulf-2's activity in the tumor microenvironment, potentially impacting HS 6-*O*-sulfation editing (Figure 11). Further evaluation of this regulatory interaction in physiological and pathological conditions was warranted to fully understand its implications for HSulf-2 function and potential therapeutic interventions (Panigrahi et al., 2024).

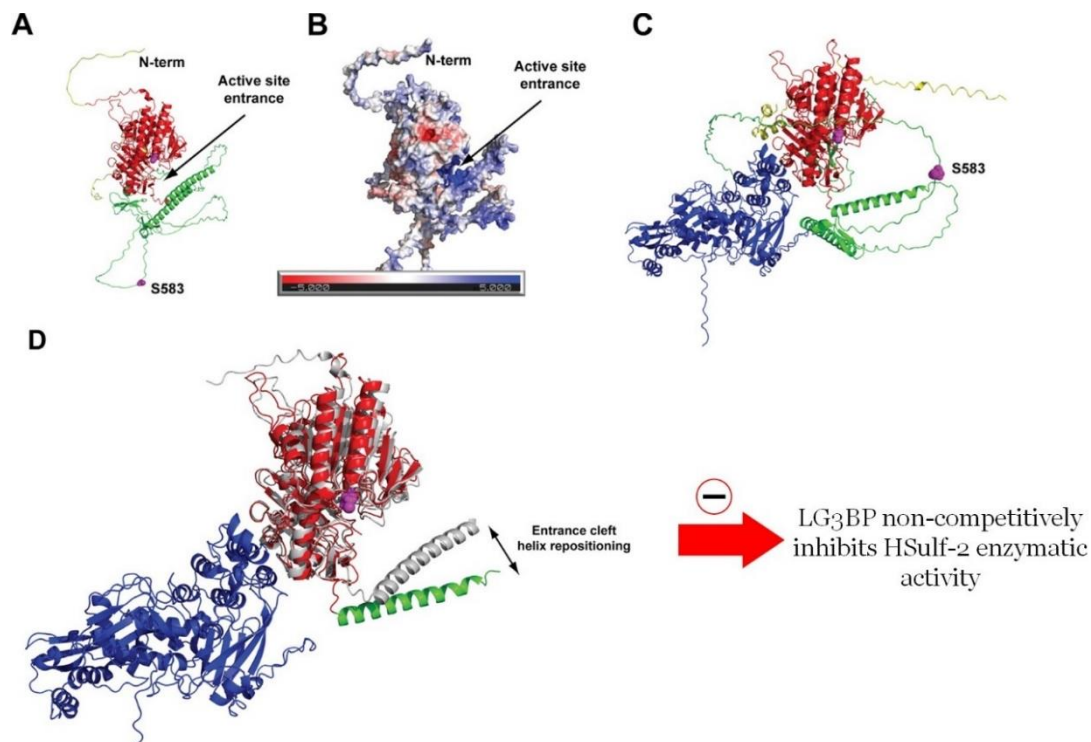


Figure 11: AlphaFold model of HSulf-2 and HSulf-2/LG3BP complex and its impact on HSulf-2 activity. A, HSulf-2 structure with catalytic core (red), hydrophilic domain (green), N/C-termini (yellow), and active site Cys88 and Ser583 (magenta). B, HSulf-2 electrostatic surface with positively charged active-site entrance (arrow). C, HSulf-2/LG3BP complex with LG3BP (blue) and HSulf-2 (colored as in A). D, overlay of HSulf-2/LG3BP complex (colored) and free HSulf-2 (grey), showing repositioning of entrance cleft helix (684–716) upon LG3BP binding, remodeling active-site entrance. Updated from (Panigrahi et al.2024).

8.3 Innovative approaches and future directions

Since their development in 1975, monoclonal antibodies (mAbs) have been sought for therapeutic applications in the treatment of various diseases, including cancer (Berger et al. 2002). The development of monoclonal antibodies targeting HSulfs, particularly HSulf-2, has shown promise not only as a diagnostic and prognostic tool but also as a potential therapeutic strategy. Primarily developed for immunoassays, these antibodies provide a foundation for identifying specific epitopes and potentially creating tumorigenic-perturbing agents.

In 2015, Singer et al. developed a novel sandwich ELISA for HSulf-2 detection using two highly specific monoclonal antibodies (5D5 and 8G1), which demonstrated high specificity for HSulf-2 without cross-reactivity to HSulf-1 (Mark S. Singer et al., 2015). The developed assay allowed the quantification of HSulf-2 in plasma and serum, highlighting the relevance of HSulf-2 mAbs as a diagnostic tool to detect blood levels of HSulf-2. Such developments not only enhance the ability to assess HSulfs' pathophysiological implications but also lay the groundwork for potential epitope-based targeting strategies for their regulation and inhibition. The therapeutic potential of targeting HSulf-2 using monoclonal antibodies was further demonstrated by Luo et al. in cholangiocarcinoma (CCA). The 5D5 HSulf-2-specific monoclonal antibody proved efficacy in

targeting HSulf-2 in the tumor microenvironment of a CCA xenograft model (Luo et al., 2021). The study revealed that upregulation of HSulf-2 in CCA leads to increased activity of a novel signaling HSulf-2-PDGFR β -YAP pathway that was identified to promote tumor growth and chemotherapy resistance. Importantly, the 5D5 mAb effectively inhibited PDGFR β -YAP signaling and suppressed tumor growth *in vivo* by neutralizing HSulf-2's action (Figure 12). These findings not only elucidated the mechanism of HSulf-2's involvement in CCA progression but also demonstrated the potential of epitope-based targeting for HSulf-2 inhibition in a cancer-related pathway.

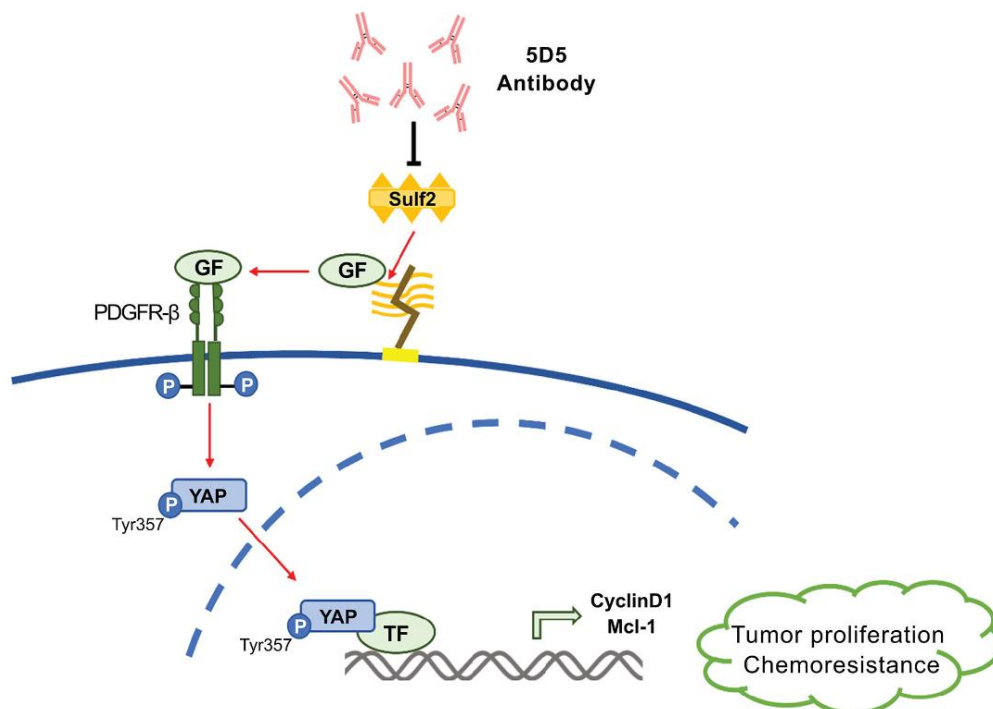


Figure 12: Proposed model for the impact of HSulf-2 monoclonal antibody 5D5 on the inhibition of the PDGFR β -YAP signaling pathway and CCA growth. Updated from (Luo et al., 2021).

Leveraging insights from the efficacy of epitope-based targeting inhibition and regulation strategies, future research could focus on developing highly specific inhibitors targeting the unique hydrophilic domain (HD) of HSulf-1 and HSulf-2. One way could be to develop HD-specific mAbs, which would lay a playground for HD implications in disease- and cancer-related pathways. The epitope information from these antibodies could further guide the design of small molecule inhibitors or peptide mimetics specifically targeting the HD domain, potentially leading to a new class of HSulf inhibitors with improved efficacy and reduced side effects. Another potential strategy would be targeting the CS/DS chain tethered to HSulf-2. As demonstrated by recent research, this PTM seems to impact the activity of HSulf-2 significantly (Seffouh et al., 2023; Panigrahi et al., 2024). Building upon this and on the fact that hyaluronidase, an enzyme that could

remove the CS chain within the tumoral microenvironment, has been linked to cancer progression and metastasis in various cancers (McAtee et al., 2014), targeting hyaluronidase could be a novel strategy for HSulf-2 regulation. Targeting hyaluronidase can indirectly down-regulate HSulf-2 activity and its interaction with LG3BP, ultimately reducing HSulf-2's pro-malignant effects.

9 Current understanding and structural challenges

HSulf-1 and HSulf-2 present a fascinating dichotomy of similarity and discrepancies. Their complex physiological and pathological implications have made them attractive yet puzzling study subjects. The scope of HSulf research is vast, spanning medical, biological, structural, and analytical fields, illustrating how it is challenging to grasp in its entirety. Two decades of dedicated research attempted to decipher the intricate mechanisms and functions of these unique enzymes. However, their complexity has often eluded precise categorization. While a global understanding of HSulfs is emerging, progress has been hindered by a significant missing piece: the lack of high-resolution 3D structures. The lack of high-resolution structural information limits our understanding of how they act at the molecular level and hinders the development of specific therapeutic strategies for HSulf-associated diseases.

Over the past decade, several studies and PhD projects have attempted to tackle the structural characterization of HSulfs, particularly HSulf-2, using various techniques such as small-angle X-ray scattering, mass spectrometry, NMR spectroscopy, crystallization, and cryo-EM. Despite these efforts, a high-resolution 3D structure of HSulfs remains elusive, primarily due to the protein's intrinsic flexibility and complex post-translational modifications. To date only Six of the seventeen human sulfatases, including Arylsulfatases A, B, and C (Ghosh, 2005), Iduronate-2-sulfatase (IDS) (Demydchuk et al., 2017), N-acetylgalactosamine-6-sulfatase (GALNS) (Rivera-Colón et al., 2012), and N-sulfoglucosamine sulfohydrolase (SGSH) (Sidhu et al., 2014), have been structurally characterized by X-ray crystallography. These enzymes share a conserved globular α/β sandwich structure with highly superimposable active site residues, suggesting a common catalytic mechanism for sulfate removal. The catalytic domains of HSulfs are hypothesized to exhibit structural homology with crystallized sulfatases based on sequence analysis and functional similarities. However, the unique features of HSulfs, particularly their hydrophilic domains and complex post-translational modifications, set them apart. Consequently, we still lack HSulf-specific molecular information that could provide a detailed understanding of their catalytic mechanisms and substrate interactions.

In the lack of experimentally determined high-resolution structures, advancements in structural

prediction, primarily through AlphaFold, have yielded valuable insights into HSulf structures (Figure 13). AlphaFold generates structural predictions by combining evolutionary information from multiple sequence alignments with physical constraints, iteratively refining models using experimental electron density maps (Jumper et al., 2021; Terwilliger et al., 2023). For both HSulf-1 (AF-Q8IWU5-F1) and HSulf-2 (AF-Q8IWU6-F1), the catalytic domains were modeled using bacterial sulfatases as templates: primarily Acetylglucosamine-6-sulfatase from *Bacteroides uniformis* (PDB IDs: 7lj2_A_1 and 7lha_A_1) and N-sulphoglucosamine sulfohydrolase from *Akkermansia muciniphila*. (PDB ID: 7ebp_A_1). These bacterial sulfatases share relatively low sequence identity (21-23%) with HSulfs but provided structural templates with high confidence (E-values in the 10^{-23} range) and good resolution (1.80-2.40 Å), suggesting conservation of the core catalytic domain architecture despite significant sequence divergence. The divergence primarily stems from the uniqueness of the HD domain, for which no homologous structures exist in current databases. Therefore, while AlphaFold provides a valuable starting point, resolving the actual three-dimensional structures of HSulfs through experimental methods remains a key priority to fully understanding their specific structural features and functional mechanisms.

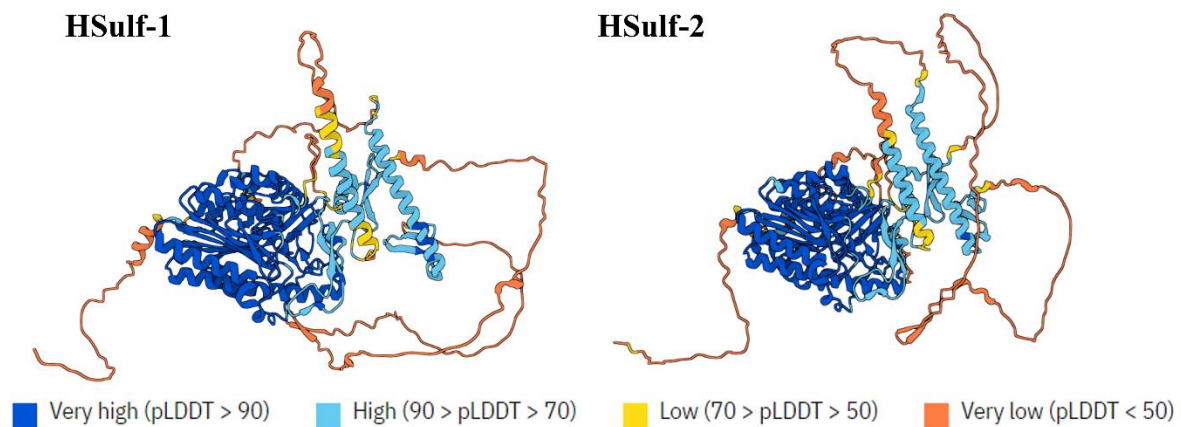


Figure 13: Predicted structure of HSulf-1 (AF-Q8IWU6-F1-v4) and HSulf-2 (model version AF-Q8IWU5-F1-v4) generated using AlphaFold2 (Jumper et al., 2021). Color code indicates prediction confidence: dark blue (very high), light blue (high), yellow (low), and orange (very low). Orange regions indicate areas of uncertainty or potential flexibility. Regions with pLDDT below 50 may be unstructured in isolation or highly flexible.

Aims of PhD

Heparan sulfate (HS) is a sulfated polysaccharide involved in various cellular processes through interactions with various protein effectors controlled by saccharide domains with rich sulfation patterns. Heparan sulfate is one of the few cellular components that cells use outside their compartments to serve as their instrument — but sometimes also their Trojan horse — and their communication tool with the extracellular environment. This external tool must be constantly remodeled to adjust its “sulfate code”, according to the cell’s needs. This task is delegated to the human endosulfatases, HSulfs, unique sulfatases in every respect, and the only ones that act outside the cell. The human endosulfatases HSulf-1 and HSulf-2 play a crucial role in numerous physiological and pathological processes through their ability to remodel heparan sulfate (HS). These unique endosulfatases act regioselectively to remove 6-*O*-sulfate groups from the functional domains of HS, thus altering ligand binding properties and modulating signaling pathways. Despite extensive research on HSulfs over the past two decades, many aspects of their structure and function remain unclear. This knowledge gap stems from two main challenges: (1) unique structural characteristics that hinder the determination of their three-dimensional structure and (2) the complexity of their HS substrates, which complicates the analytical characterization of their function in relation to their structure.

Moreover, several studies have produced conflicting results, showing similar enzymatic activities *in vitro* but revealing redundant, overlapping, or opposing functions *in vivo*. Depending on the biological context, HSulfs often display form-dependent discrepancies. These divergent activities are particularly evident in cancer research, where HSulf-1 generally exhibits anti-oncogenic properties, while HSulf-2 is often linked to pro-oncogenic effects. Therefore, ongoing research aims to identify the reasons behind this intriguing difference between the two HSulf forms.

Considering these analytical difficulties and conflicting aspects, my PhD project aimed to comprehensively characterize the structural and functional properties of HSulf-1 and HSulf-2, trying to present a link between the unique structural characteristics revealed so far and their functional impact on these unique endosulfatases. To this end, we have focused our study on three aspects:

1. Investigating the structural elements influencing HSulf-2 oligomerization, with particular emphasis on two key features: the recently discovered CS/DS GAG chain and the hydrophilic domain (HD). While previous studies had identified key structural features and post-translational

modifications that could dictate HSulf interaction and action on natural substrates, the direct impact of these elements on HSulf native conformation remained poorly understood. To address this, we focused on the molecular determinants of HSulf native conformation by characterizing the impact of post-translational modifications and domain structure on the oligomerization state.

2. Understanding the functional characteristics of HSulf endosulfatase activity, particularly the preferences for such sulfated oligosaccharide substrate and structure-function relationships. We developed a novel endosulfatase assay to assess HSulfs' reactivity towards specific oligosaccharide sequences, enhancing our understanding of their specificity for structural variations in HS polysaccharides. Leveraging this approach, as well as the availability of synthetic oligosaccharides, we conducted a comparative analysis of HSulf-1 and HSulf-2 to investigate potential differences in their catalytic properties and to understand the impact of specific structural features on their endosulfatase activity, primarily for the HSulf-2 paralog.

3. Finally, we investigated potential inhibitors of HSulf activity. Due to their high implication in physiopathological processes, mainly in cancer, several studies have focused on the potential of specific small molecule inhibitors as potential therapeutic tools. Sulfamate modification emerged as an effective strategy to modify natural substrate subsets and construct specific inhibitors for HSulfs. Following this rationale, we evaluated sulfamate-modified oligosaccharides as inhibitors of HSulf activity.

The following results section is divided into three chapters, each detailing one of the above-mentioned aspects of our study. We then conclude with a discussion that contextualizes our findings within the existing literature and identifies new questions arising from these advancements in the characterization of HSulf-1 and HSulf-2. By integrating our results with current knowledge, we aim to provide a comprehensive understanding of these unique enzymes and highlight areas for future investigation in this field.

**Chapter II: Characterization of the
impact of post-translational
modifications and domain structure on
HSulf oligomerization and size**

1 AFM analysis: impact of GAG chain on protein size

The discovery of a chondroitin sulfate glycosaminoglycan (GAG) chain attached to HSulf-2, leading to its reclassification as a member of the proteoglycan family, represents a significant breakthrough in HSulfs research (El Masri et al., 2022). This crucial post-translational modification contributes significantly to the enzyme's molecular weight and structure. Initial identification of this modification stemmed from unexpected observations within pioneer studies on the biochemical characterization of the enzyme (Seffouh, 2018; A. Seffouh et al., 2019). Previous studies using size exclusion chromatography coupled to multi-angle laser light scattering (SEC-MALLS) and small-angle X-ray scattering (SAXS) revealed that the GAG chain causes a substantial increase in the apparent molecular weight of HSulf-2, from 239-240 kDa for the GAG-deficient mutant to 423-700 kDa for the wild-type. Additionally, SAXS analysis suggested an elongated shape for the wild-type enzyme, with a maximum dimension (D_{max}) of 40 ± 3 nm, compared to 24 nm for the GAG-deficient mutant (El Masri et al., 2022).

To investigate the impact of the GAG chain on HSulf-2's size and structure at the single-molecule level, we used atomic force microscopy (AFM) imaging. AFM allows direct visualization of individual HSulf-2 molecules under near-physiological conditions, providing resolution at the single-molecule level. This level of detail is valuable because it can capture molecular-level heterogeneity in molecular populations that may be averaged out in bulk solution-based techniques such as SAXS (Costa et al., 2016).

We compared wild-type HSulf-2 with its GAG chain to the HSulf-2-SG mutant lacking the SG dipeptide motif essential for GAG attachment. AFM imaging was conducted in liquid (50 mM Tris buffer, 10 mM $MgCl_2$, pH 7.5) to simulate physiological conditions, using ultra-sharp tips (1 nm radius of curvature) to minimize artifacts. The AFM images, representative of numerous scans, revealed distinct characteristics for the HSulf-2 wild-type (Figure 14A) and HSulf-2-SG mutant (Figure 14B). The wild-type HSulf-2 images exhibited a greater variety in spot size and intensity, with larger and brighter spots potentially representing oligomers or small aggregates. In contrast, the HSulf-2-SG mutant images displayed a more uniform distribution of smaller particles, with fewer larger spots. This difference in size distribution and uniformity between the wild-type and mutant forms suggests potential oligomeric states of both forms of HSulf-2 under near-native conditions, with the wild-type showing a higher propensity for larger assemblies, as demonstrated below by particle size measurement.

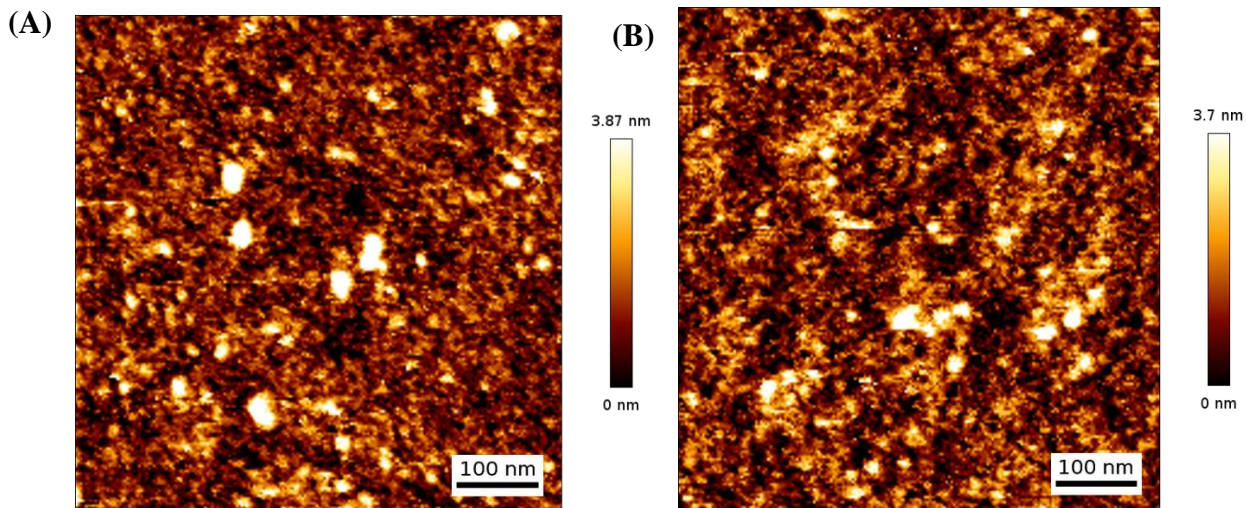


Figure 14: AFM images of HSulf-2 wild-type (A) and SG mutant (B). Scale bars: 100 nm. Height scale: 0-3.87 nm (A) and 0-3.7 nm (B).

Quantitative analysis of lateral size measurements (Figure 15) revealed an average size of 35.1 ± 10.5 nm for wild-type HSulf-2, compared to 22.9 ± 8.5 nm for the HSulf-2-SG mutant. This represents a 53% increase in average size for the wild-type enzyme, attributed to the presence of the GAG chain. Notably, both enzyme forms showed a shift towards larger sizes than their calculated averages, supporting the potential for oligomerization observed in AFM images. The size distribution histograms (Figure 15) illustrate this trend, with extended tails towards larger sizes for both wild-type HSulf-2 (blue bars) and the HSulf-2-SG mutant (red bars). The wild-type distribution extends further, up to 70 nm, while the mutant's distribution is more concentrated in the 10-40 nm range.

While the GAG chain (approximately 20-25 kDa, El Masri et al., 2022) accounts for only about 25% of HSulf-2's molecular weight, it induces a 50% increase in the enzyme's size under native conditions. This disproportionate impact highlights the significant impact of the GAG chain on HSulf-2's hydrodynamic properties.

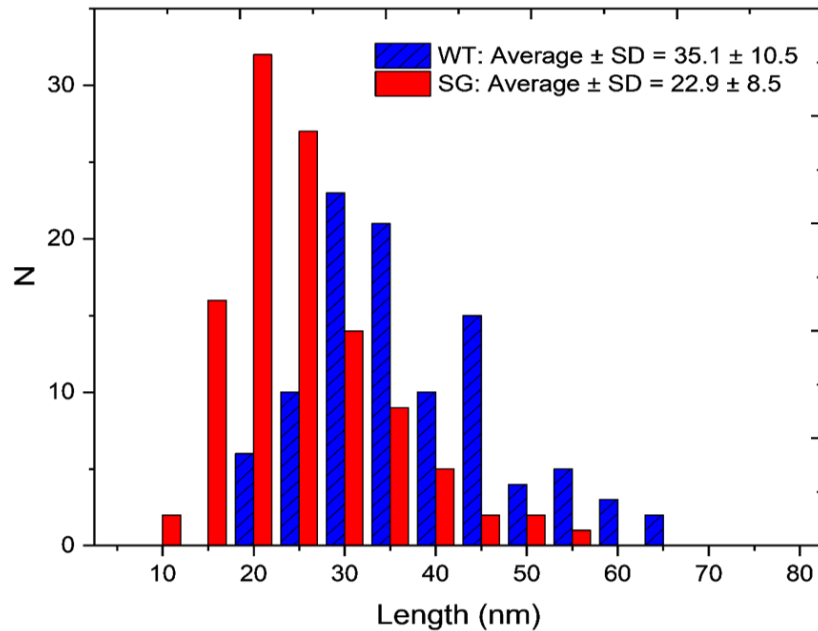


Figure 15: Histograms showing the lateral size distribution of wild-type HSulf-2 (WT, blue bars) and HSulf-2-SG mutant (SG, red bars) as measured by AFM. N represents the number of individual molecules observed at each size range.

Our AFM results corroborated previous SEC-MALLS and SAXS data, confirming that the GAG chain substantially increases HSulf-2's hydrodynamic volume. The broader size distribution observed in wild-type HSulf-2 likely reflects the heterogeneity and polydispersity introduced by the GAG chain. Collectively, these findings provide compelling evidence that the GAG chain significantly influences the hydrodynamic properties of HSulf-2, inducing a substantial increase in the overall hydrodynamic volume of the enzyme. This could account for enhancing HSulf-2's conformational flexibility and modulating its interactions within the extracellular matrix, thus influencing its distribution and activity.

2 Structural features related to the oligomerization of HSulf-2

The HSulf-2 recombinant protein used for these experiments was kindly provided by our collaborator Dr. Romain Vives from the Institut de Biologie Structurale (IBS) de Grenoble. The recombinant protein was expressed in HEK293 cells and purified according to the protocol described by Seffouh *et al.* in their work (A. Seffouh *et al.*, 2019).

The protein has a SNAP-tag at the N-terminal region and a HisTag at the C-terminal, both attached to the protein through short sequences that are cleavable by TEV protease (Figure S1 in supplementary data).

The wild-type protein is expected to have a theoretical mass of 139.9 kDa, corresponding to the whole protein (98.151 kDa), SNAP-tag (21.6 kDa), HisTag (2.2 kDa), and N-glycosylation (~18 kDa).

Table 4 : Theoretical molecular masses of HSulf-2 with SNAP/His Tags. Updated from (Bilong, 2022).

Average Mass (kDa)	Entire HSulf-2	N-terminal chain	C-terminal chain
Primary sequence without tags	98,151	59,338	38,831
Primary sequence with SNAP/HisTags	121,951	80,938	41,031

2.1 Impact of the GAG chain

Building on the observed shift towards sizes larger than the calculated averages for both enzyme forms as revealed by AFM measurements, which further supported the potential for oligomerization, we wanted to focus on the oligomerization aspects of HSulf-2 in solution.

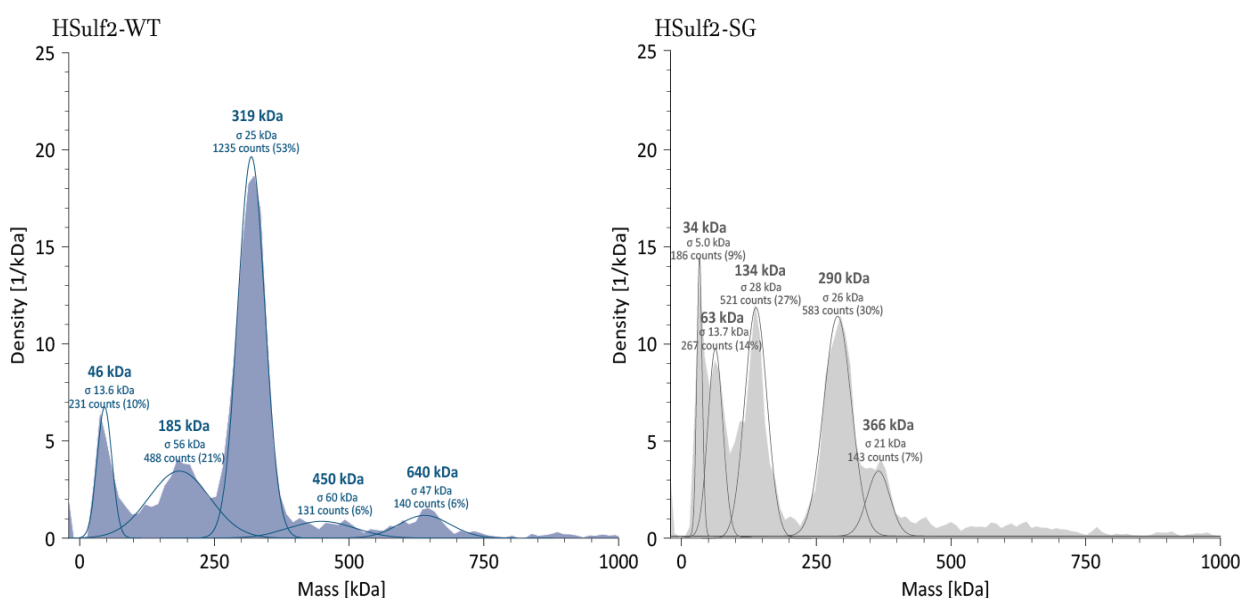


Figure 16: Mass photometry analysis of HSulf-2 wild-type (Blue) and HSulf-2-SG mutant (Grey) analyzed at 5 nM in 15 mM Tris, 2.5 mM CaCl₂, 2.5 mM MgCl₂, pH 7.5. Mass distribution profiles show the relative abundance of different molecular species for both enzyme forms. The y-axis shows the density (1/kDa) of particles detected within each mass range. Major peaks are labeled with their corresponding masses and percentage of total counts.

To this end, we employed mass photometry, a biophysical approach that enables mass estimation of proteins in their native state and provides insights into the oligomeric states of proteins in solution.

Mass photometry analysis revealed distinct oligomerization profiles for HSulf-2 wild-type and HSulf-2-SG mutant (Figure 16). The wild-type predominantly showed a major peak at 319 kDa,

likely corresponding to dimers and representing approximately 53% of the total protein population based on peak area. A smaller peak at 185 kDa, likely representing monomers, accounted for about 21% of the population, indicating a strong tendency for dimerization. In contrast, the HSulf-2-SG mutant showed a more balanced distribution between species, with peaks likely corresponding to dimers (290 kDa, ~30% of the population) and monomers (134 kDa, ~27% of the population), suggesting that the GAG chain promotes dimerization in the wild-type. Both forms exhibited lower mass species (34-63 kDa), which could represent degradation products or stable subdomains, and minor higher-order oligomers (>350 kDa). The wild-type displayed broader peaks, suggesting greater structural heterogeneity, likely due to the GAG chain. This heterogeneity may be linked to the coexistence of both GAG-free and GAG-bearing HSulf-2 forms. These results highlight the potential impact of the GAG chain on HSulf-2's oligomerization behavior and structural diversity. The data revealed two key findings: first, HSulf-2 primarily exists as a dimer in solution, aligning with previous literature (Morimoto-Tomita et al., 2002) that reported the presence of presumed SDS-resistant dimers (~250 kDa) in Western blotting analysis. Our study confirms this dimeric state under native conditions without constraints on the protein. Second, the GAG chain appears to favor dimerization, indicating its potential role in stabilizing the oligomerization state of the enzyme. However, the mutant lacking the GAG chain also showed a tendency to dimerize, albeit in a lower proportion compared to the wild type. This observation suggests that while the GAG chain promotes dimerization, it is not the sole factor responsible for this oligomeric state. To elucidate this phenomenon further, we investigated additional structural features that could contribute to the dimerization tendency of HSulf-2.

2.2 Impact of the hydrophilic domain (HD)

The recently available AlphaFold-predicted structure for HSulf-2 reveals two alpha-helical elements within the hydrophilic domain (HD) (Figure 17). The first helix spans positions 621-654, and the second helix spans positions 684-715. These helices are predicted with high confidence (pLDDT > 70) and are in close proximity, suggesting potential coiled-coil structures. Coiled coils are known to mediate protein-protein interactions and oligomerization, providing a structural basis for potential dimerization (Szczepaniak et al., 2021). Earlier studies (Morimoto-Tomita et al., 2002) identified a coiled-coil region spanning amino acid positions 623-658 within the HD of HSulf-2. To validate and correlate with the AlphaFold-predicted structure, we employed two additional prediction tools: CoCoNat (Madeo et al., 2023) and DeepCoil (Ludwiczak et al., 2019). These analyses confirmed the presence of a coiled-coil domain primarily in the first helix, with a significant probability (0.68) of forming an antiparallel dimer. While the first helix exhibits strong coiled-coil characteristics, the second helix may play structural roles related to stability or

interactions distinct from the main coiled-coil region. These computational predictions support and expand upon previous studies, highlighting the likelihood of coiled-coil-mediated protein-protein interactions, especially the formation of antiparallel dimers, within the first alpha-helical region of HSulf-2's hydrophilic domain.

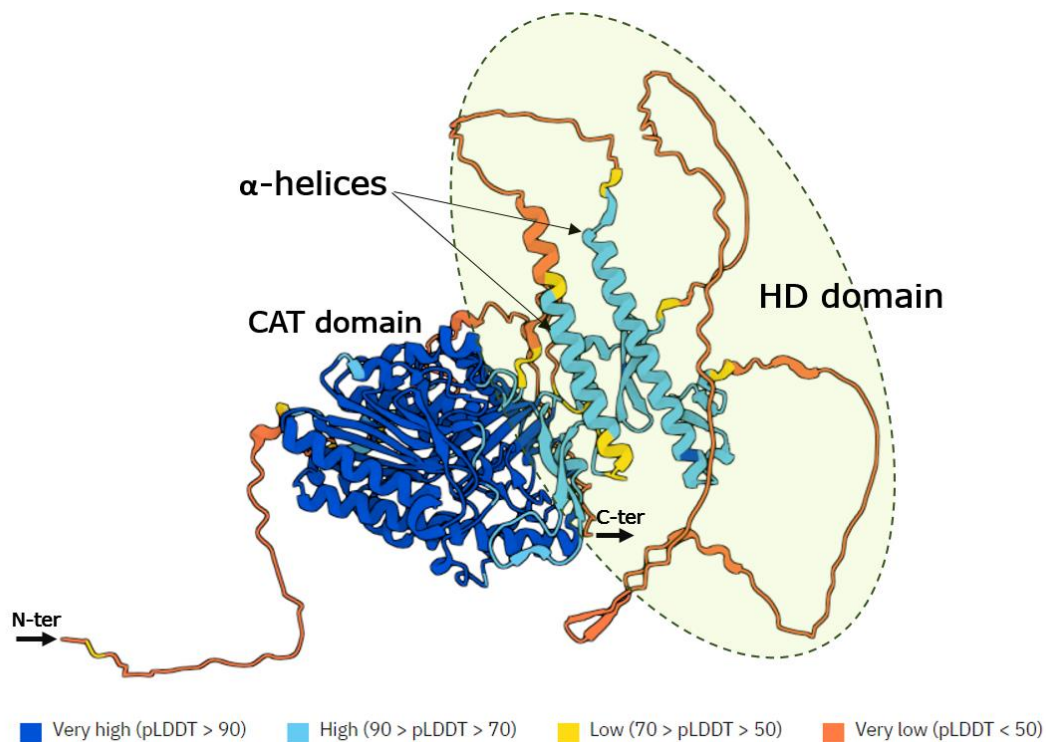


Figure 17: Predicted structure and key features of HSulf-2 based on AlphaFold2 modeling. Annotated predicted structure of HSulf-2 (UniProt ID: Q8IWU5) generated using AlphaFold2 (Jumper et al., 2021). The original AlphaFold2 prediction (model version AF-Q8IWU5-F1-v4) was obtained from the AlphaFold Protein Structure Database (Varadi et al., 2024). Color code indicates prediction confidence: dark blue (very high), light blue (high), yellow (low), and orange (very low). The hydrophilic domain (HD) is highlighted with a green dashed outline, with prominent alpha-helices labeled. The catalytic domain and a major part of the C-terminal domain are represented with high confidence (dark blue) due to sequence homology with human lysosomal glucosamine-6-sulfatase (HG6S). This model represents HSulf-2 without furin cleavage and, therefore, lacks the disulfide bridges linking the N-terminal and C-terminal regions. Arrows, circles, and annotations have been added to highlight specific regions of interest and structural features.

Given this structural prediction and the observed dimerization tendency of HSulf-2, even in the absence of the GAG chain, we decided to investigate the potential of the isolated HD domain to dimerize. Our aim was to determine whether the HD domain itself, independent of the GAG chain, could contribute to the oligomerization behavior of HSulf-2. The isolated HD domain (Theoretical pI/Mw: 9.67 / 35500.65) was expressed and purified by Clément Demongin in our laboratory using an *E. coli* bacterial system. It's important to note that this expression system lacks eukaryotic post-translational modifications, including furin cleavage. Consequently, the HD domain is produced as a non-cleaved form. Initial quality control analysis and sample identification using MALDI-TOF

mass spectrometry confirmed the presence of both monomeric (37.122 kDa) and dimeric (73.882 kDa) species (Figure 18).

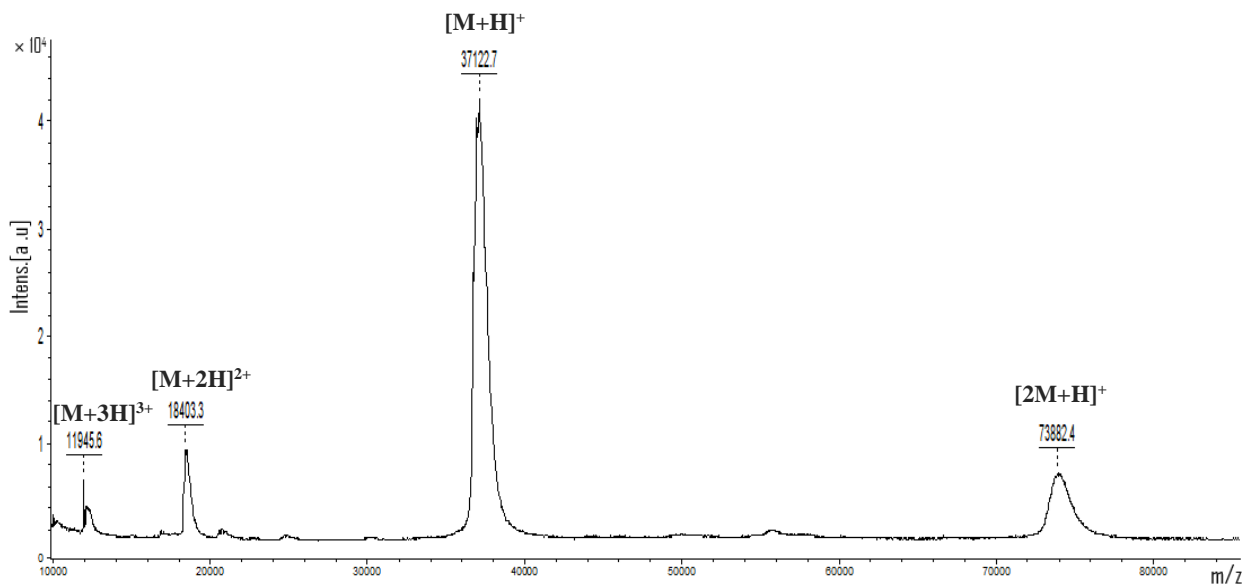


Figure 18: MALDI-TOF mass spectrum of the isolated HD domain of HSulf-2 acquired in positive linear mode. 1 μ l of the isolated HD domain (1.15 μ g) was mixed 1:1 with sinapinic acid (SA) matrix in water/acetonitrile/trifluoroacetic acid (50%/50%/0.1%). The spectrum shows multiple peaks: a dominant peak at m/z 37122.7, corresponding to the monomeric HD domain $[M+H]^+$ or a doubly charged dimer $[M+2H]^{2+}$, a peak at m/z 73882.4, representing the dimeric form $[2M+H]^+$. Additional peaks at m/z 18403.3 and 11945.6 may correspond to the monomer in doubly $[M+2H]^{2+}$ and triply $[M+3H]^{3+}$ charged states, respectively.

To characterize the oligomerization state of the HD domain under non-denaturing conditions, we performed size exclusion chromatography (SEC) analysis (Figure 19A). The SEC revealed a peak at 3.5 minutes corresponding to a species >66 kDa, which aligns with the expected dimeric form of the HD domain at 74 kDa. This suggested that the isolated HD domain has a tendency to form dimers in native conditions. In addition to SEC analysis and to further investigate its oligomerization behavior, we employed mass photometry (MP) which allowed us to quantify the distribution of different oligomeric species at various protein concentrations under near-native conditions (Figure 19B). The results showed the presence of both monomeric (39-55 kDa) and dimeric (66-88 kDa) forms of the HD domain. As the concentration increased from 5 nM to 50 nM, we observed a clear shift from predominantly monomeric species to dimeric species. This concentration-dependent shift towards dimeric species provided strong evidence for the HD domain's tendency to dimerize as protein concentration increases in solution.

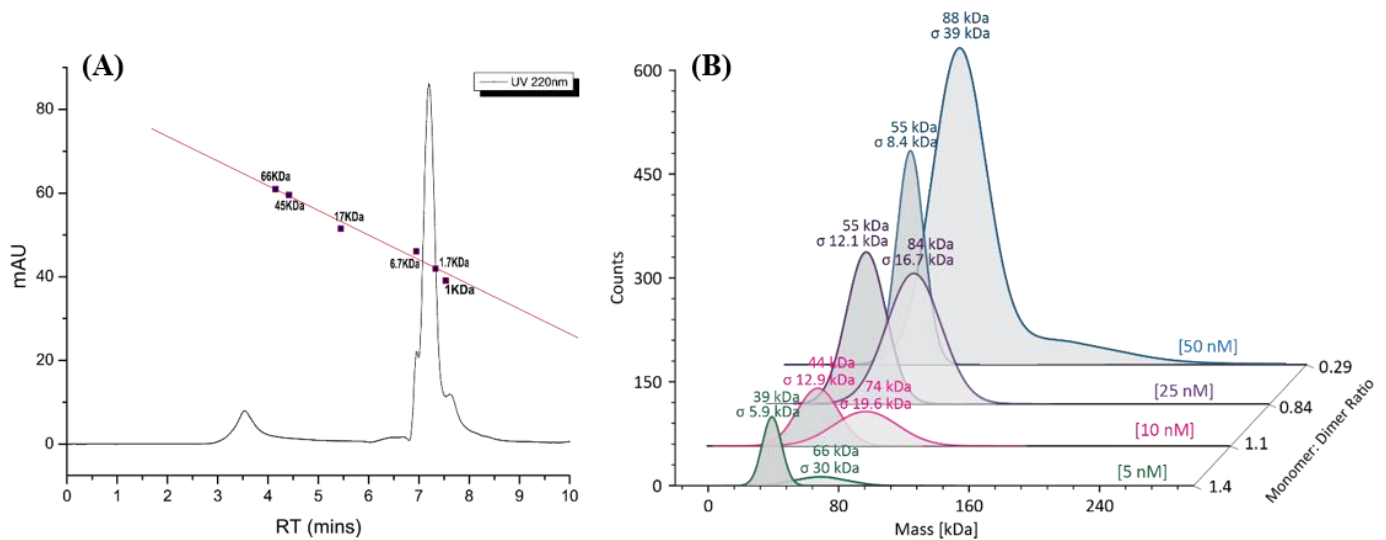


Figure 19: Analysis of the HD domain under native conditions. (A) Size exclusion chromatography (SEC) profile of the HD domain (5 μ g injected onto an AdvanceBio SEC 120Å column with a molecular weight range of 1,000 to 80,000 Da). The main peak at approximately 3.5 minutes corresponds to the HD domain. The larger peak at around 7.5 minutes is attributed to salts in the buffer composition, as verified by a blank buffer injection (150 mM sodium phosphate buffer, pH 7). (B) Mass photometry (MP) analysis of the HD domain at different concentrations (5 nM, 10 nM, 25 nM, and 50 nM) in 50 mM HEPES, 30 mM NaCl, pH 7. A different color represents each concentration. The monomer: dimer ratio for each concentration is indicated on the right side of the graph.

These results supported our initial hypothesis regarding the dimerization potential of the hydrophilic domain, demonstrating that the HD domain had an intrinsic tendency to dimerize, even when expressed in a bacterial system, where post-translational modifications such as glycosylation or furin cleavage do not occur. This confirmed that the HD domain could self-associate independently of the GAG chain present in full-length HSulf-2. Given these findings, we concluded that the HD domain likely serves as the primary driving force behind the dimerization process of HSulf-2. To further elucidate this mechanism, we next focused on characterizing specific mutations within the HD domain to identify regions critical for oligomerization.

2.3 Impact of mutations within the hydrophilic domain (HD)

Building on our findings with the isolated HD domain, we next examined several HSulf-2 mutants to further elucidate the specific regions within the HD domain that are critical for oligomerization (Figure S1). These mutants, generously provided by our collaborators at the Institute of Structural Biology, Grenoble, were initially designed for structural studies using cryo-electron microscopy (cryo-EM). We recognized their potential to offer valuable insights into the oligomerization behavior of HSulf-2. The first mutant we analyzed, HSulf-2-HDC, was a deletion variant lacking the central region of the HD domain (17 kDa) between residues D507 and C660 (Figure 20). This deleted segment comprised the unstructured region and one of the alpha helices. To maintain the

overall structure of the enzyme, this region was replaced with an SGSGGS linker, connecting the remaining parts of the HD domain and resulting in a full-length single-chain protein.

The two other mutants had more targeted modifications within the HD domain (Figure 20). HSulf-

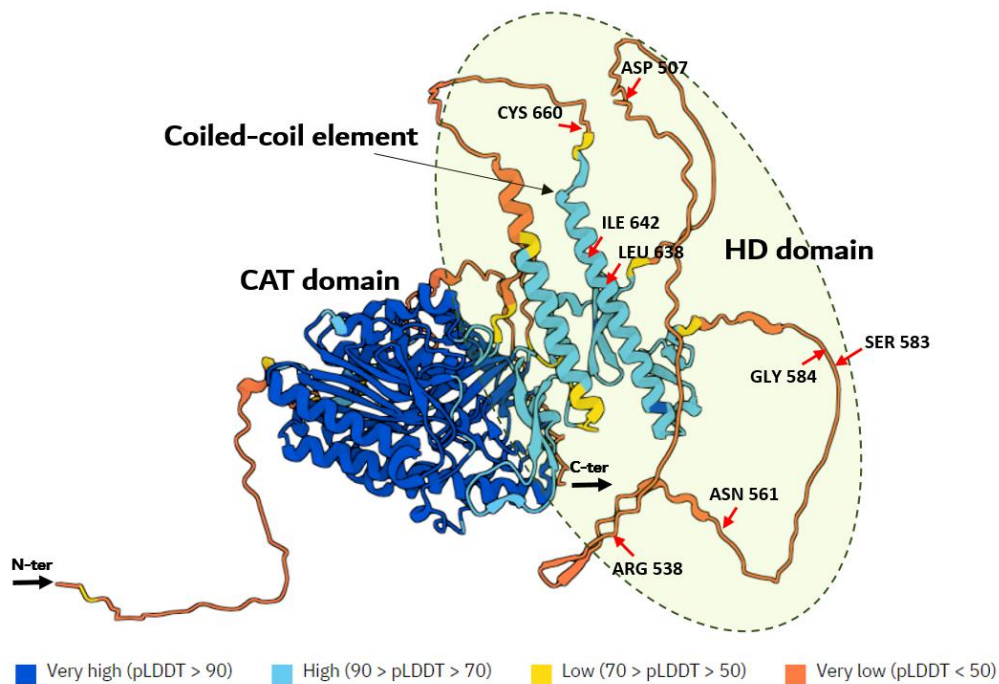


Figure 20: AlphaFold2 predicted structure of HSulf-2 (Jumper et al., 2021), highlighting domains and mutation sites. The hydrophilic domain (HD, green outline) contains the coiled-coil element where LEU638 and ILE642 are targeted in the DelC mutant. ASN561 is the site of the N561Q mutation. The region between ASP507 and CYS660 defines the truncated area in the HDC mutant. ARG538 indicates the furin cleavage site, and SER583-GLY584 marks the GAG attachment site. N-ter and C-ter denote protein termini.

2-DelC involved substituting two residues within the alpha helix of dimerization, specifically leucine 638 and isoleucine 642, with tryptophan. These mutations were strategically designed to introduce steric hindrance, potentially disrupting dimerization without compromising the overall helix organization. HSulf-2-N561Q featured a single amino acid substitution, changing an asparagine residue to glutamine at position 561, which is a site for N-glycosylation (Seffouh et al., 2023). To investigate how these mutations affect HSulf-2's oligomerization behavior, we compared these mutants to the wild-type HSulf-2 using mass photometry analysis (Figure 21).

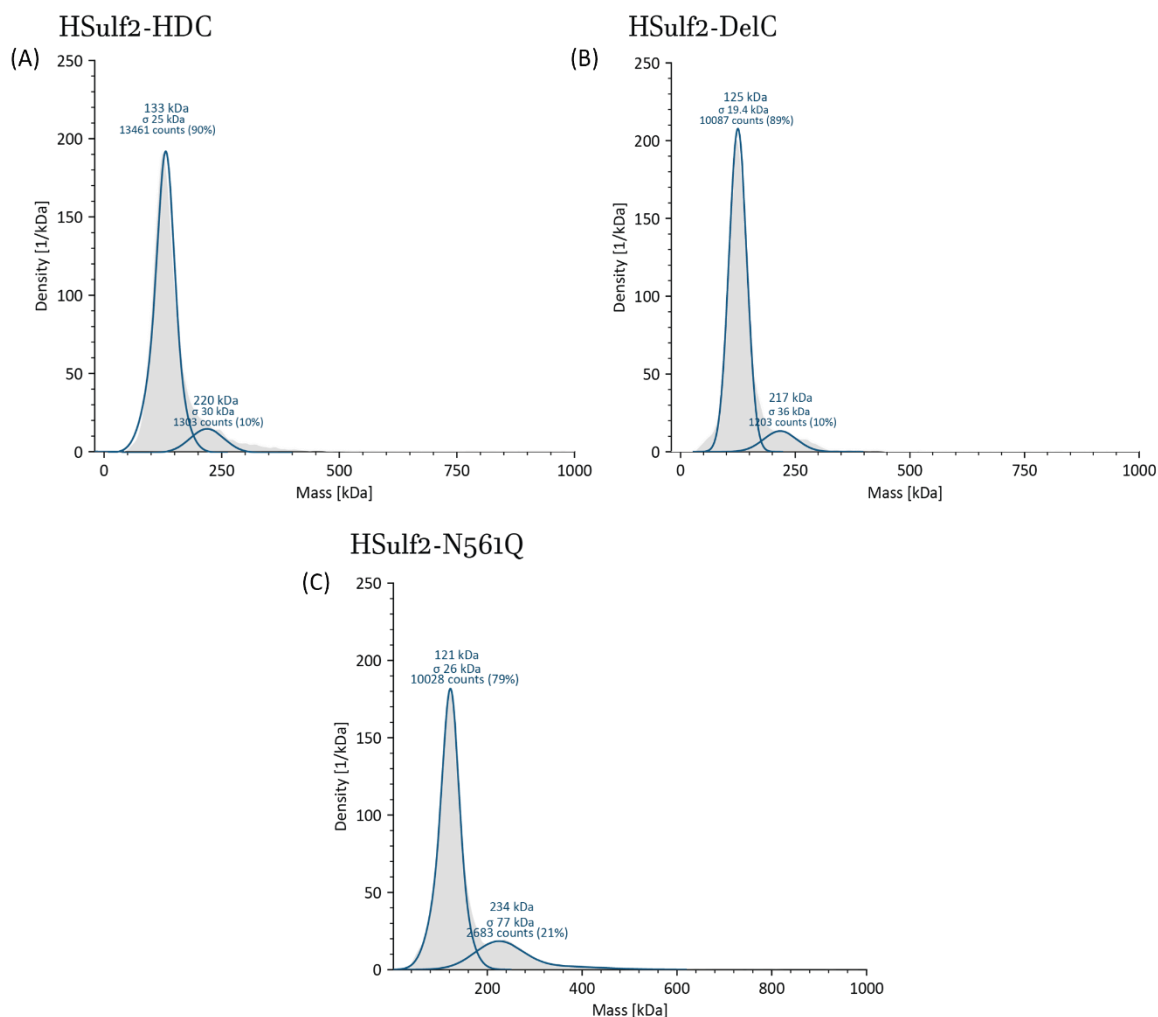


Figure 21: Mass photometry analysis of HSulf-2 variants. (A) HSulf-2-HDC, (B) HSulf-2-DelC, and (C) HSulf-2-N561Q were analyzed at 5 nM in 15 mM Tris, 2.5 mM CaCl₂, 2.5 mM MgCl₂, pH 7.5. Mass distribution profiles show relative abundance of molecular species. Y-axis: particle density (1/KDa). Major peaks, corresponding to monomers for all three variants, are labeled with masses and percentage of total counts.

As expected for HSulf-2-HDC (Figure 21A), the deletion mutation within the central region of the HD domain, which included the coiled-coil element, induced a significant monomeric tendency. Approximately 90% of the total counts consisted of monomers (133 kDa), with only a minor dimeric proportion (10% at 220 kDa). This result strongly supported the critical role of the deleted region in promoting dimerization. When we examined the HSulf-2-DelC mutant (Figure 21B), where leucine and isoleucine residues were substituted with tryptophan, we noted similar effects to the HDC mutant, with 89% of the total counts corresponding to monomeric species (125 kDa) and 10% dimeric species (217 kDa). This further highlighted the importance of these specific amino acids within the coiled-coil element for maintaining the enzyme's dimerization capacity. Interestingly, we observed that the point mutation of asparagine 561 to glutamine in HSulf-2-N561Q induced effects similar to HSulf-2-HDC and HSulf-2-DelC (Figure 21C). This unexpected result suggested that this single N-glycosylation site played a crucial role in the enzyme's

oligomerization, potentially as important as the structural elements such as the alpha helix, which highlighted the complex interplay of structural elements and post-translational modifications in HSulf-2's oligomerization.

These observations for the DelC and N561Q mutants were consistent across two independent enzyme preparations, confirming their reliability. However, given the unexpected results, particularly with the N561Q point mutation, we sought to verify whether these mutations could have caused any loss or alterations within the HD sequence. To investigate this, we performed tryptic digestion followed by Nano-Liquid Chromatography-Mass Spectrometry (Nano-LC-MSe) to assess the sequence coverage of these constructs (Table 5), with a specific focus on the HD domain. This analysis aimed to confirm that the observed effects were indeed due to the intended mutations and not because of any unintended sequence alterations or truncations.

Table 5: Sequence coverage analysis of HSulf-2 wild-type and mutant constructs. The table presents the percentage of sequence coverage for both the full-length protein and the HD domain in HSulf-2-WT, HSulf-2-DelC, and HSulf-2-N561Q constructs. Each construct (3 µg) underwent tryptic digestion at a trypsin-to-protein ratio of approximately 1:7.5. Protein sequencing was conducted using Byonic v5.3.5 (Protein Metrics). The data shown are averages derived from three independent replicates.

	HSulf2-WT			HSulf2-DelC			HSulf2-N561Q		
	1	2	3	1	2	3	1	2	3
Full length sequence coverage %	86.87%	86.28%	86.17%	84.98%	87.7%	89.59%	80.14%	82.86%	83.92%
Average	86.44%			87.42%			82.3%		
HD domain coverage %	80%	82.71%	78.98%	78.3%	77.63%	80.67%	55.25%	64%	62%
Average	80.56%			78.86%			60.42%		

The sequence coverage analysis revealed high overall coverage for all three HSulf-2 variants (WT, DelC, and N561Q), with full-length sequence coverage averaging over 82% for each construct (Table 1). Specifically, for the HD domain, both the wild-type and DelC mutant showed similar coverage at around 80%. In contrast, the N561Q mutant had a lower coverage of about 60%. Although there was no significant sequence loss, the N561Q mutation likely affected the accessibility of adjacent peptides within the HD domain, reducing their detectability during the analysis.

To further characterize the structural integrity and oligomeric state of the HSulf-2 wild-type and mutant proteins, we conducted SDS-PAGE analysis under both reducing and non-reducing conditions (Figure 22A). This approach allowed us to compare the protein profiles in the presence and absence of disulfide bonds to further understand the impact of these mutations on the structure and oligomeric state and to identify any potential changes in protein stability. Noteworthy, as mentioned in the introduction section (Page 14), HSulf-2 contains six disulfide bridges: four intra-chain bridges within the hydrophilic domain (HD) and two inter-chain bridges connecting the C-terminal and N-terminal chains (Bilong, 2022).

SDS-PAGE analysis of HSulf-2-WT and its mutants revealed distinct profiles under both reducing and non-reducing conditions. In non-reducing conditions, HSulf-2-WT showed a broad band around 250 kDa, likely representing the dimer. This band appeared with low intensity, possibly due to the GAG chain affecting protein staining efficiency. Additionally, a band just above 130 kDa was observed, which might correspond to the monomer (N-terminal and C-terminal chains linked by disulfide bonds) with PTMs. A band at 40-50 kDa indicated the presence of some GAG-free HSulf-2.

Under reducing conditions, HSulf-2-WT exhibited three distinct bands: an intense band at 95 kDa (N-terminal chain with SNAP-tag), a lighter band at 75 kDa (likely N-terminal chain without tag), and a band at 50 kDa (C-terminal chain). The prominent 95 kDa band suggests a predominance of GAG-modified HSulf-2. Typically, we would expect the 50 kDa band, representing the C-terminal chain, to intensify under reducing conditions. However, its intensity remained similar to that observed in non-reducing conditions. This unexpected result likely stems from GAG chain interference with Coomassie staining in the glycosylated population, masking the true abundance of the C-terminal fragment.

In contrast, both HSulf-2-N561Q and HSulf-2-DelC mutants displayed similar profiles in both reducing and non-reducing conditions. We observed an intermediate band around 100-130 kDa in non-reducing conditions, corresponding to the monomer as observed in mass photometry. Notably, the band corresponding to the monomeric species of the wild type (>130 kDa) showed a clear shift compared to the mutants, suggesting the absence of the glycosaminoglycan (GAG) chain in the N561Q and DelC mutant forms. Multiple bands below 50 kDa were also present in both conditions for the mutants.

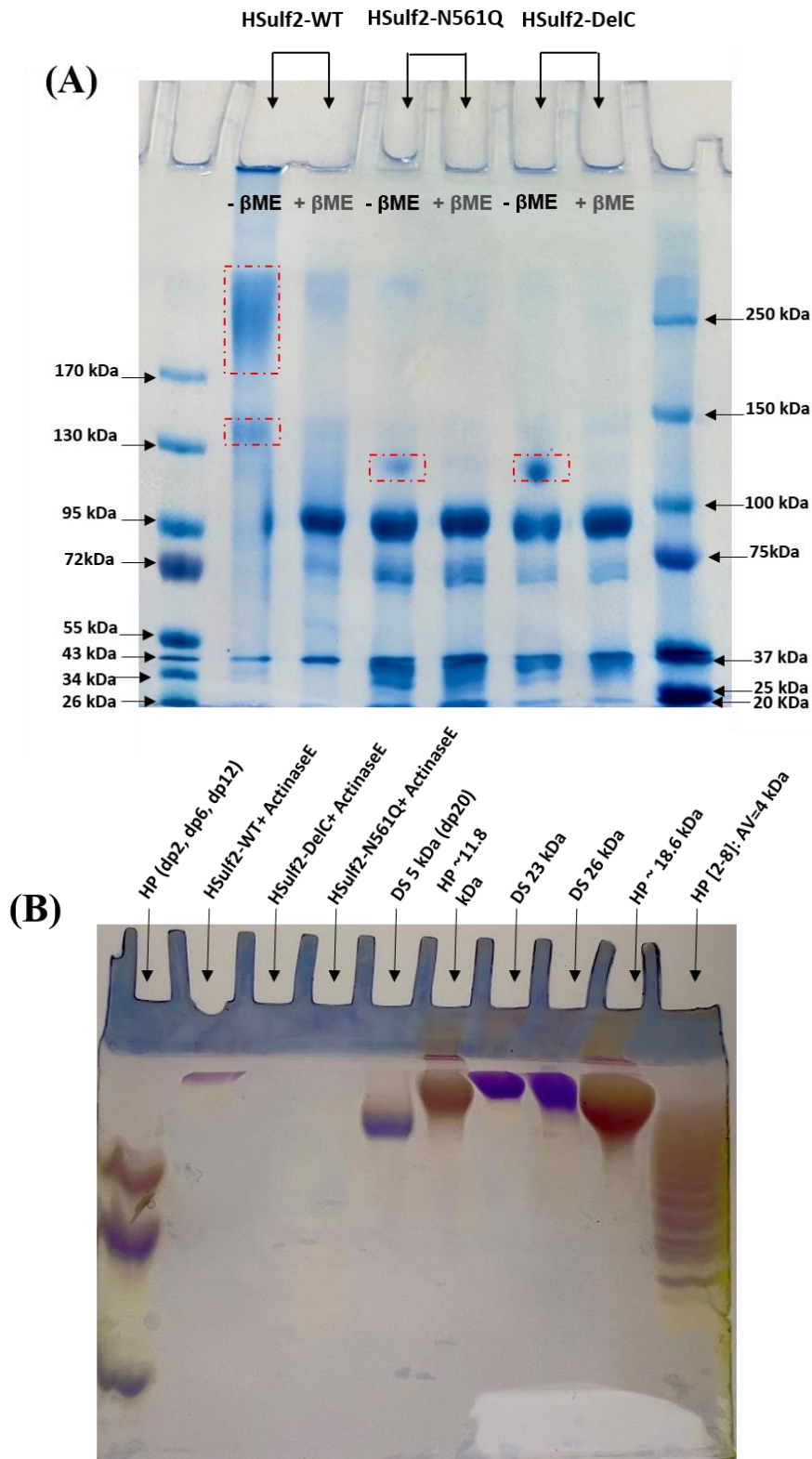


Figure 22: Electrophoretic analysis of HSulf-2 variants. (A) SDS-PAGE analysis (10% acrylamide) of HSulf-2-WT, DelC, and N561Q (3 μ g each) under reducing conditions with β -mercaptoethanol (+ β -ME) and non-reducing conditions without β -mercaptoethanol (- β -ME), revealed by Coomassie Blue staining. Molecular weight markers are indicated by black arrows. Red dashed boxes highlight monomer species for each enzyme form. (B) C-PAGE analysis (27% acrylamide) of HSulf-2-WT, DelC, and N561Q (3 μ g each), revealed by Stains-All staining. Black arrows indicate molecular weight markers of heparin and dermatan sulfate.

The similarity between reducing and non-reducing conditions for these mutants suggested that the mutations had disrupted the disulfide bond formation. The absence of higher molecular weight bands (above 170 kDa) in non-reducing conditions for both mutants, which are present in the wild-type, confirmed the low tendency to oligomerization. The presence of intense bands corresponding to the short chain (around 50 kDa) in both reducing and non-reducing conditions strongly suggested an effect on GAG modification, as the GAG chain typically causes the short chain to be undetectable in SDS-PAGE analysis.

To specifically verify the presence of the GAG post-translational modification, we performed C-PAGE electrophoresis (27%) on oligo/polysaccharides from the wild-type and both mutants after Actinase E treatment (Figure 22B). Actinase E cleaves a small peptide containing the SG motif, essential for GAG chain attachment, isolating the entire polyanionic GAG chain for detection. This method allows for the separation and visualization of the GAG chain. We observed a band around 25 kDa for the wild-type, which was absent in both mutants, indicating low or absent glycosylation for the mutants and highlighting the impact of these mutations on GAG formation.

To further investigate the GAG chain's role in HSulf-2 oligomerization, we treated the wild-type and mutants with hyaluronidase to degrade the GAG chain. Mass photometry analysis revealed significant differences in their oligomeric profiles. The wild-type HSulf-2 (Figure 23C) showed a marked shift in oligomeric distribution after hyaluronidase treatment, with a reduction in higher molecular weight species, confirming the strong relationship between the GAG chain and dimerization. In contrast, the N561Q (Figure 23A) and DelC-T (Figure 23B) mutants exhibited minimal changes in their oligomeric profiles post-treatment, supporting previous findings that these mutations disrupted GAG chain formation or attachment. The lack of significant shifts in the mutants suggested that the GAG chain was either absent or present in very low amounts. These results provided additional evidence that the N561Q and DelC mutations altered the balance of GAG formation and consequently impacted the oligomerization behavior of HSulf-2.

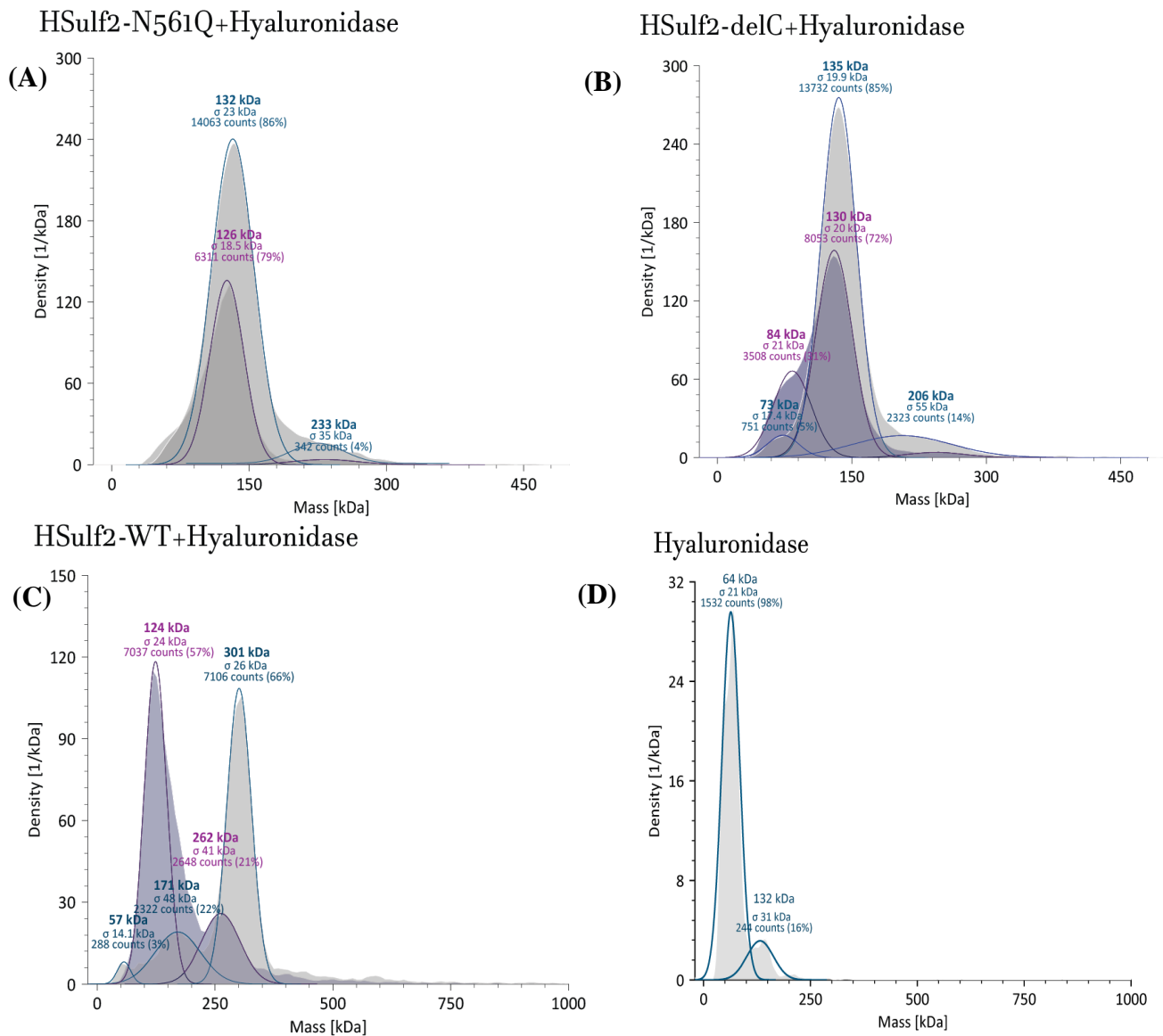


Figure 23: Mass photometry analysis of HSulf-2 wild-type and mutants (N561Q and DelC-T) with and without hyaluronidase treatment. Samples were analyzed at 50 nM in 15 mM Tris, 2.5 mM CaCl₂, 2.5 mM MgCl₂, pH 7.5. (A) HSulf-2-N561Q, (B) HSulf-2-DelC-T, (C) HSulf-2-WT, and (D) Hyaluronidase control. Untreated samples are shown in grey/blue, while hyaluronidase-treated samples are in violet.

Collectively, our investigations demonstrated that both the N-glycosylation site affected by the N561Q mutation and the region targeted by the DelC mutation play crucial roles in maintaining the proper structure, oligomerization, and post-translational modifications of HSulf-2. These mutations led to altered processing and potentially impaired GAG attachment, highlighting the importance of these regions for the enzyme's integrity and function. Furthermore, our findings reveal a synergy between the disruption of the alpha-helix structure and the perturbation of GAG formation on protein dimerization. This suggests that the GAG chain acts as a key modulator for the stability of the dimerization process, underscoring its significance in HSulf-2's overall structural integrity and functional capacity.

2.4 Oligomerization tendencies of HSulf-1 versus HSulf-2

We also tried to compare the oligomerization tendencies of the wild-type HSulf-1 and HSulf-2. Due to low expression rates encountered by our collaborator, HSulf-1 in solution form was rarely available, limiting our structural characterization analyses. We conducted mass photometry analysis of both HSulf-1 and HSulf-2 (Figure 24).

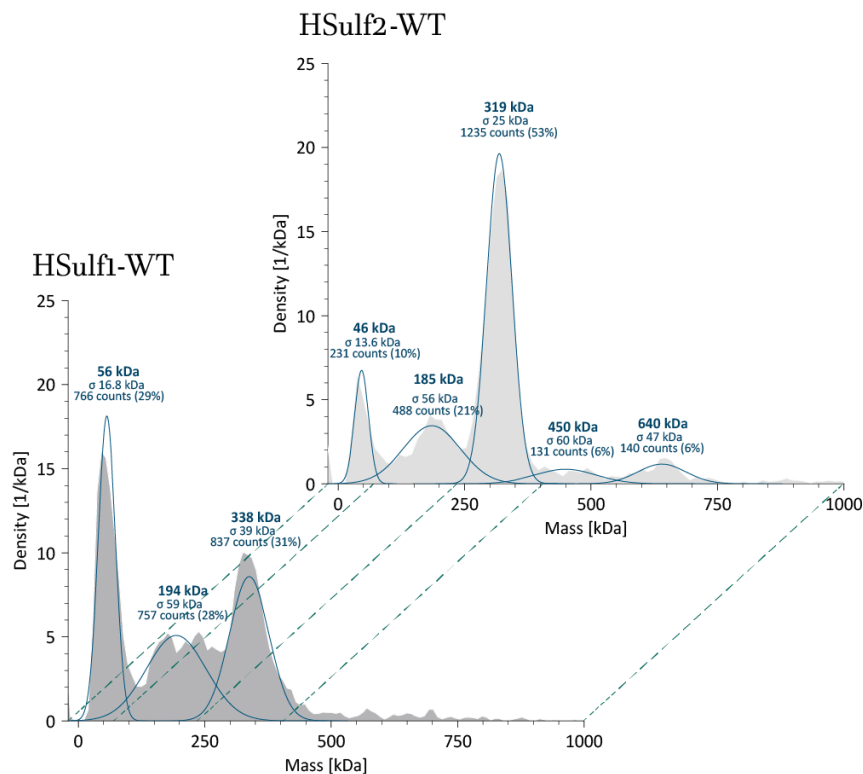


Figure 24: Mass photometry analysis of HSulf-2 wild-type (Light grey) and HSulf-1 wild-type (Grey). Samples were analyzed at 5 nM in 15 mM Tris, 2.5 mM CaCl₂, 2.5 mM MgCl₂, pH 7.5. Mass distribution profiles show the relative abundance of different molecular species for both forms of the enzyme. The y-axis shows the density (1/KDa) of particles detected within each mass range. Major peaks are labeled with their corresponding masses and percentage of total counts.

Similar oligomerization tendencies were observed for both enzymes, albeit with notable differences. HSulf-1 displayed a more balanced distribution between dimeric (338 kDa, 31%) and monomeric (194 kDa, 28%) forms. In contrast, HSulf-2 exhibited a stronger tendency to dimerize, with the dimeric form (319 kDa) accounting for 53% of the total population, while the monomeric form (185 kDa) represented 21%. HSulf-1 contains a coiled-coil region spanning amino acid positions 639–673 within its hydrophilic domain (HD), as initially reported by Morimoto-Tomita *et al.* (2002). This structural feature likely contributes to the observed dimer population in HSulf-1. However, given our findings about the GAG chain strongly modulating the dimerization process in HSulf-2 and the reported absence of this modification on HSulf-1 (El Masri *et al.*, 2022) we sought to verify the presence of this post-translational modification on HSulf-1. To examine this

variable, we conducted C-PAGE analysis for both isoforms (Figure 25).

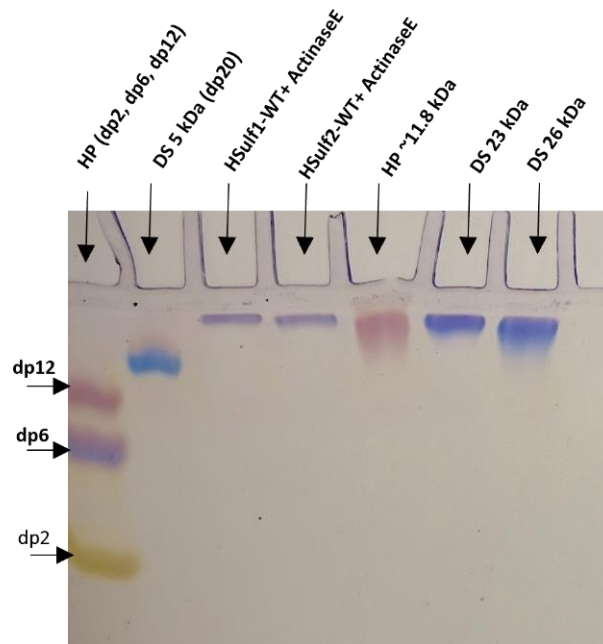


Figure 25: C-PAGE analysis (27% acrylamide) of HSulf-1-WT and HSulf-2-WT (3 μ g each), revealed by Stains-All staining. Black arrows indicate molecular weight markers of heparin and dermatan sulfate.

Unexpectedly, C-PAGE analysis revealed a band corresponding to 23-26 kDa for both HSulf-1 and HSulf-2 (Figure 25), suggesting the presence of a GAG chain on HSulf-1 as well, which does not fall in line with established knowledge about HSulf-1. To investigate this surprising result and further characterize the enzyme isoforms, we performed tryptic digestion followed by nanoLC-MS analysis. Each isoform was queried against both its own and the opposite isoform's sequence database. HSulf-1 showed 69.43% sequence coverage against its own database, while HSulf-2 exhibited 81.06% coverage. Cross-querying against the opposite isoform's database resulted in lower sequence homology (58.21% for HSulf-1 against HSulf-2's database and 59.74% for HSulf-2 against HSulf-1's database) (Table 6).

Table 6: Sequence coverage analysis of HSulf-1 and HSulf-2 by nanoLC-MS. Tryptic digests (1:7.5) of HSulf-1 and HSulf-2 (3 μ g each) were analyzed by nanoLC-MS. The resulting spectra were queried against their corresponding databases and cross-queried against each other.

	Full-length sequence coverage (%)	HSulf-1-WT	HSulf-2WT
Queried Database	HSulf-1-WT	69.43%	59.74%
	HSulf-2WT	58.21%	81.06%

These results indicated awaited distinct sequences for the two isoforms while also highlighting their partial sequence similarity, which was consistent with the known 64% sequence homology. The observed sequence coverage patterns strongly indicated that our samples represented distinct isoforms. These findings, along with the unexpected presence of a potential GAG chain on our HSulf-1 sample, warranted additional investigation into possible similar *O*-glycosylation on HSulf-1, as well.

2.5 Oligomerization Tendency Upon Substrate Binding

Having established the role of the GAG chain and specific mutations in the oligomerization behavior of HSulf-2, we next sought to investigate whether the interaction with the substrate could influence oligomerization. To determine whether heparin polysaccharide directly influences HSulf-2 oligomerization or enhances an existing tendency, we analyzed HSulf-2-heparin complexes using mass photometry. This approach allowed us to quantify changes in the distribution of oligomeric species upon substrate binding. We incubated HSulf-2 with heparin in solution and then examined the resulting complexes.

We initially focused on the DelC mutant, which exhibited minor dimer species in the absence of substrate. We tested several ratios of enzyme to heparin polysaccharide, ranging from 1:5 to 1:500, to determine if increasing substrate concentration could promote oligomerization. While no significant increase was observed for the dimer species at any of the tested ratios (Figure 26), we did notice small shifts for the minor dimer forms of the DelC mutant upon substrate addition. With increased substrate concentration, we also observed a more pronounced shift of the monomer species towards higher masses, indicating the binding of the substrate to the monomeric form of the DelC mutant.

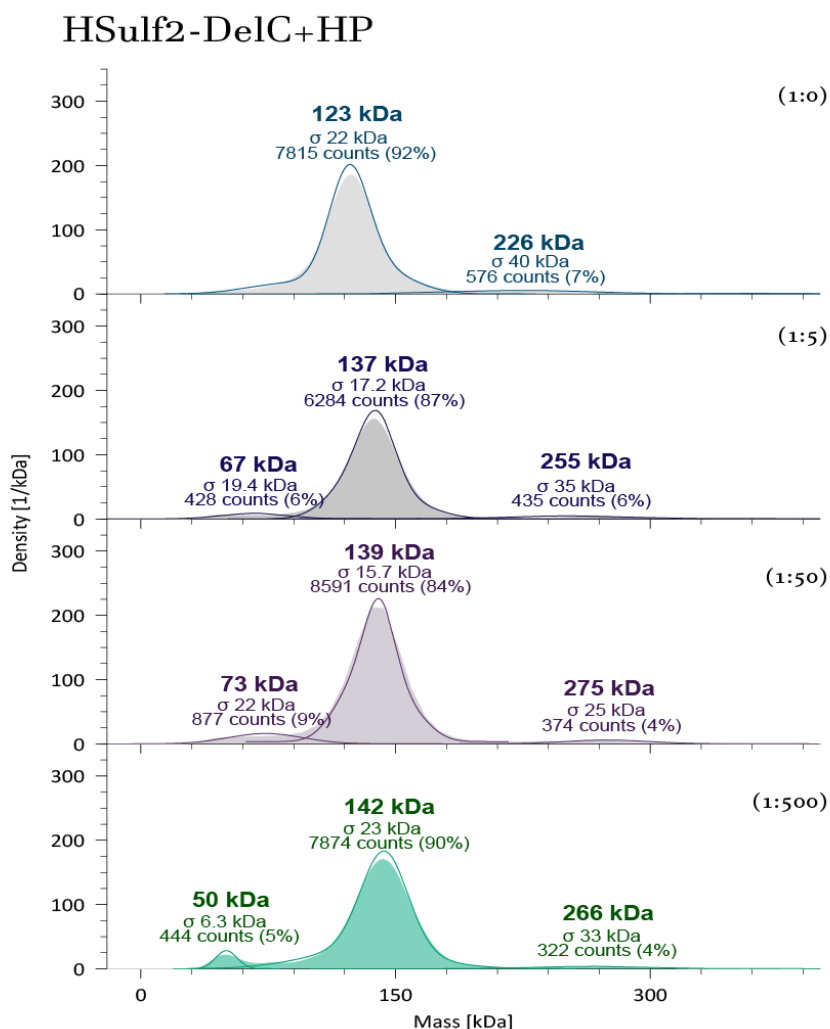


Figure 26: Mass photometry analysis of HSulf-2-DelC (10nM) with increasing ratios of heparin polysaccharide (~16.7kDa), stoichiometry ranging from 1:0 to 1:500 enzyme: polysaccharide. Mass distribution profiles show the relative abundance of different molecular species for both enzyme forms. The y-axis shows the density (1/KDa) of particles detected within each mass range. Major peaks are labeled with their corresponding masses and percentage of total counts.

To extend our investigation, we assessed the effect of substrate interaction on the wild-type forms of HSulf-1 and HSulf-2, as well as on HSulf-2-N561Q, which exhibited similar tendencies to those of DelC. Upon addition of heparin polysaccharide, we observed notable shifts for both the monomeric and dimeric species of HSulf-1 and HSulf-2 (Figure 27). These shifts suggested that the substrate binds to both oligomeric forms of the wild-type enzymes. Similarly, the HSulf-2-HDC mutant showed a shift mainly for the monomeric species after adding heparin (Figure 27C).

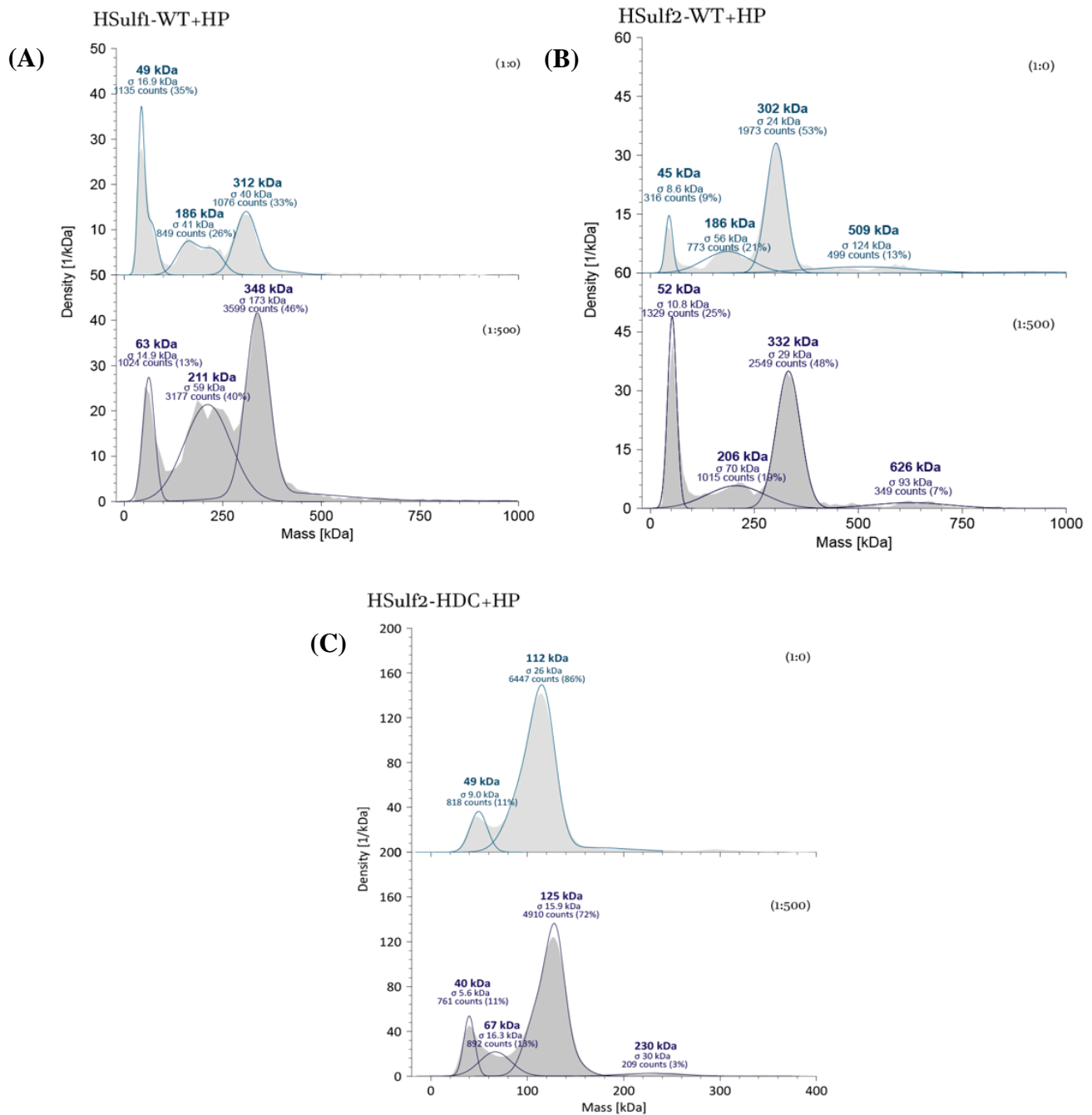


Figure 27: Mass photometry analysis of HSulf-1-wild-type (A), HSulf-1-wild-type (B), and HSulf-2-HDC (C) (10nM each) with a ratio of heparin polysaccharide (~16.7kDa) of 1:500 enzyme:polysaccharide. Mass distribution profiles show the relative abundance of different molecular species for three forms of the enzyme. The y-axis shows the density (1/KDa) of particles detected within each mass range. Major peaks are labeled with their corresponding masses and percentage of total counts.

These preliminary results indicated that adding heparin had no direct impact on the dimer/monomer ratio. Using mass photometry, we assessed the capacity of both monomeric and dimeric forms to bind to heparin. The observed shift for the HDC mutant, which lacks the inner region of the HD domain, confirmed previous studies on the capacity of the N-terminal and C-terminal regions of HD to bind effectively to the substrate, regardless of the presence of the inner region. As reported by Frese et al. (2009), eliminating only the internal, less conserved region of the HD enhances HSulf secretion without affecting enzymatic activity or substrate specificity.

In summary, our mass photometry analysis revealed that monomeric and dimeric forms of wild-type HSulfs and the HSulf-2-N561Q mutant can bind to heparin. We observed a stoichiometry of (1 monomer: 1 heparin molecule) and (1 dimer: 1 heparin molecule). These findings suggest that substrate interaction does not directly influence the oligomerization tendency of these enzymes. Furthermore, the results obtained with the HDC mutant support the importance of the N-terminal and C-terminal regions of the HD domain in substrate recognition, consistent with previous studies.

**Chapter III: Functional
Characterization of HSulf Endosulfatase
Activity: Substrate Preferences and
Structure-functional Relationships**

HSulfs have been the subject of ongoing research focusing on understanding the specific molecular determinants that govern their function in the fine-tuned regulation of heparan sulfate (HS) biological properties. Despite significant progress in this field, several key questions remain unanswered. These include the molecular determinants for HSulf substrate specificity, the structure-function relationships that dictate HSulf action, and the differences between the two HSulf isoforms. Notably, despite sharing the same substrate and having a strong sequence homology of 64%, these isoforms exhibit distinct biological consequences upon their subtle action on HS.

In this chapter, we detail our approach to characterizing HSulf endosulfatase activity, with a focus on substrate preferences and structural elements that may influence this activity. By using oligosaccharides of defined lengths and structures, we aimed to explore how variations in oligosaccharide composition and sulfation patterns affect the activity of HSulf-1 and HSulf-2, potentially revealing isoform-specific preferences. Additionally, we investigated the relationship between structure and function by assessing the impact of mutations in key structural features, such as the GAG chain and the HD domain.

1 Methodological considerations

Traditionally, two main assays have been used to study HSulf enzymatic activity: the 4-Methylumbelliferyl sulfate (4-MUS) assay, which measures overall arylsulfatase activity through fluorescence detection of desulfated 4-methylumbelliferone, and the heparin desulfation assay, which directly assesses HSulf activity on heparin substrates (Morimoto-Tomita et al., 2002; Saad et al., 2005). Both methods, however, have notable limitations. The 4-MUS assay, though sensitive, lacks specificity for HS endosulfatase activity as it measures overall arylsulfatase activity with K_m values in the millimolar range (Vives et al., 2014). The heparin desulfation assay offers better specificity but is more complex, requiring several steps, including enzymatic depolymerization by heparinases after HSulf's reaction to analyze the desulfated products. Additionally, it relies on heparin, a polysaccharide with considerable heterogeneity due to structural diversity, source-dependent composition, and preparation methods. This variability can affect HSulf binding and activity, potentially introducing variability in assays.

To overcome these limitations, we chose to use heparin-like oligosaccharides that mimic the NS functional domains of HS. These substrates provide a chemically defined and homogeneous alternative. This approach ensures specificity and minimal variability, which is essential for the detailed mechanistic studies needed to understand how HSulfs process their substrates.

To effectively monitor the desulfation process of oligosaccharides by HSulfs, we employed a HILIC-MS method developed in our laboratory (Poyer et al., 2021). This method relies on Hydrophilic interaction chromatography (HILIC), which has emerged as an excellent technique for separating saccharidic

compounds based on their hydrophilic behavior (Buszewski and Noga, 2012), gaining popularity for separating glycans and sulfated oligosaccharides derived from GAG depolymerization (Gill et al., 2013; Ouyang et al., 2016). We used a ZIC-cHILIC silica column grafted with zwitterionic phosphorylcholine groups, combining hydrophilic partitioning with weak electrostatic interactions for excellent selectivity of polar and charged compounds (Di Palma et al., 2011).

This approach offered several advantages for our analysis. First, it enabled the separation of oligosaccharides that differ only in their sulfation patterns, including variations in the number and position of sulfate groups. Second, this method relies on volatile organic solvents like acetonitrile for separation, making it compatible with mass spectrometry coupling to enable precise detection and characterization of intact substrates and desulfated products. Lastly, it allows us to avoid derivatization or extensive sample preparation, often required in traditional oligosaccharide analysis. The combination of ZIC-cHILIC separation with electrospray ionization mass spectrometry (ESI-MS) provided a robust analytical strategy, complementing our use of substrates with defined sequences to accurately characterize HSulf activity on oligosaccharides of varying lengths and sulfation patterns.

For all the conducted assays, we utilized two types of enzyme preparations: NTA bead-bound HSulf-1 and HSulf-2 expressed in Chinese hamster ovary cells (CHO) and HSulfs in solution expressed in human embryonic kidney 293F (HEK293F) cells (provided by collaborators Dr. Kenji Uchimura from UGSF, Lille and Dr. Romain Vivès from IBS, Grenoble, respectively). The enzymes in solution consisted of HSulf-1 and HSulf-2 WT enzymes, as well as HSulf-2 mutant constructs. Prior to each experiment, enzyme activity was validated using the 4-MUS arylsulfatase assay. All comparative data sets are generated using enzymes from the same preparation to account for batch-to-batch variability. For the comparative analysis of HSulf-1 and HSulf-2, we primarily used NTA bead-bound HSulf enzymes (referred to as bead-HSulfs in the text).

2 Comparative analysis of HSulf-1 and HSulf-2 activity on oligosaccharide substrates of defined sequence

Previous studies using the heparin desulfation assay have shown that HSulfs prefer NS domains in HS chains, particularly the trisulfated [IdoA(2S)-GlcNS(6S)] motif, and can desulfate [UA-GlcNS6S] disaccharides, highlighting the importance of *N*-Sulfation for substrate recognition. (Lamanna et al., 2008; Pempe et al., 2012). Given these findings and that HSulfs exhibit arylsulfatase activity on small compounds like 4-MUS, we sought to determine the smallest carbohydrate-based compound that HSulfs could process as a substrate within their catalytic site, thereby establishing the minimum size requirements for HSulf activity.

To this end, we conducted enzymatic reactions using two 6-*O*-sulfated disaccharides: monosulfated Δ UA-GlcAc6S and disulfated Δ UA-GlcNS6S, with both HSulf-1 and HSulf-2. Using our HILIC-MS method, we monitored the *m/z* 458.06 and 496.00 ions corresponding to the intact substrate species for Δ UA-GlcAc6S and Δ UA-GlcNS6S, respectively, over a 24-hour reaction period to detect any desulfated species. Our results showed no desulfation for either substrate with either enzyme after 24 hours (Figure 28A, 28B).

Our results suggested that HSulfs require larger substrates for their sulfatase activity despite their ability to act on small artificial substrates like 4-MUS. This implies that HSulfs have further requirements beyond the mere presence of 6-*O*-sulfation, which are only met at the polysaccharide level and which they cannot access when reacting with dp2 alone. Furthermore, this suggested that oligosaccharides with HS backbone need to bind first to HSulf to be processed, in contrast to small compounds like 4-MUS, which can interact with the catalytic site through mechanisms that may involve their aryl ring structure.

Our observations aligned with previous knowledge, indicating a minimum required size that corresponds to an octasaccharide to occupy the catalytic domain binding sites (A. Seffouh et al., 2019).

Previous studies using the heparin desulfation assay established that the minimum size for sulfatase activity is a tetrasaccharide (Δ UA2S-GlcNS6S-Ido2S-GlcNS6S), showing minor desulfation extent (Saad et al., 2005). Additionally, other studies reported that HSulf-2 removes 6-*O*-sulfate groups that are not within the critical antithrombin (AT)-binding region (Pempe et al., 2012; Saad et al., 2005). Building on these observations, we proceeded with oligosaccharides longer than dp2, focusing on a pentasaccharide (Fondaparinux) that mimics the AT-binding sequence in heparin and contains a 3-*O*-sulfate group (Figure 28F). Using the same assay conditions as for the disaccharides, we monitored the *m/z* 712.49 ion, corresponding to the singly desulfated product species, within a 24-hour reaction time. We observed minor singly desulfated species for both enzymes after 24 hours, with HSulf-1 showing slightly less activity (3% peak area) compared to HSulf-2 (6% peak area) (Figures 28C and 28D).

These results suggested that endosulfatase activity may require a minimum substrate length of approximately four to five saccharide units for effective binding to the catalytic domain and processing by the active site, consistent with the previously reported results on the tetrasaccharide.

To further evaluate the impact of oligosaccharide chain length on HSulfs activity, we employed an octasaccharide (commercial source, Iduron) with a similar structure to Fondaparinux, also containing a 3-*O*-sulfate group (Figure 28F). We monitored the *m/z* 722.02 ion, corresponding to the doubly desulfated species. After 24 hours, both HSulfs generated singly and doubly sulfated species, with a reduced proportion of the intact species containing four 6-*O*-sulfate groups, as shown in the chromatogram (Figure 28E). HSulf-2 exhibited enhanced activity compared to HSulf-1, with only 24% of the substrate remaining intact compared to 58% for HSulf-1. HSulf-2 produced predominantly singly desulfated species (62% of total peak area) compared to HSulf-1 (38%). Additionally, HSulf-2 generated more doubly desulfated species (13.5% of total peak area) than HSulf-1 (3.4%). This difference in activity between HSulfs was consistent with the trend observed with Fondaparinux. The heightened activity of both HSulf-1 and HSulf-2 on this longer substrate confirmed that their activity is length-dependent. Furthermore, these results demonstrate that HSulfs can act on oligosaccharide sequences containing 3-*O*-sulfate groups.

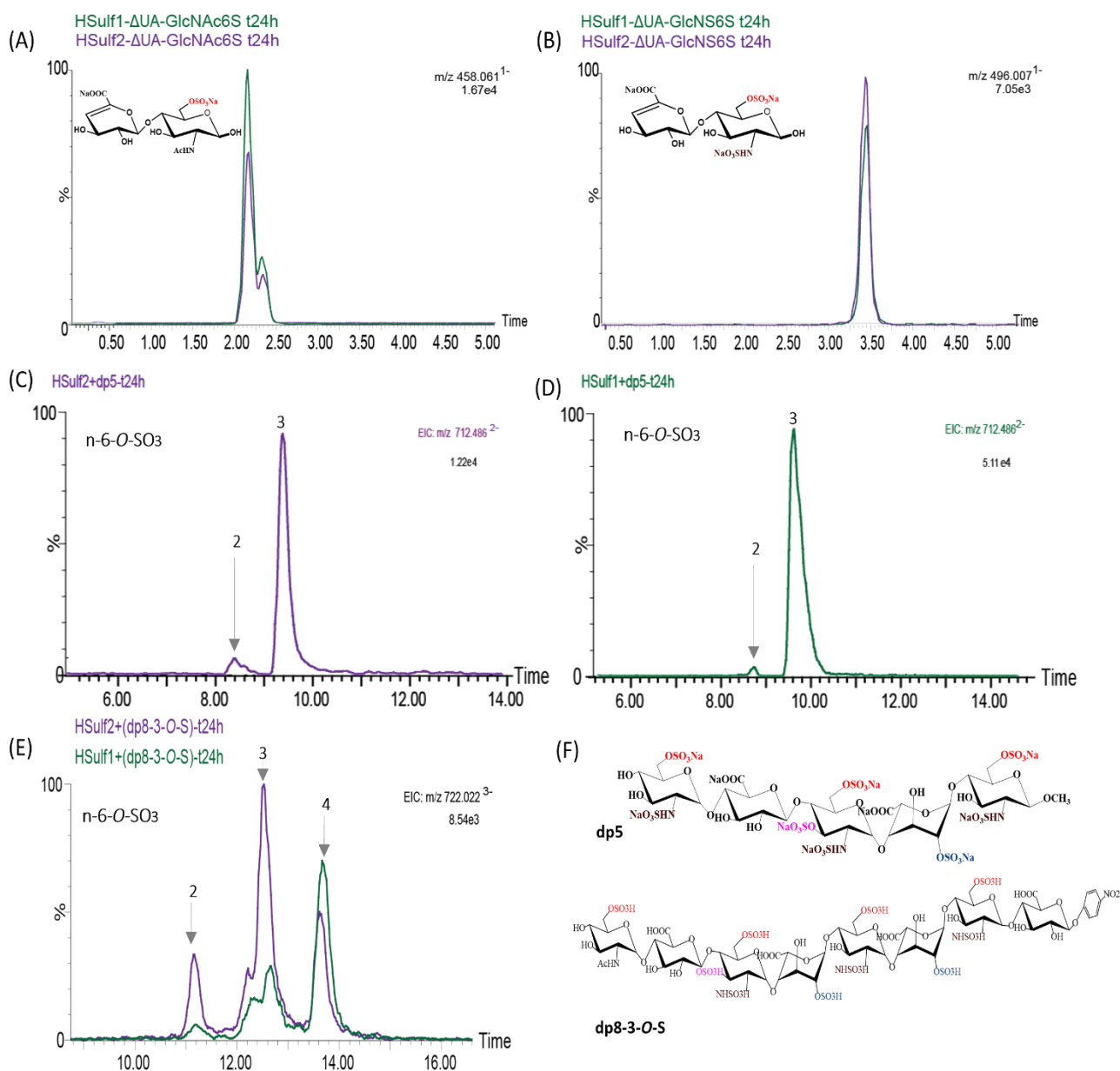
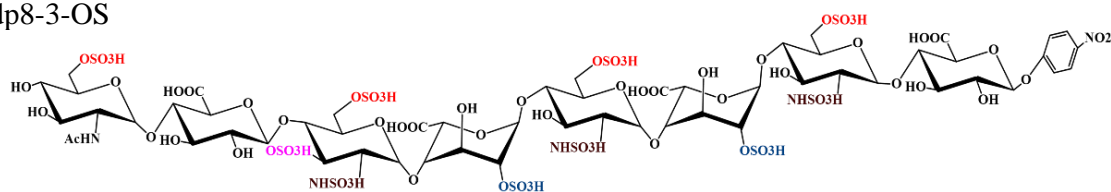


Figure 28: Extracted ion chromatograms illustrating the reactivity of HSulf-1 and HSulf-2 with oligosaccharides of varying lengths after 24h reaction time: (A) Δ UA-GlcNAc6S: green trace (HSulf-1), purple trace (HSulf-2). (B) Δ UA-GlcNS6S: green trace (HSulf-1), purple trace (HSulf-2). (C) Pentasaccharide (Fondaparinux): purple trace (HSulf-2), arrows indicating the number of remaining 6-O-sulfates after 24h. (D) Pentasaccharide (Fondaparinux): green trace (HSulf-1), arrows indicating the number of remaining 6-O-sulfates after 24h. (E) Octasaccharide: green trace (HSulf-1), purple trace (HSulf-2), arrows indicating the number of remaining 6-O-sulfates after 24h reaction course. (F) Structures of the oligosaccharides: pentasaccharide (Fondaparinux) and octasaccharide (dp8-3-O-S). Chromatograms obtained using Hydrophilic Interaction Liquid Chromatography (HILIC). Separation performed on a ZIC-chILIC column (150 \times 2.1 mm, 3 μ m) with a zwitterionic phosphorylcholine stationary phase. Mobile phase A: 7.5 mM ammonium formate (pH 4.0); B: acetonitrile. Elution performed with a gradient of increasing percentage of ammonium formate.

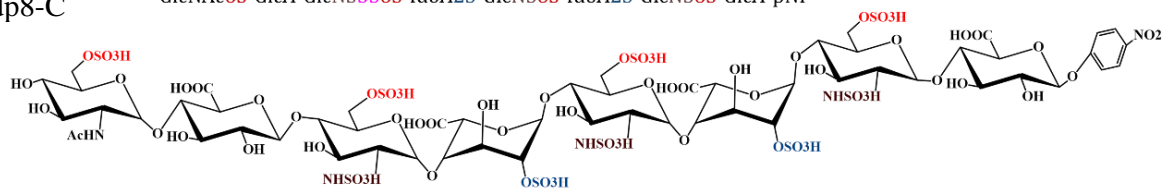
To further elucidate the substrate specificities of HSulf-1 and HSulf-2, we conducted a comparative assay using four structurally distinct octasaccharides from commercial source (Iduron), including dp8-3-OS (Figure 29). All octasaccharides contained four 6-*O*-sulfate groups on their glucosamine residues but differed in other key structural features. dp8-3-OS and dp8-C were identical except for an additional 3-*O*-sulfate group in dp8-3-OS, with both containing two IdoA2S residues. dp8-B and dp8-A differed from dp8-C and dp8-3-OS by having N-sulfation on all glucosamine residues. Additionally, dp8-B contained two IdoA2S residues, while dp8-A had only one, replaced by a GlcA in the corresponding position. With this approach, we aimed to confirm and better understand the impact of 3-*O*-sulfation, the N-acetylation or sulfation of the glucosamine at the non-reducing end, and the impact of IdoA2S residue on HSulf activity.

dp8-3-OS



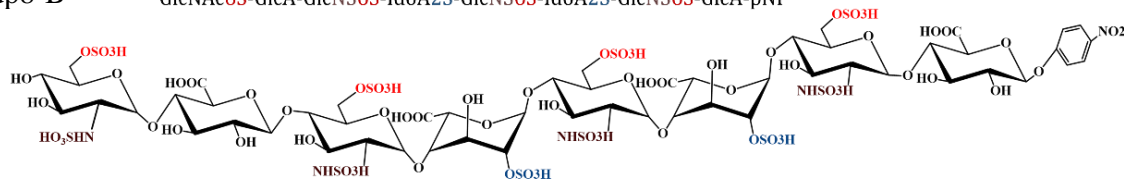
dp8-C

GlcNAc_{6S}-GlcA-GlcNS_{3S}6S-IdoA_{2S}-GlcNS_{6S}-IdoA_{2S}-GlcNS_{6S}-GlcA-pNP



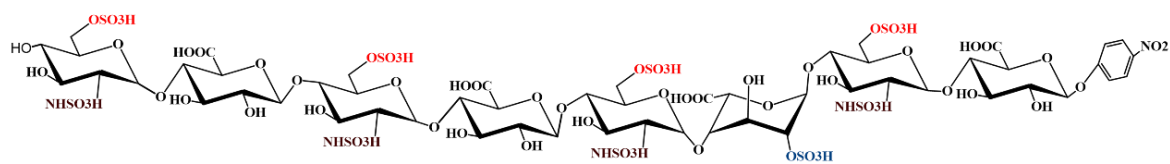
dp8-B

GlcNAc_{6S}-GlcA-GlcNS_{6S}-IdoA_{2S}-GlcNS_{6S}-IdoA_{2S}-GlcNS_{6S}-GlcA-pNP



dp8-A

GlcNS_{6S}-GlcA-GlcNS_{6S}-IdoA_{2S}-GlcNS_{6S}-IdoA_{2S}-GlcNS_{6S}-GlcA-pNP



GlcNS_{6S}-GlcA-GlcNS_{6S}-GlcA-GlcNS_{6S}-IdoA_{2S}-GlcNS_{6S}-GlcA-pNP

Figure 29: Structures of the four heparan sulfate octasaccharides (dp8-3-OS, dp8-C, dp8-B, and dp8-A, Iduron) tested for HSulf-1 and HSulf-2 activity. Color coding indicates different sulfate groups: 6-*O*-sulfates (red), N-sulfates (brown), 2-*O*-sulfates (blue), and 3-*O*-sulfate (magenta). The para-nitrophenyl (pNP) group marks the reducing end of the oligosaccharide.

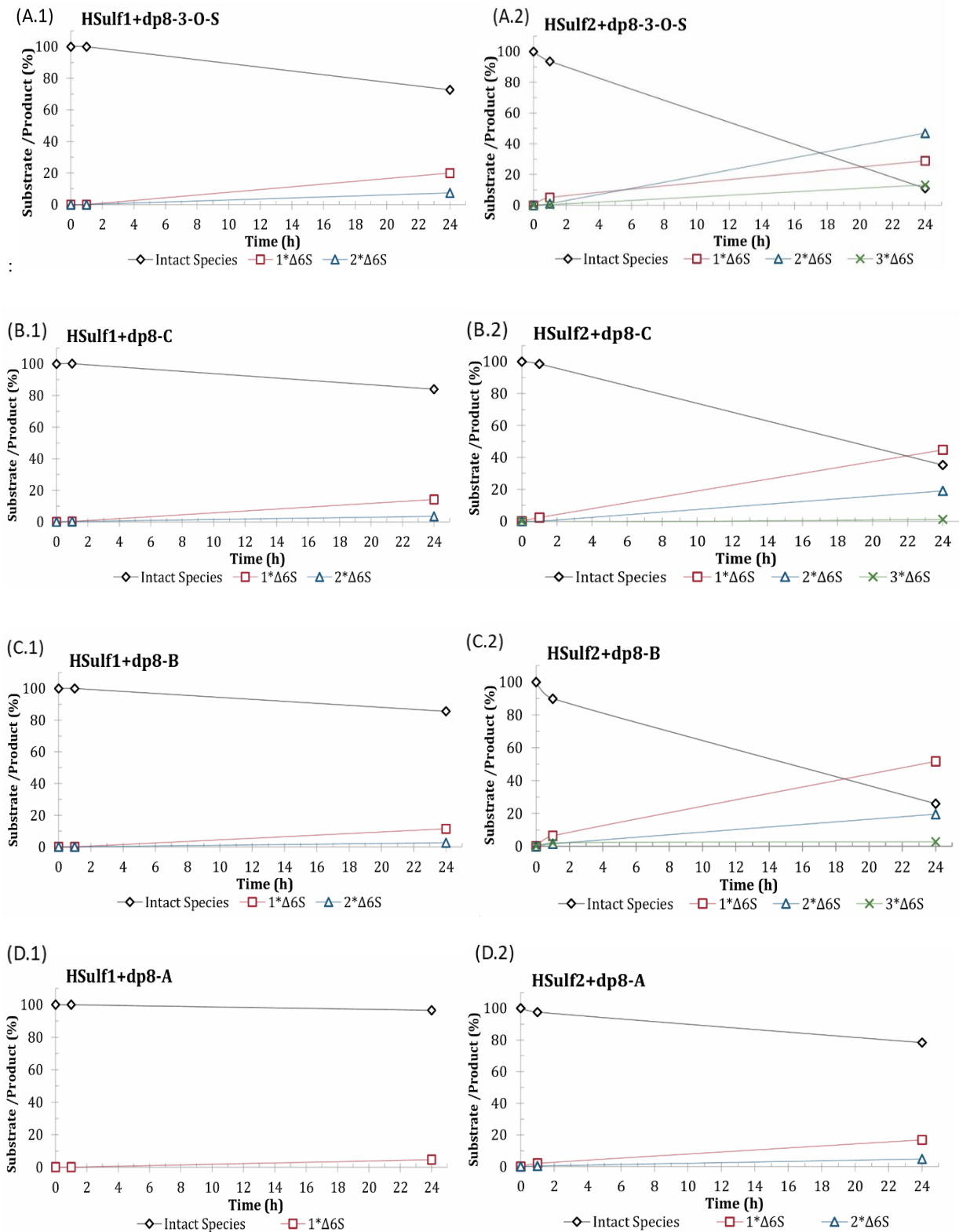


Figure 30: Endosulfatase activity of HSulf-1 and HSulf-2 measured by HILIC-MS on four octasaccharide substrates (dp8-C, dp8-3-O-S, dp8-A, and dp8-B) over 24 hours. Graphs represent the ratio of the intact substrate (black diamonds) and desulfated products: 1Δ6S (red squares), 2Δ6S (blue triangles), and 3Δ6S (green crosses). Percentages correspond to the sum of intensities of each species divided by the sum of all present species at each time point of the reaction course. Background method-induced desulfation was subtracted from all measurements. dp8: octasaccharide; Δ6S: removal of 6-O-sulfate group

Within a 24-hour reaction time, HSulf-2 demonstrated consistently pronounced desulfation across all octasaccharide substrates compared to HSulf-1 (Figure 30). Compared to HSulf-1, HSulf-2 displayed a more extensive desulfation pattern for dp8-3-*O*-S, reaching up to doubly-desulfated products (2 Δ 6S) and leaving only about 11% of the intact species, with 2 Δ 6S as the major product (Figure 30A.2). In contrast, for dp8-C, 35% of intact species remained, with singly desulfated species (1 Δ 6S) as the main product (Figure 30B.2). This confirmed the previously observed reduced activity of HSulf-1 compared to HSulf-2 on dp8-3-*O*-S. This effect remained consistent in the absence of the 3-*O*-sulfate group with dp8-C.

dp8-B (Figure 30C.1, 30C.2), which recently was demonstrated to be a substrate of HSulf-2 (Benicky et al., 2023), displayed a similar desulfation pattern to dp8-C, from which it differs by *N*-sulfation on the glucosamine in place of *N*-acetylation at the non-reducing end. A moderate enhancement in the final ratio of singly desulfated species was observed for dp8-B compared to dp8-C. This indicated that while *N*-acetylation at the non-reducing end does not significantly alter HSulf reactivity (mainly for HSulf-2), *N*-sulfation shows good concordance for substrate specificity.

dp8-A (Figure 30D.1, 30D.2), which differs from dp8-B by the presence of only one IdoA2S residue instead of two, appeared to be the least targeted by both enzymes, with HSulf-2 desulfating only 22% of the intact species within 24 hours.

Overall, these results showed that HSulf-2 was more reactive towards this set of oligosaccharides compared to HSulf-1, which presented low desulfation rates, slightly enhanced in the presence of 3-*O*-sulfation. The presence of 3-*O*-sulfation (dp8-3-*O*-S) or additional IdoA2S (dp8-B vs. dp8-A) appears to enhance desulfation, particularly for HSulf-2. These findings suggest that HSulf-2 has less stringent structural requirements than HSulf-1 for substrate recognition and desulfation. Higher overall sulfation density correlated with increased enzymatic activity, which may result from facilitated enzyme-substrate interactions and a more favorable binding environment. The presence of IdoA2S residues provides higher conformational diversity, potentially facilitating enzyme binding and activity, which may explain the impaired reactivity towards dp8-A for both enzymes due to its reduced IdoA2S content. Interestingly, the presence of GlcNAc6S (dp8-C) or GlcNS6S (dp8-B) at the non-reducing end did not induce a significant impact, indicating that the enzymes recognize either form. However, this could potentially influence the initial binding or orientation of the substrate.

Previous studies reported that HSulf-1 and HSulf-2 act in a processive enzymatic mechanism, leading to an oriented 6-*O*-desulfation from the non-reducing end towards the reducing end on heparin octasaccharides of four constitutive [UA(2S), GlcNS(6S)] units (Seffouh et al., 2013).

With this in mind, we sought to investigate the impact of the 6-*O*-sulfate group positioning on HSulf-1 and HSulf-2 activity. We conducted assays on a series of oligosaccharides of defined structure. These were provided by our collaborators, Dr. Christine Le Narvor and David Bonnaffé from the Institut de Chimie Moléculaire et des Matériaux d'Orsay (ICMMO), Université Paris-Saclay, France. The series consisted of octasaccharides with a [IdoA(2S), GlcNS(6S)]₄ backbone, systematically lacking one 6-*O*-sulfate and one 2-*O*-sulfate group on a single disaccharide unit. This modification was sequentially positioned from the non-reducing end toward the reducing end. The resulting oligosaccharides were denoted as I3III, II3II, III3I, and IIII3, where **I3** indicates the position of the modified disaccharide within the octasaccharide sequence (Figure 31).

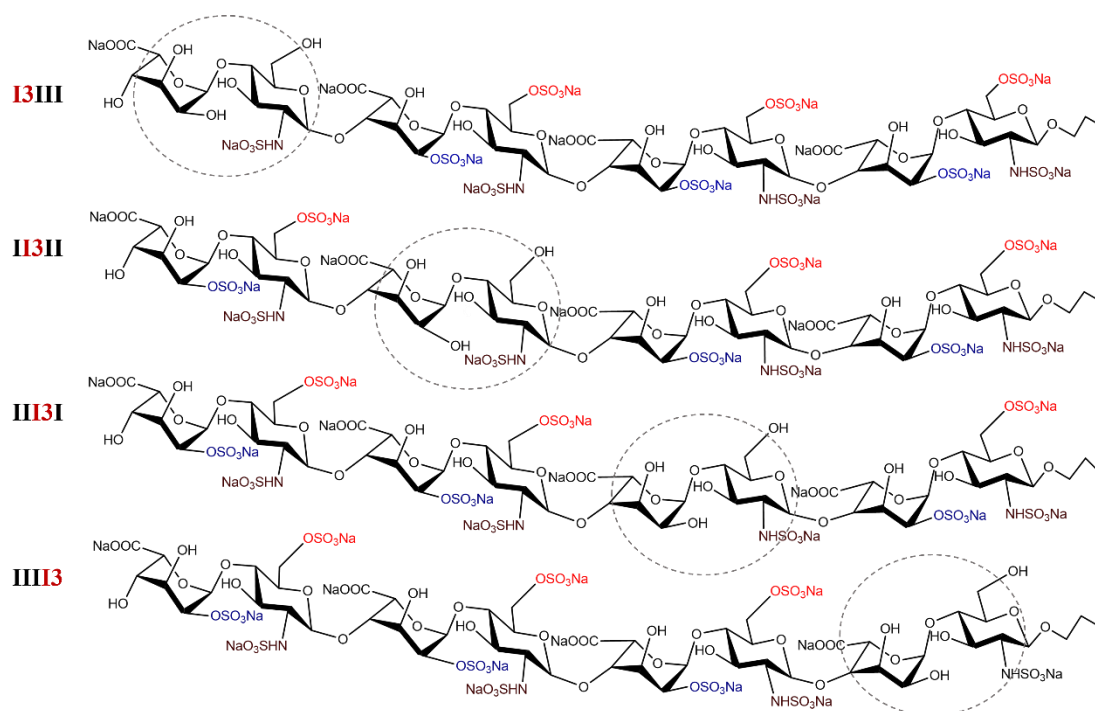


Figure 31: Structures of synthetic heparan sulfate octasaccharides tested for HSulf-1 and HSulf-2 activity. Color coding indicates different sulfate groups: 6-*O*-sulfates (red), N-sulfates (brown), 2-*O*-sulfates (blue), and 3-*O*-sulfate (magenta). The propyl group marks the reducing end. Each structure features an [IdoA(2S), GlcNS(6S)]₄ backbone, with one 6-*O*-sulfate and one 2-*O*-sulfate missing on different GlcNS units in each oligosaccharide. The variations are labeled as I3III, II3II, III3I, and IIII3, indicating the specific position of the missing sulfate groups within the sequence.

For this assay, we used unbound forms of HSulf-1 and HSulf-2 due to a partial loss in activity observed with the bead-bound preparations (however, despite their reduced activity, we could verify using the most reactive substrate that the bead-bound enzymes followed the same activity pattern). The oligosaccharides were incubated with HSulfs for 0, 1, 4, 24, and 32 hours. We included systematic controls consisting of oligosaccharides without the enzyme incubated under the same buffer and temperature conditions and samples incubated with denatured enzymes. These controls allowed us to distinguish enzyme-specific effects from potential spontaneous degradation or non-specific interactions.

Within 32 hours of enzymatic reaction, HSulf-2 consistently exhibited a more pronounced desulfation pattern than HSulf-1. This behavior was consistent with our earlier findings using bead-bound enzymes on the dp8-pnP series (Figure 30). When examining the enzymatic activities of HSulf-1 and HSulf-2 on octasaccharide substrates (I3III, II3II, III3I, and III3), we observed distinct desulfation patterns (Figure 32), suggesting that each enzyme has unique structural requirements.

Both enzymes exhibited the highest reactivity with I3III. HSulf-2 showed more rapid and extensive desulfation, leading to 95% desulfation of the intact species within 32h (Figure 32A.2) compared to 50% for HSulf-1 (Figure 32A.1). HSulf-2 was able to reach up to doubly desulfated (2 Δ 6S) production while HSulf-1 did not go beyond singly desulfated species. This result indicated that despite the absence of the 6-*O*-Sulfate group on the non-reducing end, the reactivity of the two enzymes towards the I3III substrate was maintained. This may be related to their action as endosulfatases within the HS chain and also likely results from the presence of three consecutive 6-*O*-sulfated disaccharides after the non-6-*OS* disaccharide at non-reducing-end, providing an optimal length (dp6) of substrate sequence for enzyme recognition and processivity. The formation of doubly desulfated products is observed only for HSulf-2, suggesting that potentially, for a dp6 after the non-reducing end, HSulf-2 is able to maintain its processive mechanism. This is evidenced by the decrease of singly desulfated species in favor of the increase of doubly desulfated ones after 24h reaction time. In contrast, for HSulf-1, the singly desulfated species remained predominant.

With II3II, both enzymes exhibited the lowest reactivity. HSulf-2 led to 15% desulfation of the intact species only after 24h reaction time compared to only 5% for HSulf-1 (Figure 32, B). This low reactivity may be due to the lack of a sufficiently long sequence of 6-*O*-sulfated disaccharides at either end. Specifically, the absence of a sequence superior to dp2 6-*OS* from the non-reducing end and a sequence superior to dp4 6-*OS* before the reducing end potentially disrupts the minimum recognition sequences required for efficient enzyme binding and activity.

With III3I, both enzymes exhibited enhanced activity compared to the II3II octasaccharide. HSulf-1 led to 60% desulfation of the intact species within 32h reaction time compared to 45% for HSulf-2. Additionally, HSulf-1 generated 50% singly desulfated species compared to 40% with HSulf-2 (Figure

32, C). This pattern suggested that a dp4 6-OS sequence at the non-reducing end meets minimum enzyme requirements regarding the sequence size they target at the non-reducing end. This observation concurs with the tendencies observed with II3II, which has a dp2-6-OS at the non-reducing end.

Interestingly, both HSulf-1 and HSulf-2 demonstrated low reactivity with IIII3, despite the presence of a dp6-6-OS sequence at the non-reducing end of this octasaccharide (Figure 32, D). After 24h reaction time, HSulf-1 led to 28% desulfation of the intact species compared to 36% for HSulf-2. Additionally, HSulf-1 generated 30% singly desulfated species compared to 24% with HSulf-2.

These results presented contradictory elements to those we observed with I3III and III3I regarding the importance of the non-reducing end for HSulfs activity. However, they suggested that the final position of 6-OS relative to the oligosaccharide's reducing end is crucial for HSulfs' reactivity towards the octasaccharide, probably for substrate binding. This observation aligns with a previous study by Seffouh *et al.* (2013), which claimed that once the enzyme reaches the reducing end of an S-domain, the absence of further downstream 6-*O*-sulfates dramatically reduces HSulf affinity for its substrate, allowing the enzyme to be released from the desulfated domain.

The apparent discrepancy among I3III, III3I, and IIII3 underscores the complexity of HSulf substrate interactions, suggesting the need for further investigation with additional replicates to confirm these findings. While the significance of the non-reducing end was evident, the role of the reducing end should not be underestimated. Our results with I3III indicate that HSulfs exhibit endosulfatase activity within the oligosaccharide sequence, expanding on previous understandings of their activity primarily at the polysaccharide level (Morimoto-Tomita *et al.*, 2002).

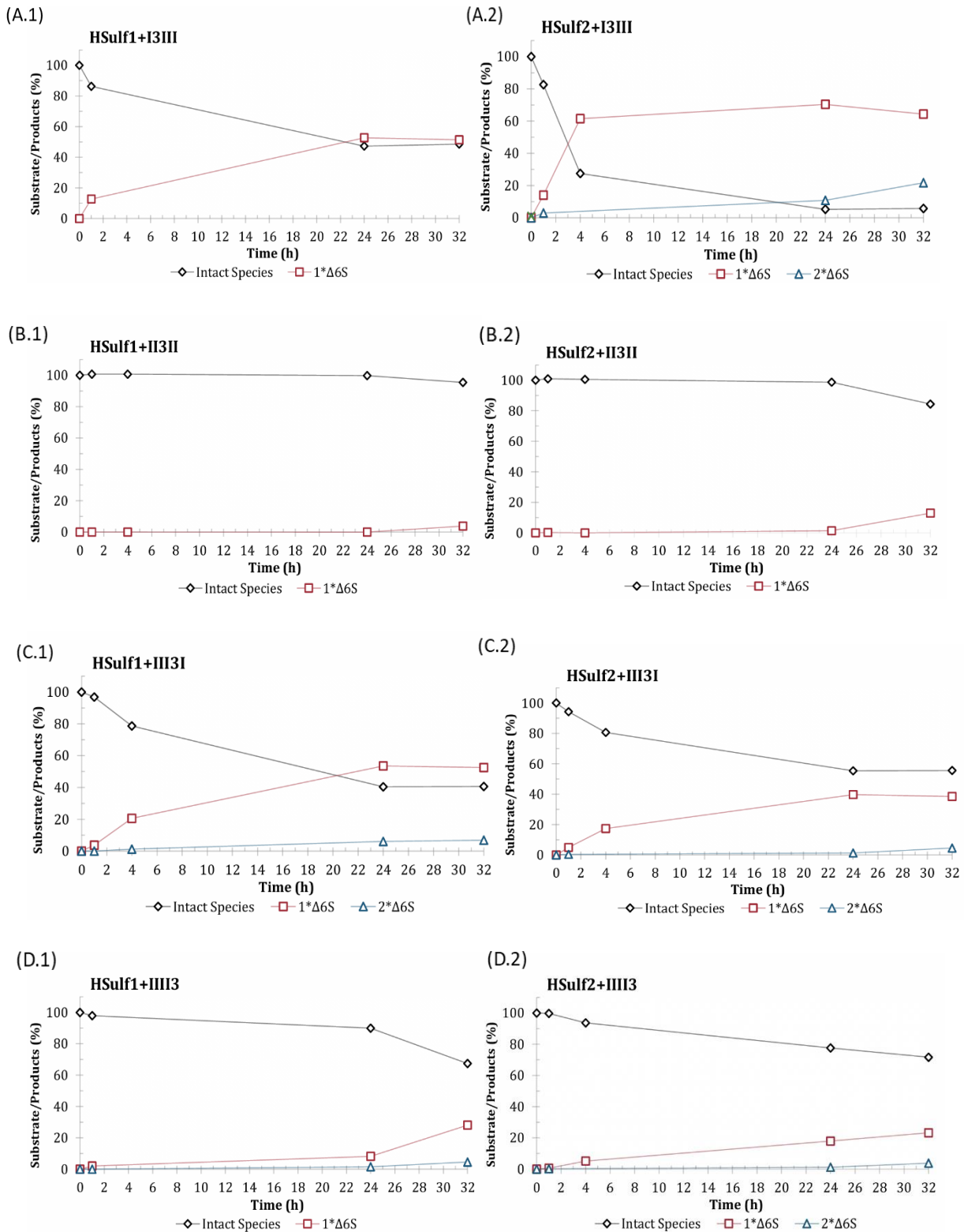


Figure 32: Endosulfatase activity of HSulf-1 and HSulf-2 measured by HILIC-MS on four octasaccharide substrates (I3III, II3II, III3I, and III3) over 32 hours. Graphs represent the ratio of intact substrate (black diamonds) and desulfated products: 1Δ6S (red squares), and 2Δ6S (blue triangles). Percentages correspond to the sum of intensities of each species divided by the sum of all present species at each time point of the reaction course. Background method-induced desulfation was subtracted from all measurements. dp8: octasaccharide; Δ6S: removal of 6-O-sulfate group

3 Impact of structural variations on the endosulfatase activity of HSulf-2

In order to investigate the impact of structural variations on the function of HSulf-2, we sought to establish a correlation between structural specificities and functional consequences on enzymatic activity. Using HSulf-2 mutant constructs, we investigated the impact of several mutations affecting structural features within HSulf-2, focusing on the GAG chain and the HD domain. For that, we conducted enzymatic assays on two substrates: Fondaparinux (dp5) and dp8-3-*O*-S, which we described in the previous section (Figure 28, page 81).

3.1 Impact of the (CS/DS) GAG chain on HSulf-2 endosulfatase activity

To evaluate the impact of the glycosaminoglycan (GAG) chain on HSulf-2 activity, we conducted comparative assays using two enzyme variants: the wild-type HSulf-2 WT and the SG mutant. In the SG mutant, the serine residue (S583) of the dipeptide SG is replaced with alanine, resulting in the loss of the tethered GAG chain. The SG mutation had previously been observed to enhance arylsulfatase activity on 4-methylumbelliferyl sulfate (4-MUS) in our laboratory (Bilong, 2022). We extended this investigation to study its impact on the endosulfatase activity using previously described pentasaccharide and octasaccharide substrates (Figure 33).

For the Fondaparinux, HSulf-2 WT completely desulfated the intact species within 48h reaction time, with a concomitant increase in singly, doubly, and triply desulfated products, leading to a majoritary singly desulfated species (1 Δ 6S) reaching 43% (Figure 33A.1).

The SG mutant displayed markedly faster reactivity towards Fondaparinux (Figure 33A.2), completely consuming the intact species within four hours. This was accompanied by a rapid increase in singly desulfated species (1 Δ 6S), which decreased as doubly and triply desulfated products accumulated, reaching 44% and 38% within 48 hours.

These results indicated that the SG mutation enhances HSulf-2's enzymatic activity, increasing both its rate and extent of desulfation on the dp5 substrate. To confirm this observation, we performed the same analysis on a longer oligosaccharide (dp8-3-*O*-S).

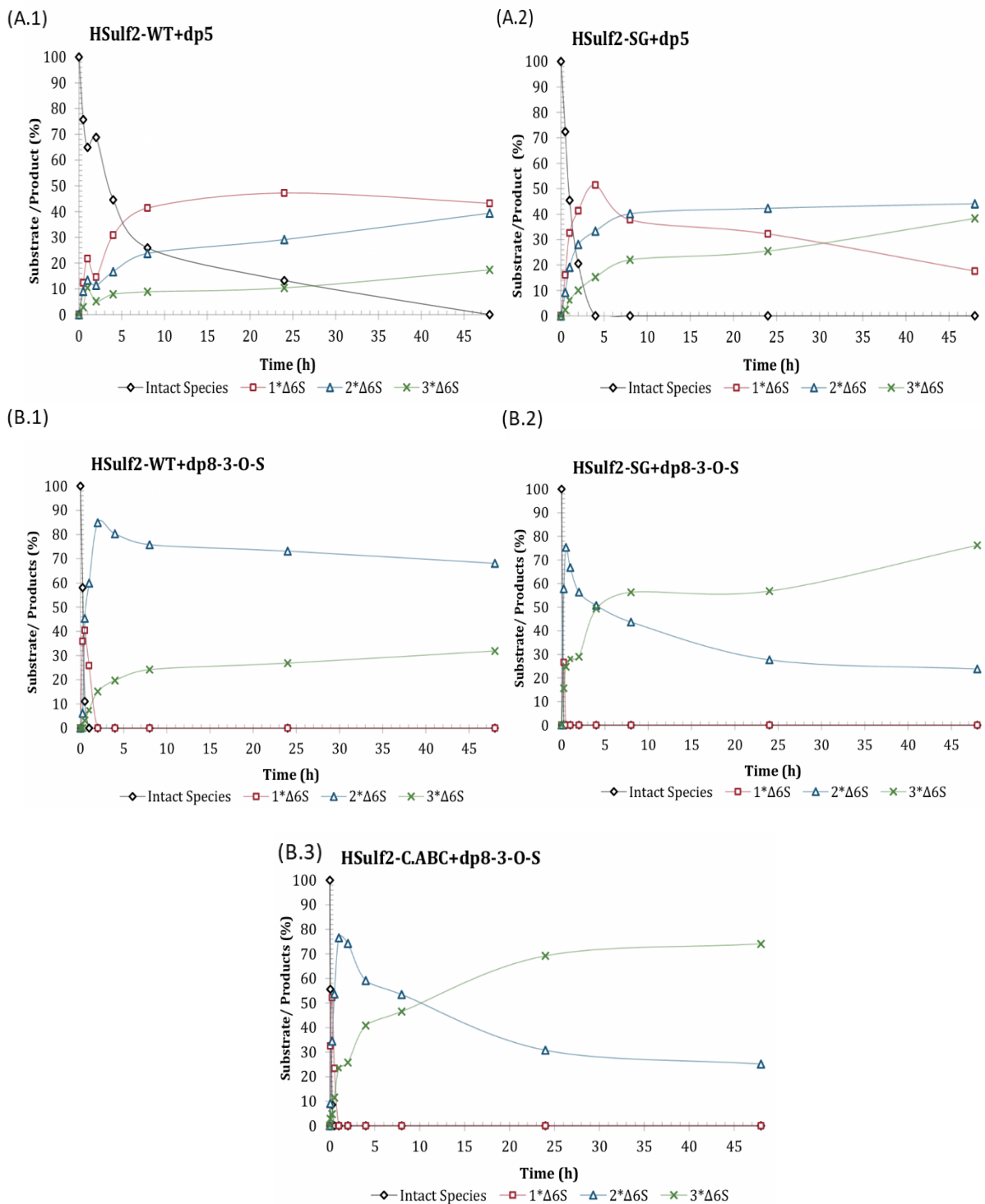


Figure 33: Impact of GAG chain on the endosulfatase activity of HSulf-2 measured by HILIC-MS on 3-*O*-sulfated oligosaccharide substrates (Fondaparinux: dp5 and dp8-3-*O*-S) over 48 hours. Graphs represent the ratio of the intact substrate (black diamonds) and desulfated products: 1Δ6S (red squares), 2Δ6S (blue triangles), and 3Δ6S (green crosses). Percentages correspond to the sum of intensities of each species divided by the sum of all present species at each time point of the reaction course. Background method-induced desulfation was subtracted from all measurements. dp8: octasaccharide; Δ6S: removal of 6-*O*-sulfate group.

For dp8-3-*O*-S, HSulf-2 WT showed rapid initial desulfation, with intact species decreasing to about 60% within the first 15 minutes. This was accompanied by complete consumption of singly desulfated species (1 Δ 6S) and a parallel increase in doubly desulfated products (2 Δ 6S), reaching 85% in 2 hours and remaining dominant throughout the 48 hours. The triply desulfated products (3 Δ 6S) gradually increased, reaching 32% by 48 hours.

The SG mutant exhibited even more rapid and extensive desulfation, completely consuming intact species in the first 15 minutes. The doubly desulfated products peaked quickly and then decreased in favor of the triply desulfated products, which became dominant, reaching about 76% by 48 hours.

These results confirmed the marked heightened activity of the SG mutant compared to the wild-type with a more extensive and rapid desulfation of both substrates.

To confirm this effect, we assayed the endosulfatase activity of HSulf-2 after treatment with chondroitinase ABC to remove its CS/DS saccharidic component consisting of the GAG chain. The chondroitinase ABC-treated HSulf-2 showed an enhanced activity profile, with rapid complete consumption of the intact species within a few minutes. This treated form exhibited faster consumption of the intact species compared to the wild-type (Figure 33B.1), though not as rapid as the SG mutant (Figure 33B.2).

The distribution of desulfated products generated by the chondroitinase ABC-treated HSulf-2 resembled that of the SG mutant, though the transition between species was less rapid. Initially, doubly desulfated products were predominant, but over time, they gradually decreased as triply desulfated products accumulated, reaching 74% by 48 hours.

These results further confirmed HSulf-2's ability to process substrates with either acetylated or *N*-sulfated glucosamine at the non-reducing end and verified that HSulf-2 is fully capable of recognizing and processing HS sequences containing a 3-*O*-S motif.

Most significantly, our experiments with dp8-3-*O*-S revealed that the removal of the GAG chain substantially enhances HSulf-2's endosulfatase activity. This effect was confirmed with the enhancement of activity observed with genetic mutation (SG mutant) and enzymatic treatment (chondroitinase ABC). The SG mutant showed the most significant increase in desulfation activity, suggesting that the complete absence of the GAG chain allows for more efficient and extensive substrate processing. This enhanced activity might be due to improved substrate access or conformational changes in HSulf-2 following GAG removal. In contrast, the enzymatically deglycosylated HSulf-2 exhibited a similar but less pronounced effect, likely because of residual CS/DS saccharidic units and tetrasaccharide linkers remaining after chondroitinase ABC treatment.

This assay also revealed an interesting aspect of the desulfation reaction for both the wild-type and SG mutant forms of HSulf-2 on Fondaparinux. We observed the production of two distinct populations of the doubly desulfated species (with one 6-OS group remaining) for both enzyme forms (Figure 34A and 34B).

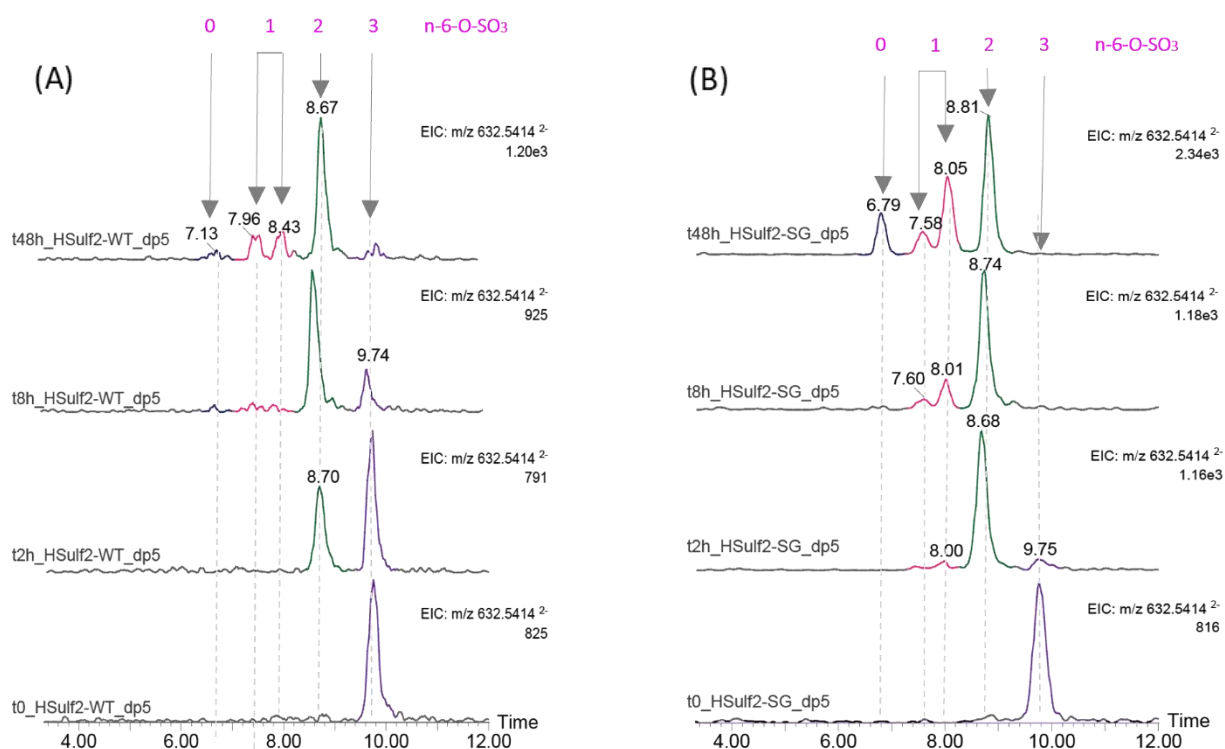


Figure 34: Extracted ion chromatograms of the triply desulfated species $[M-10Na+8H-3SO_3]^{2-}$ (m/z 632.52), showing the progression of HSulf-2 desulfation reaction on Fondaparinux (dp5) at $t=0, 2, 8,$ and $48h$. (A) HSulf-2 WT and (B) HSulf-2 SG mutant. Arrows and numbers (0-3) indicate the remaining 6-O-Sulfate groups. Color coding: intact species (purple), singly desulfated species (green), doubly desulfated species (pink), and triply desulfated species (blue). The m/z 632.52 is detected for all species due to method-induced desulfation, reflecting the predominant species at each time point. Retention times correspond to enzyme-induced desulfation, verified by extracting m/z values for intact, singly, doubly, and triply desulfated species.

This observation challenges the expected processive mechanism of HSulf-2's endosulfatase activity, where sulfate groups are typically removed sequentially from the non-reducing end toward the reducing end. Instead, our results suggest a more complex desulfation pattern for the Fondaparinux substrate. Initially, the enzyme appears to remove one sulfate group at a specific position, resulting in a single population of singly desulfated species. In the subsequent desulfation step, two distinct populations of doubly desulfated species emerge, indicating that the second sulfate removal can occur at two different positions. Last, a single population of triply desulfated species is observed.

Based on the structure of Fondaparinux and this observed desulfation pattern, we hypothesize that the first sulfate group removed is most likely the 6-OS on the GlcNS3S6S residue, which contains a 3-O-S group and is adjacent to the IdoA2S. The second desulfation step then involves the removal of either the 6-OS at the non-reducing end or the next 6-OS towards the reducing end. This hypothesis presents a potential explanation for the observed two populations of doubly desulfated species. It suggests a more flexible

desulfation mechanism for HSulf-2 on shorter oligosaccharides like Fondaparinux, possibly due to substrate size constraints that do not fill the requirements of the processive mechanism dictated by HSulf-2.

This pattern was consistent regardless of the presence or absence of the GAG chain. However, the increased activity in the absence of the GAG chain led to more pronounced and observable distinct populations of doubly desulfated species for the SG mutant enzyme.

Unlike the desulfation pattern seen with Fondaparinux, both the wild-type and SG mutant forms of HSulf-2 showed a single uniform population for each desulfated species on the dp8-3-*O*-S substrate (Figures 35A and 35B). This suggests a more processive mechanism for this longer oligosaccharide, aligning with HSulf-2's expected endosulfatase activity, where sulfate groups are removed sequentially from the non-reducing end toward the reducing end.

These patterns were consistent across other mutant species on both Fondaparinux and dp8-pnP substrates, supporting the idea that the pentasaccharide might represent a threshold length between fully processive endosulfatase activity and a more flexible desulfation pattern. We propose that this behavior could be due to the pentasaccharide's length being on the borderline of optimal substrate binding and processing by the HD domain for presentation to the active site.

Specifically, the longer dp8-3-*O*-S substrate likely provides enough length for stable interactions with the catalytic domain through binding to HD, allowing for a processive mechanism. In contrast, the shorter Fondaparinux may result in weaker interactions with HD, potentially leading to more flexibility and varied desulfation patterns.

This hypothesis offers a potential explanation for the observed differences in desulfation patterns between the two substrates and suggests that HSulf-2's mechanism may depend on substrate length. The enzyme seems to adapt its desulfation process based on oligosaccharide length, with longer substrates favoring a processive mechanism and shorter ones allowing for more flexible desulfation.

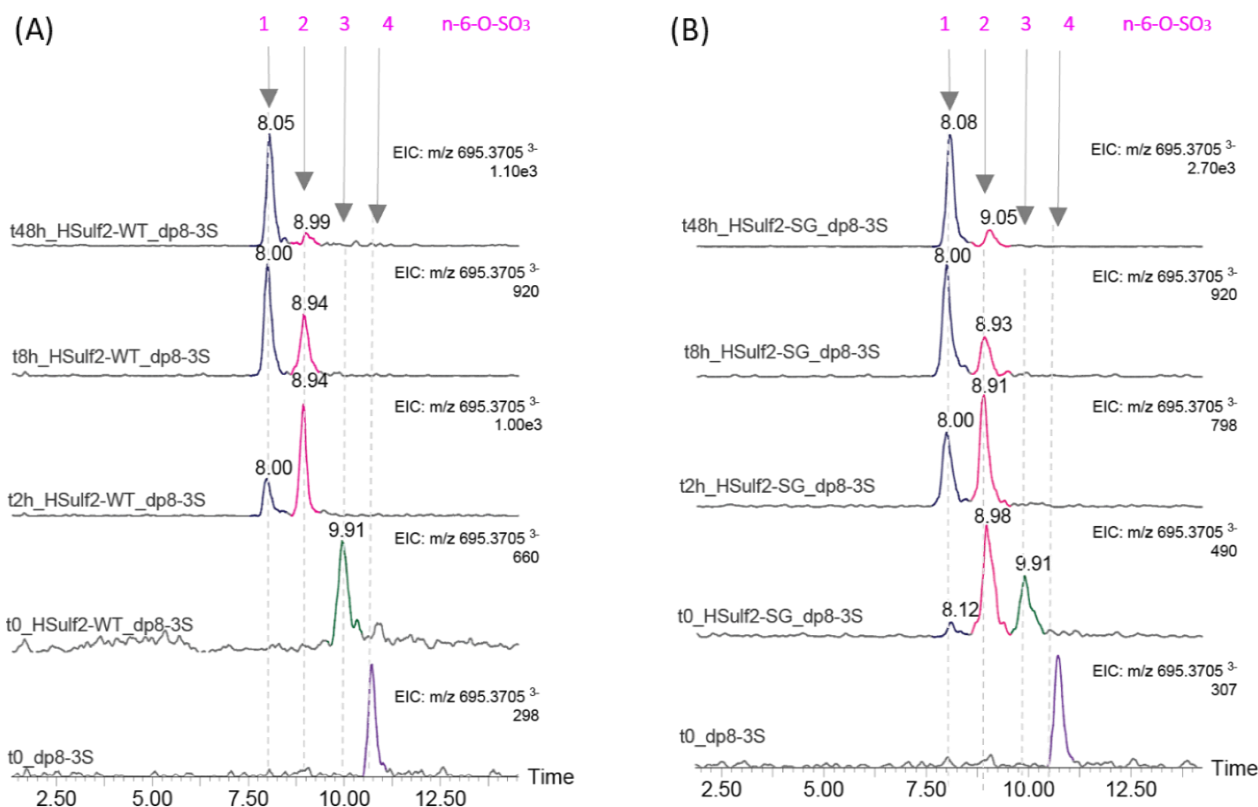


Figure 35: Extracted ion chromatograms of the triply desulfated species $[M-3H-3SO_3]^{3-}$ m/z 695.37 portraying the progression of HSulf-2 desulfation reaction on dp8-3-*O*-S and the present species at $t=0$, 2, 8, and 48h. (A) HSulf-2 WT and (B) HSulf-2 SG mutant. Arrows and numbers (1-4) indicate the remaining 6-*O*-Sulfate groups. Color coding: intact species (purple), singly desulfated species (green), doubly desulfated species (pink) and triply desulfated species (blue). The m/z 695.37 is detected for all species due to method-induced desulfation, reflecting the predominant species at each time point. Retention times correspond to enzyme-induced desulfation, verified by extracting m/z values for intact, singly, doubly, and triply desulfated species.

It is important to note that while these observations provide valuable insights into HSulf-2's 6-*O*-desulfation mechanism, further studies are warranted to confirm this aspect of HSulf-2's behavior. Additional experiments with a range of oligosaccharide lengths like dp4 and dp6 could help pinpoint the exact threshold for processive activity and provide a more detailed understanding of how substrate length influences HSulf-2's 6-*O*-desulfation mechanism. Future investigation should include testing a Δ HHD mutant to determine whether Fondaparinux desulfation relies solely on the catalytic domain or requires cooperative action between the catalytic and hydrophilic domains of HSulf-2.

3.2 Impact of mutations within the HD domain on HSulf-2 endosulfatase activity

To further investigate the impact of structural variations within HSulf-2, we assayed mutants within the HD domain, including DelC, N561Q, and the HDC mutants we characterized in the first chapter of the results section (Figure S1). Another form of the HDC mutant was used: HDC-TEV+PNGaseF with TEV protease treatment to remove the SNAP-tag and PNGase treatment for deglycosylation.

We first conducted comparative assays to evaluate the activities of wild-type HSulf-2, DelC, and N561Q mutants from the same sample preparation on the octasaccharide dp8-C lacking the 3-*O*-S group (Figure 36).

For the dp8-C substrate, HSulf-2 WT showed gradual desulfation over time, achieving approximately 95% desulfation of intact species after 24 hours. Within this period, HSulf-2 WT completely consumed the singly desulfated species, resulting in a mixture of doubly desulfated (50%) and triply desulfated (40%) products (Figure 36A).

In contrast, the HSulf-2-DelC variant exhibited much faster desulfation, consuming 97% of intact species in just one hour. This variant quickly produced triply and tetra-desulfated products, which dominated by 24 hours at 58% and 37%, respectively (Figure 36B). The HSulf-2-N561Q variant demonstrated an even more rapid initial desulfation, with 99% of intact species desulfated in one hour. Over time, the distribution of desulfated products shifted from triply desulfated (72% in one hour) to tetra-desulfated species (60% at 24 hours), suggesting continued enzyme activity on partially desulfated substrates (Figure 36D).

Notably, both mutant variants showed significantly enhanced desulfation rates and extents compared to the wild-type, with the ability to generate tetra-desulfated species not observed with the wild-type enzyme.

Furthermore, to assess the impact of N-glycosylation on endosulfatase activity, we performed a non-denaturing PNGaseF treatment on the wild-type enzyme. HSulf-2 is extensively *N*-glycosylated, with 9 out of 12 potential sites occupied (Benicky et al., 2023; Seffouh et al., 2023). PNGaseF, which cleaves *N*-linked glycoproteins at the innermost GlcNAc-asparagine bond, was used to remove these *N*-glycans while preserving the enzyme's native structure. The PNGaseF-treated wild-type enzyme (Figure 36C) showed faster initial desulfation of the dp8-C than the untreated wild-type (Figure 36A).

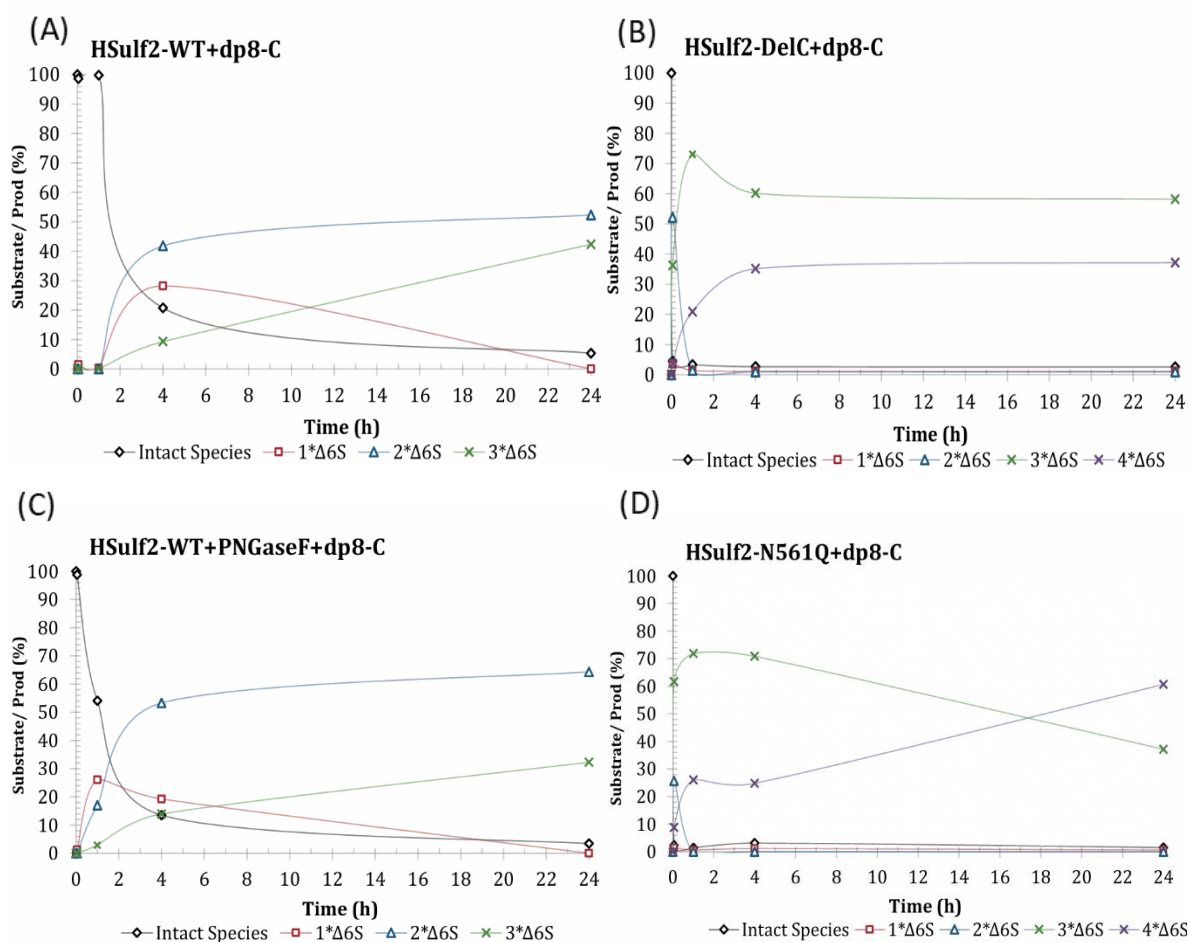


Figure 36: Impact of structural modifications on the endosulfatase activity of H sulf2 measured by HILIC-MS on the dp8-C octasaccharide over 48 hours. (A) H sulf2-WT, (B) H sulf2-DelC mutant, (C) H sulf2-WT+PNGaseF, and (D) H sulf2-N561Q mutant. Graphs represent the ratio of the intact substrate (black diamonds) and desulfated products: 1Δ6S (red squares), 2Δ6S (blue triangles), 3Δ6S (green crosses), and 4Δ6S (purple x's). Percentages correspond to the sum of intensities of each species divided by the sum of all present species at each time point of the reaction course. Background method-induced desulfation was subtracted from all measurements. dp8: octasaccharide; Δ6S: removal of 6-O-sulfate group.

Within the first hour, the PNGaseF-treated enzyme exhibited faster initial desulfation rates, reducing intact species to 46%, compared to 1% for the wild-type while portraying a similar pattern of generated desulfated products to the wild-type. These results did not correlate with findings by Benicky *et al.* (2023), reporting a dramatic 90% loss of H sulf2 activity upon partial deglycosylation. Our results align more closely with our recently reported findings (Seffouh 2023), who reported that reduced N-glycosylation profiles were sufficient to sustain H sulf2 integrity. Our observation of maintained and even enhanced activity for PNGaseF-treated H sulf2 indicates that while N-glycosylation clearly plays a role in modulating H sulf2 function, its effects may vary depending on the specific substrate and reaction conditions as well as on the extent of N-glycosylation.

Following these initial experiments, and with a second preparation of H sulf2 that included all previously mentioned (DelC, N561Q, and HDC) mutant forms, we wanted to further confirm and assess the impact

of the different mutations on the activity of HSulf-2 (Figure 37). We used Fondaparinux for this set of experiments due to a lack of dp8-C and dp-3-*O*-S availability. The pentasaccharide substrate was treated with HSulf-2 WT and mutants, with samplings taken at 0, 1, 4, and 24 hours throughout the reaction time course.

Most mutants exhibited increased initial rates and production of doubly desulfated species. Notably, although these mutations target distinct modifications, they all share the absence of the GAG chain, as shown in the first chapter.

The HDC+TEV+PNGaseF variant displayed rapid initial desulfation, with 50% of intact species desulfated within an hour. In contrast, HDC showed more gradual desulfation, consuming 15% of intact species in the same timeframe. The DelC variant exhibited rapid initial desulfation, achieving 40% desulfation compared to 30% for the N561Q mutant within the first hour.

The wild-type HSulf-2 demonstrated gradual desulfation, with 65% of intact species desulfated over 24 hours, primarily producing singly desulfated (1ΔS) products, which reached about 45% at 24 hours. It's important to note that while the wild-type showed reduced activity compared to previous Fondaparinux results—likely due to variability in enzyme preparations—the desulfation patterns remained consistent.

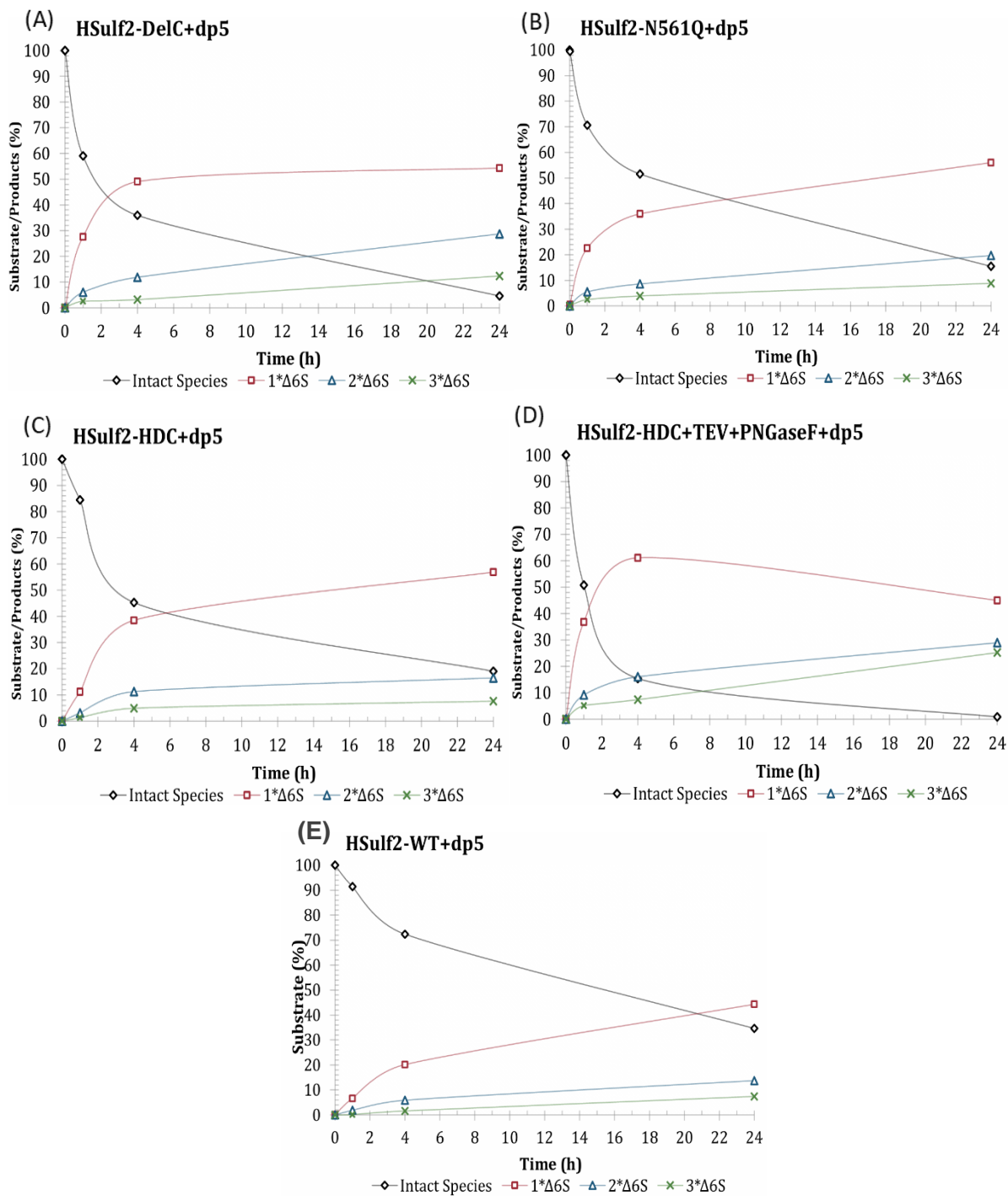


Figure 37: Impact of structural modifications on the endosulfatase activity of HSulf-2 measured by HILIC-MS on Fondaparinux over 24 hours. (A) HSulf-2-DelC mutant, (B) HSulf-2-N561Q mutant, (C) HSulf-2-HDC, (D) HSulf-2-HDC-TEV+PNGaseF, and (E) HSulf-2-WT. Graphs represent the ratio of the intact substrate (black diamonds) and desulfated products: 1 Δ 6S (red squares), 2 Δ 6S (blue triangles), and 3 Δ 6S (green crosses). Percentages correspond to the sum of intensities of each species divided by the sum of all present species at each time point of the reaction course. Background method-induced desulfation was subtracted from all measurements. dp8: octasaccharide; Δ 6S: removal of 6-O-sulfate group.

These findings suggested that mutations targeting specific regions within the HD domain, such as the internal region (HDC mutant), the helix of dimerization (DeIC mutant), and the glycosylation site near the secondary Furin cleavage site (N561Q), do not appear to reduce HSulf activity. Instead, the enhanced activity observed in these mutants likely results from a combined effect with the absence of the GAG chain, which we previously demonstrated to have a significant impact on HSulf activity. The modifications to the HD domain, removal of glycosylation sites, or alterations in GAG chain attachment could contribute to this enhancement. Still, their individual effects cannot be isolated from the impact of GAG chain absence. Moreover, the results of the HDC-TEV+PNGase mutant with Fondaparinux indicated that N-glycosylation is not strictly required for enzyme activity. This finding supports the results obtained with the PNGaseF-treated wild-type on dp8-C.

3.3 Comparative ion mobility-mass spectrometry (IM-MS) analysis of HSulf-1 and HSulf-2 desulfation patterns on Fondaparinux substrate

Our HILIC-MS analysis revealed heterogeneous desulfation patterns of Fondaparinux by HSulf-2, leading to two populations of doubly desulfated species. To further investigate this phenomenon, we employed ion mobility-mass spectrometry (IM-MS). This technique has emerged as a powerful tool for biomolecular analysis, including glycosciences, since the early 2000s (Fenn and McLean, 2008).

IM-MS offers superior resolving power for distinguishing isomers, which is particularly valuable for analyzing complex carbohydrate structures (Gray et al., 2016). In ion mobility spectrometry (IMS), gas-phase ions are separated based on size and shape as they interact with a buffer gas under an electric field. This separation is influenced by the ions' three-dimensional structure, making IMS effective for differentiating isomers and conformers (Lanucara et al., 2014). The mobility of an ion depends on its collision cross-section (CCS), allowing IMS to resolve structurally similar compounds that mass spectrometry alone cannot distinguish.

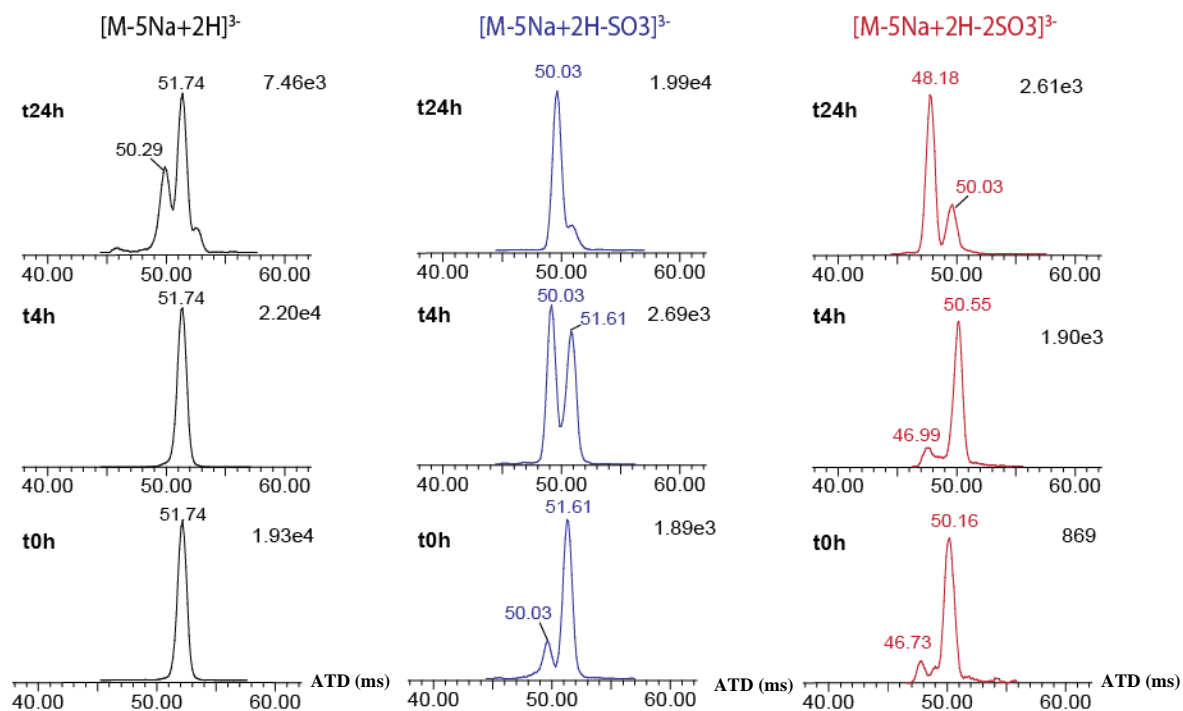
We specifically used cyclic ion mobility spectrometry coupled with mass spectrometry (cIMS-MS), a recent advancement that provides enhanced separation through multi-pass experiments (Giles et al., 2019). This approach improves the resolution of closely related isomeric species, crucial for elucidating subtle structural changes during HSulf-mediated desulfation.

To capture the time-dependent evolution of desulfation products, we conducted flow injection analysis (FIA) of samples taken at various time points from the reaction of HSulfs with Fondaparinux. The resulting mixtures were analyzed using cIMS-MS to resolve isomeric intermediates not distinguishable by HILIC-MS alone.

The cIMS-MS data revealed distinct desulfation patterns for Fondaparinux by HSulf-1 and HSulf-2 over 24 hours. We particularly monitored three species in the 3- charge state: intact (m/z 537.96, $[M-5Na+2H]^{3-}$), singly desulfated (m/z 511.31, $[M-5Na+2H-SO_3]^{3-}$), and doubly desulfated (m/z 484.65, $[M-5Na+2H-2SO_3]^{3-}$). Both enzymes showed similar overall desulfation trends but with distinct isomeric distributions (Figure 38A, 38B).

For the intact species, a single peak at the arrival time distributions (ATDs) of 51.74 ms gradually developed a shoulder at 50.29 ms by 24 hours, suggesting some conformational changes. Indeed, such second peak was ascribed to the emergence of at least one different pattern of counter-ions distribution (Na/H) within Fondaparinux backbone. The ATDs from desulfated forms, exhibited shorter times than the intact ones, as expected from smaller size pentasaccharide. Moreover, their ATDs shifted to shorter times with increasing reaction time, indicating a reduction in the overall size of the pentasaccharide according to the desulfation progression. The singly desulfated species initially showed two peaks (50.03 ms and 51.61 ms) for HSulf-1. That denoted the initial presence of desulfated forms traces, presumably due to sample or instrument conditions. HSulf-1 showed a faster transition to the 50.03 ms peak, while HSulf-2 maintained a more balanced distribution between (50.03 ms and 51.61 ms) over time. Regarding the doubly desulfated species, the initial ATDs were still lower than the singly desulfated ones (50.16 and 50.69 ms for HSulf-1 and HSulf-2), confirming the overall size reduction. HSulf-1 exhibited a single peak at 48.18 ms whereas HSulf-2 produced two distinct peaks at 48.18 ms and 50.03 ms by 24 hours.

(A) HSulf-1+Fondaparinux



(B) HSulf-2+Fondaparinux

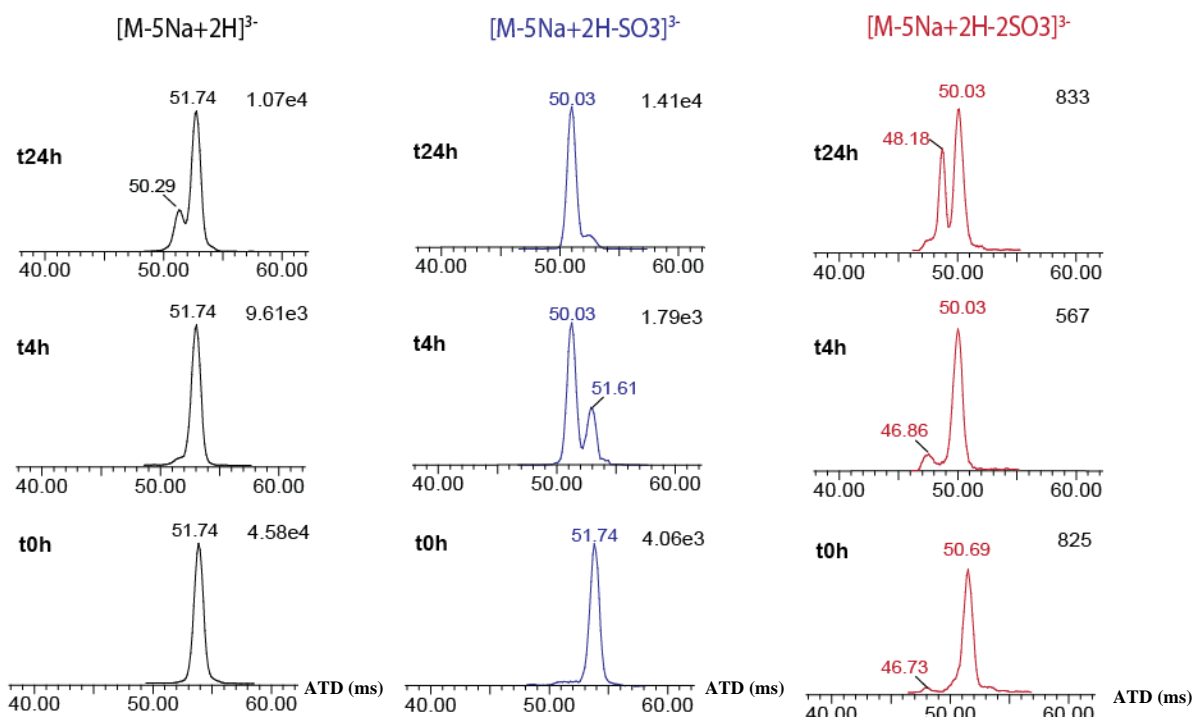


Figure 38: Time-course analysis of Fondaparinux desulfation by HSulf-1 and HSulf-2 using cyclic ion mobility mass spectrometry (cIMS-MS). (A) HSulf-1 + Fondaparinux. (B) HSulf-2 + Fondaparinux. Arrival time distributions (ATDs) are shown for three ionic species: intact Fondaparinux (m/z 537.96, $[M-5Na+2H]^{3-}$) (black trace), singly desulfated (m/z 511.31, $[M-5Na+2H-SO_3]^{3-}$) (blue trace), and doubly desulfated (m/z 484.65, $[M-5Na+2H-2SO_3]^{3-}$) (red trace) at t0h, t4h, and t24h (bottom to top in each panel). The x-axis represents ATD in milliseconds (ms).

The formation of multiple isomeric species, particularly for doubly desulfated products, suggests that both enzymes may remove sulfate groups from different positions on the Fondaparinux substrate. However, this could also arise from variations in counter-ion distribution.

The cIMS-MS technique highlights the complexity of substrate processing by HSulf-1 and HSulf-2. Distinct ATDs and multiple isomers of the intact substrate and desulfated species were observed in the (4⁻) and (5⁻) charge states (Figures S2 and S3 in Supplementary Information), confirming the intricate nature of Fondaparinux processing by HSulfs across different ionic forms.

To distinguish between desulfation patterns and counter-ion effects, future work will involve combining ion mobility with MS/MS to pinpoint specific sites of sulfate removal. We also plan to calculate collision cross-section (CCS) values and extend this approach to longer oligosaccharides than Fondaparinux for a more comprehensive understanding of HSulf activity on oligosaccharide substrates of defined sequence.

Chapter IV: Inhibitory effect of synthetic oligosaccharides with defined structures and modifications on HSulf activity



HSulf-1 and HSulf-2 have emerged as significant targets for small-molecule inhibition, with ongoing research identifying several compounds that offer valuable insights into their molecular mechanisms and therapeutic applications. As described earlier in the introduction section (see page 42), these inhibitors include phenyl sulfonyl derivatives, HS mimics, substrate sulfamate analogs, and trichloroethylsulfamates. Given the dual arylsulfatase (ARS) and endosulfatase activities of HSulfs, alongside the known inhibitory potential of sulfamate substituents, we utilized an arylsulfatase assay to examine the impact of competitive substrates on HSulfs activity.

Our aim was to explore the effect of synthetic oligosaccharides with defined structures and modifications on HSulfs activity. By comparing desulfation rates and profiles in the presence or absence of these potential inhibitors, we sought to elucidate their influence on HSulfs' functionality.

1 Evaluation of sulfamate-modified oligosaccharides as inhibitors of HSulf activity

We aimed to leverage the established knowledge of sulfamate groups as potent inhibitors of sulfatases, a strategy proven effective across various sulfatase enzymes. This approach was initially developed for steroid sulfatase inhibition (Woo et al., 2000), where sulfamate groups were shown to act as substrate mimics, binding to the active site but resisting hydrolysis. The proposed mechanism involved the formation of a covalent bond with the catalytic formylglycine (FGly) residue in the enzyme's active site, creating a stable enzyme-inhibitor complex (Bond et al., 1997; S. R. Hanson et al., 2004). Building on this foundational work, Schelwies *et al.* (2010) extended the sulfamate inhibitor approach specifically to HSulfs, demonstrating its potential for these enzymes. This strategy has since been further developed, with recent studies exploring various sulfamate-modified heparan sulfate (HS) oligosaccharides as HSulfs inhibitors (Chiu et al., 2020; Kennett et al., 2023).

To extend and further explore this approach, we investigated the inhibitory effects of a series of sulfamate-modified heparan sulfate (HS) synthetic oligosaccharides specifically designed to target HSulfs activity. These compounds were synthesized and kindly provided by our collaborator, Dr. Christine Le Narvor, from the Institut de Chimie Moléculaire et des Matériaux d'Orsay (ICMMO), Université Paris-Saclay, France. The design strategy of these compounds aimed at combining the specificity of HS oligosaccharides with the inhibitory power of sulfamate groups, potentially leading to potent and selective HSulf inhibitors.

The oligosaccharides we tested have the general structure of GlcNS6-(-OSO₂NH₂)-(IdoA2S-GlcNS6S)_n-propyl, where "n" represents the number of repeating disaccharide units. The chain lengths vary from trisaccharide (n=1) to nonasaccharide (n=4), allowing us to assess how chain length influences inhibitory efficacy. The sulfate group at the non-reducing end glucosamine residue (-OSO₃H) is replaced with a sulfamate group (-OSO₂NH₂), and a propyl linker is present at the reducing end.

We conducted a competition-based assay against the fluorogenic pseudosubstrate 4-methylumbelliferyl sulfate (4-MUS) to evaluate the inhibitory effects of these sulfamate-modified oligosaccharides at a fixed concentration of 50 μM on HSulf-2 wild-type (WT) and the N561Q, DeIC, SG, and HDC mutants (Figure 39).

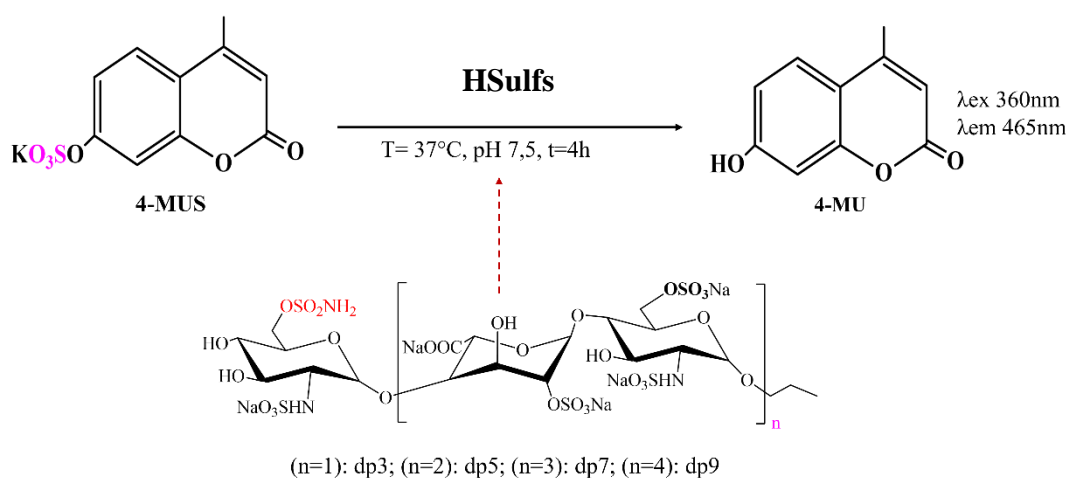


Figure 39: Schematic representation of the Arylsulfatase fluorogenic assay used to measure HSulf activity and inhibition. The primary reaction shows HSulfs catalyzing the hydrolysis of 4-methylumbelliferyl sulfate (4-MUS, 10 mM) to produce the fluorescent product 4-methylumbelliferone (4-MU), as indicated by a solid arrow. Sulfamate-oligosaccharide inhibitors are depicted as competing with 4-MUS for the enzyme's active site, shown by a dashed red arrow.

This initial screening was designed to provide insight into the influence of oligosaccharide length and the sulfamate modification at the non-reducing end on inhibition efficacy across different HSulf-2 constructs and to assess the impact of structural features, particularly within the HD domain and regarding the presence of the GAG chain. Our results revealed distinct inhibition patterns across the HSulf-2 constructs (Figure 40). Generally, all HSulf-2 mutants exhibited heightened sensitivity to the oligosaccharide inhibitors compared to WT. Despite variations in overall sensitivity, the relative inhibitory trends among dp3, dp5, dp7, and sulfamate-dp9 were largely consistent across the HSulf-2 constructs, with sulfamate-dp9 consistently inducing complete inhibition.

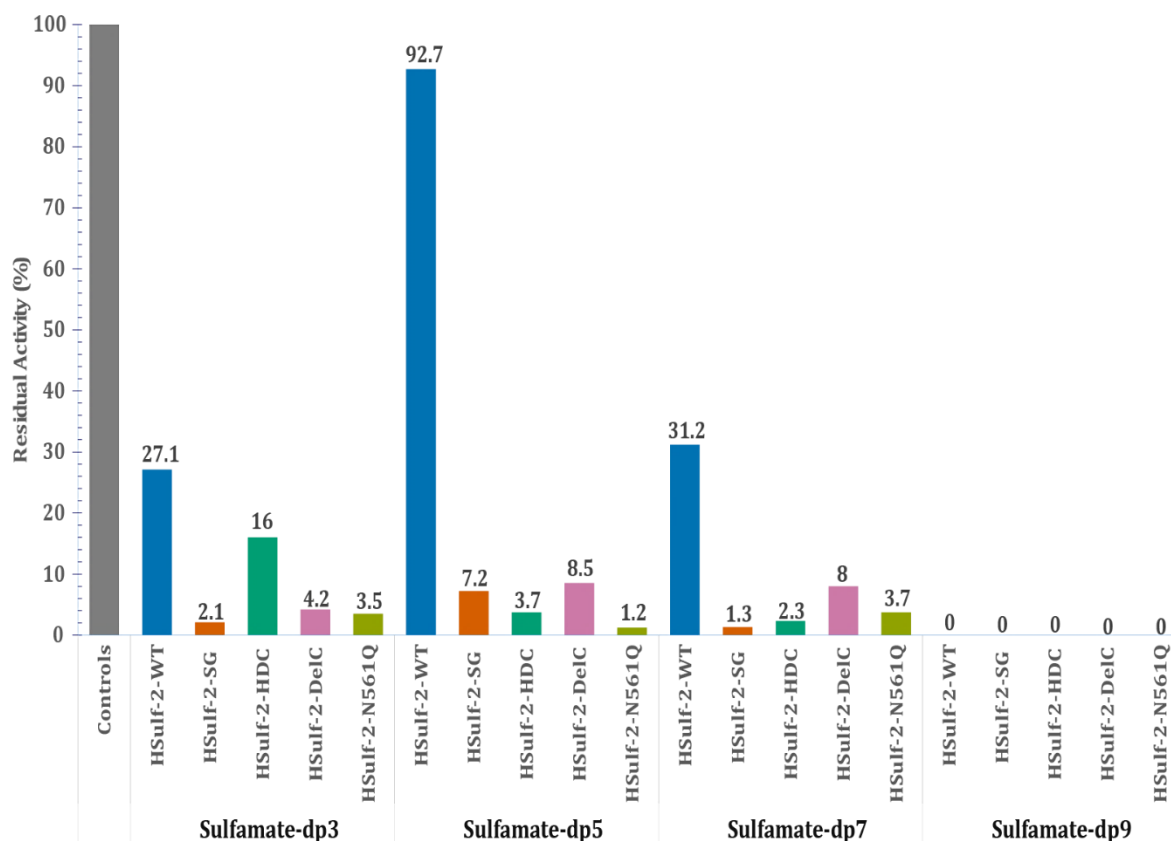


Figure 40: Inhibitory effects of Sulfamate-oligosaccharides (50 μ M) on HSulf-2 WT and mutants. Bars represent the percentage of residual activity compared to the control with no inhibitor (100%, gray bar). The data shown are from single measurements. Sulfamate-oligosaccharides of varying lengths (dp3, dp5, dp7, and sulfamate-dp9) were tested against HSulf-2 WT (blue) and its mutants: N561Q (orange), SG (green), HDC (pink), and DelC (light green). Complete inhibition or negative slopes are represented as 0% remaining activity.

All mutants share the strongest inhibition by sulfamate oligosaccharides, whether they carry a point mutation or a deletion of part of HD, suggesting that these alterations in the HSulf-2 structure make the enzyme more sensitive to the action of these inhibitors. We can hypothesize that this increased sensitivity is related to the structural and functional characteristics of these mutants that we have highlighted (see Chapter II, page 62), namely the absence of a GAG chain, an exclusively monomeric form, and higher sulfatase activity. We specifically showed that the mutants exhibit sulfatase activity four times higher than the WT with respect to the 4MUS substrate and under the same experimental conditions as those used in these inhibition experiments. Given this higher sulfatase activity, the pronounced drop in activity upon adding sulfamate-oligosaccharides appears all the more significant. It indicates their effectiveness in disrupting and inhibiting the catalytic mechanism of HSulf-2.

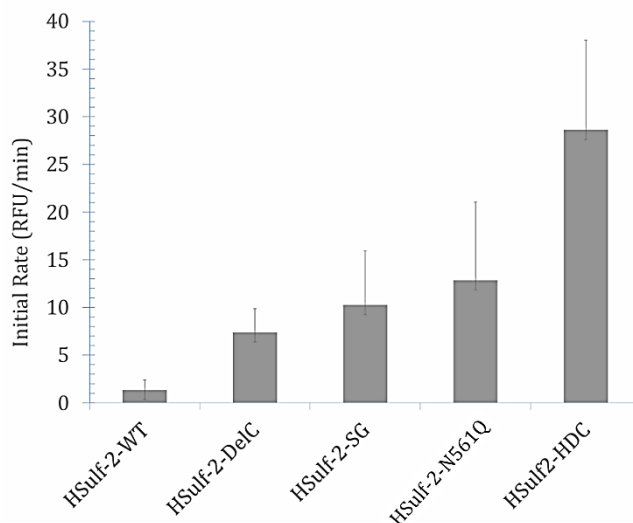


Figure 41: Average initial rates (Relative Fluorescence Units (RFU)/min) of HSulf-2 WT and mutant enzymes with 10 mM 4-MUS. The data represented is from triplicate measurements.

Regarding the possible mechanism of inhibition, a key consideration is that these mutants share the common feature of lacking the glycosaminoglycan (GAG) chain, as demonstrated by our C-PAGE analysis (Chapter II, page 67), and are in monomeric form. The absence or reduction of GAG chains may have contributed to increased inhibitor accessibility due to reduced electrostatic repulsion between the polyanionic GAG chain and the sulfamate-oligosaccharides. Similarly, we can hypothesize that the dimeric association may also hinder access to the active site. This mechanism potentially explains both the increased baseline activity and the heightened susceptibility to inhibition by sulfamate-oligosaccharides observed in the mutant constructs.

The strong inhibition by sulfamate-oligosaccharides confirmed the value of the sulfamate chemical function and its insertion into sulfated oligosaccharide sequences to achieve potent and specific inhibition. This specificity could be attributed to the structural similarity of these compounds to their natural substrates, unlike the pseudosubstrate 4-MUS, as previously suggested (Schelwies et al., 2010). This specificity relies on the interaction of sulfamate oligosaccharides with the HD domain, which is fully present in the point mutants and partially missing in the HDHC mutant. However, in the latter, the patches of positively charged residues at the C-terminal regions of the HD domain involved in the interaction with sulfated substrates are retained.

The consistent observation of sulfamate-dp9 achieving complete inhibition across all HSulf-2 constructs, including the WT, underscored the potent inhibitory capacity of this oligosaccharide length. This effect persisted regardless of the structural specificity of each construct, indicating that sulfamate-dp9

effectively inhibited HSulf-2 activity, irrespective of the presence or absence of the GAG chain and the mutations introduced within the HD domain. One possible interpretation is that HD binds with high affinity to the sulfamate oligosaccharides and presents them to the catalytic domain through the binding site around the catalytic pocket, hindering access for the 4-MUS pseudosubstrate. The interaction with these binding sites within the catalytic domain, as well as the C-terminal and N-terminal regions of the HD domain, identified as heparan sulfate (HS) binding sites (Frese et al., 2009; Ilham et al., 2019), may also induce conformational changes that rendered the entry of 4-MUS into the catalytic site unfavorable. However, further replicates were needed to confirm these trends and accurately assign structure-activity relationships.

To investigate whether the observed inhibitory effects of the sulfamate-modified oligosaccharides were consistent across the two HSulf forms, we also conducted similar inhibition tests on HSulf-1. However, the significantly lower baseline activity of HSulf-1 compared to HSulf-2 (Figure 42) made it difficult to define the range of inhibition for HSulf-1 clearly. Despite this limitation, we attempted to measure the effects of the oligosaccharide inhibitors on HSulf-1; preliminary results (not shown) showed similar trends to those observed with HSulf-2. This observation suggested a similar pattern of inhibition across both HSulf forms.

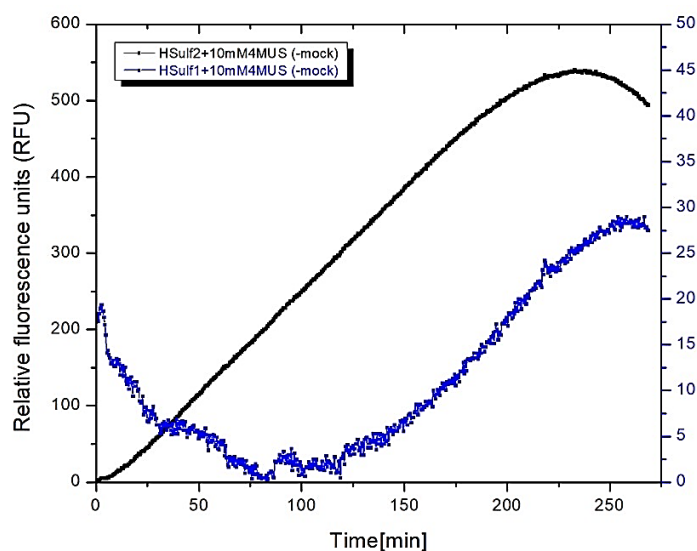


Figure 42: Aryl-sulfatase activity of HSulf-1 (blue) and HSulf-2 (black) (1 μ g each) with 10 mM 4-MUS. Traces represent the emitted fluorescence upon 4-MUS desulfation reaction catalyzed by HSulfs within 4 hours. Background fluorescence of 4-MUS without the enzyme was accounted for with mock subtraction.

2 Effect of the length of heparin oligosaccharides as competitive inhibitors (dp2, dp5, dp6 and dp8).

To further elucidate the impact of oligosaccharide length on HSulf-2 arylsulfatase inhibition, independent of the sulfamate modification, we evaluated the inhibitory effects of various heparan/heparin oligosaccharides. These oligosaccharides included dp2 (Δ UA–GlcNS6S), dp5: Fondaparinux (GlcNS6S–GlcA–GlcNS3S6S–IdoA2S–GlcNS6S1Me), dp6 (UA,2S–GlcNS6S–IdoA2S–GlcNS6S–IdoA2S–GlcNS6S), and dp8-C (GlcNAc6S–GlcA–GlcNS6S–IdoA2S–GlcNS6S–IdoA2S–GlcNS6S–GlcA–pnp), which were either enzymatically generated post-HP degradation using heparinases or chemically synthesized (Figure S6). These oligosaccharides' varying lengths and structures allowed for a lengthwise comparison with the previously tested sulfamate-modified oligosaccharides.

We conducted competition assays using the HSulf-2 SG mutant due to its heightened responsiveness compared to the wild type, as observed in our previous experiments. This allowed for more sensitive inhibition detection and showed generally similar trends to the wild type, making it a suitable construct to study.

The results revealed a length-dependent inhibitory effect of oligosaccharides on the SG mutant of HSulf-2 (Figure 43). Shorter oligosaccharides (dp2 and dp5) exhibited moderate inhibition, with 10.2% and 17.9% residual activities, respectively. In contrast, longer oligosaccharides (dp6 and dp8) completely inhibited HSulf-2 activity. Interestingly, HSulf-2 does not hydrolyze the 6-*O*-sulfated dp2, yet, it appears as an inhibitor of sulfatase activity here. This result suggests that dp2 accesses the catalytic domain, competing with 4-MUS, but because HD does not present it due to its short length, it is not properly positioned relative to the catalytic residues.

By comparing these results with previously tested sulfamate-modified HS oligosaccharides, we observed a consistent trend of increased inhibition with oligosaccharide length, with one notable exception. In both sets, dp5 showed slightly less inhibitory effect than other lengths, regardless of sulfamate modification. However, sulfamate-modified dp5 demonstrated higher inhibition (7.2% residual activity) compared to unmodified dp5 (17.87% residual activity), highlighting the enhancing effect of sulfamate modification in inhibition.

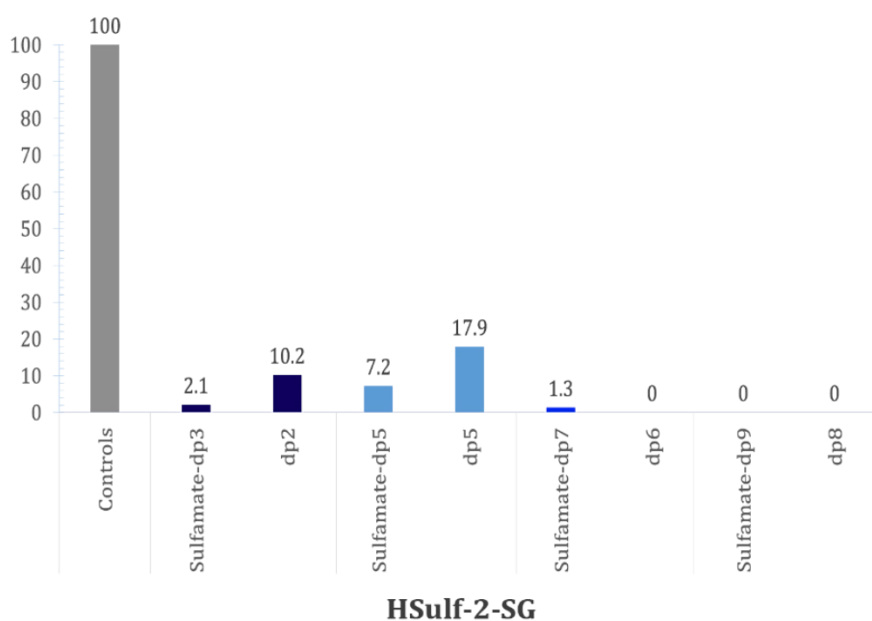


Figure 43: Comparison of inhibitory effects of sulfamate-modified oligosaccharides (dp3, dp5 (fondaparinux), dp7, sulfamate-dp9) to unmodified heparin oligosaccharides (dp2, dp5, dp6, dp8) at 50 μ M concentration on HSulf-2 SG mutant activity. Bars represent the percentage of remaining activity compared to those with no inhibitor (100%). The data shown are from single measurements. Cases of complete inhibition or negative slopes are represented as 0% remaining activity.

These results highlighted that oligosaccharide length and sulfamate modification were crucial for efficient inhibition in competition with 4-MUS. Longer oligosaccharides increased the inhibitory effect, as evidenced by the complete inhibition observed with dp6 and dp8. However, the consistently reduced efficacy of dp5 across both modified and unmodified series suggested that optimal inhibition depended on a complex interplay of factors beyond mere chain length and sulfamate modification for HSulf-2-SG. This observation implied that the inhibitory effect relied on a more complex mechanism, possibly involving specific structural features to induce conformational change. In the case of HSulfs, this required sufficient size, which we suggested beyond dp5, to guarantee interaction with binding sites. These findings underscored the importance of considering multiple molecular characteristics when designing potential HSulf-2 inhibitors.

3 Inhibitory effect of the sulfamate dp9 on HSulf-2 SG mutant and wild-type arylsulfatase activity

Considering the observed length-dependent effect and the higher efficacy of the sulfamate nonasaccharide (sulfamate-dp9) from our previous results, we aimed to characterize its inhibitory potential further. To achieve this, we prioritized optimizing enzyme use and gaining a more precise understanding of the inhibition mechanism by focusing our subsequent experiments on HSulf-2 WT and the SG mutant. Consequently, we conducted dose-response experiments to assess the inhibitory potency of sulfamate-dp9 on these two enzyme forms. The sulfamate-dp9 was tested at a concentration range from 50 nM to 50 μ M against 10 mM of the 4-MUS substrate. This range was chosen to span several orders of magnitude below the previously tested 50 μ M, which induced complete inhibition in the previous assays.

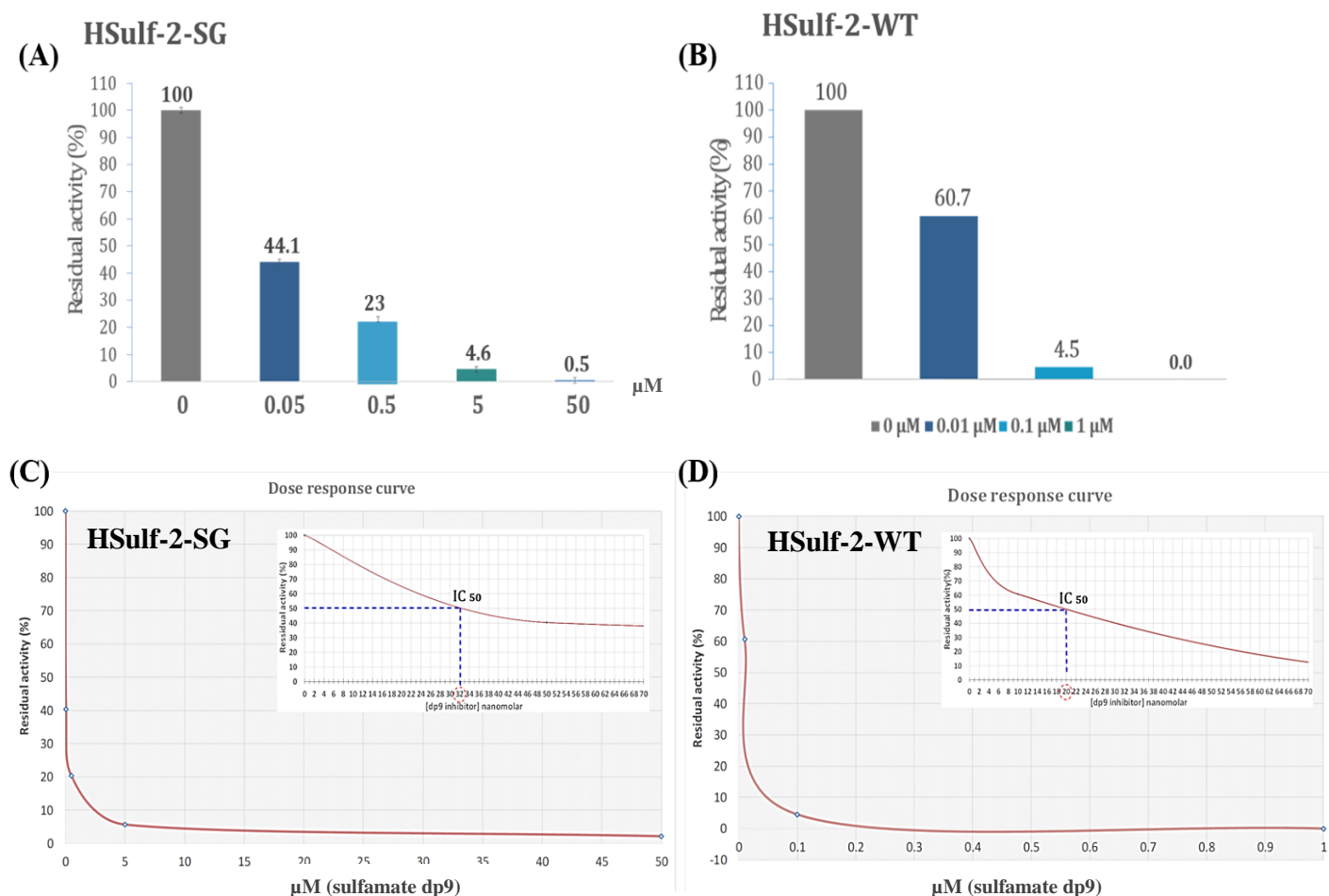


Figure 44: Inhibitory effects of sulfamate-dp9 oligosaccharide on the arylsulfatase activity of HSulf-2 SG mutant and wild-type (WT) (1 μ g each) in the presence of 10 mM 4-MUS. (A) Residual activity (%) of the SG mutant at varying concentrations of sulfamate-dp9 oligosaccharide in μ M. (B) Residual activity (%) of HSulf-2 WT at varying concentrations of sulfamate-dp9 oligosaccharide in μ M. (C) Dose-response curve for the SG mutant, depicting the percentage of residual activity as a function of sulfamate-dp9 concentration. (D) Dose-response curve for HSulf-2 WT, illustrating the percentage of residual activity as a function of sulfamate-dp9 concentration, with the IC₅₀ value determined graphically. 4-MUS hydrolysis rates in the absence of the sulfamate-sulfamate-dp9 were set to 100%.

Our initial experiments with the SG mutant revealed a clear dose-dependent response to sulfamate-dp9 (Figure 44A). As the oligosaccharide concentration increased, we observed a corresponding decrease in residual enzyme activity. Notably, even at the lowest concentration tested (50 nM), sulfamate-dp9 demonstrated significant inhibitory effects, with an average residual activity of 44.3% across two replicates. This marked inhibition at such low concentrations underscored the potency of sulfamate-dp9 as an inhibitor of HSulf-2 activity. The dose-response relationship between residual activity and sulfamate-dp9 concentration for the SG mutant was characterized by a steep decline in residual activity, particularly at lower sulfamate-dp9 concentrations (Figure 44C). This profile allowed for the graphical determination of the IC₅₀ value, which was calculated to be 32 nM for the SG mutant. To compare these findings with HSulf-2 WT, we tested a reduced but proportionally similar range of inhibitor concentrations (0.01, 0.1, 1 μM), starting at 10 nM (Figure 44B). HSulf-2 WT exhibited marked responsiveness to sulfamate-dp9, with 4.5% residual activity observed at 0.1 μM compared to an average of 23% at 0.5 μM for the SG mutant. Analysis of the dose-response relationship for HSulf-2 WT yielded an IC₅₀ of 20 nM. Despite the apparent higher sensitivity of HSulf-2 WT at specific concentrations, the overall IC₅₀ values suggest similar sensitivity to sulfamate-dp9 for both the WT and SG mutant (Figure 44B).

To estimate the IC₅₀ more accurately for the SG mutant, a 4-parameter logistic (4PL) model was applied to the data using Origin. The 4PL model is represented by the equation:

$$y = A1 + \frac{A2 - A1}{1 + \left(\frac{x}{IC_{50}}\right)^p}$$

where *y* is the response, *A1* and *A2* are the minimum and maximum asymptotes, *x* is the concentration of the inhibitor, *x* is the IC₅₀, and *p* is the slope factor. Due to the limited number of data points in the lower range of the sigmoid curve, *A1* was fixed to 0 (Figure S4). This approach provided an IC₅₀ value of 31.45 ± 9.34 nM for the SG mutant, consistent with the graphically determined value. We also applied the 4PL model to the limited HSulf-2 WT data, which yielded an estimated IC₅₀ of 34.68 nM. Despite the insufficient number of data points for HSulf-2 WT, it is noteworthy that this estimate falls within the same range (20-35 nM) as the IC₅₀ determined for the SG mutant. However, due to the limited data for HSulf-2 WT, this estimate should be interpreted with caution and considered preliminary. Further experiments with more data points and replicates for both constructs are necessary to validate these findings and enable a more robust comparison of their sensitivity to sulfamate-dp9 inhibition.

To further characterize the inhibitory mechanism of sulfamate-dp9, we tested a range of 4-MUS concentrations to evaluate the inhibitory effect of sulfamate-dp9 across varying substrate concentrations. We observed a consistent increase in inhibition with increasing concentrations of sulfamate-dp9 at 1 mM and 10 mM 4-MUS substrate concentrations (Figure 45). This pattern suggested a potential non-competitive inhibition mechanism, as the inhibitory effect persisted across different substrate concentrations, indicating that the inhibitory effect of sulfamate-dp9 is maintained independent of the 4-MUS concentration.

In non-competitive inhibition, the inhibitor binds to a site distinct from the substrate-binding site, causing a conformational change in the enzyme that results in reducing the catalytic activity without directly competing with the substrate (Berg et al., 2002). This mechanism is consistent with our earlier hypothesis that sulfamate oligosaccharides might bind to HSulf-2 through the HS binding sites located within HD and the catalytic domains consecutively, potentially causing conformational changes that affect HSulf arylsulfatase activity. However, this interpretation raises two important questions: firstly, are these sulfamate compounds substrates of HSulfs in addition to being inhibitors? And secondly, could their inhibitory effect be due to more complex interactions beyond simple binding-induced conformational changes?

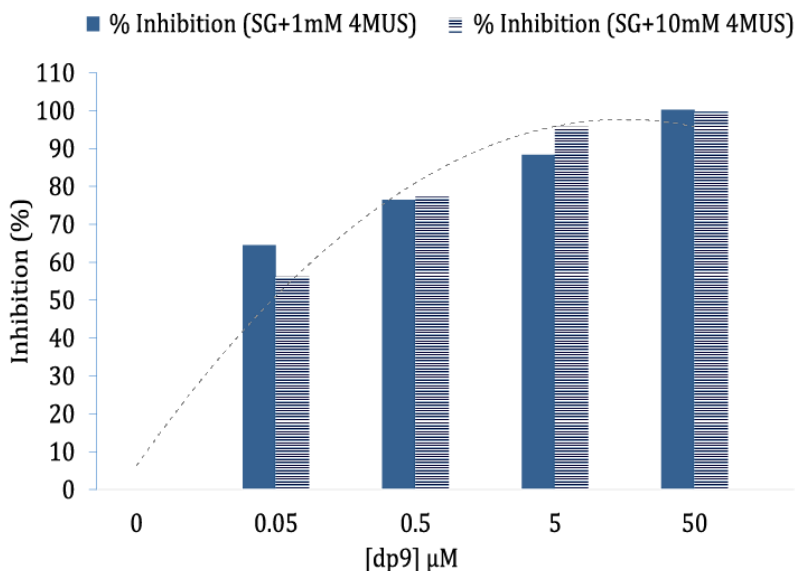


Figure 45: Inhibition of SG mutant by sulfamate-dp9 at different 4-MUS concentrations. The bar graph illustrates the percentage inhibition of the SG mutant by varying concentrations of sulfamate-dp9 (0, 0.05, 0.5, 5, and 50 μM) in the presence of two substrate concentrations: 1 mM (solid, blue bars) and 10 mM (striped, blue bars) 4-MUS. The dotted line shows the trend of increasing inhibition with higher sulfamate-dp9 concentrations, highlighting the dose-dependent inhibitory effect of sulfamate-dp9 on the SG mutant. X-axis: μM (sulfamate-dp9).

4 Inhibitory effect of the sulfamate dp9 on HSulf-1 and HSulf-2 endosulfatase activity

To investigate the potential dual role of sulfamate-dp9 as both a potential inhibitor and substrate, we conducted the HILIC-MS endosulfatase assay of HSulf-1 and HSulf-2 using the sulfamate nonasaccharide (sulfamate-dp9) as substrate. Remarkably, both enzymes could remove 6-*O*-sulfate groups from sulfamate-dp9, with maximum removal of three 6-*O*-Sulfate groups observed within 30 hours of reaction time (Figure 46). To ensure the validity of these results, we included controls using denatured enzymes and the oligosaccharide without enzymes, which confirmed that the desulfation was indeed enzymatic and not an artifact of the experimental conditions

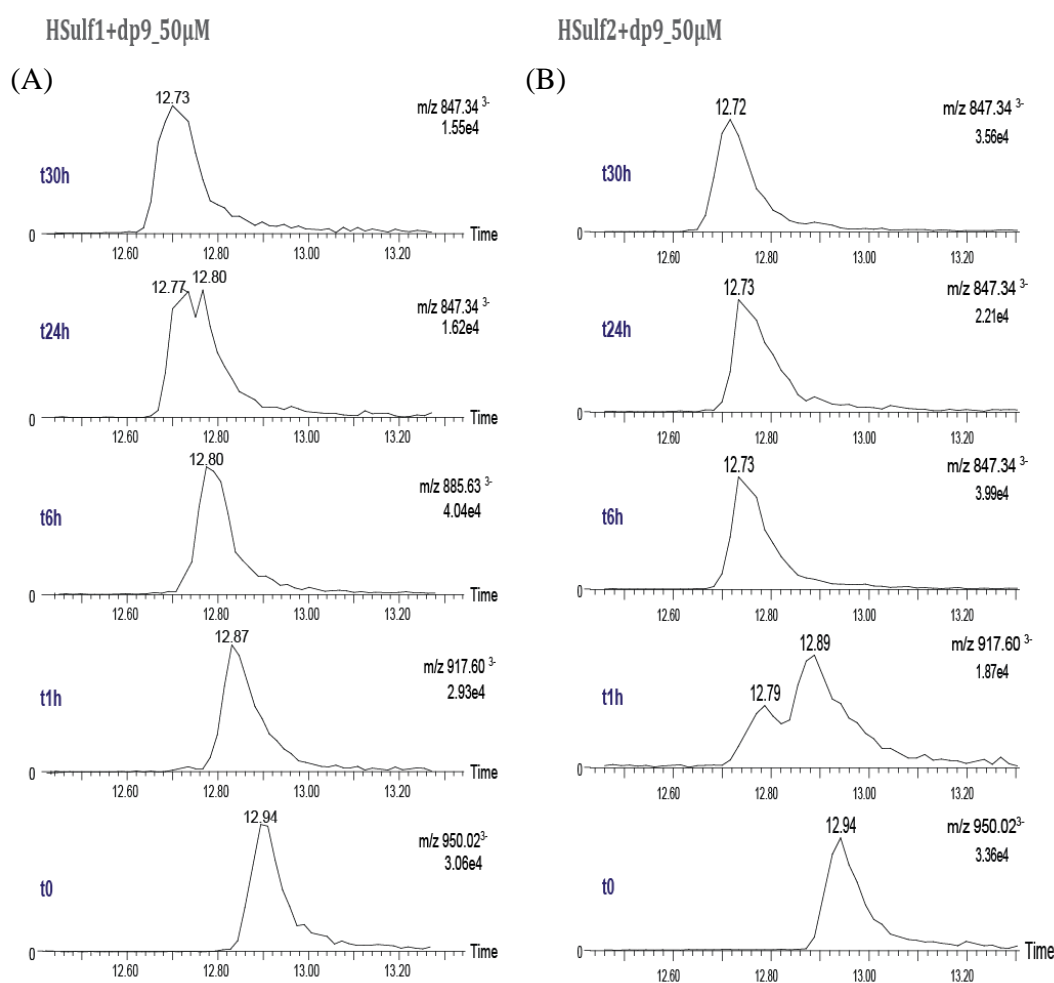


Figure 46: Time-course analysis of sulfamate-dp9 desulfation by HSulf-1 and HSulf-2. HILIC-MS extracted ion chromatograms showing the enzymatic processing of (sulfamate-dp9) by HSulf-1 (A) and HSulf-2 (B) over 30 hours. Chromatograms are arranged from bottom to top, representing time points t0, 1h, 6h, 24h, and 30h. Triply charged species are shown with m/z values indicating intact sulfamate-dp9 (950.02³⁻), singly desulfated (917.60³⁻), doubly desulfated (885.63³⁻), and triply desulfated (847.34³⁻) forms. Peak shifts from right to left reflect increasing desulfation over time. Changing intensities and retention times demonstrate progressive sulfate removal by both enzymes, confirming sulfamate-dp9 as a substrate for HSulf-1 and HSulf-2.

Having established that sulfamate-dp9 can act as a substrate for HSulfs, we next examined its impact on the desulfation of the dp8-C, (dp8-C: GlcNAc6S-GlcA-GlcNS6S-IdoA2S-GlcNS6S-IdoA2S-GlcNS6S-GlcA-pnp). HSulf-1 and HSulf-2 were preincubated with sulfamate-dp9 for 30 minutes prior to the addition of dp8-C at a 1:5 inhibitor-to-substrate ratio. The reaction was monitored over a 48-hour time course, with samples taken at 0, 1, 6, 24, and 48 hours to assess the effect of sulfamate-dp9 on the desulfation rates of dp8-C compared to controls without the inhibitor (Figure 47).

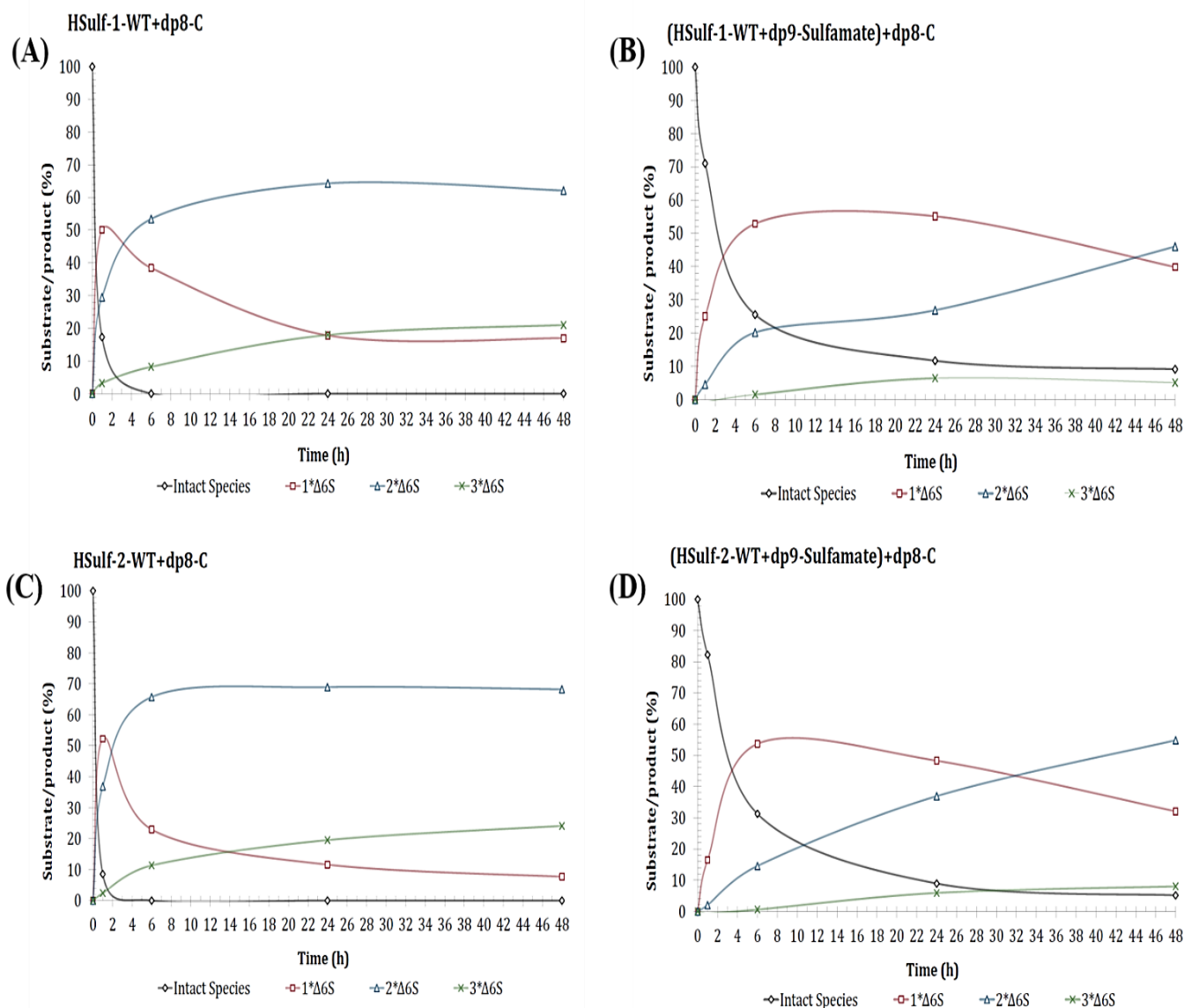


Figure 47: Time-course analysis of HSulf-1 and HSulf-2 desulfation activity on dp8-C with and without sulfamate-dp9 inhibitor. The graphs show the desulfation of synthetic octasaccharide dp8-C by HSulf-1 (A, B) and HSulf-2 (C, D) over 48 hours. Panels A and C represent control reactions without inhibitor, while B and D show reactions with sulfamate-dp9 present. The y-axis shows the percentage of substrate/product, and the x-axis displays reaction time in hours. Data points were collected at 0, 1, 6, 24, and 48 hours. Color code: Black - Intact dp8-C species, Red - Singly desulfated species (1 Δ 6S), Blue - Doubly desulfated species (2 Δ 6S), Green - Triply desulfated species (3 Δ 6S). The graphs illustrate the evolution of intact substrate and generated desulfated products over time, demonstrating the inhibitory effect of sulfamate-dp9 on both HSulf-1 (B) and HSulf-2 desulfation activity (D).

In the presence of sulfamate-dp9 (Figure 47B, 47D), we observed a significant decrease in the initial desulfation rates of dp8-C for both HSulf-1 and HSulf-2 compared to the control reactions (Figure 47A, 47C). For HSulf-1, the initial reaction rate (Figure 47B) showed a marked decrease, with only about 30% of the substrate desulfated after one hour, compared to approximately 90% for the control reaction (Figure 47A). Similarly, HSulf-2 activity was notably reduced, with the inhibited reaction (Figure 47D) showing a slower rate of only about 20% compared to nearly 100% of the substrate desulfation within the first hour in the absence of sulfamate-dp9 (Figure 47C). This inhibitory effect persisted throughout the 48-hour time course for both enzymes with consistently lower levels of desulfation than controls. The presence of sulfamate-dp9 significantly altered the distribution of desulfated products for both HSulf-1 and HSulf-2 at 48 hours. We observed the formation of only 15% doubly and triply desulfated species and, consequently, the persistence of singly desulfated species in the reaction medium. These changes suggest that in the presence of sulfamate-dp9, the enzymes could not reach the later stages of the desulfation process, leading to an accumulation of singly desulfated intermediates.

The dual role of sulfamate-dp9 as both a substrate and an inhibitor highlights the complex interaction between sulfamate oligosaccharides and HSulfs. The sulfamate modification does not entirely prevent enzyme recognition, indicating flexibility in substrate binding. The simultaneous processing of both compounds suggests a complex mechanism involving competitive substrate behavior and potential allosteric effects. These findings warrant further investigation into the precise mechanism of inhibition.

In comparison to the competition assay with 4-MUS, the endosulfatase assay revealed more specific effects, suggesting a complex interplay between sulfamate oligosaccharides and HSulfs. Future studies using this assay could provide deeper insights into the kinetics and structural basis of inhibition, uncovering nuances in the mechanism that were not apparent in the less specific 4-MUS-based assays. Such investigations could be crucial for understanding the full potential of these sulfamate oligosaccharides as tools for studying HSulf function and as potential therapeutic agents.

Chapter V: Discussion and Perspectives

HSulfs are a unique class of sulfatases that have garnered significant attention due to their distinctive structural features and far-reaching functional implications. Despite causing only a 4-5% reduction in overall heparan sulfate (HS) sulfation, HSulfs dramatically alter HS binding properties, highlighting the profound impact of their targeted modifications. Over the past two decades, these enzymes have been the subject of increasing scientific interest, with studies focusing on various aspects, including their physiological impact, their role in pathological processes, particularly in cancer, and the characterization of their structure-function relationships. One of the most striking features of HSulfs is their structural complexity, which sets them apart from other sulfatases. They possess a hydrophilic domain that is exclusive to their subfamily, and recently, HSulf-2 has been classified as both a sulfatase and a proteoglycan, a rare dual classification that highlights the exceptional nature of these enzymes. The intricate post-translational modifications and the unique domain organization of HSulfs raise intriguing questions about their impact on enzyme activity, as well as the potential interplay between these modifications. In this PhD research, we aimed to elucidate further the relationship between the structural properties and functional characteristics of HSulfs, seeking to provide a rationale for their unique features within the sulfatase family.

1 Impact of post-translational modifications (PTMs) and domain organization on HSulfs structure and function

Our approach focused on investigating the structural characteristics and oligomerization tendencies of HSulfs under native-like conditions. We placed particular emphasis on the impact of post-translational modifications (PTMs), primarily of the GAG chain, on protein size and the role of specific structural features such as the hydrophilic domain. We examined both wild-type HSulfs and mutants targeting specific structural elements. To assess relationships between structural features and functionality of HSulfs, we conducted parallel activity assays to understand the direct impact of structural elements and mutations on HSulf activity. This combined approach was designed to correlate structural properties with functional consequences regarding the enzyme activity, with a particular focus on the HSulf-2 enzyme.

Our work has demonstrated for the first time the use of atomic force microscopy (AFM) to characterize HSulf-2, with the unique feature of doing so in solution to closely mimic biological conditions, thereby preserving its native structure. Using AFM under these native-like conditions, we observed a clear impact of the GAG chain on the size of HSulf-2 at the single-molecule level, expanding on previous observations made using techniques such as small-angle X-ray scattering (SAXS) and size-exclusion chromatography coupled with multi-angle laser light scattering (SEC-MALLS) (El Masri *et al.* 2022). Additionally, we noticed a clear tendency for HSulf-2 to form larger assemblies, suggesting the presence of oligomeric states. This tendency was enhanced by the glycosaminoglycan (GAG) chain for the wild-type enzyme compared to the GAG-deficient mutant. These findings prompted us to focus specifically on the oligomerization aspect of HSulf-2, which was further confirmed by mass photometry analysis. Both the wild-type and the GAG-deficient mutant tended to dimerize, with a more pronounced tendency for the wild-type, indicating that while the GAG chain is involved in this phenomenon, it primarily relies on an intrinsic feature of the protein. Previous work by Tang & Rosen (2009) suggested that the C-terminal region might be responsible for multimerization. The presence of coiled-coils (A623 - E658), as reported by Morimoto-Tomita *et al.* (2002), further supports the idea that the hydrophilic domain (HD), through its double alpha helices, mediates oligomerization.

These observations prompted us to explore two critical aspects of HSulf-2 oligomerization. First, we aimed to determine whether the intrinsic structural feature responsible for dimerization is located within the hydrophilic domain (HD) and if this domain facilitates physiologically relevant dimerization of HSulf-2 under native conditions. Second, we sought to understand the modulatory role of the glycosaminoglycan (GAG) chain on the HD-driven oligomerization process, examining how this unique post-translational modification influences the oligomeric state of HSulf-2.

Mass photometry and size exclusion chromatography analysis of the isolated hydrophilic domain (HD)

of HSulf-2 under native conditions confirmed its intrinsic tendency for dimerization. It is worth noting that isolated HD was produced in an *E.coli* expression system. This finding underscored the HD's crucial role in the oligomerization tendency of HSulf-2, independent of eukaryotic post-translational modifications, such as the GAG chain formation. Further investigation using HSulf-2 mutants to characterize the impact of the HD regions on the whole protein provided additional support for the HD's implication on oligomerization. A truncation mutant within the HD domain (HDC), lacking the central region D483 to C636, showed a strong tendency towards monomeric forms compared to the wild type. Similarly, mutants targeting the coiled-coil element (delC, where Leu638 and Ile642 are replaced by tryptophan) and a glycosylation site proximal to furin cleavage sites (N561Q, where asparagine is replaced by glutamine) also exhibited increased monomeric tendencies, providing additional evidence for the critical role of these structural features within HD in oligomerization.

The analysis of delC and N561Q mutants using SDS-PAGE unexpectedly revealed similar profiles under reducing and non-reducing conditions, *i.e.*, the monomer state being the main form of both mutants. This observation prompted us to consider the role of disulfide bonds in HSulf-2's structural integrity and oligomerization, building upon previous work in our laboratory by Mélanie Bilong (2021). This work identified key disulfide bonds within the HD domain, with 8 out of 10 cysteine residues implicated in disulfide bridge formation (C446, C455, C464, C477, C504, C506, C660, C662) concentrated within this region. Notably, these disulfide bridges were also observed in the isolated HD expressed in bacterial systems, suggesting their formation is intrinsically driven by the protein sequence. The proximity of the delC and N561Q mutations to the residues C660 and C662 involved in the intra-chain disulfide bridge in HSulf-2 may alter the overall structure of HD and, somehow, impact the balance of disulfide bridge formation (Figure 48).

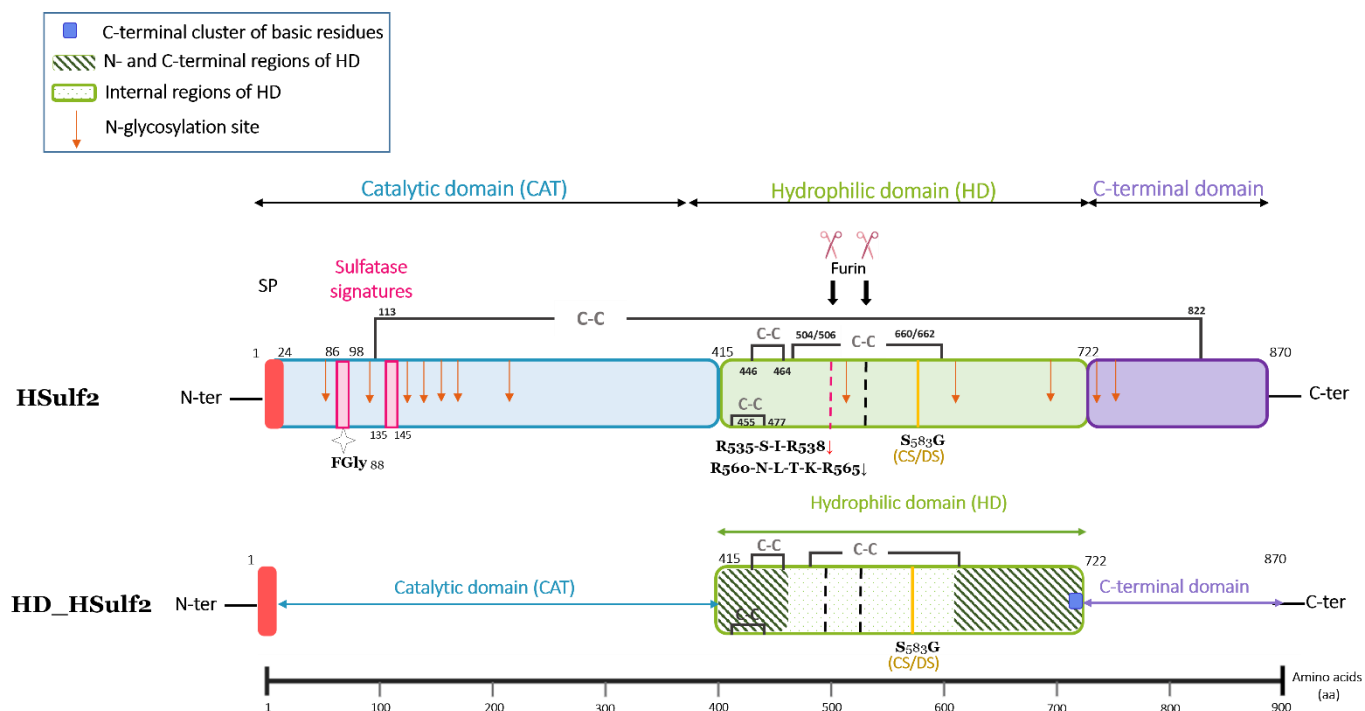


Figure 48: Schematic representation of key structural elements and residues within full-length HSulf-2 and its isolated hydrophilic domain (HD_HSulf-2). SP: signal peptide.

Interestingly, the delC and N561Q mutants, despite targeting residues different from the SG dipeptide motif essential for GAG attachment, displayed a lack of GAG chain, as evidenced by the C-PAGE analysis. While the mechanisms by which N-glycosylation or coiled-coil element mutations affect GAG chain attachment remain unclear, these findings suggest a crucial role for the N561 glycosylation site in both HSulf-2 oligomerization and GAG chain attachment. These observations suggested a complex interplay between the coiled-coil element, disulfide bridges, and the GAG chain within the HD domain in promoting dimer formation. We hypothesize that disulfide bridges might provide a structural conformation that favors dimerization, with the GAG chain potentially stabilizing this conformation. These findings collectively underscore the intricate relationship between specific structural elements of the HD domain, post-translational modifications, and HSulf-2's oligomerization behavior. The GAG chain, in conjunction with the coiled-coil region and disulfide bridges, appears to be tightly implicated in mediating the multimerization process of HSulf-2 by stabilizing a conformational state favorable for protein-protein interaction. Although the impact of the GAG chain was further demonstrated upon hyaluronidase treatment of HSulf-2 wild type and mutants, with a clear shift to predominantly monomeric species for the wild type, it would be valuable for future studies to examine the oligomerization behavior of cysteine mutants. This approach could further elucidate the role of disulfide bridges in HSulf-2's oligomerization state and provide a more comprehensive understanding of the interplay between structural elements and post-translational modifications in regulating HSulf-2 oligomerization. Our investigation

into the structure-function relationships of HSulf-2 revealed key insights into the interplay between structural features (glycosaminoglycan (GAG) chain, oligomerization state) and enzymatic activity. Compared to the wild-type enzyme, we observed enhanced aryl and endosulfatase activity upon GAG removal, whether through the SG mutation or chondroitinase ABC treatment. Interestingly, similar effects were observed for the HDC, delC, and N561Q mutants. While targeting different amino acids within the hydrophilic domain (HD), these mutations shared two critical features: the absence of the GAG chain and a predominant tendency towards monomeric forms, as confirmed by mass photometry analysis. The apparent contrast between dimerization and activity raises intriguing questions about the physiological regulation of HSulf-2 function. The similar impact on activity observed across different mutations implies that the GAG chain is a major governor in this situation, inducing a specific modulation of enzyme activity. We propose that the GAG chain promotes a conformational change, thus inducing a more stabilized dimeric state of the protein that dictates a certain pattern of activity.

Our observation that the absence or removal of the GAG chain significantly enhanced HSulf-2 activity supports and expands upon recent findings in the field. Research by Panigrahi *et al.* (2024) demonstrated that HSulf-2 can directly bind to extracellular matrix (ECM) proteins, particularly galectin-3-binding protein (LG3BP), which is a key regulator of cancer-stroma interactions. Their study assessed how the glycosaminoglycan (GAG) chain affects this interaction and the enzyme's activity. Co-immunoprecipitation experiments indicated a direct interaction between HSulf-2 and LG3BP, suggesting this binding may also occur *in vivo*. Notably, the study highlighted that chondroitin sulfate (CS) modification of HSulf-2 influences its interaction with LG3BP. When the CS chain was removed using chondroitinase ABC treatment, HSulf-2's binding to LG3BP increased, as shown by enhanced pulldown of HSulf-2. Targeted MS analysis revealed that the presence of the CS/DS GAG chain inversely correlates with LG3BP binding affinity, and a mutant form of HSulf-2 lacking the CS chain interacted more efficiently with LG3BP. These findings, along with our results, suggest a complex regulatory mechanism for HSulf-2 activity. The GAG chain plays a critical role in regulating HSulf-2's interaction with ECM proteins and influences its oligomerization state and enzymatic activity. Our data showing enhanced activity upon GAG removal, coupled with the predominance of monomeric forms in GAG-deficient mutants, aligns with this model.

Collectively, these observations hint at a sophisticated regulatory mechanism where the GAG chain promotes the stabilization of dimeric forms of the enzyme, potentially limiting interaction with other protein counterparts. When the GAG chain is removed, the interaction with proteins like LG3BP is enhanced, yet this binding decreases HSulf-2's activity. This suggests that both dimerization and protein-protein interactions serve as mechanisms for regulating HSulf-2 activity in the extracellular environment. This multifaceted regulation highlights the importance of considering both structural features and the

cellular context when studying HSulf-2 function. Future studies should aim to further elucidate how these different regulatory mechanisms are balanced *in vivo* and how they might be altered in pathological conditions.

Protein-liquid-liquid phase separation (LLPS) is an emerging concept that explains complex protein interactions and functions in cellular environments (Alberti et al., 2019). While HSulf-1 and HSulf-2 have FuzDrop scores (a phase separation propensity predictor) of respectively 0.49 and 0.36, i.e., below the typical LLPS threshold of 0.6, recent literature suggests that proteins with lower propensities can still participate in LLPS as clients or modulators (Alberti et al., 2019; Bianchi et al., 2023). HSulfs possess intrinsically disordered regions (IDRs) in the HD domain and engage in multivalent interactions, traits linked to LLPS participation (Jo et al., 2022). Their ability to bind extracellular matrix proteins aligns with LLPs' "scaffold" concept (Alberti et al., 2019). Given these features, we hypothesize that HSulfs may act as clients or modulators in extracellular LLPS processes, potentially being recruited into existing or forming condensates. This could create specific compartmentalization at the cell surface enriched with enzymatic effectors involved in modulating sulfation patterns and binding properties of heparan sulfate. This hypothesis suggests new research directions, such as investigating HSulf co-localization with extracellular condensates and examining how condensate properties might affect HSulf activity, potentially revealing new insights into their roles in extracellular matrix regulation and disease processes.

Our comparative analysis of HSulf-1 and HSulf-2 revealed unexpected similarities in their oligomerization tendencies and post-translational modifications. Contrary to the established understanding that only HSulf-2 harbors a glycosaminoglycan (GAG) chain (El Masri et al., 2022), our C-PAGE analysis unexpectedly detected a polyanionic component on HSulf-1 similar to the GAG chain observed on HSulf-2. This finding challenges previous understanding of the structural differences between these forms. The potential presence of a GAG-like modification on HSulf-1 warrants further investigation using approaches similar to those used for HSulf-2 to fully characterize this modification.

Investigating substrate binding's impact on the oligomeric state of HSulf-1 and HSulf-2, including the delC and HDC mutants of HSulf-2, provided intriguing insights into the interplay between substrate interaction and protein oligomerization. Using heparin (HP) as a substrate analog, we observed that substrate binding did not directly alter the oligomerization state of either HSulf form or their mutants. However, the interaction of HP with both dimeric and monomeric forms for the wild-type, and mainly with the monomeric form for the mutants, aligns with previous studies identifying multiple heparan sulfate (HS) binding sites within HSulfs. These findings complement the work of Seffouh *et al.* (2019), who identified novel HS binding sites within the catalytic domain of HSulf-2, and Milz *et al.* (2013), who characterized heparin interaction sites in the hydrophilic domain (HD). Multiple binding sites across different domains likely enable HSulfs to interact with their substrate in various oligomeric states,

suggesting a sophisticated mechanism for substrate recognition and processing. While HP as a substrate analog offered valuable preliminary insights, it's important to recognize the limitations of this approach. Future studies using the natural HS substrate will be essential for accurately representing physiological conditions and precisely characterizing the interplay between substrate binding and oligomerization in the context of HSulf function. These investigations might uncover subtle differences in substrate interaction between oligomeric states or isoforms that weren't evident with the more highly sulfated HP analog.

2 6-*O*-endosulfatase assay for the functional characterization of HSulfs

Unlike the methods used so far, which only provide an indirect view of HSulf enzyme activity through disaccharide analysis and at an end-point, our study introduces a novel 6-*O*-endosulfatase activity assay based on synthetic heparin and heparan sulfate oligomers, utilizing HILIC-MS for separation and detection of substrates and products at various time points of the enzymatic reaction. This approach allowed us to confirm and extend previous findings about substrate specificity while comparing the two HSulf forms on a range of synthetic oligosaccharides with defined lengths, structures, and sulfation patterns. By directly assessing enzyme action on substrates mimicking the sulfated regions within natural HS, we gained more control over structural complexity without the need for depolymerization of heterogeneous polysaccharides as commonly used for endosulfatase assays (Saad et al., 2005; Uchimura et al., 2006).

Our results supported and expanded upon earlier findings regarding the minimum size requirement for HSulf activity on HS/HP oligosaccharides. We found that neither HSulf-1 nor HSulf-2 reacted with mono- or di-sulfated disaccharides, confirming that the minimum substrate size is greater than dp2. This observation is consistent with initial studies by Saad *et al.* (2005) and Huang *et al.* (2014), which identified a fully sulfated tetrasaccharide (Δ UA2S-GlcNS6S-Ido2S-GlcNS6S) as the smallest substrate for HSulf-2. More recent research by Chiu *et al.* (2020) showed HSulf-1 activity on a trisulfated trisaccharide (Ido2S-GlcNS6S-Ido2S), further refining our understanding of substrate size requirements.

Based on established knowledge and our experimental observations, we propose that HSulf activity and minimum size requirements should be considered in two distinct modes. The first is an arylsulfatase-like activity, similar to that observed with 4-MUS, primarily relying on the catalytic domain alone. For this mode, we hypothesize that substrates must have a contained size or steric volume (e.g., 4-MUS) to freely diffuse and directly access the catalytic site without the involvement of other HSulf domains and be desulfated in an exo-sulfatase-like manner. If the 6-*O*-sulfated disaccharides, although similar in size to 4-MUS, are not substrates for this arylsulfatase activity, it is likely because their much more polar nature requires specific interactions with the active site that only longer structures can fulfill.

The second mode is endosulfatase activity, where the substrate binds to the hydrophilic domain (HD) to be presented to the catalytic site and acted on in a processive manner. This involves recruitment by the HD and binding to the two HS binding sites in the catalytic domain, as identified by Seffouh *et al.* (2019), thus requiring larger substrates to effectively engage both the HD and the catalytic domain binding sites.

Our results with the pentasaccharide Fondaparinux and sulfated octasaccharide substrates further supported this perspective. Analysis of Fondaparinux revealed the production of uniform mono-desulfated and tri-desulfated species, along with two distinct populations of di-desulfated species (two retention

times corresponding to the same extracted ion of m/z 672.5 $[M-10Na+8H-2SO_3]^{2-}$). In contrast, octasaccharides exhibited uniform populations of mono- to tri-desulfated species. This organized desulfation pattern for dp8 oligosaccharides, previously demonstrated by Seffouh *et al.* (2013), was further confirmed by our results, indicating the sequential desulfation of one species at a time along the reaction time course. We hypothesize that the pentasaccharide represents a boundary between endo-activity and arylsulfatase-like activity of HSulfs. We propose that a minimum length exceeding the pentasaccharide is required for binding to the hydrophilic domain (HD) and subsequent processing in an organized, processive manner from the non-reducing to the reducing end. It would be valuable to investigate this effect on a hexasaccharide with a structure similar to the assayed penta- and octasaccharides to validate this hypothesis further.

Notably, we observed effective HSulf activity on the pentasaccharide motif essential for antithrombin binding, challenging previous evidence such as that reported by Pempe *et al.* (2012). While they suggested that Sulf-2 removes 6-*O*-sulfate groups only from regions outside the critical AT-binding pentasaccharide sequence, our results with fondaparinux demonstrated that HSulfs, primarily HSulf-2, effectively hydrolyze this biologically relevant sequence. Our examination of a series of octasaccharides with varying sulfation patterns further revealed that HSulfs effectively act on substrates containing 3-*O*-sulfate (3-*OS*) motifs, with an observed relative enhancement in activity in their presence. These observations align with recent work by Timm *et al.* (2023), who reported a correlation between the 3-*OS* motif and enhanced HSulf-1 activity. These findings could thus have significant implications for our understanding of HSulf function, given the rarity and biological importance of 3-*O*-sulfation in HS chains, which, while occurring in only about 1% of HS disaccharides, its biological relevance is disproportionately high, creating specific binding sites for various proteins and influencing critical processes from blood coagulation to neuronal function (Thacker *et al.*, 2014). Notably, it is involved in the binding and internalization of tau protein, potentially playing a role in Alzheimer's disease progression (Zhao *et al.*, 2020). Rauch *et al.* (2018) demonstrated that overexpression of extracellular endosulfatases (Sulf1 & Sulf2), which selectively cleave 6-*O* sulfate of HSPGs, dramatically decreased tau uptake in human central nervous system cell lines, further confirming the action of HSulfs within 3-*O*-sulfated regions within HS.

We believe that processing sequences with this rare motif is not coincidental. The presence of 3-*OS* may act as a marker for highly sulfated regions, which are preferred substrates for HSulfs, explaining the observed enhanced activity. This interpretation suggests that HSulfs have a preference for 3-*OS*-containing substrates, suggesting that these rare modifications could play a significant role in directing HSulf activity within the complex landscape of HS chains.

Furthermore, as introduced in the previous section, our assay enabled a direct comparison between wild-type HSulf-2 and mutant constructs, allowing us to link structural features to enzymatic activity. All

mutants sharing a common feature - the absence of the GAG chain - exhibited clearly enhanced activity. We utilized this heightened activity to investigate the extent of maximum desulfation, which further confirmed our observations on fondaparinux and octasaccharides regarding the generated populations of desulfated species.

Notably, the mutants could remove up to four 6-*O*-sulfate groups from octasaccharides, regardless of the presence of the para-nitrophenol group (pNP) near the 6-*O*-sulfate at the reducing end. This is particularly interesting as Seffouh *et al.* (2013) previously showed that HSulfs typically removed up to three 6-*O*-sulfate groups from octasaccharide substrates, leaving the last one on the reducing end intact. The enhanced desulfation observed in the mutants suggests a potential loss of strict processivity, likely due to mutations within the HD domain, which acts as the engine for this mechanism.

Based on these observations, we propose that the GAG chain may “collaborate” strongly with the HD domain for HSulf activity. It likely plays a crucial role in modulating substrate access and enzyme conformation, which in turn dictates processivity. This interplay between the GAG chain and the HD domain appears essential for maintaining the specific activity pattern observed for the HSulf-2 wild-type.

When comparing the two HSulf isoforms, we consistently observed higher reactivity and more pronounced desulfation by HSulf-2 compared to HSulf-1 across all tested substrates, including the 4-MUS substrate. These observations led us to consider that HSulf-1 potentially exhibits more stringent substrate specificity than HSulf-2. Alternatively, the observed difference in activity might result from HSulf-1 presenting different structural composition preferences for HS sequence subsets than the ones we tested, which consisted of highly sulfated sequences. This view aligns with recent work by Timm *et al.* (2023), who proposed a more nuanced understanding of HSulf substrate specificity. Their study suggested that HSulf-2, in particular, favors sequences with higher sulfate content and charge density, characteristics more prevalent in heparin and heparin-like substrates. They suggest that specificity might be determined by the frequency of preferred binding sites within the HS chain, which could be higher for HSulf-2 compared to HSulf-1.

Moreover, despite the presumed absence of a GAG chain on HSulf-1, we still observed lower activity than HSulf-2, for which we clearly demonstrated that the absence of the GAG chain induces a significant increase in activity. Given our observations in the first section regarding detecting the GAG chain on HSulf-1, we strongly recommend further investigation into the potential GAG chain modification of HSulf-1.

In conclusion, our assay provides a powerful tool for studying HSulf activity and substrate specificity at the molecular level. This method enables screening of structure-function relationships of HSulfs, as demonstrated with our mutant constructs of HSulf-2, which could be valuable for further investigations,

mainly for the HSulf-1 isoform. Future perspectives include utilizing this assay to screen for potential HSulf inhibitors or activators and to assess their impact on the endosulfatase activity of HSulfs.

3 Inhibitory effects of synthetic oligosaccharides on HSulf activity

Studies on the inhibition of human endosulfatases HSulf-1 and HSulf-2 are relatively recent and still limited: compared to other enzymes involved in the modification of GAGs, such as heparanases, the number of studies specifically targeting the inhibition of HSulfs remains modest. A key objective in characterizing human endosulfatases HSulf-1 and HSulf-2 is designing specific inhibitors to combat cancer, neurodegenerative diseases, and inflammation and immunity-related pathologies. This specificity involves two levels: distinguishing endosulfatases from arylsulfatases and differentiating between HSulf-1 and HSulf-2. Our study investigated the inhibitory effects of synthetic oligosaccharides on HSulf activity using a competitive inhibition assay with 4-methylumbelliferyl sulfate (4-MUS) as a fluorogenic pseudosubstrate. These oligosaccharides, synthesized based on Quellier's work (2020), incorporated a sulfamate group known as a sulfatase-specific inhibiting chemical function, building upon pioneering carbohydrate-based sulfamate inhibitors (Schelwies *et al.* 2010). Our results support this strategy's effectiveness; sulfamate-modified oligosaccharides (dp3, dp5, dp7, dp9) showed distinct inhibitory patterns across HSulf-2 constructs, with dp9 consistently inducing complete inhibition at 50 μ M.

Our results align with and extend the work of Chiu *et al.* (2020) and Kennett *et al.* (2024), who demonstrated the inhibitory potential of short sulfamate oligosaccharides on HSulf activity using 4-methylumbelliferyl sulfate (4-MUS) competition assays. Chiu *et al.* identified sulfonamide-modified trisaccharide IdoA(2S)-GlcNS(6Sulfamate)-IdoA(2S) with an IC₅₀ value of 0.53 μ M against HSulf-1. Kennett *et al.* developed a trisulfated disaccharide inhibitor, IdoA(2S)-GlcNS(6Sulfamate), specifically targeting HSulf-2, with an IC₅₀ value of 39.8 μ M. In our study, dp9 showed remarkable potency as an inhibitor of the arylsulfatase on 4-MUS, with IC₅₀ values of 20 nM for HSulf-2 WT and 32 nM for the SG mutant. This significant improvement in inhibitory potency compared to the trisaccharide and disaccharide inhibitors from Chiu and Kennett's studies highlights the importance of oligosaccharide length and structure in determining inhibitory efficacy against HSulfs.

To further assess the impact of oligosaccharide length on competition with 4-MUS, we assayed several lengths of heparin oligosaccharide substrates without the sulfamate modification (dp2, dp5, dp6, dp8). This experiment revealed length-dependent inhibitory effects on the HSulf-2 SG mutant, with longer oligosaccharides exhibiting more potent inhibition. These results suggest that the sulfamate oligosaccharides' inhibition potency stems from two factors: the sulfamate modification and the better affinity to HSulf-2 due to their oligosaccharide nature.

We observed reduced inhibition efficacy of dp5 in both modified and unmodified series with HSulf-2.

This suggests that dp5 may serve as a threshold between arylsulfatase-like and endosulfatase activities, being just below the required length for HD processing while still capable of interacting with this domain. This finding highlights the importance of considering multiple molecular characteristics when designing potential HSulf inhibitors, particularly the interplay between oligosaccharide length and the enzyme's catalytic and HD domains.

Moreover, our study emphasizes the need to consider both aryl and endosulfatase activities in HSulf inhibition. We used a HILIC-MS assay to assess sulfamate dp9 as both an inhibitor and a substrate for HSulfs. Our results revealed a complex interaction: while sulfamate dp9 effectively competed with 4-MUS for the enzyme's active site, the 6-*O*-endosulfatase HILIC-MS assay showed that both HSulf-1 and HSulf-2 could still remove sulfate groups from this compound, despite the presence of a sulfamate group at position 6 of the non-reducing end glucosamine. This indicates that dp9 acts more as a substrate for HSulfs rather than a classical inhibitor, highlighting the nuanced nature of HSulf-substrate interactions. Comparative assays using dp8 instead of 4-MUS as substrate showed reduced desulfation when HSulfs were preincubated with the sulfamate-modified compound, which could indicate that the inhibitor first binds to a site other than the active site (allosteric inhibition); in this case, the HD domain, before being presented to the active site to prevent substrate binding or transformation.

We propose that these compounds act as substrate-based inhibitors or "slow substrates" for HSulfs, exhibiting competitive binding, slow turnover, and potential product inhibition. This mechanism offers unique advantages in selectivity and sustained inhibition, positioning these compounds as promising leads for developing novel HSulf-targeted therapies. The complexity of the enzyme-inhibitor interaction underscores the need for thorough characterization using a variety of assay types. To better understand the exact mode of inhibition, further investigations—such as detailed kinetic analyses and time-dependent inhibition studies—are essential. These studies would provide valuable insights into the mechanism of action and help guide the optimization of these compounds for enhanced potency and selectivity against HSulfs.

Furthermore, positioning the sulfamate group within the inhibitor sequence appears to be a critical factor in determining the efficacy of HSulf inhibitors. This insight became particularly evident when comparing different disaccharide inhibitors. The arrangement IdoA(2S)-GlcNS(6Sulfamate) demonstrated significantly improved potency against Sulf-2 with an IC₅₀ value of 39.8 μ M \pm 18.3, compared to its GlcNS(6Sulfamate)-IdoA(2S) counterpart, which showed only 20% inhibition at 0.7 mM (Kennett et al., 2024; Chiu et al., 2020). This stark difference in inhibitory potential, despite both compounds being disaccharides with a sulfamate modification, suggests that the specific arrangement of the sulfamate group relative to other structural elements is crucial for effective HSulf inhibition.

Given these findings, we propose that future design of oligosaccharide inhibitors, particularly those targeting the endosulfatase activity of HSulfs, should carefully consider the position of the 6-sulfamate group within the chain. For dp2 inhibitors, the IdoA(2S)-GlcNS(6Sulfamate) arrangement seems optimal. However, for longer oligosaccharides (dp3, dp5, dp7, dp9), it would be valuable to systematically explore various positions of the sulfamate group to determine if there's an optimal location or pattern for maximal inhibition.

To further understand the structural requirements for HSulf inhibition, conducting comparative studies with Glucosamine-6-sulfatase (G6S) would be valuable. G6S shares strong homology with HSulfs but lacks the HD domain. This comparison could clarify the role of the HD domain in endosulfatase activity inhibition, its importance in inhibitor binding and efficacy, and provide insights into structural features crucial for HSulf-specific inhibition.

This comprehensive approach could lead to the development of highly specific and potent HSulf inhibitors. By fine-tuning the sulfamate position to match the enzyme's substrate preferences and optimizing the inhibitor structure for interaction with the HD domain, tailored inhibitors could offer improved efficacy and selectivity. Such advancements could enhance therapeutic strategies for conditions where HSulf activity is implicated, such as certain cancers.

Finally, developing specific inhibitors for each form of human endosulfatases HSulf-1 and HSulf-2 remains challenging due to their structural and functional similarities. To date, the lack of crystallographic structures of HSulf-1 and HSulf-2 prevents the identification of subtle differences in the conformation of their active site or HD domain, which could be exploited to design inhibitors that selectively bind to either enzyme. The contribution of 3D structural modeling, currently underway in the laboratory (thesis of Jianjun Tao), should help progress toward this goal.

We believe that exploiting the specificities of the HD domain and its differences in binding between HSulf-1 and HSulf-2 could constitute a target for differentiated inhibitors. Furthermore, the HILIC-MS method is suitable for high-throughput screening of small molecule libraries. It could allow 1) the identification of compounds that show a selective affinity for the active site of HSulf-1 or HSulf-2 and 2) the development of specific mimetic substrates for each enzyme, depending on their affinity for the HD domain and the differences in the sulfation motifs they target. Combining these two approaches could serve as a foundation for designing selective inhibitors targeting both the HD domain and the catalytic site.

Other avenues remain to be explored for discovering specific inhibitors of HSulfs, including the development of monoclonal antibodies recognizing unique epitopes on HSulf-1 or HSulf-2 or antibodies conjugated to small inhibitory molecules to enhance specificity by precisely targeting the localization of

HSulfs in tissues. Finally, the 2024 Nobel Prize in Medicine on the role of microRNAs in post-transcriptional regulation of genes also highlights a promising pathway: the development of siRNA or shRNA specifically targeting the transcripts of HSulf-1 or HSulf-2 could selectively inhibit the expression of one or the other enzyme at the genetic level. A few studies report RNA interference (siRNA) or genetic knockout approaches for SULF1 and SULF2 genes (Lai et al., 2010; Yue et al., 2008; Zheng et al., 2013). These approaches are mainly employed in model systems to understand the role of these enzymes. Although different from direct enzymatic inhibition, this approach could complement pharmacological strategies.

Chapter VI: Materials and Methods

1 Endosulfatase activity assay

1.1 Hydrophilic Interaction Liquid Chromatography - MS analysis

- Enzymatic reaction:

Buffers: several buffer compositions were systematically evaluated to optimize both substrate and products detection in mass spectrometry analysis while maintaining enzyme activity. The following compositions were assessed in order:

1. 50 mM Tris, 10 mM MgCl₂, pH 7.5
2. 20 mM Tris, 5 mM MgCl₂, pH 7.5
3. 50 mM Tris, 5 mM MgCl₂, pH 7.5
4. 20 mM Tris, 5 mM CaCl₂, pH 7.5
5. 50 mM Tris, 5 mM CaCl₂, pH 7.5
6. 50 mM Tris, 5 mM MgCl₂, 5 mM CaCl₂, pH 7.5
7. 15 mM Tris, 2.5 mM MgCl₂, 2.5 mM CaCl₂, pH 7.5
8. 25 mM Tris, 2.5 mM MgCl₂, 2.5 mM CaCl₂, pH 7.5

Firstly, the effect of reducing Tris concentration was investigated while evaluating the impact of different divalent cations. The buffers containing only MgCl₂ or CaCl₂ were compared to assess their respective effects on enzyme activity. It was highlighted that CaCl₂ enhanced the activity. However, to balance the commonly used MgCl₂ in activity assays and the enhancement effects of CaCl₂, subsequent tests were performed with buffers containing both MgCl₂ and CaCl₂ at reduced concentrations. The Tris concentration was further optimized to minimize salt interference in mass spectrometry analysis while maintaining enzyme activity.

According to such criteria, and after thorough evaluation, a buffer composed of 15 mM Tris, 2.5 mM MgCl₂, 2.5 mM CaCl₂, and pH 7.5 was kept for further studies.

➤ *Immobilized HSulfs:*

HSulf-1 and HSulf-2 enzymes were kindly provided by our collaborator, Dr. Ushiko Uchimura, from the Institute for Structural and Functional Glycobiology at the University of Lille. The enzymes were received immobilized on 1 µm diameter Ni-NTA HisPur™ magnetic beads (ThermoFisher). Approximately 1-2 µg of HSulfs were bound to the metal beads. The beads were first resuspended in 100 µL of Tris buffer

used for the assay. Then, 10 μL of the bead suspension (containing $\approx 0.1\text{-}0.2 \mu\text{g}$ of HSulf) were mixed with 9-30 μL of oligosaccharide solution (15-50 μM final concentration). The oligosaccharide solutions were prepared as follows: disaccharides and octasaccharides were initially dissolved in pure water to 1 mM, then diluted in buffer to 100 μM ; fondaparinux was initially at 2.3 mM in pure water, then diluted to 125 μM in buffer. Buffer was added to complete the reaction volume to 60 μL . The mixture was incubated with gentle agitation (350 rpm) at 37°C for 24 to 48h. Throughout the reaction course, aliquots of 10 μL from the reaction mixture were collected for analysis. Each aliquot was set in a magnetic tube rack (Qiagen) to separate the beads from the reaction products. The supernatant (10 μL) was transferred to another tube for further analysis. The final sample composition was then adjusted to match the initial chromatography gradient conditions, consisting of 35% reaction products in water and 65% acetonitrile (MeCN), with a final volume of 30 μL in the vial. This method allowed for efficient separation of the enzyme from the reaction products, facilitating the analysis of HSulf activity on oligosaccharides of different lengths.

➤ *HSulfs in solution:*

HSulf enzymes and their mutant constructs were kindly provided by our collaborator, Dr. Romain Vivès, from the Laboratory of Structure and Activity of Glycosaminoglycans at the Institute of Structural Biology, Grenoble. The enzymes were received in a buffer of 50 mM Tris, 300 mM NaCl, 5 mM MgCl_2 , and 5 mM CaCl_2 at pH 7.5. Enzyme assays were optimized through a series of experiments with varying enzyme and substrate concentrations. The reaction mixture was prepared with 3 μg of HSulf (wild-type or mutant) and oligosaccharide substrate at a final concentration of 50 μM in a total volume of 50 μL using Tris buffer to maintain a 1:100 enzyme-to-substrate molar (E/S) ratio during the assay. Subsequently, the substrate concentration was reduced to 40 μM to approximate a 1:90 E/S ratio, allowing efficient use of synthetic substrates. To economize the enzyme, only 1 μg of HSulf was used in the final protocol. Incubation was carried out at 37°C for 24 to 48 h with gentle agitation (500 rpm). Throughout the reaction course, 5 μL aliquots were taken at 0, 1, 2, 8, 24, and 48h to monitor the progress of the reaction. Two control experiments were also conducted simultaneously involving (1) the inactivated enzyme (heated to 95°C for 5 min) mixed with the corresponding substrate concentration and (2) oligosaccharides incubated in buffer at the same temperature reaction. The final sample composition (5 μL aliquote + 9 μL pure water + 26 μL MeCN) was adjusted to match the initial chromatography gradient conditions: 35% reaction products in water and 65% acetonitrile (MeCN) at a final volume of 40 μL in the vial.

- Conditions of chromatographic separation:

Hydrophilic Interaction Liquid Chromatography (HILIC) analyses were performed using an ACQUITY UPLC H-Class system (Waters). The separation was conducted on a ZIC-cHILIC column (SeQuant® ZIC®-cHILIC, 3 µm particle size, 100 Å pore size, 150 × 2.1 mm dimensions, PEEK-coated HPLC analytical column). Such column is composed of a silica stationary phase grafted with zwitterionic phosphorylcholine groups, providing a 1:1 charge balance between positive and negative charges.

Mobile phases were freshly prepared and degassed. Briefly, the UPLC mobile phases were as follows: solvent A was 7.5 mM ammonium formate (NH₄HCO₂) adjusted to pH 4.0 using formic acid and solvent B was acetonitrile. Prior to analysis, the column was conditioned using the following gradient: 50% solvent A and 50% solvent B for 10 min, then activated using 10% solvent A and 90% solvent B for 10 min at a flow rate of 0.3 mL/min. Column temperatures was set in a range of 20 to 30°C, representing different temperatures used across multiple experiments. The target sample temperature was set to 8.0 ± 0.5°C. Oligosaccharide samples (2-10 µL) were injected onto the column, corresponding to 10-62.5 pmol of analyte.

Two main elution gradients were employed, depending on the analyzed desulfated oligosaccharide:

- A short gradient: 35% A from 0 to 10 min, 50% A in 10 min, 100% A in 1 min, 100% A for 5 min, 10% A in 1 min, 10% A for 3 min, 35% A in 1 min, and 35% A for 4 min of column reconditioning.
- A long gradient: 35% A from 0 to 15 min, 65% A in 15 min, 95% A in 1 min, 95% A for 2 min, 0% A in 1 min, 0% A for 3 min, 100% A in 1 min, 100% A for 4 min, 10% A in 3 min, 10% A for 5 min, 35% A in 1 min, and 35% A for 6 min of column reconditioning.

Both gradients were performed at a constant flow rate of 0.3 mL/min. The column was reconditioned between each series of injections by running a blank sample (35% A and 65% B) using the same analytical conditions. UV detection was performed at 232 nm with a λ range of 220-250 nm. At the end of the analysis batch, the column was washed with 50% solvent B and 50% solvent C (H₂O) for 10 min to remove residual salts, then equilibrated with 80% solvent B and 20% solvent C for short-term storage.

- MS analysis conditions:

The ZIC-cHILIC column was coupled to a quadrupole time-of-flight (Q-TOF) mass spectrometer (Xevo G2 QTof, Waters). Mass spectrometry analysis was conducted in negative ion mode. The electrospray ionization (ESI) source parameters were optimized to minimize in-source fragmentation of labile sulfate groups. The capillary voltage was initially set to -2.5 kV and later adjusted to -1.5 kV. The source temperature was set to 80 °C, with a sampling cone voltage of 20 V and a source offset of 10 V. Gas flow

rates were set to 20 and 800 L/h for the cone gas and the desolvation gas, respectively. The experiments were performed in resolution mode (mass resolution >40,000 FWHM measured on the m/z 956 as $[M + 6H]^{6+}$) with a mass-to-charge range of 50-1200 m/z . The instrument was calibrated daily using 5 mM sodium formate (NaF) solution in a mixture of H₂O/ MeCN/Formic acid (50:50:0.1, v/v/v) for the mass range 50–1200 m/z . Leucine enkephalin (200 pg/ μ L) in 50:50 acetonitrile/water + 0.1% formic acid was used as an internal standard and constantly infused as a lock mass. After the acquisition, data were analyzed using MassLynx software (version 4.1, Waters).

1.2 Flow Injection-Ion mobility-MS analysis

-Enzymatic reactions:

HSulfs (3 μ g in solution or 0.3-0.6 μ g on 30 μ L of beads, see section 1.1 HSulfs part) were mixed with heparin pentasaccharide in a total reaction volume of 150 μ L, with a final substrate concentration of 50 μ M. Reactions were initially performed in 20 mM Tris, 5 mM MgCl₂ buffer (pH 7.5) at 37°C. However, the buffer was subsequently optimized to 15 mM Tris, 2.5 mM MgCl₂, and 2.5 mM CaCl₂ (pH 7.5). To ensure enough detection of oligosaccharides by FIA (flow injection analysis) without any desalting or separation steps while maintaining the original buffer conditions, some sample preparation was slightly modified. Briefly, the reaction mixture was adjusted to contain 1 μ g of HSulfs and a final substrate concentration of 250 μ M in a total volume of 50 μ L. Substrate modification was monitored by samplings throughout the time course from 0 to 24 h. Two control experiments in the same conditions were also conducted simultaneously with, on the one hand, the inactivated enzyme (heated at 95°C for 5 min) and, on the other hand, the substrate. Then, the samples were diluted by 10-fold in water/acetonitrile (MeCN) 40:60. In detail, 1 μ L of the sample was diluted in a final volume of 40 μ L, resulting in final oligosaccharide concentrations of 25 μ M (initial conditions) or 31 μ M (optimized conditions).

- Flow injection analysis:

Sample preparation for Flow Injection Analysis FIA-Ion mobility (FIA-IM-MS) analysis was optimized to ensure adequate detection and analysis of enzymatically generated products without additional desalting or purification techniques. Fondaparinux concentrations ranging from 12.5 μ M to 50 μ M in a water-organic solvent mixture were tested to determine the limit of detection (LOD). Good signal-to-noise ratios ($S/N > 3/1$) were obtained for concentrations of 20 μ M and higher. FIA was performed using an ACQUITY UPLC M-Class system, which enabled precise fluidic control with programmable injection sequences bypassing the chromatography column. The sample manager temperature rack was set to $8.0 \pm 0.5^\circ\text{C}$. A volume of 10 μ L of each sample was injected directly into the mobile phase consisting of 100% H₂O, with flow rates of 0.05 to 0.2 mL/min. This approach resulted in rapid effective analysis times of 2 min per sample. A blank run was performed between samples, consisting of 60% MeCN.

- Ion mobility-mass spectrometry:

Ion mobility-mass spectrometry (IM-MS) experiments were conducted using a Waters SELECT SERIES Cyclic IMS instrument equipped with an electrospray ionization (ESI) source. This instrument combines cyclic ion mobility separation with time-of-flight mass spectrometry. Mass spectra were acquired in negative ion mode over a mass range of m/z 50-1200 (mass resolution $> 60,000$ FWHM measured on the m/z 956 as $[M + 6H]^{6+}$ in V mode). The instrument was calibrated using sodium formate (NaF) across this mass range. The ESI source was operated with a capillary voltage of 1.5 kV and a sample cone voltage of 20 V. Source and desolvation temperatures were set to 80°C and 280°C, respectively. Desolvation and cone gas flows were set at 800 L/h and 20 L/h, respectively, and Nitrogen was used as the buffer gas for cyclic ion mobility separation (40 mL/min, 1.69 mbar). The cyclic IMS device was operated with a traveling wave pulse height of 15.0 V and a velocity of 375 m/s. The total cycle time of 71.4 ms comprised three steps: inject (10.00 ms), separate (35.00 ms), and eject and acquire (26.40 ms). This configuration resulted in 4-5 passes of monitored ions through the 98 cm cyclic IMS path. Data acquisition and processing were performed using MassLynx (version V4.2) software.

2 Arylsulfatase activity assay

This test setup was designed to control the activity upon reception of the enzymes, assess the effect of different experimental parameters on the arylsulfatase activity of HSulf enzymes, and screen the potential inhibitory effects of some oligosaccharides.

- Enzymatic reactions:

The enzymatic reactions were carried out using HSulf enzymes, either immobilized on beads or in solution (see previous sections), and the fluorogenic synthetic substrate 4-methylumbelliferyl sulfate (4-MUS). The reactions were performed in a 96-well plate with a maximum volume of 100 μ L per well. The buffer composition was adapted concurrently with the endosulfatase assay to ensure optimal enzyme activity and to standardize experimental conditions across both assays. For HSulfs on beads, 0.2 μ g of the enzyme was mixed with 10 mM 4-MUS in the appropriate Tris assay buffer (containing 15-50 mM Tris, with either 2.5-10 mM $MgCl_2$ or 2.5-10 mM $CaCl_2$ or both, at pH 7.5). For HSulfs and mutant constructs in solution, the enzyme amount was initially set to 3 μ g but later reduced to 1 μ g, as previously explained, and combined with 10 mM 4-MUS in the corresponding assay buffer. Control samples included a buffer control (100 μ L of assay buffer) to subtract background noise and a blank control (10 mM 4-MUS in assay buffer). 4-MUS control stock solutions were prepared at 50 mM and stored at 4°C until use.

- 4-MUS/HS Oligosaccharide competition assay:

To evaluate the potential inhibitory effects of HS oligosaccharides on HSulf arylsulfatase activity, various HS oligosaccharides of defined length and structure were tested. HSulf enzymes (1 μg) were incubated with 50 μM HS oligosaccharides in the corresponding buffer. Prior to microplate readings, 10 mM of 4-MUS substrate was added to initiate the reaction. Also, two Control experiments were conducted, including (1) enzyme with the substrate but without oligosaccharides and (2) oligosaccharides with the substrate but without enzyme, to assess the specific effects of HS oligosaccharide addition. For HS oligosaccharides showing inhibitory effects, a range of concentrations (50 nM-50 μM) was tested to determine the half-maximal inhibitory concentration (IC₅₀).

- 4-Methylumbelliferone (4-MU) calibration curve:

Standard curves were generated using 4-Methylumbelliferone (4-MU) at concentrations ranging from 0 to 1 μM . A 1 mM 4-MU stock solution was prepared in dimethyl sulfoxide (DMSO) and stored at 4°C, protected from light. Working solutions of 1 μM and 10 μM 4-MU were prepared by diluting the stock solution in the appropriate assay buffer. Two sets of dilutions were prepared: a nanomolar range (0-100 nM) using the 1 μM working solution and a broader range (0-1 μM) using the 10 μM working solution. All dilutions were made in the assay buffer, with a final volume of 100 μL per well.

- Spectrophotometric Analysis:

The spectrophotometric analysis of the arylsulfatase activity assay was performed using a Varioskan microplate reader (Thermo Scientific) controlled by the SkanIt software (Thermo Scientific). The instrument was set up using a Greiner UV-star Microplate, 96-well, COC, chimney well, black (reference 655809), the black frame, and the chimney shape, allowing for a reduction in light diffusion and crosstalk between the wells. The SkanIt software session was configured with the appropriate plate template, and the measurement parameters were defined as follows: a kinetic loop with 750 readings taken every 20 seconds, fluorescence excitation at 360 nm and emission at 465 nm, and absorbance measured at 362 nm. Before initiating the assay, the temperature was set to 37°C, and the plate was allowed to equilibrate for 15 minutes. The prepared assay plate was then placed in the Varioskan microplate reader, the enzyme was added at last, and the kinetic measurement was started using the above predefined parameters. After the completion of the kinetic run, the fluorescence and absorbance data were exported in CSV format and analyzed using Origin software to determine the arylsulfatase activity. The background signal was corrected by manual subtraction of the control measurements (4-MUS in buffer) from the sample readings.

3 Atomic force microscopy analysis

- System setup :

Atomic force microscopy (AFM) experiments were conducted using a Nanowizard 4 microscope (JPK Bruker) in Quantitative Imaging (QI) mode, which provides non-destructive imaging, high-resolution capabilities in liquid environments, and quantitative data on mechanical and adhesive properties, making it ideal for studying delicate protein samples in their native state (Chopin et al., 2013). Ultrasharp Mikromash tips (1 nm radius of curvature, 20 N/m spring constant, NanoAndMore, France) were used for imaging.

Freshly cleaved mica surfaces were used for the AFM experiments due to their atomically flat and clean nature. A piece of double-sided tape was placed onto the mica and gently pulled off, starting from one edge, to remove a thin layer and expose a fresh surface. The resulting cleaved mica is optically flat, transparent, and free from contamination, making it ideal for AFM imaging of proteins.

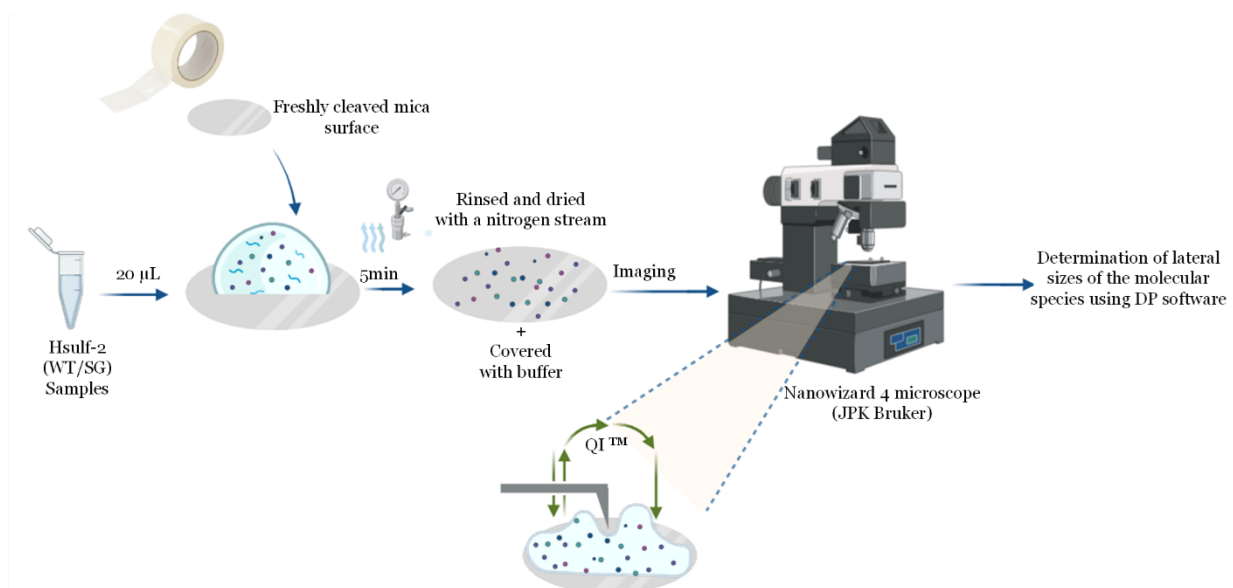


Figure 49: AFM analysis workflow.

- Sample preparation:

HSulf-2 samples (wild-type and SG mutant construct) were diluted to 50 µg/µL in 50 mM Tris buffer containing 10 mM MgQuantitative Imaging (QI), pH 7.5. Twenty microliters of this solution were immediately deposited on the freshly cleaved mica surface (10 mm diameter, grade V1, NanoAndMore, France) to avoid contamination. After 5 min, the mica surface was rinsed with ultrapure water and dried with a nitrogen stream to stop protein adsorption. The mica surface was then covered with a 50 mM Tris buffer containing 10 mM MgCl₂, pH 7.5, to rehydrate the adsorbed proteins before imaging.

-Imaging Parameters:

The vertical displacement speed of the tip was 25 $\mu\text{m/s}$, and images were collected at a minimum of 126 pixels \times 126 pixels over 600 nm \times 600 nm scanning areas. The force setpoint was at 3–10 nN, and the reference force height at 1 nN was extracted from the force curves using the Data Processing (DP) software (JPK/Bruker). The lateral size of the molecular species (in the x-y plane) was determined using the DP software Section Analysis tool.

4 Mass photometry analysis:

-System setup :

Mass Photometry (MP) experiments were conducted using a Refeyn Two^{MP} mass photometry instrument (Refeyn Ltd., Oxford, UK) with an Accurion i4 vibration isolation bench. For data acquisition, Refeyn Acquire^{MP} software was used to capture movies, and Refeyn Discover^{MP} software was employed for data analysis, both utilizing standard settings. 1.5H high-precision glass coverslips (Refeyn), either as it is or after poly-L-lysine coating, were used in conjunction with reusable self-adhesive silicone sample 6-well cassettes (Refeyn: 3 mm ID, 11 mm \times 15 mm OD, 1 mm Depth). Before analysis, a small drop of immersion oil (Zeiss Immersol) was applied to the objective lens. Any excess oil was wiped with a Whatman lens tissue. Next, flip and mount the prepared coverslip-gasket assembly so the red autofocus laser is roughly centered. Secure the coverslip with the provided magnets. The objective focus was adjusted using the corresponding sample buffer (10-18 μL). Samples were prepared using a droplet dilution technique. An initial buffer droplet was placed in the well, followed by adding and mixing appropriate volumes of calibrant, protein, or protein-oligosaccharide solution. This resulted in a final volume of 20 μL and a concentration typically ranging from 5 to 50 nM, depending on the sample analyzed. Recordings were taken for a 60-120 second video length according to the sample. After mass photometry experiments, the coverslip is discarded, and the objective is cleaned with Whatman lens tissue and isopropanol. The gasket well is emptied, rinsed with water or buffer, then soaked in 0.5% detergent solution (Tween-20 or SDS) for 30-60 min. Gaskets are thoroughly rinsed, optionally sonicated for 5-10 min, rinsed again, and air-dried. Before reuse, gaskets are inspected for damage and replaced if necessary to prevent contamination in future experiments.

- Calibration:

To cover the full range of the analyzed proteins and their expected oligomers/interaction complexes, we used a combination of calibrants: Bovine Serum Albumin (BSA, Sigma) with its main monomeric species at 66 kDa, Beta-amylase from sweet potato (Sigma Ref.A8781) exhibiting monomer, dimer, and tetramer species at 56, 112, and 224 kDa respectively, and Bovine Thyroglobulin (Sigma Ref. 609310) primarily

present as dimers at 670 kDa. Calibration stock solutions were prepared in PBS 5% glycerol at 2 mg/mL (corresponding to 30 μ M of the monomer) for Albumin, 5.6 mg/mL (100 μ M monomer) for Beta-amylase and 10 mg/mL (15 μ M dimer) for Thyroglobulin. Working solutions were prepared by diluting the stock to 30-50 nM in the corresponding buffer immediately before use. Mass photometry measurements were then conducted at a final concentration of 5 nM in the sample well, using the same buffer composition as for the analyzed protein or protein/complex. The ratiometric contrast to mass calibration curve was then generated using the recorded contrast of the different oligomerization states of the calibrants.

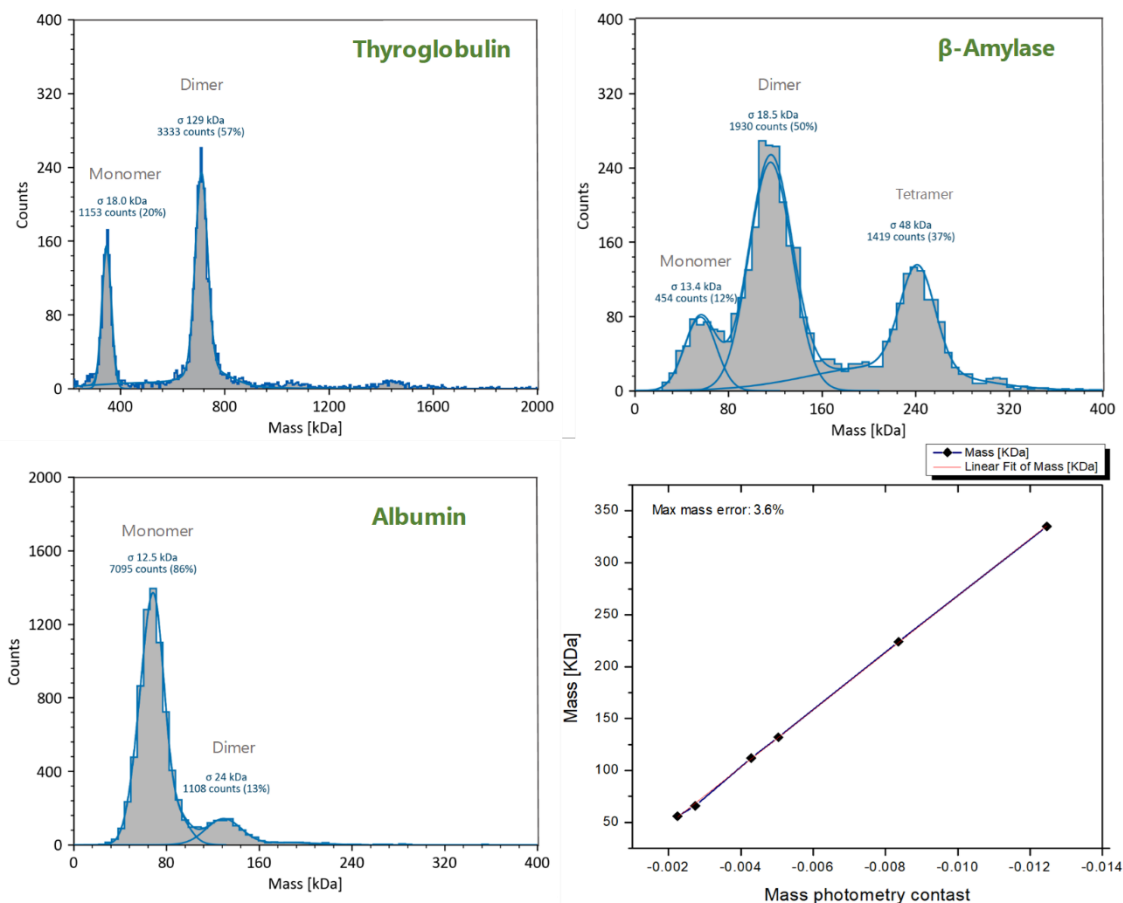


Figure 50: Example of a calibration curve with protein standards for mass photometry analysis.

- Determination of oligomerization state of HSulf:

HSulfs wild-type and mutant working solutions of 100-500 nM were prepared in 15 mM Tris, 2.5 mM CaCl_2 , and 2.5 mM MgCl_2 pH 7.5. Recordings were conducted in regular image size (Range) at a final 5-50 nM concentration in the sample well.

- Investigation of HSulf-Heparin interaction:

Stock solutions of heparin (Novo Nordisk, ~16.7 kDa) were prepared in ultrapure water at 20 mg/mL. These were diluted in 15 mM Tris, 2.5 mM CaCl_2 , and 2.5 mM MgCl_2 pH 7.5 to 10-100 μ M working

solutions. HSulf wild-type and mutant constructs were used to analyze their binding to heparin. HSulf constructs, at a final concentration of 10 nM, were incubated with varying concentrations from 50 nM to 5 μ M of heparin. Samples were prepared by adding the appropriate volume of heparin to the buffer droplet containing HSulf, resulting in a final volume of 20 μ L. Recordings were taken for a 60-90 second video length.

5 Size exclusion chromatography analysis

Size Exclusion Chromatography (SEC) analyses were performed using an Agilent 1260 Infinity II Bio GPC system coupled to a detector. The separation was conducted on an AdvanceBio SEC column (2.1 x 150 mm, 1.9 μ m particle size, 120 Å pore size, PEEK-lined; Agilent Technologies, part number PL1980-3250 PK) with a molecular weight range of 1,000 to 80,000 Da. The mobile phase consisted of 150 mM sodium phosphate buffer (pH 7.0), filtered twice through a Durapore 0.22 μ m PVDF membrane (47 mm diameter) before use. The mobile phase was run isocratically for 15 min at a 0.1 mL/min flow rate. Column temperature was maintained at 30°C. Sample injection volumes ranged from 1 to 5 μ L, not exceeding 1% of the column volume. Before analysis, the system was thoroughly purged to avoid air bubbles and ensure optimal performance. Samples and protein standards were prepared at concentrations ranging from 0.2 to 1 mg/mL and filtered using Millex-GV4 0.22 μ m syringe filters (Millipore) before transferring into autosampler vials. Detection was performed using a multiple wavelength detector (MWD) set at two wavelengths: 280 nm and 220 nm, both with a bandwidth of 3 nm. Chromatograms were recorded in milli-absorbance units (mAU). The Agilent AdvanceBio SEC 130 Å Protein Standard was used for system calibration, containing five proteins with molecular weights of 1, 1.6, 6.7, 17, and 45 kDa. The standard was reconstituted to a concentration of 1 mg/mL, 150 mM Sodium Phosphate, pH 7.0, and 5 μ L was injected for calibration runs. Additionally, separate protein standards were used, including albumin (66 kDa, 1 mg/mL), of which 1 μ g was injected. The calibration curve was generated using the retention times of the standard proteins to establish the relationship between the molecular weight and elution volume. After each batch of injections, a blank injection with only water was performed to rinse the injection system, and the column was rinsed with 100% H₂O to remove salts from the system.

6 Protein sequencing

- Tryptic digestion :

Proteolysis of HSulf and mutant constructs was performed with the following steps:

Sample preparation. 3 μg of HSulf was combined with 2.5 μL of 8 M urea (2 M final). Volume was, adjusted to 10 μL with 50 mM ammonium bicarbonate (NH_4HCO_3 , pH 8.0), then incubated for 1 h with gentle agitation (350 rpm) at room temperature.

Reduction and alkylation. 1.2 μL of 50 mM Dithiothreitol (DTT) (5 mM final) and 0.8 μL of 50 mM ammonium bicarbonate was added to the previous solution (total volume 12 μL) and incubated for 1 h at 37°C under agitation (500 rpm). Subsequently, 1 μL of 250 mM Iodoacetamide (IAA) (20 mM final) was added, and the solution was incubated 45-min room temperature in the dark.

Urea dilution. 7 μL of 50 mM ammonium bicarbonate (pH 8.0) was added to dilute urea to 1 M final concentration (total volume 20 μL), compatible with the trypsin activity.

Tryptic digestion. 1 μL of sequencing-grade modified trypsin (0.4 $\mu\text{g}/\mu\text{L}$) was added, achieving a trypsin-to-protein ratio of approximately 1:7.5 to ensure efficient digestion. The reaction mixture (final volume 21 μL) was incubated overnight at 37°C. The reaction was stopped by heating the sample at 95°C for 5 min. Samples were then stored at -20°C until further analysis.

- Desalting with ZipTip C18

HSulf peptides from in-solution tryptic digestion were purified/desalted using ZipTip C18 (Millipore) following the manufacturer's protocol. This step is crucial for removing urea, salts, too-high buffer concentration, and other contaminants that may interfere with nanoLC-MS/MS analysis. Pipet slowly to avoid introducing air into the packing material and to maximize peptide binding.

Conditioning. Set a P20 pipettor to 10 μl , place ZipTip C18 on P10 pipettor. Aspirate 10 μL of acetonitrile, discard to waste, and repeat three times.

Phase Hydration. ZipTip C18 was equilibrated with 0.1% trifluoroacetic acid (TFA) in water. Aspirate 10 μL of 0.1% TFA, discard to waste, and repeat three times. TFA or other ion-pairing agents are necessary to maintain an acidic pH (≤ 4) for maximum peptide phase binding efficiency.

Sample loading. Peptides were bound to the C18 phase. Slowly aspirate 10 μL of sample and expel the liquid back into the tube; repeat 30 times.

Washing. Bound peptides were desalted. Aspirate 10 μL of 0.1% TFA solution and expel into waste; repeat the wash step 3 times.

Elution. Peptides were eluted sequentially with various acetonitrile content. Aspirate and expel the 10 μL aliquot of elution solution at 50:50:0.1 and 80:20:0.1 acetonitrile/water/TFA (v/v/v) mixtures in an elution tube (20 μL final).

The entire desalting procedure was repeated twice to ensure complete removal of urea. Eluted peptides (total volume 40 μL =2 \times 20 μL) were concentrated using a vacuum centrifuge (speed-vac) for 30-40min at ambient temperature (typically 25-37°C). Dried peptide samples were stored at -80°C until nanoLC-MS/MS analysis.

- Nano-LC-MSE analysis:

Sample preparation: Dried peptide samples were resuspended in 30 μL of water/acetonitrile/formic acid (98:2:0.1, v/v/v), sonicated for 10 min, and transferred to vials before injection.

Chromatography: Analyses were performed using an ACQUITY UPLC M-Class system (Waters) coupled to a SELECT SERIES Cyclic IMS mass spectrometer (Waters). Tryptic digest (5 μL) was injected onto a nanoEase M/Z Symmetry C18 trap column (5 μm particle size, 100 Å pore size, 180 μm x 20 mm) for desalting and concentration, at 5 $\mu\text{L}/\text{min}$ for 2 min using 99.5% solvent A (water/0.1% formic acid) and 0.5 % solvent B (acetonitrile/0.1% formic acid). Peptide separation was performed on a nanoEase M/Z HSS T3 C18 column (1.8 μm particle size, 100 Å pore size, 75 μm x 100 mm) at 400 nL/min. The gradient profile was: 5% B for 5 min, 5-35% B over 50 min, 35-85% B over 10 min, 85% B for 15 min, decreasing to 3% B in 1 min, followed by re-equilibration at 95% A for 9 min. Injections were performed in experimental triplicates, interspersed with blanks of digested BSA (0.2 μL) to prevent cross-contamination and provide a reference for assessing background noise. The column was connected to a glass emitter tip (186003932, Waters).

Mass Spectrometry. The SELECT SERIES Cyclic IMS, equipped with a time-of-flight (TOF) analyzer (mass resolution >60,000 FWHM measured on the m/z 956 as $[\text{M} + 6\text{H}]^{6+}$ in V mode), operated in positive nanoelectrospray ionization mode (ES+) using MS^E data acquisition. Two functions alternated rapidly: (1) Low energy: TOF MS scan (50-2000 m/z, 0.5 s scan time, 0.010 s inter-scan delay, 6.0 eV trap and 4.0 eV transfer collision energies); (2) High energy: TOF MS scan (50-2000 m/z, 0.5 s scan time, 0.010 s inter-scan delay, 6.0 eV trap and 60.0-100.0 eV ramped transfer collision energies). A third function for reference mass correction, *i.e.*, lock mass (Leucine enkephalin, 546.2766-566.2766 m/z), used a 0.2 s scan time and 0.005 s inter-scan delay. The ADC Sample Frequency was 7.2 GHz. The capillary voltage was initially set to 2.5 kV. The source temperature was set at 80°C, with a sampling cone at 40 V and a source offset of 10 V. Gas flow rates were set at 20 and 350 L/h for the one gas and the purge gas, respectively, and nanoflow gas was set to 0.30 bar. Data were analyzed using MassLynx software (version 4.2, Waters).

- Protein identification software:

Bioinformatic analysis for protein sequencing was performed using Licensed Byonic v5.3.5 software from Protein Metrics. The HSulf sequence database was prepared in FASTA format, and the database research options included decoys and common contaminants.

Digestion and instrument parameters were configured as follows: tryptic digestion, targeting cleavage sites at arginine (R) and lysine (K) residues on the C-terminal side, with semi-specific digestion specificity and allowing for up to two missed cleavages. Mass tolerance settings included a precursor mass tolerance of 10 ppm, with recalibration using Leucine-Enkephalin (556.2771 m/z). The fragmentation type was set to QTOF/HCD, with a fragment mass tolerance of 40 ppm. The Byonic search included the following variable chemical modifications: Carbamidomethyl (+57.021464) at C (common1), Carbamyl (+43.005814) at NTer and K (common1), Deamidated (+0.984016) at N and Q (common1), Oxidation (+15.994915) at M (common1), Pyridylethyl (+105.057849) at C (rare2), and FormylGly (-17.992806) at C (rare1), and Xlink Disulfide (-2.015650) at cysteine (C) for disulfide bonds. A list of 132 human N-glycans databases was also included as a potential modification in the sequence research. Advanced spectrum input options included charge states of 1, 2, 3, and 4, a maximum precursor mass of 10,000 Da, precursor and charge assignments computed from MS, a maximum of 10 precursors per MS² for MS^E, and a smoothing width of 0.01 m/z. The protein false discovery rate (FDR) threshold was set to 2% (50 reverse counts). Following the Byonic search, results were analyzed using Byonic Viewer v5.3.44. The analysis focused primarily on comparing sequence coverages between wild-type and mutant enzymes while also evaluating identified peptides, glycopeptides, peptide scores, and peptide-spectrum matches (PSMs).

7 Sodium dodecyl-sulfate polyacrylamide gel electrophoresis (SDS -PAGE)

- Gel Preparation:

The gels (7.3 × 8.3 × 0.1 cm; height × width × thickness) were prepared using the Mini-PROTEAN 3 Cell (Biorad) as follows:

Component	Volume (μL)
Resolving Gel (10% acrylamide)	
MilliQ water	4785
40% Acrylamide/Bisacrylamide (29:1)	2500
1.5 M Tris pH 8.8	2500
10% Sodium dodecyl sulfate (SDS)	100
10% Ammonium persulfate (APS)	100
N, N, N', N'-Tetramethylethylenediamine (TEMED)	15
Stacking Gel (5% acrylamide)	
MilliQ water	2220
40% Acrylamide/Bisacrylamide (29 :1)	625
0.5 M Tris pH 6.8	2000
10% Sodium dodecyl sulfate (SDS)	100
10% Ammonium persulfate (APS)	50
N, N, N', N'-Tetramethylethylenediamine (TEMED)	5

For each gel, the APS and TEMED polymerization reagents were added last to allow time to mix and fill the cassette with the gel solutions before polymerization. The gels were allowed to polymerize for 25-45 min, depending on the room temperature.

- Sample preparation:

3 μg of protein samples were dissolved in 3 μL of 5X Laemmli buffer stock solution, and the volume was adjusted to a maximum of 15 μL with water (1X Laemmli buffer final) The final using ultrapure . The 5X Laemmli buffer consisted of 5% SDS, 50% glycerol, 0.1% bromophenol blue, and 250 mM Tris-HCl (pH

6.8). For reducing conditions, 5% β -mercaptoethanol (BME) was freshly added before use; alternatively, the buffer was prepared without BME for non-reducing conditions. Samples were then denatured by heating at 95°C for 5 min.

- Sample loading and gel electrophoresis:

Samples and molecular weight markers were loaded onto the polyacrylamide gel using gel loading tips. Two protein molecular weight standards were used: Precision Plus Protein Dual Color Standards (10–250 kDa, Bio-Rad REF 1610374) and PageRuler Prestained Protein Ladder (10-170 kDa, Euromedex, REF 06P-0111). 10-15 μ L of the sample was loaded into wells, and 5 μ L of the corresponding molecular weight markers (2 μ g of protein) was also loaded into distinct wells. Another well was devoted to bromophenol blue as a dye front indicator to monitor electrophoresis progress. Electrophoresis was conducted using a Tris-Glycine-SDS running buffer (25 mM Tris, 192 mM glycine, 0.1% SDS, pH 8.3). A 10X stock solution of Tris-Glycine buffer (without SDS) was prepared and can be stored at 4°C for further use.

The working solution was diluted 100 mL of the 10X stock with 890 mL of ultrapure water, then 10 mL of 10% SDS solution was added to a final volume of 1 L. This 1X working buffer was kept at 4°C until use.

The electrophoresis protocol consisted of three stages: an initial voltage of 50 V for 10 min, followed by 70 V for 10 min, and finally, 200 V until the dye front reached the bottom of the gel. The total running time was typically around 60 minutes.

- Gel Staining:

Following electrophoretic separation, the gel was stained using a Coomassie-based protein stain (Instant Blue™) through gentle agitation for 20 min at room temperature. To reduce background staining and so enhance protein band visibility, the gel was subsequently destained in ultrapure water under gentle agitation for 1 to 12h. Destaining time must be adjusted to ensure an optimal contrast between protein bands and gel background. After destaining, the gel was immersed in fresh ultrapure water and stored at 4°C. The stained gel was then placed on a light table (UVP Visi-White Transilluminator, Analytik Jena) with a transparent sheet underneath for imaging and analysis.

8 Carbohydrate Gel Electrophoresis (C-PAGE)

- Gel Preparation:

The gels (7.3 × 8.3 × 0.1 cm; height × width × thickness) were prepared using the Mini-PROTEAN 3 Cell (Biorad) as follows:

Polymerization was carried out in a 100 mM Tris-HCl buffer, pH 7.8, composed of 6% and 27% /10% polyacrylamide/bis-acrylamide for the stacking and resolving gels, respectively.

Component	Volume (μL)		
	Resolving Gel		Stacking Gel
	27% acrylamide	10% acrylamide	6% acrylamide
MilliQ water	384	2934	1180
40% Acrylamide/Bisacrylamide	4050	1500	300
Tris-HCl (100mM, pH 7.8)	1500	1500	500
10% Ammonium persulfate (APS)	60	60	20
N, N, N',N'- Tetramethylethylenediamine (TEMED)	6	6	2

- Sample preparation, gel loading, and electrophoresis:

HSulf-2 (3-6 μg), either untreated or treated with 20% (w/w) Actinase E and/or 10 mU CSase ABC, was suspended in a solution containing 10% glycerol (3-5 μL of 50% glycerol) and 10% phenol red (1 μL), in a final loaded volume of 7-15 μl.

Molecular weight markers were loaded as 2-3 μg per well and include:

- Heparin (HP) oligosaccharide ladder: Dp2, Dp6, Dp12.
- Enoxaparin (Lovenox): 2-8 kDa, average MW 4 kDa
- Dermatan sulfate (DS): Dp20, 5 kDa.
- Unfractionated heparin: 11.8 kDa.
- Unfractionated heparin (UFH): 18.6 kDa.
- Chondroitin sulfate B (CS-B) or (DS): 23 and 26 kDa.

Samples and molecular weight markers were loaded using gel loading tips. Electrophoresis was conducted using a Tris-Acetic acid running buffer (40 mM Tris, 40 mM acetic acid, pH 7.8). A 10X stock solution of Tris-Acetic acid buffer was prepared by dissolving 48 g of Trisma Base (400 mM) and 400 mM Acetic Acid in water, adjusting the volume to 1 L and the pH to 7.8 with 8 M NaOH. This stock solution can be stored at 4°C for further use. The working solution was diluted 100 mL of the 10X stock with 900 mL of ultrapure water to a final volume of 1 L. This 1X working buffer was kept at 4°C until use. The electrophoresis was performed at a constant voltage of 200 V for 31-45 min until the dye front reached the bottom of the gel.

- Gel staining:

Following electrophoretic separation, the gel was stained using a diluted “Stains-All.” The solution was prepared by dissolving 0.15 g of commercial Stains-All in 15 mL of ethanol and adding of 15 mL of water. The staining procedure was carried out in the dark to preserve the light-sensitive dye. The gel was gently agitated in the staining solution, protected by aluminum foil, for 20 min. It was then transferred to a water bath and kept in the dark overnight. To complete the destaining process, the gel was exposed to light for 1 h, which caused the Stains-All to precipitate on the gel surface. The precipitated stain was then carefully wiped off using fingertips, with many precautions due to the fragility of C-PAGE gels and the highly staining nature of the Stains-All solution. Alternatively, destaining methods using a 25:75 (v/v) isopropanol/water or extended light exposure were used cautiously to prevent over-destaining of low-intensity bands. Following the staining and destaining process, the gel was then placed on a light table (UVP Visi-White Transilluminator, Analytik Jena) with a transparent sheet underneath for imaging and analysis. The analysis was based on the color code for glycosaminoglycan identification as described by Andrade *et al.* (Andrade et al., 2018).

9 Enzymatic treatments of HSulfs

- ActinaseE Proteolysis:

ActinaseE, a mixture of proteases that cleave at the carboxylic groups of glutamic and aspartic acids (C-terminal side), was used to release the glycosaminoglycan (GAG) chain from the protein core of HSulf-2. 1.2 µL of ActinaseE (0.5 mg/ml, 20% w/w) was mixed with 3 µg of HSulf in a final volume of 12 µL of buffer (20 mM Tris-HCl pH 7.2). After vortex agitation and centrifugation, the mixture was incubated for 24 h at 37°C. The reaction was stopped by heating at 95°C for 5 min.

- PNGaseF Deglycosylation:

Peptide-N-Glycosidase F (PNGaseF) cleaves the N-glycopeptide bond between asparagine and the first

N-acetylglucosamine (GlcNAc) of the glycosidic chain. The N-deglycosylation of HSulf-2 was performed under non-denaturing conditions following the manufacturer's protocol (Promega). Briefly, 3 μg of HSulf-2 was diluted in 50 mM ammonium bicarbonate buffer (pH 7.8) to a final volume of 18 μL . Then, 2 μL of PNGaseF was added, and the mixture was incubated at 37°C overnight prior to further reactions.

- Hyaluronidase Deglycosylation:

Hyaluronidase is an endoglycosidase that randomly cleaves β -N-acetyl hexosamine-(1-4)-glycosidic bonds in hyaluronic acid and chondroitin sulfates. 1 μL hyaluronidase (1000 U/mL) was added to 1 μg HSulf in a buffer of 20 mM sodium phosphate, 77 mM NaCl, pH 7, in a final volume of 10 μL . The mixture was incubated at 37°C overnight, and the depolymerization was stopped by heating at 95°C for 5 min.

- Chondroitinase ABC Depolymerisation

Chondroitinase ABC is a lyase that catalyzes the degradation of polysaccharides containing (1-4)- β -D-hexosamine and (1-3)- β -D-glucuronic or (1-3)- α -L-iduronic linkages into unsaturated disaccharides. It acts on chondroitin 4-sulfate, chondroitin 6-sulfate, dermatan sulfate, and slowly on hyaluronic acid. 1 μL chondroitinase ABC (50 mU) was added to 3 μg HSulf in a buffer composed of 20 mM Tris-HCl, pH 7.2, in a final volume of 12 μL . The mixture was incubated at 37°C overnight, and the depolymerization was stopped by heating at 95°C for 5 min.

Materials

Ultra-pure water (18.2 M Ω) produced by a Milli-Q apparatus (Millipore) was used for all the conducted experiments.

Solvents :

Acetonitrile, $\geq 99.9\%$ (Sigma-Aldrich, 34967, CAS 75-05-8)

Ethanol, $\geq 99\%$ (VWR, 20821, CAS 64-17-5)

Formic acid, 98-100% (Sigma-Aldrich, 111670, CAS 64-18-6)

Glycerol, $\geq 99.5\%$ (Carlo-Erba, 453752, CAS 56-81-5)

Isopropanol, $\geq 99.9\%$ (Honeywell Riedel-de Haën™, 67-63-0, CAS 67-63-0)

Methanol, $\geq 99.8\%$ (Sigma-Aldrich, 320390, CAS 67-56-1)

Salts and other reagents:

2-Mercaptoethanol, $\geq 99.0\%$ (Sigma, 805740, CAS 60-24-2)

4-Methylumbelliferone, $\geq 98\%$ (Sigma-Aldrich, M1381-100G, CAS 90-33-5)

4-Methylumbelliferyl sulfate potassium salt (Sigma-Aldrich, M7133-1G, CAS55870-30-3)

40% Acrylamide/Bis Solution, 37.5:1 (Bio-Rad, 1610148EDU, CAS 79-06-1, 110-26-9)

Ammonium bicarbonate, $\geq 99.0\%$ (Sigma-Aldrich, A6141, CAS 1066-33-7)

Ammonium formate, $\geq 99.0\%$ (Sigma-Aldrich, 70221, CAS 540-69-2)

Ammonium persulfate, $\geq 98\%$ (Sigma-Aldrich, A3678-25G, CAS 7727-54-0)

Bromophenol blue (Sigma, B0126, CAS 62625-28-9)

Calcium chloride, $\geq 93.0\%$ (Sigma-Aldrich, C5670, CAS 10043-52-4)

Dimethyl sulfoxide, $\geq 99.0\%$ (Sigma-Aldrich, CAS 67-68-5)

DL-Dithiothreitol, $\geq 98\%$ (Sigma-Aldrich, D0632, CAS 3483-12-3)

Iodoacetamide, $\geq 99\%$ (Sigma-Aldrich, I1149, CAS 144-48-9)

Instant Blue™ Protein Stain (Expedeon, Cambridgeshire, UK)

Magnesium chloride hexahydrate, 99.0-102.0% (Sigma-Aldrich, M2670, CAS 7791-18-6)

Phenol red (Fluka, 32661, CAS 143-74-8)

Phosphate-buffered saline (PBS) (Sigma-Aldrich, P4417)

SDS solution 10% (Thermo, CAS 151-21-3)

Sodium chloride, $\geq 99.5\%$ (Sigma-Aldrich, S9625, CAS 7647-14-5)

Sodium formate (Sigma-Aldrich, 71735, CAS 141-53-7)

Sodium hydroxide, $\geq 97.0\%$, pellets (Aldrich, 221465, CAS 1310-73-2)

Sodium phosphate tribasic anhydrous, technical grade (Alfa Aesar, 013438, CAS 7601-54-9)

Stains-All, $\sim 95\%$ purity, powder (Sigma-Aldrich, E9379, CAS 7423-31-6)

TEMED (N,N,N',N'-Tetramethylethylenediamine), $\geq 99\%$ (Bio-Rad, 161-0800, CAS 110-18-9)

Tris base (Tris[hydroxymethyl]aminomethane) (Bio-Rad, 1610719, CAS 77-86-1)

Tris(carboxyethyl)phosphine, HCl (Sigma, C4706, CAS 51805-45-9)

Trizma hydrochloride, $\geq 99.0\%$ (Sigma-Aldrich, T3253, CAS 1185-53-1)

Tween 20 (Riedel-Haen, 63158, CAS 9005-64-5)

- Oligosaccharides & polysaccharides :

Fondaparinux; $\geq 95\%$ (Sigma-Aldrich, SML1240-5MG)

Heparin (16.7 kDa) (Novovo Nordisk, KBJ 6056-1)

3-O-Sulfated Series dp8 (IDURON, M08 S10b); 99%

Structure: GlcNAc6S-GlcA-GlcNS3S6S-IdoA2S-GlcNS6S-IdoA2S-GlcNS6S-GlcA-pNP

2-O-Sulfated Series dp8 (IDURON, M08 S10a); 90%

Structure: GlcNAc6S-GlcA-GlcNS6S-IdoA2S-GlcNS6S-IdoA2S-GlcNS6S-GlcA-pNP

2-O-Sulfated Series dp8 (IDURON, M08 S09a); 99%

Structure: GlcNS6S-GlcA-GlcNS6S-GlcA-GlcNS6S-IdoA2S-GlcNS6S-GlcA-pNP

2-O-Sulfated Series dp8 (IDURON, M08 S09b); 99%

Structure: GlcNAc6S-GlcA-GlcNS6S-IdoA2S-GlcNS6S-IdoA2S-GlcNS6S-GlcA-pNP

Heparin Disaccharide dp2 ; $>95\%$ (IDURON, HD004)

Structure: Δ UA – GlcNS,6S (II-S)

Heparin Disaccharide dp2 ; >95% (IDURON, HD008)

Structure: Δ UA – GlcNAc,6S (II-A)

Dermatan Sulfate oligosaccharide dp20 (IDURON, DSO20)

Δ HexA - GalNAc,4S – (IdoA – GalNAc,4S)9

Unfractionated heparin (16 kDa) (Celsus Laboratories Inc)

Enoxaparin sodium (Lovenox) (2-8 kDa, average MW 4 kDa) (Sanofi)

Dermatan sulfate (23 and 26 kDa) (kindly supplied by Ifremer)

- Calibrant peptides and proteins :

Bovin Albumin (Sigma-Aldrich, A-8531, CAS 9048-46-8)

Pierce™ Bovine Serum Albumin Standard, 2 mg/mL (Thermo Scientific, 23209)

Bovin Thyroglobulin (Sigma-Aldrich, T-9145, CAS 9010-34-8)

β -Amylase (Sweet potato) (Sigma-Aldrich, A-8781, CAS 9000-91-3)

SEC 130 Å Protein Standard Mix (Agilent AdvanceBio, part number 5190-9416)

Leucine Enkephalin, Lockspray (Waters, reference 186006013)

Enzymes:

Actinase E, ≥ 4 U/mg (Sigma-Aldrich, P6911)

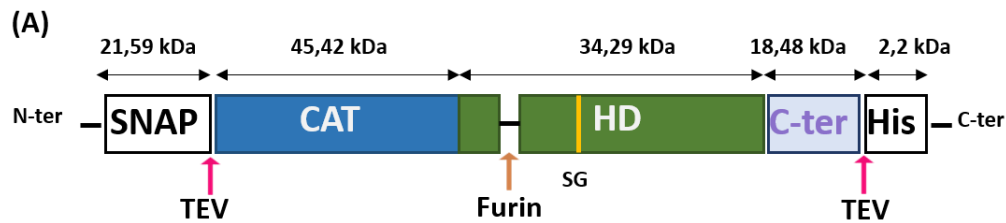
Chondroitinase ABC (Sigma-Aldrich, C2905)

Hyaluronidase (Sheep testes), ≥ 300 U/mg (Sigma-Aldrich, H2126)

PNGase F, $\geq 10,000$ U/mL (Promega, V483A)

Sequencing grade modified trypsin (Promega, V511C)

Supplementary Information

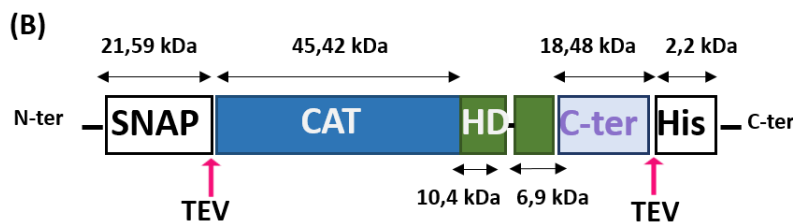


→ **HSulf-2 WT**: (SNAP/His + ~ 18 kDa N-glycosylation) : 139,9 kDa

→ **HSulf-2 SG**: Δ SG ($S_{583} \Rightarrow A$) + (SNAP/His + ~ 18 kDa N-glycosylation): ~139,9 kDa

→ **HSulf-2 DelC**: ($L_{638} \Rightarrow W$; $L_{642} \Rightarrow W$) + (SNAP/His + ~ 18 kDa N-glycosylation): ~139,9 kDa

→ **HSulf2-N561Q**: ($N_{561} \Rightarrow Q$) + (SNAP/His + ~ 18 kDa N-glycosylation): ~139,9 kDa

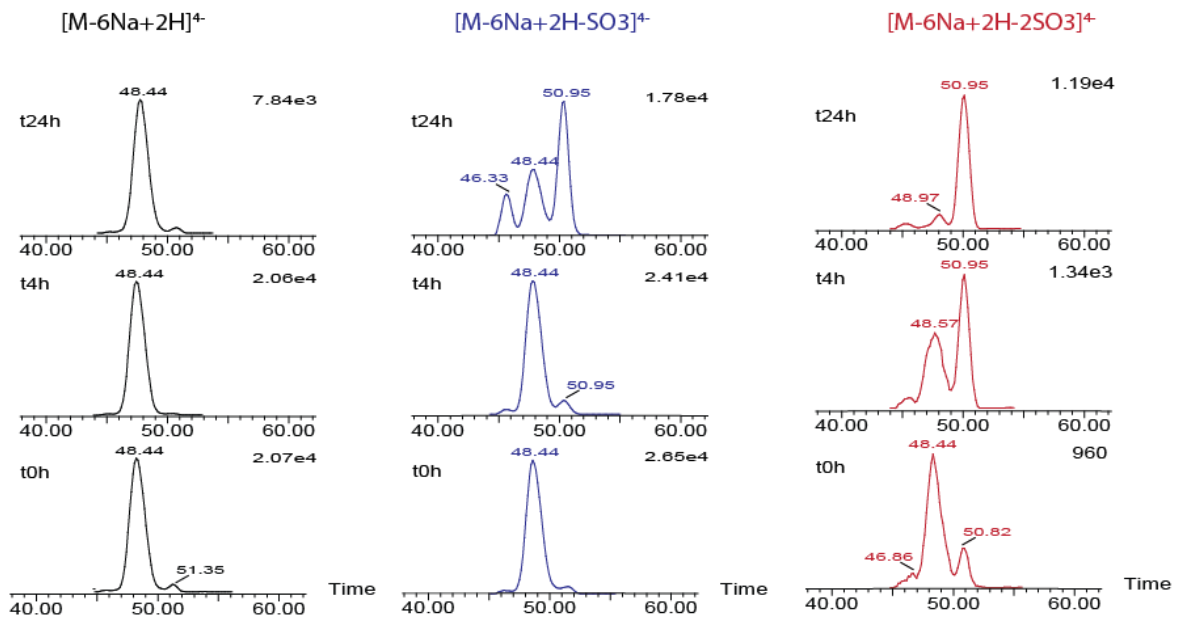


→ **HSulf-2 HDC**: Δ HDC (-17kDa) + (SNAP/His + ~ 18 kDa N-glycosylation): 122,9 kDa

→ **HSulf-2 HDC+TEV+PNGaseF**: Δ HDC (-17kDa) – (SNAP/His + ~ 18 kDa N-glycosylation): 81,2 kDa

Figure S1: HSulf-2 wild-type and mutant constructs sequence composition (updated from (Cretinon, 2022)). (A) Full-length HD domain constructs, including HSulf-2 WT (full-length protein with GAG chain on HD domain and furin cleavage site), HSulf-2 SG ($S583A$ mutation eliminating GAG chain attachment), HSulf-2 DelC ($L638W$ and $L642W$ mutations in the helix of dimerization), and HSulf-2-N561Q ($N561Q$ mutation near furin cleavage site); (B) Modified HD domain constructs including HSulf-2 HDC with SGSGGS linker (truncated HD domain $\Delta 17kDa$) and HSulf-2 HDC+TEV+PNGaseF (HDC construct treated with TEV protease and PNGaseF). All constructs feature N-terminal SNAP and C-terminal His tags for expression in HEK293F and purification, with molecular weights indicated for each domain and construct.

HSulf-1 + Fondaparinux



HSulf-2 + Fondaparinux

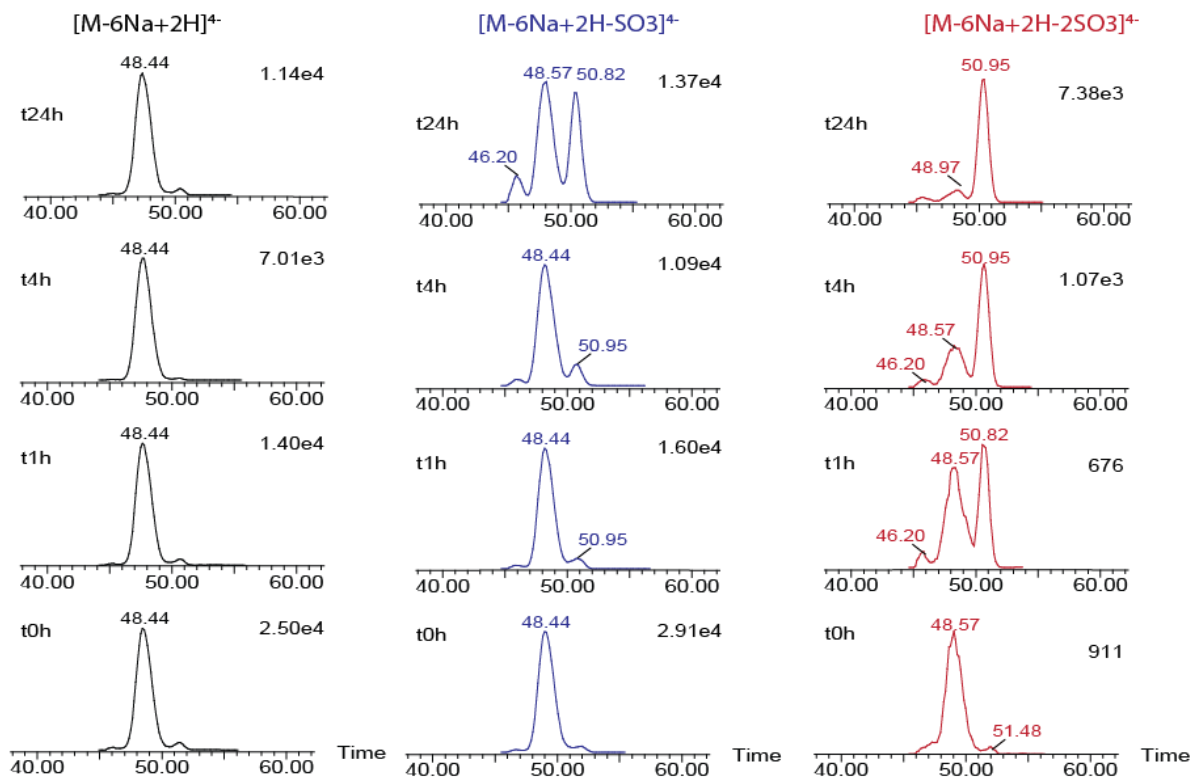
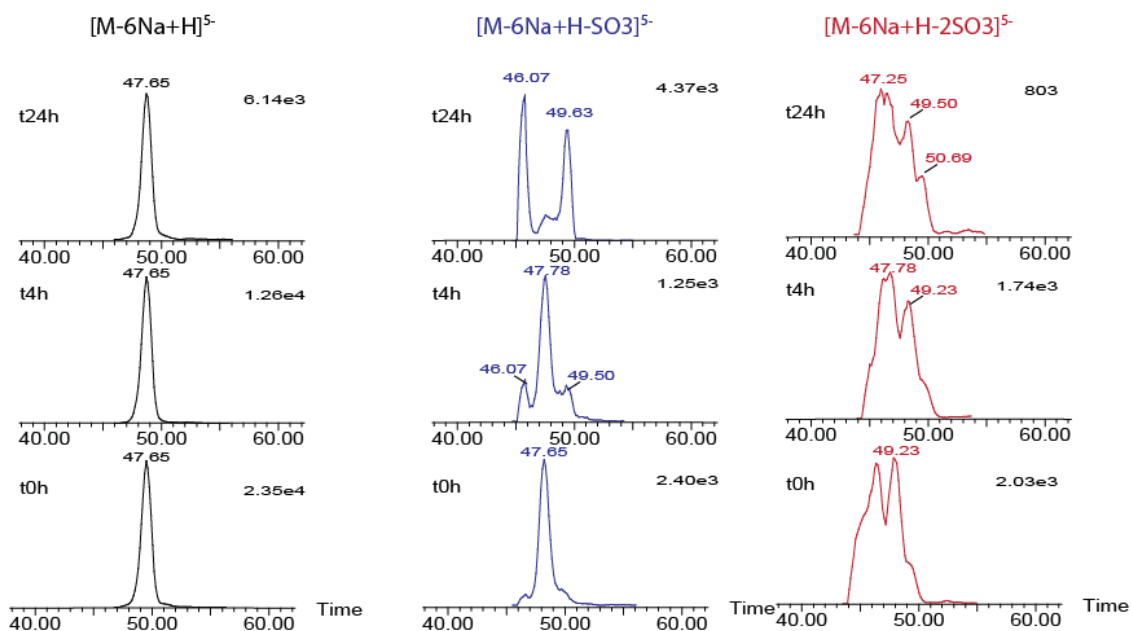


Figure S2: Time-course analysis of Fondaparinux desulfation by HSulf-1 and HSulf-2 using cyclic ion mobility mass spectrometry (cIMS-MS). (A) HSulf-1 + Fondaparinux. (B) HSulf-2 + Fondaparinux. Arrival time distributions (ATDs) are shown for three ionic species: intact Fondaparinux $[M-6Na+2H]^+$ (black trace), mono-desulfated $[M-6Na+2H-SO_3]^+$ (blue trace), and di-desulfated $[M-6Na+2H-2SO_3]^+$ (red trace) at three-time points: t0h, t4h, and t24h (bottom to top in each panel). The x-axis represents ATD in milliseconds (ms).

HSulf-1+Fondaparinux



HSulf-2+Fondaparinux

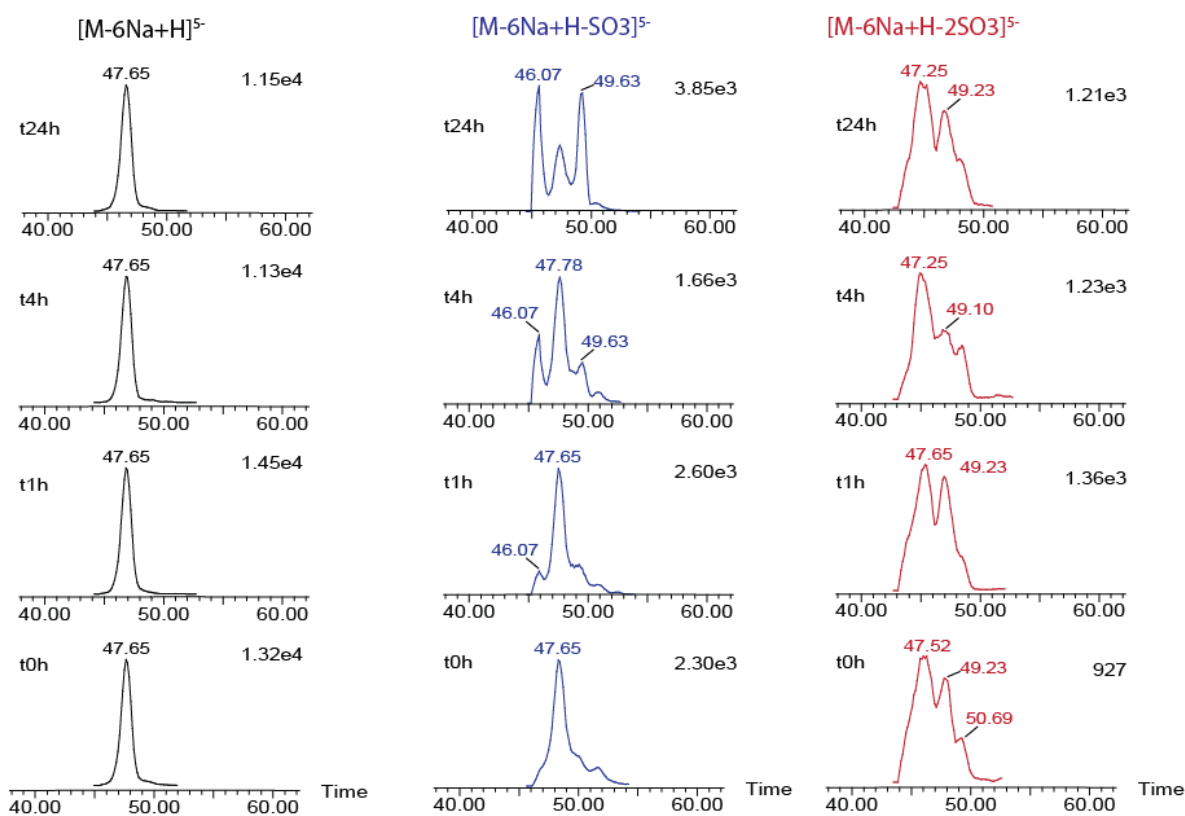


Figure S3: Time-course analysis of Fondaparinux desulfation by HSulf-1 and HSulf-2 using cyclic ion mobility mass spectrometry (cIMS-MS). (A) HSulf-1 + Fondaparinux. (B) HSulf-2 + Fondaparinux. Arrival time distributions (ATDs) are shown for three ionic species: intact Fondaparinux $[M-6Na+H]^{5-}$ (black trace), mono-desulfated $[M-6Na+H-SO_3]^{5-}$ (blue trace), and di-desulfated $[M-5Na+H-2SO_3]^{5-}$ (red trace) at three-time points: t0h, t4h, and t24h (bottom to top in each panel). The x-axis represents ATD in milliseconds (ms).

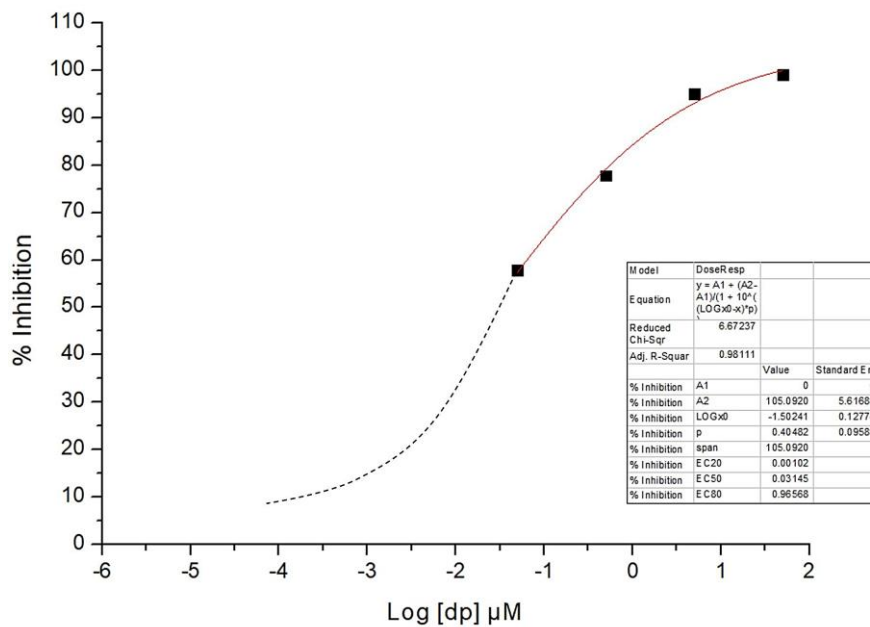


Figure S4: Dose-response curve of HSulf-SG inhibition by sulfamate-dp9 oligosaccharide.

Data points represent mean values \pm standard error (n = 2). The solid line represents the fitted four-parameter logistic (4PL) model. The dashed portion of the curve at lower concentrations indicates the region where experimental data points are lacking.

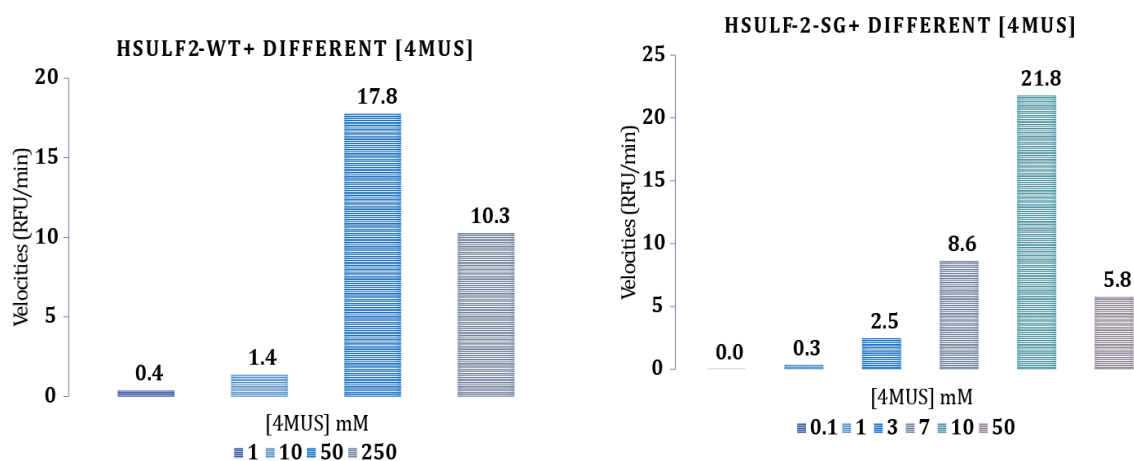
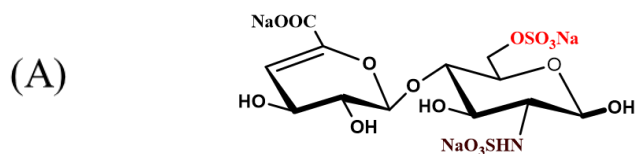


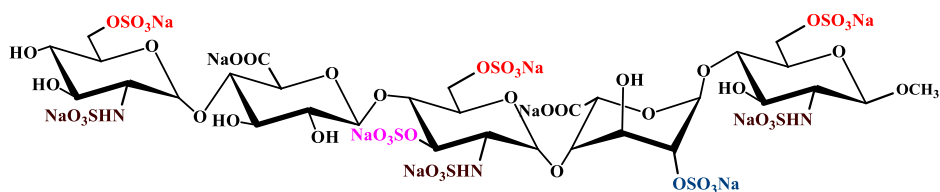
Figure S5: Arylsulfatase activity of HSulf-2 and SG mutant at different 4-MUS concentrations. The figure shows the enzymatic activity of the HSulf-2 wild type (left panel) and the SG mutant (right panel) measured as velocities (RFU/min) at various concentrations of the substrate 4-methylumbelliferyl sulfate (4-MUS). Both enzymes show increasing activity with higher substrate concentrations but with different patterns and magnitudes of response. The SG mutant exhibits higher overall activity than wild-type HSulf-2, particularly at lower substrate concentrations.



dp2 (ΔUA-GlcNS6S):

Unsaturated heparin disaccharide produced by enzymatic depolymerization of porcine heparin with bacterial heparinase.

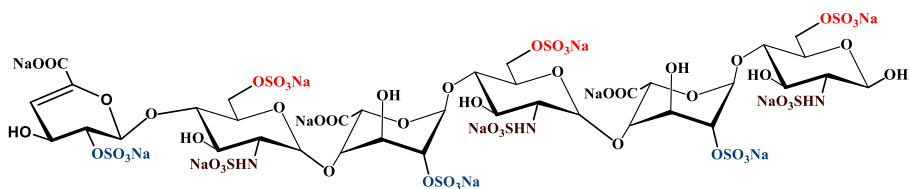
(B)



dp5 (GlcNS6S-GlcA-GlcNS3S6S-IdoA2S-GlcNS1Me6S):

Chemically synthesized pentasaccharide that mimics the active sequence of heparin.

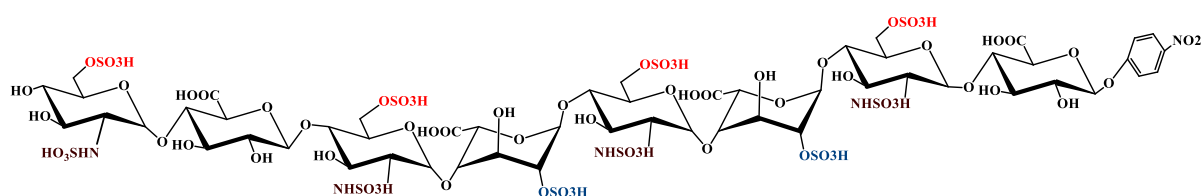
(C)



dp6 (UA,2S-GlcNS,6S-IdoA,2S-GlcNS,6S-IdoA,2S-GlcNS,6S):

Prepared by controlled partial depolymerization of unfractionated heparin using Heparinase I, followed by separation via gel filtration.

(D)



dp8 (GlcNAc6S-GlcA-GlcNS6S-IdoA2S-GlcNS6S-IdoA2S-GlcNS6S-GlcA-pnp): Heparin oligosaccharide, enzymatically synthesized with a p-nitrophenol (pNP) group at the end terminal.

Figure S6: Chemical structures of Heparin oligosaccharides (A) Disaccharide. (B) Pentasaccharide. (C) Hexasaccharide. (D) Octasaccharide

Supplementary Table S 1 Comprehensive Overview of Sulfs' Physiological Implications: From Signaling Pathways to Biological Functions

Physiological Implications of Sulfs	Pathway/Process	Conducted Analysis/Experiment	Key Findings	Sulf Ortholog/Paralog; Model	Reference
Growth Factor Signaling Regulation	FGF ¹ signaling	-Knockout mouse models (knock-out phenotypes) -Cell culture experiments with Sulf overexpression or knockdown -Biochemical assays to measure growth factor binding to heparan sulfate	Sulfs repress FGF signaling	-Sulf1 and Sulf2 (Mouse) -Sulf2 (Human)	-(Higginson et al., 2012; Lamanna et al., 2006; Sugaya et al., 2008) -(Uchimura et al., 2006)
	VEGF ² signaling		Sulfs affect VEGF signaling, influencing angiogenesis	-Sulf1 (Human) -Sulf2 (Human)	-(J. Lai et al., 2004; Lai et al., 2003; J. P. Lai et al., 2004) -(Uchimura et al., 2006)
	HBEGF ³ signaling		HSulf-1 interferes by inhibiting HBEGF-dependent cell proliferation and survival	-Sulf1 (Human)	-(Li et al., 2005)
	TGFβ ⁴ signaling		HSulf-1 can act as both a positive and negative regulator of TGFβ signaling	-Sulf1 (Human)	-(Narita et al., 2006; Yue et al., 2008)
	GDNF ⁵ signaling		HSulf-1 and HSulf-2 enhance GDNF signaling by decreasing GDNF binding to heparan sulfate	-Sulf1 and Sulf2 (Human)	-(Ai et al., 2007)

Morphogen Regulation	Wnt ⁶ signaling	-In situ hybridization to detect Sulf expression patterns -Genetic manipulation in model organisms (e.g., Drosophila, Xenopus) -Analysis of morphogen gradients and target gene expression	Sulfs modulate Wnt signaling by affecting its interaction with Frizzled (Fz) receptors	-Sulf1 (Quail) -Sulf1 and Sulf2 (Mouse) -Sulf1 and Sulf2 (Human) -Sulf1 (Xenopus)	-(Dhoot et al., 2001; Ai et al., 2003) - (Nawroth et al., 2007; Hitchins et al., 2012) -(Tang and Rosen, 2009) - (Fellgett et al., 2015)
	TGFβ/BMP ⁷ signaling		Sulfs influence BMP activity by modulating its interaction with inhibitors like Noggin	-Sulf1 (Quail) -Sulf1 (Xenopus) -Sulf1 and Sulf2 (Mouse)	-(Viviano et al., 2004) -(Freeman et al., 2008) -(Otsuki et al., 2010; Nakamura et al., 2021)
	Hedgehog/Shh ⁸ signaling		Sulfs regulate Hedgehog distribution and signaling	-Sulf1 (Chick) -Sulf1(Drosophila) -Sulf1 (Human) -Sulf1 (Xenopus) -Sulf1 and Sulf2 (Mouse)	-(Danesin et al., 2006) -(Wojcinski et al., 2011) -(MA et al., 2011) -(Ramsbottom et al., 2014) -(Jiang et al., 2017)
Embryonic Development	Neural development and axon guidance	-Knock out phenotypes -Histological analysis of embryonic tissues -Gene expression profiling during	Sulfs influence neuronal plasticity, oligodendrocyte specification, and esophageal innervation	-Sulf1 (Chick) -Sulf1 and Sulf2 (Mouse) -Sulf1 and Sulf2 (Rat)	-(Danesin et al., 2006) -(Kalus et al., 2015; Aizawa et

		development			al., 2019) -(Joy et al., 2015)
	Skeletal development		Sulfs regulate bone volume, chondrogenesis, and cartilage homeostasis	-Sulf1 (Quail) -Sulf1 and Sulf2 (Mouse)	-(Zhao et al., 2007) -(Ratzka et al., 2008)
	Cardiovascular development		Sulfs play crucial roles in cardiovascular development and endothelial cell activity	-Sulf1 and Sulf2 (Mouse) -Sulf1 and Sulf2 (Human)	-(Korf-Klingebiel et al., 2019) -(Justo et al., 2022)
	Spermatogenesis and reproductive biology		Sulfs regulate the spermatogonial stem cell niche	Sulf1 and Sulf2 (Mouse)	-(Langsdorf et al., 2007)
	Glial cell development		Sulfs influence glial cell development and astrocyte subtype generation	Sulf1 and Sulf2 (Mouse)	-(Higginson et al., 2012; Ohayon et al., 2019; Touahri et al., 2012)
Tissue Homeostasis and Repair	Muscle regeneration and satellite cell function	-Injury models (e.g., muscle regeneration, liver regeneration) -Cell culture models of differentiation and proliferation -Analysis of extracellular matrix composition	Sulfs regulate satellite cell differentiation and myoblast fusion	-Sulf1A / Sulf1 and Sulf2 (Mouse)	-(Gill et al., 2010; Langsdorf et al., 2007; Tran et al., 2012)
	Cartilage homeostasis and osteoarthritis		Sulfs support cartilage homeostasis by regulating BMP and FGF signaling pathways	-Sulf1 and Sulf2 (Human) -Sulf1 and Sulf2 (Mouse)	-(Otsuki et al., 2008) -(Otsuki et al., 2010)

	Angiogenesis and vascular biology		HSulf-1 affects vascular smooth muscle cell behavior	-Sulf1 (Human)	-(Sala-Newby et al., 2005)
	Inflammatory responses		Sulfs influence leukocyte infiltration and chemokine interactions	-Sulf1 and Sulf2 (Mouse) -Sulf1 and Sulf2 (Human)	-(Nakamura et al., 2013; Oshima et al., 2019) -(S. Zhang et al., 2012; El Masri et al., 2020)
	Tissue regeneration and wound healing		Sulfs modulate Wnt signaling in hepatocyte proliferation and tissue regeneration	-Sulf1 and Sulf2 (Mouse) -Sulf1 and Sulf2 (Xenopus)	-(Nakamura et al., 2013) -(Wang and Beck, 2015)
	Renal function and glomerular filtration		Sulf1 plays a role in renal function and glomerular filtration	-Sulf1 (Zebrafish)	-(Schenk et al., 2019)
Stem Cell Regulation	Stem cell differentiation	-Isolation and culture of stem cells from Sulf knockout mice -Differentiation assays -Gene expression analysis of stem cell markers	Sulfs regulate stem cell differentiation and niche maintenance	-Sulf1 and Sulf2 (Mouse) -Sulf1 (Drosophila)	(Langsdorf et al., 2007; Levings et al., 2016; Takemura and Nakato, 2017)
	Spermatogonial stem cell niche			-Sulf1 and Sulf2 (Mouse)	-(Langsdorf et al., 2011)

Cell Signaling and Behavior	Cell cycle and nuclear events	-Cell migration assays -Proliferation and apoptosis assays -Analysis of cell adhesion and extracellular matrix interactions	Sulfs are involved in cell cycle-related nuclear events	-Sulf1 and Sulf2 (Human)	-(Krishnakumar et al., 2018)
	Chemokine regulation		Sulfs affect chemokine binding to HS, influencing their distribution and activity	-Sulf2 (Human)	-(Uchimura et al., 2006; Pichert et al., 2012)
	Neuronal plasticity and behavior		Sulfs influence neuronal plasticity and behavior	-Sulf1 and Sulf2 (Mouse)	(Kalus et al., 2009)
	Cellular stress response		HSulf-1 modulates cellular responses to cadmium-induced stress in lung cells	-Sulf1 (Human)	(H. Zhang et al., 2012)

¹**FGF**: Fibroblast Growth Factor signaling, involved in cell proliferation, differentiation, and tissue repair (Ornitz and Itoh, 2015). ²**VEGF**: Vascular Endothelial Growth Factor signaling, crucial for angiogenesis and blood vessel formation (Ferrara et al., 2003). ³**HBEGF**: Heparin-Binding EGF-like Growth Factor signaling, important for cell proliferation and survival. ⁴**TGFβ**: Transforming Growth Factor Beta signaling regulates cell growth, differentiation, and apoptosis (Massagué, 2012). ⁵**GDNF**: Glial cell-derived Neurotrophic Factor signaling, essential for neuronal survival and differentiation. ⁶**Wnt**: Wingless/Integrated signaling, critical for embryonic development and tissue homeostasis (Komiya and Habas, 2008). ⁷**TGFβ/BMP**: Transforming Growth Factor Beta/Bone Morphogenetic Protein signaling, involved in embryonic development and tissue regeneration (Katagiri and Watabe, 2016). ⁸**Hedgehog/Shh**: Hedgehog/Sonic Hedgehog signaling is crucial for embryonic development and cell fate determination (Ingham and McMahon, 2001).

Supplementary Table S 2 : Comprehensive Overview of HSulfs' Pathological Implications

Organ/System	Pathology		HSulf-1	HSulf-2
Central Nervous System (Brain and Spinal Cord)	Non-cancer related	-Alzheimer's disease		Sulf2 shows decreased expression in Alzheimer's disease patients' brains (Roberts et al., 2017).
		-Protein aggregation diseases	Both Sulf1 and Sulf2 are involved in preventing HS domain accumulation in cerebral amyloid plaques and regulating Tau internalization through 6-O sulfation on heparan sulfate proteoglycans (HSPGs) (Hosono-Fukao et al., 2012; Rauch et al., 2018).	
	Cancer-related	-Brain tumors		Sulf2 regulates signaling and growth in malignant glioma (Phillips et al., 2012)
		-Glioblastoma -Malignant glioma	Both Sulf1 and Sulf2 have been identified as candidate cancer-causing genes in brain tumors and are involved in tumor progression (Johansson et al., 2005, 2004). They alter glycosylation in brain cancer (Lemjabbar-Alaoui et al., 2015) and promote tumor invasion in glioblastoma through Heparan Sulfate Glycosaminoglycans (Tran et al., 2017).	
Head and Neck	Cancer-related	-Squamous cell carcinoma	Sulf1 inhibits head and neck squamous cell carcinoma by modulating HGF-mediated tumor cell invasion and signaling (J. P. Lai et al., 2004).	Sulf2 plays a significant role in head and neck carcinoma development and progression . Its expression is associated with carcinoma development (Flowers et al., 2016), affects patient survival (Yang et al., 2020), and promotes invasiveness through interactions with cancer-associated fibroblasts (Mukherjee et al., 2023).
			Sulf1 upregulation correlates with poor survival in the early stages, while Sulf2 significantly impacts survival in the later stages of head and neck squamous cell carcinoma (HNSC) development (Yang et al., 2022).	

Respiratory System (Lungs)	Non-cancer related	- Cadmium/Bleomycin-induced lung injury -Idiopathic pulmonary fibrosis	Sulf1 over-expression sharpens cadmium-induced injury to lung cells (H. Zhang et al., 2012).	Sulf2 is overexpressed in idiopathic pulmonary fibrosis , and its epithelial deletion exacerbates bleomycin-induced lung injury (Yue et al., 2013; Yue, 2017).
	Cancer-related	-Lung cancer		Sulf2 plays an essential role in lung cancer, the leading cause of cancer deaths, promoting human lung carcinogenesis and serving as a potential diagnostic and prognostic marker. (Lemjabbar-Alaoui et al., 2010; Lui et al., 2016).
			Both Sulf1 and Sulf2 alter lung glycosylation and serve as promising blood-based biomarkers for the detection of early-stage non-small cell lung cancer (Lemjabbar-Alaoui et al., 2015; Yang et al., 2021).	
Cardiovascular System (Heart and Blood Vessels)	Non-cancer related	-Cardiovascular development and disease	Both Sulf1 and Sulf2 modulate cell signaling and sulfation in cardiovascular development and disease (Justo et al., 2021).	

Digestive System	Non-cancer related	<ul style="list-style-type: none"> -Type 2 diabetes -Liver fibrosis -Cirrhosis -Obesity 		<p>Sulf2 hepatic overexpression in type 2 diabetes suppresses remnant lipoprotein uptake (Chen et al., 2010) and strongly predisposes to elevated triglycerides in obesity and diabetes (Hassing et al., 2014). At the molecular level, Sulf2 inhibits very low-density lipoprotein interaction with hepatocyte heparan sulfate, affecting triglyceride-rich particle clearance (Hassing et al., 2012). In liver pathology, Sulf2 has elevated serum levels in cirrhosis patients (M. S. Singer et al., 2015) and regulates liver fibrosis through the TGF-beta signaling pathway (Nakamura et al., 2021).</p>
	Cancer-related	<ul style="list-style-type: none"> -Hepatocellular carcinoma -Pancreatic cancer -Gastric cancer -Colorectal cancer 	<p>Sulf1 plays a complex role in digestive system cancers. In hepatocellular carcinoma, it inhibits tumor growth by promoting apoptosis and decreasing heparin-binding growth factor signaling (J. Lai et al., 2004; Lai et al., 2006). Restoration of silenced Sulf1 sensitizes these cancer cells to chemotherapy-induced apoptosis (Shire et al., 2015). In pancreatic cancer, Sulf1 promotes progression by interfering with heparin-binding growth factor signaling and regulating growth and invasion (Li et al., 2005; Abiatari et al., 2006). In gastric cancer, Sulf1 acts as a tumor suppressor by inhibiting cell growth and potentially by down-regulating Hedgehog signaling (MA et al., 2011). Notably, (Junnila et al., 2010) first reported an 11.6-fold overexpression of SULF1 in gastric cancer tissue compared to nonmalignant gastric tissue, further highlighting its significance in this cancer type.</p>	<p>In digestive system cancers, Sulf2 generally promotes progression. In hepatocellular carcinoma (HCC), Sulf2 enhances progression through glypican 3-dependent Wnt activation and stimulates the GLI1-STAT3 transcriptional complex. Additionally, Sulf2 promotes HCC progression via inhibition of apoptosis (Lai et al., 2010; Carr et al., 2020; C. Wang et al., 2021). Sulf2 is found to be overexpressed in 57% of HCCs and 73% of HCC cell lines, and its forced expression promotes HCC cell growth and migration, while its knockdown inhibits these processes (J. P. Lai et al., 2008). Sulf2 levels increase in cirrhosis, suggesting its potential as a biomarker (M. S. Singer et al., 2015). In pancreatic cancer, it serves as a prognostic biomarker and candidate therapeutic target (Alhasan et al., 2016). Sulf2 promotes growth and metastasis in colorectal cancer by activating Akt and Erk1/2 pathways (Tao et al., 2017) and serves as a prognostic biomarker correlated with tumor-associated macrophages in gastric cancer (T.-B. Wang et al., 2021).</p>
				<p>Both Sulf1 and Sulf2 play significant roles in pancreatic cancer, correlating with glypican-1 expression and TGF-beta, BMP, and activin receptors (Kayed et al., 2006). They promote pancreatic cancer growth and tumorigenicity (Nawroth et al., 2007), and their</p>

			splice variants differentially regulate tumor growth progression (Gill et al., 2014). In colorectal cancer , both sulfatases enhance tumorigenic potential (Vicente et al., 2015). Accordingly, in gastric cancer , Sulf1 and Sulf2 exhibit oncogenic roles, with Sulf1 stromal expression serving as a prognostic and metastasis-predictive biomarker (Hur et al., 2012).	
Renal System (Kidneys)	Non-cancer related	<ul style="list-style-type: none"> -Kidney transplantation inflammation -Childhood nephrotic syndrome -Chronic renal fibrosis -Glomerular integrity regulation -Kidney transthyretin deposits 	Sulf1 expression is repressed during inflammation in kidney transplantation (Celie et al., 2007).	Sulf2 is associated with steroid resistance in childhood nephrotic syndrome (Agrawal et al., 2021).
	Cancer-related	-Renal cancer		High levels of Sulf2 gene expression in renal cancer correlate with early stages and less invasiveness, while low levels suggest advanced stages and higher invasiveness (Kumagai et al., 2016).
			Both Sulf1 and Sulf2 play critical roles in kidney-related pathologies. They are involved in 6-O-sulfated heparan sulfate's contribution to chronic renal fibrosis (Alhasan et al., 2014) and regulate glomerular integrity by modulating growth factor signaling, which is vital for maintaining kidney function (Takashima et al., 2016). Sulf1 and Sulf2 are implicated in the accumulation of Heparan Sulfate S-domains in kidney transthyretin deposits , accelerating fibril formation and promoting cytotoxicity (Kameyama et al., 2019).	

Reproductive System	Non-cancer related	-Recurrent miscarriage	Sulf1 polymorphisms are associated with recurrent miscarriage (Zahraei et al., 2014; Taghizadeh et al., 2015).	
	Cancer-related	-Ovarian cancer -Breast cancer -Cervical cancer	In breast cancer , Sulf1 acts as a tumor suppressor. Its presence helps control cancer spread by modulating FGF2- and hypoxia-mediated migration and invasion (Khurana et al., 2011). However, when Sulf1 is lost, it leads to enhanced autocrine signaling mediated by amphiregulin, which promotes cancer progression (Narita et al., 2007). In ovarian cancer , the role of Sulf1 is more complex. While it is generally downregulated, (Backen et al., 2007) demonstrated the overexpression of Sulf1 in ovarian cancer tissues. Loss of sulf1 expression enhances tumorigenicity (He et al., 2014). Its expression is negatively regulated by variant hepatic nuclear factor 1 (Liu et al., 2009), and its polymorphisms are associated with how early ovarian cancer develops and how long patients survive (Han et al., 2011) when it's present, it tends to promote autophagy and reduce lipid droplet formation (Roy et al., 2017). Individuals exhibiting elevated SULF1 expression demonstrated an improved response to chemotherapy compared to those with low or moderate expression levels (Zeng et al., 2021).	Sulf2 predominantly promotes progression in reproductive system cancers. In breast cancer , it is upregulated and proangiogenic (Morimoto-Tomita et al., 2005) and promotes progression through regulating tumor-related factors (Zhu et al., 2016), although its inhibition reduces <i>in vivo</i> tumor growth of MDA-MB-231 breast cancer xenografts (Peterson et al., 2010). In cervical cancer , Sulf2 promotes tumorigenesis and inhibits apoptosis through ERK/AKT signaling (Jiang et al., 2020).

Musculoskeletal System (Bones, Joints, and Cartilage)	Non-cancer related	<p>-Mesomelia-synostoses syndrome</p> <p>-Intervertebral disc degeneration</p> <p>-Osteoarthritis</p> <p>-Cartilage homeostasis</p>	<p>Sulf1 deletion is associated with mesomelia-synostoses syndrome (Isidor et al., 2010), and it's expressed in degenerative intervertebral disc cells (Tsai et al., 2015). Sulf1 intra-articular injection suppresses cartilage degeneration in osteoarthritis (Otsuki et al., 2017) and contributes to intervertebral disc development and homeostasis (Otsuki et al., 2019).</p> <p>Both sulfatases maintain cartilage homeostasis by modulating BMP and FGF signaling pathways (Otsuki et al., 2010) and are involved in dysregulated heparan sulfate proteoglycan synthesis in human osteoarthritic cartilage (Chanalaris et al., 2019). The altered heparan sulfate structure influenced by Sulfs protects against osteoarthritis (Severmann et al., 2020).</p>	
	Cancer-related	-Prostate cancer bone metastasis	Sulf1 suppresses prostate cancer bone metastasis by inhibiting Wnt3A-driven growth (Brasil da Costa et al., 2020).	
Hematological System	Cancer-related	<p>-Multiple Myeloma</p> <p>-Leukemia</p>	<p>Sulf-1 and Sulf-2 effectively inhibit myeloma tumor growth <i>in vivo</i> (Dai et al., 2005).</p> <p>High levels of SULF1 gene expression were observed in T polymphocytic leukemia and acute myeloid leukemia when compared to their respective normal tissue counterparts (Bret et al., 2011) .</p>	

Multiple Systems (various parts of the body)	Non-cancer related	-Protein aggregation diseases	Sulfated glycosaminoglycans facilitate the prion-like behavior of p53 aggregates (Iwahashi et al., 2020). Heparan sulfate S-domains and extracellular sulfatases (Sulfs) are involved in various protein aggregation diseases, suggesting a broader role for these molecules in protein aggregation disease (Nishitsuji and Uchimura, 2017; Nishitsuji, 2018).	
	General Cancer	-Angiogenesis -Tumor metastasis	Sulf1 plays a crucial role in inhibiting angiogenesis and tumorigenesis <i>in vivo</i> (Narita et al., 2006), suggesting its potential as a tumor suppressor . Interestingly, tumor-necrosis factor-α induces Sulf1 expression in fibroblasts (Sikora et al., 2016) indicating its involvement in the tumor microenvironment and inflammatory processes.	The Sulf2 gene undergoes alternative splicing in developing and tumor tissues (Gill et al., 2011), suggesting its diverse roles in different cellular contexts.
			Both Sulf1 and Sulf2 are involved in the regulation of intracellular signaling through extracellular glycan remodeling (Parker and Kohler, 2010), highlighting their importance in cell-cell communication and signal transduction. They play crucial roles in modifying heparan sulfate proteoglycans in the tumor microenvironment (Hammond et al., 2014), which can influence cancer progression and metastasis. Given their significant involvement in various aspects of cancer progression, both Sulf1 and Sulf2 are considered potential therapeutic targets in tumor metastasis (Han, 2024).	

Résumé en Français

1. Introduction

La communication entre les cellules et leur microenvironnement est essentielle au fonctionnement des organismes pluricellulaires. Ce dialogue cellulaire repose sur des cascades de signalisation où les interactions protéiques sont modulées par des modifications post-traductionnelles (MPT). La sulfation, une de ces modifications enzymatiques, participe à l'établissement d'un code moléculaire régulant les fonctions biologiques. Le maintien des niveaux de sulfation joue un rôle central dans l'homéostasie de l'organisme. Les altérations de cet équilibre, qu'elles soient en excès ou en défaut, sont associées à diverses pathologies. Les sulfotransférases et les sulfatases régulent finement cet équilibre par l'ajout ou l'élimination de groupements sulfate.

La découverte des sulfatases HSulfs ajoute de la complexité au niveau de la compréhension de la régulation de la sulfatation. Ces sulfatases se distinguent des autres sulfatases humaines par leur action sur l'héparane sulfate au niveau de l'espace extracellulaire. L'héparane sulfate, un glycosaminoglycane de la matrice extracellulaire (MEC), est un médiateur des interactions cellulaires qui assure la communication entre elles et leur microenvironnement. HSulfs induisent un remodelage du degré de sulfatation du HS en catalysant spécifiquement l'hydrolyse du groupement 6-*O*-sulfate de ses résidus glucosamines. Ce remodelage a un effet sur les interactions HS/ligands et, par conséquent, module les voies de signalisation associées. Ces voies de signalisation contrôlent des processus biologiques clés tels que la croissance, la différenciation, la migration cellulaire ainsi que la réponse immunitaire

Durant ces deux dernières décennies, un intérêt croissant pour les HSulfs s'est manifesté. Cependant, plusieurs aspects de leur structure et de leur fonction restent à élucider. Ces enzymes présentent une organisation structurale particulière et modifient des substrats polysaccharidiques complexes, ce qui constitue un défi analytique pour leur analyse fonctionnelle et structurale. HSulfs engendrent également des effets biologiques et pathologiques différents, particulièrement dans le cancer. HSulf-1 montre des propriétés anti-cancéreuses, tandis que HSulf-2 favorise la progression tumorale. Cette dualité fonctionnelle, malgré une homologie de séquence de 64%, soulève des questions fondamentales sur leurs mécanismes d'action.

C'est dans ce contexte que s'inscrit mon projet de thèse, visant à établir les corrélations entre les caractéristiques structurales uniques des HSulfs et leur mécanisme enzymatique.

2. Résultats et discussion

2.1-Impact des modifications post-traductionnelles (MPT) et de l'organisation en domaines sur la structure et la fonction des HSulfs

La caractérisation de HSulf-2 par microscopie à force atomique (AFM) en conditions quasi-natives a montré l'effet de la chaîne GAG sur les dimensions moléculaires de l'enzyme. Ces données concordent avec des analyses précédentes par diffusion des rayons X aux petits angles (SAXS) et par chromatographie d'exclusion stérique couplée à la diffusion de lumière laser multi-angles (SEC-MALLS) qui suggèrent une forme allongée de l'enzyme. Cette analyse nous a permis de mettre en évidence la tendance de HSulf-2 à former des assemblages de tailles importantes, suggérant la formation d'oligomères. Cette tendance est plus prononcée pour l'enzyme de type sauvage que pour le mutant déficient en GAG.

La caractérisation de l'oligomérisation des HSulfs en conditions natives a porté sur deux aspects principaux : l'influence des modifications post-traductionnelles, notamment celle de la chaîne de glycosaminoglycane (GAG), sur le volume hydrodynamique et la taille des HSulfs, ainsi que le rôle du domaine hydrophile (HD). Nous avons comparé des formes sauvages et mutantes ciblant des éléments structuraux spécifiques de HSulf-2. Cette tendance à la dimérisation a été confirmée par photométrie de masse, suggérant une propriété intrinsèque de HSulf à dimériser. Cette observation concorde avec les travaux de Tang & Rosen (2009) qui proposent une implication du domaine C-terminal dans la multimérisation. La présence de structures en superhélice (A623-E658) au niveau du HD, identifiée par Morimoto-Tomita et al. (2002), renforce l'hypothèse d'une oligomérisation médiée intrinsèquement.

Ces résultats nous ont conduits à étudier deux aspects distincts : la capacité du domaine hydrophile (HD) à induire la dimérisation en conditions natives, et l'influence de la chaîne glycosaminoglycane (GAG) sur l'oligomérisation médiée par le HD.

Les analyses par photométrie de masse et par chromatographie d'exclusion stérique du domaine hydrophile de HSulf-2, produit dans un système bactérien (*E. coli*), ont confirmé sa capacité intrinsèque à la dimérisation en conditions natives. Ces résultats nous ont permis d'attribuer un rôle déterminant au HD dans l'oligomérisation de HSulf-2, indépendamment des modifications post-traductionnelles eucaryotes, notamment la formation de la chaîne de GAG. Notre analyse des différents mutants de HSulf-2 nous a permis de caractériser plus précisément l'implication du HD dans ce processus. Ces constructions, dont un mutant (HDC) avec délétion de la région D483-C636 ainsi que des mutants ciblant les résidus des superhélices (delC : Leu638 et Ile642 substituées par des tryptophanes) ou le site de glycosylation proche des sites de clivage de la furine (N561Q : substitution asparagine-glutamine), montrent une tendance accrue à la monomérisation. Ces résultats confirment le rôle essentiel de ces éléments structuraux du HD dans l'oligomérisation de HSulf-2.

Les analyses par SDS-PAGE des mutants delC et N561Q ont révélé leur prédominance sous forme monomérique en conditions réductrices et non réductrices. Ces résultats nous ont amenés à examiner leur position par rapport aux ponts disulfures caractérisés précédemment dans notre laboratoire (Bilong, 2021). La localisation de ces mutations à proximité des résidus C660 et C662, impliqués dans un pont disulfure inter-chaîne essentiel à la formation d'hétérodimère liant la région N-terminale à la C-terminale, suggère un lien structural. Ces observations suggèrent l'implication des ponts disulfures dans l'oligomérisation de HSulf-2, la position des mutations pourrait ainsi perturber l'équilibre oligomérique *via* leur influence sur les ponts disulfures. La génération de mutants ciblant directement ces résidus cystéine permettrait d'approfondir cette hypothèse.

Le profil C-PAGE des mutants delC et N561Q indique une absence de la chaîne de GAG, un résultat inattendu puisque ces mutations n'affectent pas le motif SG responsable de son attachement. Cette observation suggère un lien entre la structure du domaine HD et la formation du GAG. Notre analyse des différentes constructions a révélé que les altérations du site de glycosylation N561 ou de l'élément en superhélice affectent à la fois l'oligomérisation et la présence du GAG. Ces observations suggèrent une coopération entre trois éléments structuraux du HD - l'élément en superhélice, les ponts disulfures et la chaîne de GAG - dans la stabilisation de l'état dimérique. Le traitement par la hyaluronidase de la forme sauvage, induisant une transition vers des formes monomériques, confirme cette hypothèse.

Concernant les relations structure-fonction de HSulf-2, nous avons déterminé une corrélation inverse entre l'état d'oligomérisation et l'activité enzymatique. L'absence de chaîne de GAG, qu'elle soit pour les mutants SG, HDC, delC ou N561Q, favorise la forme monomérique et augmente les activités aryl et endosulfatases. La chaîne de GAG semble donc induire un changement conformationnel qui stabilise l'état dimérique et favorise l'activité enzymatique.

Pour finir, notre analyse C-PAGE a démontré la présence d'une chaîne de GAG sur HSulf-1, une caractéristique jusqu'à ce jour attribuée uniquement à HSulf-2. Cette observation ouvre de nouvelles perspectives pour une caractérisation approfondie de cette modification sur HSulf-1.

2.2-Test d'activité endosulfatase pour la caractérisation fonctionnelle des HSulfs

Nous avons mis en place un nouveau test d'activité 6-*O*-endosulfatase qui se base sur une analyse HILIC-MS d'oligosaccharides d'héparine et d'héparane sulfate de séquence bien définie. Cette méthode se distingue des analyses traditionnelles d'activité endosulfatase des HSulfs par deux aspects majeurs. Tout d'abord, elle permet un suivi cinétique direct de l'activité enzymatique comparée aux mesures traditionnelles en point final. De plus, elle se base sur l'utilisation de substrats avec des structures et motifs de sulfatation bien définis, ce qui offre un contrôle structural précis. Contrairement aux méthodes classiques qui nécessitent une étape supplémentaire de dépolymérisation de polysaccharides hétérogènes, cette approche nous a permis d'approfondir nos connaissances sur la spécificité de substrat des deux formes de HSulf-1 et HSulf-2 avec un détail à l'échelle moléculaire.

Nos résultats confirment des observations antérieures concernant la taille minimale requise pour l'activité des HSulfs sur les oligosaccharides HS/HP. Ces dernières suggèrent un tétrasaccharide entièrement sulfaté comme substrat minimal pour HSulf-2. L'absence de réactivité de HSulf-1 et HSulf-2 envers les disaccharides mono- et di-sulfatés observée dans notre analyse suggère une taille minimale de substrat supérieure à dp2. Des travaux récents ont affiné cette compréhension en démontrant l'activité de HSulf-1 sur un trisaccharide trisulfaté.

Sur la base des connaissances établies et de nos observations expérimentales, nous proposons que les exigences de taille minimale soient considérées selon deux modes distincts d'activité enzymatique, aryl- et endo-sulfatase. L'activité arylsulfatase, illustrée par la réaction avec le 4-MUS, dépend principalement du domaine catalytique. Ce mode nécessiterait des substrats de taille limitée, capables de diffuser librement vers le site catalytique sans l'intervention d'autres domaines, selon un mécanisme proche des exo-sulfatases. L'absence d'activité sur les disaccharides 6-*O*-sulfatés, malgré leur taille comparable au 4-MUS, s'expliquerait par leur polarité accrue nécessitant des interactions spécifiques avec le site actif, interactions uniquement possibles avec des structures plus étendues. L'activité endosulfatase implique, quant à elle, une interaction avec le domaine hydrophile (HD) qui présente le substrat au site catalytique pour un traitement processif, nécessitant des substrats plus longs pour engager simultanément le HD et les sites de liaison du domaine catalytique.

L'étude de HSulf-2 avec le Fondaparinux et les octasaccharides sulfatés a montré des profils de désulfatation distincts. Le traitement du Fondaparinux par HSulf-2 produit des espèces mono- et tri-désulfatées uniformes, mais génère deux populations d'espèces di-désulfatées. Les octasaccharides présentent une distribution régulière d'espèces mono-, di- et tri-désulfatées, indiquant une désulfatation progressive du substrat dp8. Ces différents profils suggèrent que le pentasaccharide constitue une structure charnière dans le mécanisme enzymatique de HSulf-2.

Nos travaux ont montré que les HSulfs sont capables d'agir sur le motif pentasaccharidique de l'antithrombine, contrairement à des observations précédentes. L'étude des octasaccharides avec différents motifs de sulfatation a mis en évidence non seulement l'activité des HSulfs sur les substrats contenant des motifs (3-OS), mais aussi une activité accrue en leur présence. Ce résultat est particulièrement pertinent compte tenu de la rareté de ce motif au niveau des chaînes HS et de son rôle crucial dans divers processus biologiques. Nous proposons que cette prise en charge par HSulfs des séquences contenant ce motif rare ne soit pas fortuite, ces motifs rares pourraient signaler des régions hautement sulfatées, substrats préférentiels des HSulfs, expliquant ainsi l'activité enzymatique accrue observée. Cette interprétation peut expliquer la préférence des HSulfs pour les substrats comportant des modifications 3-OS au sein de l'architecture complexe des chaînes HS.

L'analyse comparative entre HSulf-2 sauvage et les mutants dépourvus de chaîne de GAG a révélé une activité accrue chez ces derniers. Les mutants éliminent quatre groupements 6-O-sulfate des octasaccharides comparé à trois uniquement pour la forme sauvage. Cette observation suggère que les mutations au niveau du HD modifient le mécanisme enzymatique, révélant ainsi une coopération fonctionnelle entre la chaîne de GAG et le domaine HD qui détermine la processivité caractéristique de HSulf-2 sauvage.

HSulf-1, initialement décrite comme dépourvue de chaîne de GAG, montre une activité inférieure à celle de HSulf-2. Pour cette dernière, l'absence de GAG augmente pourtant l'activité enzymatique. La mise en évidence d'une chaîne GAG sur HSulf-1 par l'analyse C-PAGE ouvre de nouvelles perspectives et justifie une caractérisation approfondie de cette modification inattendue sur HSulf-1.

En conclusion, notre approche HILIC-MS constitue une méthode analytique résolutive pour l'étude de la spécificité de substrat des HSulfs à l'échelle moléculaire. Cette méthode servira à la caractérisation fine de HSulf-1 ainsi qu'au criblage d'inhibiteurs spécifiques des HSulfs.

2.3-Effets inhibiteurs des oligosaccharides synthétiques sur l'activité des HSulfs

Le développement d'inhibiteurs des endosulfatases humaines HSulf-1 et HSulf-2 représente un domaine d'étude relativement récent, contrastant avec les recherches plus étendues sur d'autres enzymes modificatrices des GAGs, comme les héparanases. La conception d'inhibiteurs spécifiques de ces endosulfatases constitue un enjeu majeur pour le traitement des cancers et des pathologies neurodégénératives, inflammatoires et immunitaires. Cette spécificité requiert une double sélectivité : vis-à-vis des aryl et endosulfatases d'une part, et entre HSulf-1 et HSulf-2 d'autre part.

Dans ce contexte, nous avons évalué des oligosaccharides modifiés par une fonction sulfamate (-OSO₂NH₂) introduite en position 6 de la glucosamine à l'extrémité non réductrice. Cette approche exploite la spécificité de la fonction sulfamate comme inhibiteur des sulfatases. Les tests de compétition avec le

substrat fluorogène 4-MUS ont montré que le dp9 sulfamate atteint des IC50 de 20 nM et 32 nM pour HSulf-2 WT et le mutant SG, surpassant ainsi les IC50 des inhibiteurs tri- et disaccharidiques précédemment décrits dans la littérature.

L'analyse des oligosaccharides d'héparine non modifiés a montré un lien entre la longueur des chaînes et leur pouvoir inhibiteur sur le mutant HSulf-2 SG. Ces observations suggèrent que l'efficacité des oligosaccharides sulfamates résulte d'une synergie entre la modification sulfamate et l'affinité préférentielle de HSulf-2 pour les chaînes d'oligosaccharides \geq dp8.

L'efficacité d'inhibition réduite observée pour le dp5 corrobore notre hypothèse d'une transition entre les activités arylsulfatase et endosulfatase à cette longueur. Cette taille apparaît comme un seuil : trop courte pour une interaction optimale avec le domaine HD, mais suffisante pour établir un contact initial. Cette caractéristique souligne l'importance d'adapter la longueur de l'oligosaccharide aux domaines fonctionnels de l'enzyme pour concevoir des inhibiteurs efficaces.

L'étude des composés sulfamates a mis en évidence un comportement dual. Ces composés agissent comme inhibiteurs efficaces de l'activité arylsulfatase sur 4-MUS, mais sont également reconnus comme substrats de l'activité 6-*O*-endosulfatase de HSulf-1 et HSulf-2. Cette activité de substrat est observée même en présence du groupement sulfamate en position 6 de la glucosamine non réductrice. Des essais comparatifs utilisant dp8 comme substrat ont démontré une réduction de la désulfatation après pré-incubation avec le composé sulfamate. Ce résultat suggère un mécanisme d'inhibition allostérique : l'inhibiteur interagirait d'abord avec le domaine HD avant d'être présenté au site actif, modulant ainsi la liaison ou la transformation du substrat. Cette dualité fonctionnelle des composés sulfamates suggère un mécanisme d'action complexe. L'efficacité de ces inhibiteurs pourrait reposer sur leur capacité à agir comme des substrats à « turnover » lent qui occupent le site catalytique tout en subissant une transformation enzymatique progressive. Cette caractéristique, combinée à leur affinité pour le domaine HD, ouvre des perspectives intéressantes pour le développement d'outils thérapeutiques ciblant HSulfs.

Des études précédentes ont démontré qu'un arrangement IdoA(2S)-GlcNS(6Sulfamate) présente une IC50 de $39,8 \mu\text{M} \pm 18,3$ contre HSulf-2, tandis que son homologue GlcNS(6Sulfamate)-IdoA(2S) n'induit que 20% d'inhibition à 0,7 mM (Kennett et al., 2024 ; Chiu et al., 2020). Cette différence montre que le positionnement du groupement sulfamate au niveau de la séquence oligosaccharidique est déterminant pour l'efficacité inhibitrice. Ces résultats guident la conception de nouveaux inhibiteurs oligosaccharidiques. Si l'arrangement IdoA(2S)-GlcNS(6Sulfamate) s'avère optimal pour les inhibiteurs dp2, l'optimisation pour des oligosaccharides plus longs (dp3, dp5, dp7, dp9) nécessite donc une exploration supplémentaire pour identifier les configurations maximisant l'efficacité inhibitrice. Il serait aussi intéressant de mener une étude comparative avec la Glucosamine-6-sulfatase (G6S). Cette enzyme,

qui présente une forte homologie avec le domaine catalytique des HSulfs mais est dépourvue du domaine HD, constituerait un modèle pertinent pour élucider le rôle spécifique du domaine HD dans la reconnaissance et l'efficacité des inhibiteurs. Dans leur ensemble, ces observations pourraient guider le développement d'inhibiteurs spécifiques des HSulfs, en optimisant à la fois le positionnement du groupe sulfamate et les interactions avec le domaine HD.

En conclusion, nos résultats apportent de nouvelles perspectives sur les relations structure-fonction des HSulfs, enrichissant ainsi la base de connaissances nécessaire pour un développement rationnel d'inhibiteurs spécifiques pour leur ciblage thérapeutique.

Bibliography

- Abiatari, I., Kleeff, J., Li, J., Felix, K., Buchler, M.W., Friess, H., 2006. Hsulf-1 regulates growth and invasion of pancreatic cancer cells. *J Clin Pathol* 59, 1052–8. <https://doi.org/10.1136/jcp.2005.031716>
- Agrawal, S., Ransom, R.F., Saraswathi, S., Garcia-Gonzalo, E., Webb, A., Fernandez-Martinez, J.L., Popovic, M., Guess, A.J., Kloczkowski, A., Benndorf, R., Sadee, W., Smoyer, W.E., On Behalf Of The Pediatric Nephrology Research Consortium, P., 2021. Sulfatase 2 Is Associated with Steroid Resistance in Childhood Nephrotic Syndrome. *J Clin Med* 10. <https://doi.org/10.3390/jcm10030523>
- Ai, X., Do, A.T., Kusche-Gullberg, M., Lindahl, U., Lu, K., Emerson, C.P., Jr., 2006. Substrate Specificity and Domain Functions of Extracellular Heparan Sulfate 6-O-Endosulfatases, QSulf1 and QSulf2. *J Biol Chem* 281, 4969–76. <https://doi.org/10.1074/jbc.M511902200>
- Ai, X., Do, A.T., Lozynska, O., Kusche-Gullberg, M., Lindahl, U., Emerson, C.P., Jr., 2003. QSulf1 remodels the 6-O sulfation states of cell surface heparan sulfate proteoglycans to promote Wnt signaling. *J Cell Biol* 162, 341–51. <https://doi.org/10.1083/jcb.200212083>
- Ai, X., Kitazawa, T., Do, A.T., Kusche-Gullberg, M., Labosky, P.A., Emerson, C.P., Jr., 2007. SULF1 and SULF2 regulate heparan sulfate-mediated GDNF signaling for esophageal innervation. *Development* 134, 3327–38. <https://doi.org/10.1242/dev.007674>
- Aizawa, S., Okada, T., Keino-Masu, K., Doan, T.H., Koganezawa, T., Akiyama, M., Tamaoka, A., Masu, M., 2019. Abnormal Pyramidal Decussation and Bilateral Projection of the Corticospinal Tract Axons in Mice Lacking the Heparan Sulfate Endosulfatases, Sulf1 and Sulf2. *Front Mol Neurosci* 12, 333. <https://doi.org/10.3389/fnmol.2019.00333>
- Alberti, S., Gladfelter, A., Mittag, T., 2019. Considerations and challenges in studying liquid-liquid phase separation and biomolecular condensates. *Cell* 176, 419–434. <https://doi.org/10.1016/j.cell.2018.12.035>
- Alhasan, A.A., Spielhofer, J., Kusche-Gullberg, M., Kirby, J.A., Ali, S., 2014. Role of 6-O-sulfated heparan sulfate in chronic renal fibrosis. *J Biol Chem* 289, 20295–306. <https://doi.org/10.1074/jbc.M114.554691>
- Alhasan, S.F., Haugk, B., Ogle, L.F., Beale, G.S., Long, A., Burt, A.D., Tiniakos, D., Televantou, D., Coxon, F., Newell, D.R., Charnley, R., Reeves, H.L., 2016. Sulfatase-2: a prognostic biomarker and candidate therapeutic target in patients with pancreatic ductal adenocarcinoma. *Br J Cancer* 115, 797–804. <https://doi.org/10.1038/bjc.2016.264>
- Ambasta, R.K., Ai, X., Emerson, C.P., Jr., 2007. Quail Sulf1 function requires asparagine-linked glycosylation. *J Biol Chem* 282, 34492–9. <https://doi.org/10.1074/jbc.M706744200>
- Andrade, J.P.S., Oliveira, C.P., Tovar, A.M.F., Mourão, P.A. de S., Vilanova, E., 2018. A color-code for glycosaminoglycans identification by means of polyacrylamide gel electrophoresis stained with the cationic carbocyanine dye Stains-all. *ELECTROPHORESIS* 39, 666–669. <https://doi.org/10.1002/elps.201700391>
- Appel, M.J., Bertozzi, C.R., 2015. Formylglycine, a Post-Translationally Generated Residue with Unique Catalytic Capabilities and Biotechnology Applications. *ACS Chem. Biol.* 10, 72–84. <https://doi.org/10.1021/cb500897w>
- Appel, M.J., Meier, K.K., Lafrance-Vanasse, J., Lim, H., Tsai, C.-L., Hedman, B., Hodgson, K.O., Tainer, J.A., Solomon, E.I., Bertozzi, C.R., 2019. Formylglycine-generating enzyme binds substrate directly at a mononuclear Cu(I) center to initiate O₂ activation. *Proc. Natl. Acad. Sci. U.S.A.* 116, 5370–5375. <https://doi.org/10.1073/pnas.1818274116>
- Backen, A.C., Cole, C.L., Lau, S.C., Clamp, A.R., McVey, R., Gallagher, J.T., Jayson, G.C., 2007. Heparan sulphate synthetic and editing enzymes in ovarian cancer. *Br J Cancer* 96, 1544–1548. <https://doi.org/10.1038/sj.bjc.6603747>

- Bao, L., Yan, Y., Xu, C., Ji, W., Shen, S., Xu, G., Zeng, Y., Sun, B., Qian, H., Chen, L., Wu, M., Su, C., Chen, J., 2013. MicroRNA-21 suppresses PTEN and hSulf-1 expression and promotes hepatocellular carcinoma progression through AKT/ERK pathways. *Cancer Letters* 337, 226–236. <https://doi.org/10.1016/j.canlet.2013.05.007>
- Barbeyron, T., Brillet-Guéguen, L., Carré, W., Carrière, C., Caron, C., Czjzek, M., Hoebeke, M., Michel, G., 2016. Matching the Diversity of Sulfated Biomolecules: Creation of a Classification Database for Sulfatases Reflecting Their Substrate Specificity. *PLoS ONE* 11, e0164846. <https://doi.org/10.1371/journal.pone.0164846>
- Benicky, J., Sanda, M., Panigrahi, A., Liu, J., Wang, Z., Pagadala, V., Su, G., Goldman, R., 2023. A 6-O-endosulfatase activity assay based on synthetic heparan sulfate oligomers. *Glycobiology* 33, 384–395. <https://doi.org/10.1093/glycob/cwad026>
- Berg, J.M., Tymoczko, J.L., Stryer, L., 2002. *Biochemistry, Fifth Edition*. W. H. Freeman.
- Bianchi, G., Brocca, S., Longhi, S., Uversky, V.N., 2023. Liaisons dangereuses: Intrinsic Disorder in Cellular Proteins Recruited to Viral Infection-Related Biocondensates. *IJMS* 24, 2151. <https://doi.org/10.3390/ijms24032151>
- Bilong, M., 2022. Caractérisation protéomique et structurale d'endosulfatases humaines Hsulf1 modulant la sulfatation de l'héparane sulfate et biomarqueur de progression tumorale. Paris Saclay.
- Bilong, M., Bayat, P., Bourderioux, M., Jérôme, M., Giuliani, A., Daniel, R., 2021. Mammal hyaluronidase activity on chondroitin sulfate and dermatan sulfate: Mass spectrometry analysis of oligosaccharide products. *Glycobiology* 31, 751–761. <https://doi.org/10.1093/glycob/cwab004>
- Bond, C.S., Clements, P.R., Ashby, S.J., Collyer, C.A., Harrop, S.J., Hopwood, J.J., Guss, J.M., 1997. Structure of a human lysosomal sulfatase. *Structure* 5, 277–289. [https://doi.org/10.1016/S0969-2126\(97\)00185-8](https://doi.org/10.1016/S0969-2126(97)00185-8)
- Brasil da Costa, F.H., Lewis, M.S., Truong, A., Carson, D.D., Farach-Carson, M.C., 2020. SULF1 suppresses Wnt3A-driven growth of bone metastatic prostate cancer in perlecan-modified 3D cancer-stroma-macrophage triculture models. *PLoS One* 15, e0230354. <https://doi.org/10.1371/journal.pone.0230354>
- Bret, C., Moreaux, J., Schved, J.-F., Hose, D., Klein, B., 2011. SULFs in human neoplasia: implication as progression and prognosis factors. *J Transl Med* 9, 72. <https://doi.org/10.1186/1479-5876-9-72>
- Bulleid, N.J., 2012. Disulfide Bond Formation in the Mammalian Endoplasmic Reticulum. *Cold Spring Harbor Perspectives in Biology* 4, a013219–a013219. <https://doi.org/10.1101/cshperspect.a013219>
- Buszewski, B., Noga, S., 2012. Hydrophilic interaction liquid chromatography (HILIC)—a powerful separation technique. *Anal Bioanal Chem* 402, 231–247. <https://doi.org/10.1007/s00216-011-5308-5>
- Carr, R.M., Romecin Duran, P.A., Tolosa, E.J., Ma, C., Oseini, A.M., Moser, C.D., Banini, B.A., Huang, J., Asumda, F., Dhanasekaran, R., Graham, R.P., Toruner, M.D., Safgren, S.L., Almada, L.L., Wang, S., Patnaik, M.M., Roberts, L.R., Fernandez-Zapico, M.E., 2020. The extracellular sulfatase SULF2 promotes liver tumorigenesis by stimulating assembly of a promoter-looping GLI1-STAT3 transcriptional complex. *J Biol Chem* 295, 2698–2712. <https://doi.org/10.1074/jbc.RA119.011146>
- Celie, J.W.A.M., Rutjes, N.W.P., Keuning, E.D., Soininen, R., Heljasvaara, R., Pihlajaniemi, T., Dräger, A.M., Zweegman, S., Kessler, F.L., Beelen, R.H.J., Florquin, S., Aten, J., van den Born, J., 2007. Subendothelial Heparan Sulfate Proteoglycans Become Major L-Selectin and Monocyte Chemoattractant Protein-1 Ligands upon Renal Ischemia/Reperfusion. *Am J Pathol* 170, 1865–1878. <https://doi.org/10.2353/ajpath.2007.070061>
- Chanalaris, A., Clarke, H., Guimond, S.E., Vincent, T.L., Turnbull, J.E., Troeberg, L., 2019. Heparan Sulfate Proteoglycan Synthesis Is Dysregulated in Human Osteoarthritic Cartilage. *The American Journal of Pathology* 189, 632–647. <https://doi.org/10.1016/j.ajpath.2018.11.011>
- Chau, B.N., Diaz, R.L., Saunders, M.A., Cheng, C., Chang, A.N., Warrenner, P., Bradshaw, J., Linsley, P.S., Cleary, M.A., 2009. Identification of SULF2 as a Novel Transcriptional Target of p53 by

- Use of Integrated Genomic Analyses. *Cancer Research* 69, 1368–1374. <https://doi.org/10.1158/0008-5472.CAN-08-2742>
- Chen, J., Jones, C.L., Liu, J., 2007. Using an Enzymatic Combinatorial Approach to Identify Anticoagulant Heparan Sulfate Structures. *Chemistry & Biology* 14, 986–993. <https://doi.org/10.1016/j.chembiol.2007.07.015>
- Chen, K., Liu, M.L., Schaffer, L., Li, M., Boden, G., Wu, X., Williams, K.J., 2010. Type 2 diabetes in mice induces hepatic overexpression of sulfatase 2, a novel factor that suppresses uptake of remnant lipoproteins. *Hepatology* 52, 1957–67. <https://doi.org/10.1002/hep.23916>
- Chiu, L.-T., Sabbavarapu, N.M., Lin, W.-C., Fan, C.-Y., Wu, C.-C., Cheng, T.-J.R., Wong, C.-H., Hung, S.-C., 2020. Trisaccharide Sulfate and Its Sulfonamide as an Effective Substrate and Inhibitor of Human Endo-O-sulfatase-1. *J. Am. Chem. Soc.* 142, 5282–5292. <https://doi.org/10.1021/jacs.0c00005>
- Cosma, M.P., Pepe, S., Annunziata, I., Newbold, R.F., Grompe, M., Parenti, G., Ballabio, A., 2003. The multiple sulfatase deficiency gene encodes an essential and limiting factor for the activity of sulfatases. *Cell* 113, 445–56. [https://doi.org/10.1016/s0092-8674\(03\)00348-9](https://doi.org/10.1016/s0092-8674(03)00348-9)
- Costa, L., Andriatis, A., Brennich, M., Teulon, J.-M., Chen, S.W., Pellequer, J.-L., Round, A., 2016. Combined small angle X-ray solution scattering with atomic force microscopy for characterizing radiation damage on biological macromolecules. *BMC Struct Biol* 16, 18. <https://doi.org/10.1186/s12900-016-0068-2>
- Coutinho, M.F., Prata, M.J., Alves, S., 2012. Mannose-6-phosphate pathway: A review on its role in lysosomal function and dysfunction. *Molecular Genetics and Metabolism* 105, 542–550. <https://doi.org/10.1016/j.ymgme.2011.12.012>
- Cretinon, Y., 2022. Caractérisation structurale de HSulf par microscopie électronique, cristallographie et RMN. Grenoble Alpes.
- Dai, Y., Yang, Y., MacLeod, V., Yue, X., Rapraeger, A.C., Shriver, Z., Venkataraman, G., Sasisekharan, R., Sanderson, R.D., 2005. HSulf-1 and HSulf-2 Are Potent Inhibitors of Myeloma Tumor Growth in Vivo. *Journal of Biological Chemistry* 280, 40066–40073. <https://doi.org/10.1074/jbc.M508136200>
- Danesin, C., Agius, E., Escalas, N., Ai, X., Emerson, C., Cochard, P., Soula, C., 2006. Ventral neural progenitors switch toward an oligodendroglial fate in response to increased Sonic hedgehog (Shh) activity: involvement of Sulfatase 1 in modulating Shh signaling in the ventral spinal cord. *J Neurosci* 26, 5037–48. <https://doi.org/10.1523/JNEUROSCI.0715-06.2006>
- Daško, M., Demkowicz, S., Biernacki, K., Ciupak, O., Kozak, W., Masyk, M., Rachon, J., 2020. Recent progress in the development of steroid sulphatase inhibitors – examples of the novel and most promising compounds from the last decade. *J Enzyme Inhib Med Chem* 35, 1163–1184. <https://doi.org/10.1080/14756366.2020.1758692>
- De Pascale, V., Quiccione, M.S., Tafuri, S., 2021. Heparan Sulfate Proteoglycans in Viral Infection and Treatment: A Special Focus on SARS-CoV-2 - PMC.
- Demydchuk, M., Hill, C.H., Zhou, A., Bunkóczi, G., Stein, P.E., Marchesan, D., Deane, J.E., Read, R.J., 2017. Insights into Hunter syndrome from the structure of iduronate-2-sulfatase. *Nat Commun* 8, 15786. <https://doi.org/10.1038/ncomms15786>
- Dhoot, G.K., Gustafsson, M.K., Ai, X., Sun, W., Standiford, D.M., Emerson, C.P., Jr., 2001. Regulation of Wnt signaling and embryo patterning by an extracellular sulfatase. *Science* 293, 1663–6. <https://doi.org/10.1126/science.293.5535.1663>
- Di Palma, S., Boersema, P.J., Heck, A.J.R., Mohammed, S., 2011. Zwitterionic Hydrophilic Interaction Liquid Chromatography (ZIC-HILIC and ZIC-cHILIC) Provide High Resolution Separation and Increase Sensitivity in Proteome Analysis. *Anal. Chem.* 83, 3440–3447. <https://doi.org/10.1021/ac103312e>
- Dierks, T., Dickmanns, A., Preusser-Kunze, A., Schmidt, B., Mariappan, M., Von Figura, K., Ficner, R., Rudolph, M.G., 2005. Molecular Basis for Multiple Sulfatase Deficiency and Mechanism for Formylglycine Generation of the Human Formylglycine-Generating Enzyme. *Cell* 121, 541–552. <https://doi.org/10.1016/j.cell.2005.03.001>

- Dierks, T., Schlotawa, L., Frese, M.-A., Radhakrishnan, K., Von Figura, K., Schmidt, B., 2009. Molecular basis of multiple sulfatase deficiency, mucopolidosis II/III and Niemann–Pick C1 disease — Lysosomal storage disorders caused by defects of non-lysosomal proteins. *Biochimica et Biophysica Acta (BBA) - Molecular Cell Research* 1793, 710–725. <https://doi.org/10.1016/j.bbamcr.2008.11.015>
- Diez-Roux, G., Ballabio, A., 2005. SULFATASES AND HUMAN DISEASE. *Annual Review of Genomics and Human Genetics* 6, 355–379. <https://doi.org/10.1146/annurev.genom.6.080604.162334>
- El Masri, R., 2019. Remodeling of heparan sulfate: functional and structural characterization of human endosulfatase HSulf-2. Grenoble Alpes.
- El Masri, R., Cretinon, Y., Gout, E., Vives, R.R., 2020. HS and Inflammation: A Potential Playground for the Sulfs? *Front Immunol* 11, 570. <https://doi.org/10.3389/fimmu.2020.00570>
- El Masri, R., Seffouh, A., Lortat-Jacob, H., Vivès, R.R., 2016. The “in and out” of glucosamine 6-O-sulfation: the 6th sense of heparan sulfate. *Glycoconj J* 34, 285–298. <https://doi.org/10.1007/s10719-016-9736-5>
- El Masri, R., Seffouh, A., Roelants, C., Seffouh, I., Gout, E., Perard, J., Dalonneau, F., Nishitsuji, K., Noborn, F., Nikpour, M., Larson, G., Cretinon, Y., Friedel-Arboleas, M., Uchimura, K., Daniel, R., Lortat-Jacob, H., Filhol, O., Vives, R.R., 2022. Extracellular endosulfatase Sulf-2 harbors a chondroitin/dermatan sulfate chain that modulates its enzyme activity. *Cell Rep* 38, 110516. <https://doi.org/10.1016/j.celrep.2022.110516>
- Ellgaard, L., Sevier, C.S., Bulleid, N.J., 2018. How Are Proteins Reduced in the Endoplasmic Reticulum? *Trends in Biochemical Sciences* 43, 32–43. <https://doi.org/10.1016/j.tibs.2017.10.006>
- Esko, J.D., Kimata, K., Lindahl, U., 2009. Proteoglycans and Sulfated Glycosaminoglycans, in: Varki, A., Cummings, R.D., Esko, J.D., Freeze, H.H., Stanley, P., Bertozzi, C.R., Hart, G.W., Etzler, M.E. (Eds.), *Essentials of Glycobiology*. Cold Spring Harbor Laboratory Press, Cold Spring Harbor (NY).
- Esko, J.D., Selleck, S.B., 2002. Order Out of Chaos: Assembly of Ligand Binding Sites in Heparan Sulfate. *Annu. Rev. Biochem.* 71, 435–471. <https://doi.org/10.1146/annurev.biochem.71.110601.135458>
- Feige, M.J., BRAAKMAN, I., M.HENDERSHOT, L., 2018. Disulfide Bonds in Protein Folding and Stability, in: *Oxidative Folding of Proteins: Basic Principles, Cellular Regulation and Engineering, Chemical Biology*.
- Fellgett, S.W., Maguire, R.J., Pownall, M.E., 2015. Sulf1 has ligand-dependent effects on canonical and non-canonical Wnt signalling. *Journal of Cell Science* 128, 1408–1421. <https://doi.org/10.1242/jcs.164467>
- Fenn, L.S., McLean, J.A., 2008. Biomolecular structural separations by ion mobility–mass spectrometry. *Anal Bioanal Chem* 391, 905–909. <https://doi.org/10.1007/s00216-008-1951-x>
- Ferrara, N., Gerber, H.-P., LeCouter, J., 2003. The biology of VEGF and its receptors. *Nat Med* 9, 669–676. <https://doi.org/10.1038/nm0603-669>
- Flowers, S.A., Zhou, X., Wu, J., Wang, Y., Makambi, K., Kallakury, B.V., Singer, M.S., Rosen, S.D., Davidson, B., Goldman, R., 2016. Expression of the extracellular sulfatase SULF2 is associated with squamous cell carcinoma of the head and neck. *Oncotarget* 7, 43177–43187. <https://doi.org/10.18632/oncotarget.9506>
- Foster, P.A., 2021. Steroid Sulphatase and Its Inhibitors: Past, Present, and Future. *Molecules* 26, 2852. <https://doi.org/10.3390/molecules26102852>
- Franco, B., Meroni, G., Parenti, G., Levilliers, J., Bernard, L., Gebbia, M., Cox, L., Maroteaux, P., Sheffield, L., Rappold, G.A., Andria, G., Petit, C., Ballabio, A., 1995. A cluster of sulfatase genes on Xp22.3: Mutations in chondrodysplasia punctata (CDPX) and implications for warfarin embryopathy. *Cell* 81, 15–25. [https://doi.org/10.1016/0092-8674\(95\)90367-4](https://doi.org/10.1016/0092-8674(95)90367-4)
- Freeman, S.D., Moore, W.M., Guiral, E.C., Holme, A.D., Turnbull, J.E., Pownall, M.E., 2008. Extracellular regulation of developmental cell signaling by XtSulf1. *Dev Biol* 320, 436–45. <https://doi.org/10.1016/j.ydbio.2008.05.554>

- Frese, M.-A., Milz, F., Dick, M., Lamanna, W.C., Dierks, T., 2009. Characterization of the Human Sulfatase Sulf1 and Its High Affinity Heparin/Heparan Sulfate Interaction Domain. *Journal of Biological Chemistry* 284, 28033–28044. <https://doi.org/10.1074/jbc.M109.035808>
- Fujita, K., Takechi, E., Sakamoto, N., Sumiyoshi, N., Izumi, S., Miyamoto, T., Matsuura, S., Tsurugaya, T., Akasaka, K., Yamamoto, T., 2010. HpSulf, a heparan sulfate 6-O-endosulfatase, is involved in the regulation of VEGF signaling during sea urchin development. *Mechanisms of Development* 127, 235–245. <https://doi.org/10.1016/j.mod.2009.12.001>
- Gallagher, J., 2015. Fell–Muir Lecture: Heparan sulphate and the art of cell regulation: a polymer chain conducts the protein orchestra. *Int J Experimental Path* 96, 203–231. <https://doi.org/10.1111/iep.12135>
- Gaunt, S.J., 2022. Seeking Sense in the Hox Gene Cluster. *J Dev Biol* 10, 48. <https://doi.org/10.3390/jdb10040048>
- Giles, K., Ujma, J., Wildgoose, J., Pringle, S., Richardson, K., Langridge, D., Green, M., 2019. A Cyclic Ion Mobility-Mass Spectrometry System. *Anal. Chem.* 91, 8564–8573. <https://doi.org/10.1021/acs.analchem.9b01838>
- Gill, R., Hitchins, L., Fletcher, F., Dhoot, G.K., 2010. Sulf1A and HGF regulate satellite-cell growth. *J Cell Sci* 123, 1873–83. <https://doi.org/10.1242/jcs.061242>
- Gill, R.B., Day, A., Barstow, A., Liu, H., Zaman, G., Dhoot, G.K., 2011. Sulf2 gene is alternatively spliced in mammalian developing and tumour tissues with functional implications. *Biochem Biophys Res Commun* 414, 468–73. <https://doi.org/10.1016/j.bbrc.2011.09.088>
- Gill, R.M.S., Michael, A., Westley, L., Kocher, H.M., Murphy, J.I., Dhoot, G.K., 2014. SULF1/SULF2 splice variants differentially regulate pancreatic tumour growth progression. *Experimental Cell Research* 324, 157–171. <https://doi.org/10.1016/j.yexcr.2014.04.001>
- Gill, V.L., Aich, U., Rao, S., Pohl, C., Zaia, J., 2013. Disaccharide Analysis of Glycosaminoglycans Using Hydrophilic Interaction Chromatography and Mass Spectrometry. *Anal. Chem.* 85, 1138–1145. <https://doi.org/10.1021/ac3030448>
- Gorsi, B., Whelan, S., Stringer, S.E., 2010. Dynamic expression patterns of 6-O endosulfatases during zebrafish development suggest a subfunctionalisation event for *sulf2*. *Developmental Dynamics* 239, 3312–3323. <https://doi.org/10.1002/dvdy.22456>
- Gray, C.J., Thomas, B., Upton, R., Migas, L.G., Eyers, C.E., Barran, P.E., Flitsch, S.L., 2016. Applications of ion mobility mass spectrometry for high throughput, high resolution glycan analysis. *Biochimica et Biophysica Acta (BBA) - General Subjects, Glycans in personalised medicine* 1860, 1688–1709. <https://doi.org/10.1016/j.bbagen.2016.02.003>
- Hammond, E., Khurana, A., Shridhar, V., Dredge, K., 2014. The Role of Heparanase and Sulfatases in the Modification of Heparan Sulfate Proteoglycans within the Tumor Microenvironment and Opportunities for Novel Cancer Therapeutics. *Front Oncol* 4, 195. <https://doi.org/10.3389/fonc.2014.00195>
- Han, C.H., Huang, Y.J., Lu, K.H., Liu, Z., Mills, G.B., Wei, Q., Wang, L.E., 2011. Polymorphisms in the SULF1 gene are associated with early age of onset and survival of ovarian cancer. *J Exp Clin Cancer Res* 30, 5. <https://doi.org/10.1186/1756-9966-30-5>
- Han, M., 2024. 6-O-endosulfatases in tumor metastasis: heparan sulfate proteoglycans modification and potential therapeutic targets. *Am J Cancer Res* 14, 897–916. <https://doi.org/10.62347/RXVE7097>
- Hanson, Sarah R., Best, M.D., Wong, C., 2004. Sulfatases: Structure, Mechanism, Biological Activity, Inhibition, and Synthetic Utility. *Angew Chem Int Ed* 43, 5736–5763. <https://doi.org/10.1002/anie.200300632>
- Hanson, S. R., Best, M.D., Wong, C.H., 2004. Sulfatases: structure, mechanism, biological activity, inhibition, and synthetic utility. *Angew Chem Int Ed Engl* 43, 5736–63. <https://doi.org/10.1002/anie.200300632>
- Harder, A., Moller, A.K., Milz, F., Neuhaus, P., Walhorn, V., Dierks, T., Anselmetti, D., 2015. Catch bond interaction between cell-surface sulfatase Sulf1 and glycosaminoglycans. *Biophys J* 108, 1709–1717. <https://doi.org/10.1016/j.bpj.2015.02.028>

- Hassing, H.C., Mooij, H., Guo, S., Monia, B.P., Chen, K., Kulik, W., Dallinga-Thie, G.M., Nieuwdorp, M., Stroes, E.S.G., Williams, K.J., 2012. Inhibition of hepatic sulfatase-2 In Vivo: A novel strategy to correct diabetic dyslipidemia. *Hepatology* 55, 1746–1753. <https://doi.org/10.1002/hep.25580>
- Hassing, H.C., Surendran, R.P., Derudas, B., Verrijken, A., Francque, S.M., Mooij, H.L., Bernelot Moens, S.J., Hart, L.M. 't, Nijpels, G., Dekker, J.M., Williams, K.J., Stroes, E.S.G., Van Gaal, L.F., Staels, B., Nieuwdorp, M., Dallinga-Thie, G.M., 2014. *SULF2* strongly predisposes to fasting and postprandial triglycerides in patients with obesity and type 2 diabetes mellitus. *Obesity* 22, 1309–1316. <https://doi.org/10.1002/oby.20682>
- He, X., Khurana, A., Roy, D., Kaufmann, S., Shridhar, V., 2014. Loss of HSulf-1 expression enhances tumorigenicity by inhibiting Bim expression in ovarian cancer. *Int J Cancer* 135, 1783–1789. <https://doi.org/10.1002/ijc.28818>
- Higginson, J.R., Thompson, S.M., Santos-Silva, A., Guimond, S.E., Turnbull, J.E., Barnett, S.C., 2012. Differential Sulfation Remodelling of Heparan Sulfate by Extracellular 6- *O* -Sulfatases Regulates Fibroblast Growth Factor-Induced Boundary Formation by Glial Cells: Implications for Glial Cell Transplantation. *J. Neurosci.* 32, 15902–15912. <https://doi.org/10.1523/JNEUROSCI.6340-11.2012>
- Hitchins, L., Fletcher, F., Allen, S., Dhoot, G.K., 2012. Role of Sulf1A in Wnt1- and Wnt6-induced growth regulation and myoblast hyper-elongation. *FEBS Open Bio* 3, 30–34. <https://doi.org/10.1016/j.fob.2012.11.007>
- Holmes, R.S., 2017. Comparative and Evolutionary Studies of Vertebrate Extracellular Sulfatase Genes and Proteins: SULF1 and SULF2. *J Proteomics Bioinform* 10. <https://doi.org/10.4172/jpb.1000423>
- Holmes, R.S., 2016. Comparative and Evolutionary Studies of Vertebrate Arylsulfatase B, Arylsulfatase I and Arylsulfatase J Genes and Proteins: Evidence for an ARSB-like Sub-family. *J Proteomics Bioinform* 9. <https://doi.org/10.4172/jpb.1000418>
- Holst, C.R., Bou-Reslan, H., Gore, B.B., Wong, K., Grant, D., Chalasani, S., Carano, R.A., Frantz, G.D., Tessier-Lavigne, M., Bolon, B., French, D.M., Ashkenazi, A., 2007. Secreted sulfatases Sulf1 and Sulf2 have overlapping yet essential roles in mouse neonatal survival. *PLoS One* 2, e575. <https://doi.org/10.1371/journal.pone.0000575>
- Honda, T., Kaneiwa, T., Mizumoto, S., Sugahara, K., Yamada, S., 2012. Hyaluronidases Have Strong Hydrolytic Activity toward Chondroitin 4-Sulfate Comparable to that for Hyaluronan. *Biomolecules* 2, 549–563. <https://doi.org/10.3390/biom2040549>
- Hosono-Fukao, T., Ohtake-Niimi, S., Hoshino, H., Britschgi, M., Akatsu, H., Hossain, M.M., Nishitsuji, K., van Kuppevelt, T.H., Kimata, K., Michikawa, M., Wyss-Coray, T., Uchimura, K., 2012. Heparan sulfate subdomains that are degraded by Sulf accumulate in cerebral amyloid ss plaques of Alzheimer's disease: evidence from mouse models and patients. *Am J Pathol* 180, 2056–67. <https://doi.org/10.1016/j.ajpath.2012.01.015>
- Hossain, M.M., Hosono-Fukao, T., Tang, R., Sugaya, N., van Kuppevelt, T.H., Jenniskens, G.J., Kimata, K., Rosen, S.D., Uchimura, K., 2010. Direct detection of HSulf-1 and HSulf-2 activities on extracellular heparan sulfate and their inhibition by PI-88. *Glycobiology* 20, 175–86. <https://doi.org/10.1093/glycob/cwp159>
- Huang, Y., Mao, Y., Buczek-Thomas, J.A., Nugent, M.A., Zaia, J., 2014. Oligosaccharide Substrate Preferences of Human Extracellular Sulfatase Sulf2 Using Liquid Chromatography-Mass Spectrometry Based Glycomics Approaches. *PLoS ONE* 9, e105143. <https://doi.org/10.1371/journal.pone.0105143>
- Hur, K., Han, T., Jung, E., Yu, J., Lee, H., Kim, W.H., Goel, A., Yang, H., 2012. Up-regulated expression of sulfatases (SULF1 and SULF2) as prognostic and metastasis predictive markers in human gastric cancer. *The Journal of Pathology* 228, 88–98. <https://doi.org/10.1002/path.4055>
- Ingham, P.W., McMahon, A.P., 2001. Hedgehog signaling in animal development: paradigms and principles. *Genes Dev* 15, 3059–3087. <https://doi.org/10.1101/gad.938601>

- Isidor, B., Pichon, O., Redon, R., Day-Salvatore, D., Hamel, A., Siwicka, K.A., Bitner-Glindzicz, M., Heymann, D., Kjellen, L., Kraus, C., Leroy, J.G., Mortier, G.R., Rauch, A., Verloes, A., David, A., Le Caignec, C., 2010. Mesomelia-synostoses syndrome results from deletion of *SULF1* and *SLCO5A1* genes at 8q13. *Am J Hum Genet* 87, 95–100. <https://doi.org/10.1016/j.ajhg.2010.05.012>
- Iwahashi, N., Ikezaki, M., Nishikawa, T., Namba, N., Ohgita, T., Saito, H., Ihara, Y., Shimanouchi, T., Ino, K., Uchimura, K., Nishitsuji, K., 2020. Sulfated glycosaminoglycans mediate prion-like behavior of p53 aggregates. *Proc Natl Acad Sci U S A* 117, 33225–33234. <https://doi.org/10.1073/pnas.2009931117>
- Jiang, T., Chen, Z.H., Chen, Z., Tan, D., 2020. *SULF2* promotes tumorigenesis and inhibits apoptosis of cervical cancer cells through the ERK/AKT signaling pathway. *Braz J Med Biol Res* 53, e8901. <https://doi.org/10.1590/1414-431x20198901>
- Jiang, W., Ishino, Y., Hashimoto, H., Keino-Masu, K., Masu, M., Uchimura, K., Kadomatsu, K., Yoshimura, T., Ikenaka, K., 2017. Sulfatase 2 Modulates Fate Change from Motor Neurons to Oligodendrocyte Precursor Cells through Coordinated Regulation of Shh Signaling with Sulfatase 1. *Dev Neurosci* 39, 361–374. <https://doi.org/10.1159/000464284>
- Jo, Y., Jang, J., Song, D., Park, H., Jung, Y., 2022. Determinants for intrinsically disordered protein recruitment into phase-separated protein condensates. *Chem. Sci.* 13, 522–530. <https://doi.org/10.1039/D1SC05672G>
- Johansson, F.K., Brodd, J., Eklöf, C., Ferletta, M., Hesselager, G., Tiger, C.F., Uhrbom, L., Westermarck, B., 2004. Identification of candidate cancer-causing genes in mouse brain tumors by retroviral tagging. *Proc Natl Acad Sci U S A* 101, 11334–7. <https://doi.org/10.1073/pnas.0402716101>
- Johansson, F.K., Goransson, H., Westermarck, B., 2005. Expression analysis of genes involved in brain tumor progression driven by retroviral insertional mutagenesis in mice. *Oncogene* 24, 3896–905. <https://doi.org/10.1038/sj.onc.1208553>
- Joy, M.T., Vrbova, G., Dhoot, G.K., Anderson, P.N., 2015. *Sulf1* and *Sulf2* expression in the nervous system and its role in limiting neurite outgrowth *in vitro*. *Experimental Neurology* 263, 150–160. <https://doi.org/10.1016/j.expneurol.2014.10.011>
- Jumper, J., Evans, R., Pritzel, A., Green, T., Figurnov, M., Ronneberger, O., Tunyasuvunakool, K., Bates, R., Židek, A., Potapenko, A., Bridgland, A., Meyer, C., Kohl, S.A.A., Ballard, A.J., Cowie, A., Romera-Paredes, B., Nikolov, S., Jain, R., Adler, J., Back, T., Petersen, S., Reiman, D., Clancy, E., Zielinski, M., Steinegger, M., Pacholska, M., Berghammer, T., Bodenstein, S., Silver, D., Vinyals, O., Senior, A.W., Kavukcuoglu, K., Kohli, P., Hassabis, D., 2021. Highly accurate protein structure prediction with AlphaFold. *Nature* 596, 583–589. <https://doi.org/10.1038/s41586-021-03819-2>
- Junnala, S., Kokkola, A., Mizuguchi, T., Hirata, K., Karjalainen-Lindsberg, M., Puolakkainen, P., Monni, O., 2010. Gene expression analysis identifies over-expression of *CXCL1*, *SPARC*, *SPPI*, and *SULF1* in gastric cancer. *Genes Chromosomes & Cancer* 49, 28–39. <https://doi.org/10.1002/gcc.20715>
- Justo, T., Martiniuc, A., Dhoot, G.K., 2021. Modulation of cell signalling and sulfation in cardiovascular development and disease. *Sci Rep* 11, 22424. <https://doi.org/10.1038/s41598-021-01629-0>
- Justo, T., Smart, N., Dhoot, G.K., 2022. Context Dependent *Sulf1/Sulf2* Functional Divergence in Endothelial Cell Activity. *Int J Mol Sci* 23. <https://doi.org/10.3390/ijms23073769>
- Kalus, I., Rohn, S., Puvirajesinghe, T.M., Guimond, S.E., Eyckerman-Kolln, P.J., Ten Dam, G., van Kuppevelt, T.H., Turnbull, J.E., Dierks, T., 2015. *Sulf1* and *Sulf2* Differentially Modulate Heparan Sulfate Proteoglycan Sulfation during Postnatal Cerebellum Development: Evidence for Neuroprotective and Neurite Outgrowth Promoting Functions. *PLoS One* 10, e0139853. <https://doi.org/10.1371/journal.pone.0139853>
- Kalus, I., Salmen, B., Viebahn, C., von Figura, K., Schmitz, D., D’Hooge, R., Dierks, T., 2009. Differential involvement of the extracellular 6-O-endosulfatases *Sulf1* and *Sulf2* in brain development and neuronal and behavioural plasticity. *J Cell Mol Med* 13, 4505–21. <https://doi.org/10.1111/j.1582-4934.2008.00558.x>

- Kameyama, H., Uchimura, K., Yamashita, T., Kuwabara, K., Mizuguchi, M., Hung, S.C., Okuhira, K., Masuda, T., Kosugi, T., Ohgita, T., Saito, H., Ando, Y., Nishitsuji, K., 2019. The Accumulation of Heparan Sulfate S-Domains in Kidney Transthyretin Deposits Accelerates Fibril Formation and Promotes Cytotoxicity. *Am J Pathol* 189, 308–319. <https://doi.org/10.1016/j.ajpath.2018.09.015>
- Katagiri, T., Watabe, T., 2016. Bone Morphogenetic Proteins. *Cold Spring Harb Perspect Biol* 8, a021899. <https://doi.org/10.1101/cshperspect.a021899>
- Kayed, H., Kleeff, J., Keleg, S., Jiang, X., Penzel, R., Giese, T., Zentgraf, H., Büchler, M.W., Korc, M., Friess, H., 2006. Correlation of glypican-1 expression with TGF-beta, BMP, and activin receptors in pancreatic ductal adenocarcinoma. *Int J Oncol* 29, 1139–48.
- Kennett, A., Epple, S., Van Der Valk, G., Georgiou, I., Gout, E., Vives, R.R., Russell, A., 2023. Modified minimal-size fragments of Heparan Sulfate as inhibitors of endosulfatase-2 (Sulf-2). *Chem. Commun.* 10.1039.D3CC02565A. <https://doi.org/10.1039/D3CC02565A>
- Khan, S., Fung, K.W., 馮家維, Rodriguez, E., Patel, R., Gor, J., Mulloy, B., Perkins, S.J., 2013. The Solution Structure of Heparan Sulfate Differs from That of Heparin. *Journal of Biological Chemistry* 288, 27737–27751. <https://doi.org/10.1074/jbc.M113.492223>
- Khurana, A., Jung-Beom, D., He, X., Kim, S.-H., Busby, R.C., Lorenzon, L., Villa, M., Baldi, A., Molina, J., Goetz, M.P., Shridhar, V., 2013. Matrix detachment and proteasomal inhibitors diminish Sulf-2 expression in breast cancer cell lines and mouse xenografts. *Clin Exp Metastasis* 30, 407–415. <https://doi.org/10.1007/s10585-012-9546-5>
- Khurana, A., Liu, P., Mellone, P., Lorenzon, L., Vincenzi, B., Datta, K., Yang, B., Linhardt, R.J., Lingle, W., Chien, J., Baldi, A., Shridhar, V., 2011. HSulf-1 modulates FGF2- and hypoxia-mediated migration and invasion of breast cancer cells. *Cancer Res* 71, 2152–61. <https://doi.org/10.1158/0008-5472.CAN-10-3059>
- Khurana, A., Tun, H.W., Marlow, L., Copland, J.A., Dredge, K., Shridhar, V., 2012. Hypoxia negatively regulates heparan sulfatase 2 expression in renal cancer cell lines. *Molecular Carcinogenesis* 51, 565–575. <https://doi.org/10.1002/mc.20824>
- Komiya, Y., Habas, R., 2008. Wnt signal transduction pathways. *Organogenesis* 4, 68–75. <https://doi.org/10.4161/org.4.2.5851>
- Korf-Klingebiel, M., Reboll, M.R., Grote, K., Schleiner, H., Wang, Y., Wu, X., Klede, S., Mikhed, Y., Bauersachs, J., Klintschar, M., Rudat, C., Kispert, A., Niessen, H.W., Lubke, T., Dierks, T., Wollert, K.C., 2019. Heparan Sulfate-Editing Extracellular Sulfatases Enhance VEGF Bioavailability for Ischemic Heart Repair. *Circ Res* 125, 787–801. <https://doi.org/10.1161/CIRCRESAHA.119.315023>
- Krishnakumar, K., Chakravorty, I., Foy, W., Allen, S., Justo, T., Mukherjee, A., Dhoot, G.K., 2018. Multi-tasking Sulf1/Sulf2 enzymes do not only facilitate extracellular cell signalling but also participate in cell cycle related nuclear events. *Exp Cell Res* 364, 16–27. <https://doi.org/10.1016/j.yexcr.2018.01.022>
- Kumagai, S., Ishibashi, K., Kataoka, M., Oguro, T., Kiko, Y., Yanagida, T., Aikawa, K., Kojima, Y., 2016. Impact of Sulfatase-2 on cancer progression and prognosis in patients with renal cell carcinoma. *Cancer Science* 107, 1632–1641. <https://doi.org/10.1111/cas.13074>
- Lai, J., Chien, J., Staub, J., Avula, R., Greene, E.L., Matthews, T.A., Smith, D.I., Kaufmann, S.H., Roberts, L.R., Shridhar, V., 2003. Loss of HSulf-1 up-regulates heparin-binding growth factor signaling in cancer. *J Biol Chem* 278, 23107–17. <https://doi.org/10.1074/jbc.M302203200>
- Lai, J., Chien, J.R., Moser, D.R., Staub, J.K., Aderca, I., Montoya, D.P., Matthews, T.A., Naborney, D.M., Cunningham, J.M., Smith, D.I., Greene, E.L., Shridhar, V., Roberts, L.R., 2004. hSulf1 sulfatase promotes apoptosis of hepatocellular cancer cells by decreasing heparin-binding growth factor signaling. *Gastroenterology* 126, 231–248. <https://doi.org/10.1053/j.gastro.2003.09.043>
- Lai, J.P., Chien, J., Strome, S.E., Staub, J., Montoya, D.P., Greene, E.L., Smith, D.I., Roberts, L.R., Shridhar, V., 2004. HSulf-1 modulates HGF-mediated tumor cell invasion and signaling in head and neck squamous carcinoma. *Oncogene* 23, 1439–47. <https://doi.org/10.1038/sj.onc.1207258>

- Lai, J.P., Oseini, A.M., Moser, C.D., Yu, C., Elswa, S.F., Hu, C., Nakamura, I., Han, T., Aderca, I., Isomoto, H., Garrity-Park, M.M., Shire, A.M., Li, J., Sanderson, S.O., Adjei, A.A., Fernandez-Zapico, M.E., Roberts, L.R., 2010. The oncogenic effect of sulfatase 2 in human hepatocellular carcinoma is mediated in part by glypican 3-dependent Wnt activation. *Hepatology* 52, 1680–9. <https://doi.org/10.1002/hep.23848>
- Lai, J.-P., Sandhu, D.S., Shire, A.M., Roberts, L.R., 2008. The tumor suppressor function of human sulfatase 1 (SULF1) in carcinogenesis. *J Gastrointest Cancer* 39, 149–158. <https://doi.org/10.1007/s12029-009-9058-y>
- Lai, J.P., Sandhu, D.S., Yu, C., Han, T., Moser, C.D., Jackson, K.K., Guerrero, R.B., Aderca, I., Isomoto, H., Garrity-Park, M.M., Zou, H., Shire, A.M., Nagorney, D.M., Sanderson, S.O., Adjei, A.A., Lee, J.S., Thorgeirsson, S.S., Roberts, L.R., 2008. Sulfatase 2 up-regulates glypican 3, promotes fibroblast growth factor signaling, and decreases survival in hepatocellular carcinoma. *Hepatology* 47, 1211–22. <https://doi.org/10.1002/hep.22202>
- Lai, J.P., Yu, C., Moser, C.D., Aderca, I., Han, T., Garvey, T.D., Murphy, L.M., Garrity-Park, M.M., Shridhar, V., Adjei, A.A., Roberts, L.R., 2006. SULF1 inhibits tumor growth and potentiates the effects of histone deacetylase inhibitors in hepatocellular carcinoma. *Gastroenterology* 130, 2130–44. <https://doi.org/10.1053/j.gastro.2006.02.056>
- Lamanna, W.C., Baldwin, R.J., Padva, M., Kalus, I., Dam, G.T. ten, Kuppevelt, T.V. van, Gallagher, J., Figura, K. von, Dierks, T., Merry, C., 2006. Heparan sulfate 6-O-endosulfatases: discrete in vivo activities and functional co-operativity. *The Biochemical journal* 400 1, 63–73. <https://doi.org/10.1042/BJ20060848>
- Lamanna, W.C., Frese, M.A., Balleininger, M., Dierks, T., 2008. Sulf loss influences N-, 2-O-, and 6-O-sulfation of multiple heparan sulfate proteoglycans and modulates fibroblast growth factor signaling. *J Biol Chem* 283, 27724–27735. <https://doi.org/10.1074/jbc.M802130200>
- Lamanna, W.C., Kalus, I., Padva, M., Baldwin, R.J., Merry, C.L.R., Dierks, T., 2007. The heparanome—The enigma of encoding and decoding heparan sulfate sulfation. *Journal of Biotechnology* 129, 290–307. <https://doi.org/10.1016/j.jbiotec.2007.01.022>
- Langsdorf, A., Do, A.-T., Kusche-Gullberg, M., Emerson Jr., C.P., Ai, X., 2007. Sulfs are regulators of growth factor signaling for satellite cell differentiation and muscle regeneration. *Developmental Biology* 311, 464–477. <https://doi.org/10.1016/j.ydbio.2007.08.053>
- Langsdorf, A., Schumacher, V., Shi, X., Tran, T., Zaia, J., Jain, S., Taglienti, M., Kreidberg, J.A., Fine, A., Ai, X., 2011. Expression regulation and function of heparan sulfate 6-O-endosulfatases in the spermatogonial stem cell niche. *Glycobiology* 21, 152–61. <https://doi.org/10.1093/glycob/cwq133>
- Lanucara, F., Holman, S.W., Gray, C.J., Evers, C.E., 2014. The power of ion mobility-mass spectrometry for structural characterization and the study of conformational dynamics. *Nature Chem* 6, 281–294. <https://doi.org/10.1038/nchem.1889>
- Lee, J.-Y., Song, J., LeBlanc, L., Davis, I., Kim, J., Beck, S., 2021. Conserved dual-mode gene regulation programs in higher eukaryotes. *Nucleic Acids Research* 49, 2583–2597. <https://doi.org/10.1093/nar/gkab108>
- Lemjabbar-Alaoui, H., McKinney, A., Yang, Y.W., Tran, V.M., Phillips, J.J., 2015. Glycosylation alterations in lung and brain cancer. *Adv Cancer Res* 126, 305–44. <https://doi.org/10.1016/bs.acr.2014.11.007>
- Lemjabbar-Alaoui, H., van Zante, A., Singer, M.S., Xue, Q., Wang, Y.Q., Tsay, D., He, B., Jablons, D.M., Rosen, S.D., 2010. Sulf-2, a heparan sulfate endosulfatase, promotes human lung carcinogenesis. *Oncogene* 29, 635–46. <https://doi.org/10.1038/onc.2009.365>
- Levings, D.C., Arashiro, T., Nakato, H., 2016. Heparan sulfate regulates the number and centrosome positioning of Drosophila male germline stem cells. *Mol Biol Cell* 27, 888–96. <https://doi.org/10.1091/mbc.E15-07-0528>
- Li, J., Kleeff, J., Abiatari, I., Kayed, H., Giese, N.A., Felix, K., Giese, T., Buchler, M.W., Friess, H., 2005. Enhanced levels of Hsulf-1 interfere with heparin-binding growth factor signaling in pancreatic cancer. *Mol Cancer* 4, 14. <https://doi.org/10.1186/1476-4598-4-14>

- Li, J.-P., Kusche-Gullberg, M., 2016. Heparan Sulfate: Biosynthesis, Structure, and Function, in: International Review of Cell and Molecular Biology. Elsevier, pp. 215–273. <https://doi.org/10.1016/bs.ircmb.2016.02.009>
- Liu, C.-J., 2014. Adjuvant heparanase inhibitor PI-88 therapy for hepatocellular carcinoma recurrence. *WJG* 20, 11384. <https://doi.org/10.3748/wjg.v20.i32.11384>
- Liu, P., Gou, M., Yi, T., Xie, C., Qi, X., Zhou, S., Deng, H., Wei, Y., Zhao, X., 2012. Efficient inhibition of an intraperitoneal xenograft model of human ovarian cancer by HSulf-1 gene delivered by biodegradable cationic heparin-polyethyleneimine nanogels. *Oncol Rep* 27, 363–370. <https://doi.org/10.3892/or.2011.1550>
- Liu, P., Khurana, A., Rattan, R., He, X., Kalloger, S., Dowdy, S., Gilks, B., Shridhar, V., 2009. Regulation of HSulf-1 expression by variant hepatic nuclear factor 1 in ovarian cancer. *Cancer Res* 69, 4843–50. <https://doi.org/10.1158/0008-5472.CAN-08-3065>
- Lokeshwar, V.B., Cerwinka, W.H., Isoyama, T., Lokeshwar, B.L., 2005. HYAL1 Hyaluronidase in Prostate Cancer: A Tumor Promoter and Suppressor. *Cancer Research* 65, 7782–7789. <https://doi.org/10.1158/0008-5472.CAN-05-1022>
- Ludwiczak, J., Winski, A., Szczepaniak, K., Alva, V., Dunin-Horkawicz, S., 2019. DeepCoil—a fast and accurate prediction of coiled-coil domains in protein sequences. *Bioinformatics* 35, 2790–2795. <https://doi.org/10.1093/bioinformatics/bty1062>
- Lui, N.S., Yang, Y.W., van Zante, A., Buchanan, P., Jablons, D.M., Lemjabbar-Alaoui, H., 2016. SULF2 Expression Is a Potential Diagnostic and Prognostic Marker in Lung Cancer. *PLoS One* 11, e0148911. <https://doi.org/10.1371/journal.pone.0148911>
- Luo, X., Campbell, N.A., He, L., O'Brien, D.R., Singer, M.S., Lemjabbar-Alaoui, H., Ahn, K.S., Smoot, R., Torbenson, M.S., Rosen, S.D., Roberts, L.R., 2021. Sulfatase 2 (SULF2) Monoclonal Antibody 5D5 Suppresses Human Cholangiocarcinoma Xenograft Growth Through Regulation of a SULF2-Platelet-Derived Growth Factor Receptor Beta-Yes-Associated Protein Signaling Axis. *Hepatology* 74, 1411–1428. <https://doi.org/10.1002/hep.31817>
- MA, H.-Y., ZHANG, F., LI, J., MO, M.-L., CHEN, Z., LIU, L., ZHOU, H.-M., SHENG, Q., 2011. HSulf-1 suppresses cell growth and down-regulates Hedgehog signaling in human gastric cancer cells. *Oncol Lett* 2, 1291–1295. <https://doi.org/10.3892/ol.2011.407>
- Madeo, G., Savojardo, C., Manfredi, M., Martelli, P.L., Casadio, R., 2023. CoCoNat: a novel method based on deep learning for coiled-coil prediction. *Bioinformatics* 39, btad495. <https://doi.org/10.1093/bioinformatics/btad495>
- Mashima, R., Nakanishi, M., 2022. Mammalian Sulfatases: Biochemistry, Disease Manifestation, and Therapy. *Int J Mol Sci* 23, 8153. <https://doi.org/10.3390/ijms23158153>
- Massagué, J., 2012. TGF β signalling in context. *Nat Rev Mol Cell Biol* 13, 616–630. <https://doi.org/10.1038/nrm3434>
- Matsuzaka, Y., Yashiro, R., 2024. Classification and Molecular Functions of Heparan Sulfate Proteoglycans and Their Molecular Mechanisms with the Receptor. *Biologics* 4, 105–129. <https://doi.org/10.3390/biologics4020008>
- McAtee, C.O., Barycki, J.J., Simpson, M.A., 2014. Emerging Roles for Hyaluronidase in Cancer Metastasis and Therapy, in: *Advances in Cancer Research*. Elsevier, pp. 1–34. <https://doi.org/10.1016/B978-0-12-800092-2.00001-0>
- Mclean, J., 1959. The Discovery of Heparin. *Circulation* 19, 75–78. <https://doi.org/10.1161/01.CIR.19.1.75>
- Milz, F., Harder, A., Neuhaus, P., Breitkreuz-Korff, O., Walhorn, V., Lubke, T., Anselmetti, D., Dierks, T., 2013. Cooperation of binding sites at the hydrophilic domain of cell-surface sulfatase Sulf1 allows for dynamic interaction of the enzyme with its substrate heparan sulfate. *Biochim Biophys Acta* 1830, 5287–98. <https://doi.org/10.1016/j.bbagen.2013.07.014>
- Mohanty, S., P Chaudhary, B., Zoetewey, D., 2020. Structural Insight into the Mechanism of N-Linked Glycosylation by Oligosaccharyltransferase. *Biomolecules* 10, 624. <https://doi.org/10.3390/biom10040624>

- Morimoto-Tomita, M., Uchimura, K., Bistrup, A., Lum, D.H., Egeblad, M., Boudreau, N., Werb, Z., Rosen, S.D., 2005. Sulf-2, a proangiogenic heparan sulfate endosulfatase, is upregulated in breast cancer. *Neoplasia* 7, 1001–10. <https://doi.org/10.1593/neo.05496>
- Morimoto-Tomita, M., Uchimura, K., Werb, Z., Hemmerich, S., Rosen, S.D., 2002. Cloning and Characterization of Two Extracellular Heparin-degrading Endosulfatases in Mice and Humans. *Journal of Biological Chemistry* 277, 49175–49185. <https://doi.org/10.1074/jbc.M205131200>
- Mukherjee, P., Zhou, X., Benicky, J., Panigrahi, A., Aljuhani, R., Liu, J., Ailles, L., Pomin, V.H., Wang, Z., Goldman, R., 2023. Heparan-6- O -endosulfatase 2 promotes invasiveness of head and neck squamous carcinoma cell lines in co-cultures with cancer associated fibroblasts (preprint). *Cancer Biology*. <https://doi.org/10.1101/2023.10.05.561077>
- Nagamine, S., Keino-Masu, K., Shiomi, K., Masu, M., 2010. Proteolytic cleavage of the rat heparan sulfate 6-O-endosulfatase SulfFP2 by furin-type proprotein convertases. *Biochem Biophys Res Commun* 391, 107–12. <https://doi.org/10.1016/j.bbrc.2009.11.011>
- Nagamine, S., Koike, S., Keino-Masu, K., Masu, M., 2005. Expression of a heparan sulfate remodeling enzyme, heparan sulfate 6-O-endosulfatase sulfatase FP2, in the rat nervous system. *Developmental Brain Research* 159, 135–143. <https://doi.org/10.1016/j.devbrainres.2005.07.006>
- Nagamine, S., Tamba, M., Ishimine, H., Araki, K., Shiomi, K., Okada, T., Ohto, T., Kunita, S., Takahashi, S., Wismans, R.G.P., Van Kuppevelt, T.H., Masu, M., Keino-Masu, K., 2012. Organ-specific Sulfation Patterns of Heparan Sulfate Generated by Extracellular Sulfatases Sulf1 and Sulf2 in Mice. *Journal of Biological Chemistry* 287, 9579–9590. <https://doi.org/10.1074/jbc.M111.290262>
- Nakamura, I., Asumda, F.Z., Moser, C.D., Kang, Y.N.N., Lai, J.P., Roberts, L.R., 2021. Sulfatase-2 Regulates Liver Fibrosis through the TGF-beta Signaling Pathway. *Cancers (Basel)* 13. <https://doi.org/10.3390/cancers13215279>
- Nakamura, I., Fernandez-Barrena, M.G., Ortiz-Ruiz, M.C., Almada, L.L., Hu, C., Elswa, S.F., Mills, L.D., Romecin, P.A., Gulaid, K.H., Moser, C.D., Han, J.-J., Vrabel, A., Hanse, E.A., Akogyeram, N.A., Albrecht, J.H., Monga, S.P.S., Sanderson, S.O., Prieto, J., Roberts, L.R., Fernandez-Zapico, M.E., 2013. Activation of the Transcription Factor GLI1 by WNT Signaling Underlies the Role of SULFATASE 2 as a Regulator of Tissue Regeneration. *J Biol Chem* 288, 21389–21398. <https://doi.org/10.1074/jbc.M112.443440>
- Nakayama, K., 1997. Furin: a mammalian subtilisin/Kex2p-like endoprotease involved in processing of a wide variety of precursor proteins. *Biochem J* 327 (Pt 3), 625–635. <https://doi.org/10.1042/bj3270625>
- Narita, K., Chien, J., Mullany, S.A., Staub, J., Qian, X., Lingle, W.L., Shridhar, V., 2007. Loss of HSulf-1 expression enhances autocrine signaling mediated by amphiregulin in breast cancer. *J Biol Chem* 282, 14413–20. <https://doi.org/10.1074/jbc.M611395200>
- Narita, K., Staub, J., Chien, J., Meyer, K., Bauer, M., Friedl, A., Ramakrishnan, S., Shridhar, V., 2006. HSulf-1 inhibits angiogenesis and tumorigenesis in vivo. *Cancer Res* 66, 6025–32. <https://doi.org/10.1158/0008-5472.CAN-05-3582>
- Nawroth, R., van Zante, A., Cervantes, S., McManus, M., Hebrok, M., Rosen, S.D., 2007. Extracellular sulfatases, elements of the Wnt signaling pathway, positively regulate growth and tumorigenicity of human pancreatic cancer cells. *PLoS One* 2, e392. <https://doi.org/10.1371/journal.pone.0000392>
- Nishitsuji, K., 2018. Heparan sulfate S-domains and extracellular sulfatases (Sulfs): their possible roles in protein aggregation diseases. *Glycoconj J* 35, 387–396. <https://doi.org/10.1007/s10719-018-9833-8>
- Nishitsuji, K., Uchimura, K., 2017. Sulfated glycosaminoglycans in protein aggregation diseases. *Glycoconj J* 34, 453–466. <https://doi.org/10.1007/s10719-017-9769-4>
- Ntenti, C., Papakonstantinou, E., Fidani, L., Stolz, D., Goulas, A., 2024. The Genetics behind Sulfation: Impact on Airway Remodeling. *Journal of Personalized Medicine* 14, 248. <https://doi.org/10.3390/jpm14030248>

- Nurcombe, V., 2024. From heparan glycobiology to stem cell therapy: a historical perspective. *Academia Biology* 2.
- Ohayon, D., Escalas, N., Cochard, P., Glise, B., Danesin, C., Soula, C., 2019. Sulfatase 2 promotes generation of a spinal cord astrocyte subtype that stands out through the expression of Olig2. *Glia* 67, 1478–1495. <https://doi.org/10.1002/glia.23621>
- Ornitz, D.M., Itoh, N., 2015. The Fibroblast Growth Factor signaling pathway. *WIREs Developmental Biology* 4, 215–266. <https://doi.org/10.1002/wdev.176>
- Oshima, K., Han, X., Ouyang, Y., El Masri, R., Yang, Y., Haeger, S.M., McMurtry, S.A., Lane, T.C., Davizon-Castillo, P., Zhang, F., Yue, X., Vivès, R.R., Linhardt, R.J., Schmidt, E.P., 2019. Loss of endothelial sulfatase-1 after experimental sepsis attenuates subsequent pulmonary inflammatory responses. *Am J Physiol Lung Cell Mol Physiol* 317, L667–L677. <https://doi.org/10.1152/ajplung.00175.2019>
- Otsuki, S., Alvarez-Garcia, O., Lotz, M.K., Neo, M., 2019. Role of heparan sulfate 6-O endosulfatases in intervertebral disc homeostasis. *Histol Histopathol* 34, 1051–1060. <https://doi.org/10.14670/HH-18-107>
- Otsuki, S., Hanson, S.R., Miyaki, S., Grogan, S.P., Kinoshita, M., Asahara, H., Wong, C.H., Lotz, M.K., 2010. Extracellular sulfatases support cartilage homeostasis by regulating BMP and FGF signaling pathways. *Proc Natl Acad Sci U S A* 107, 10202–7. <https://doi.org/10.1073/pnas.0913897107>
- Otsuki, S., Murakami, T., Okamoto, Y., Hoshiyama, Y., Oda, S., Neo, M., 2017. Suppression of cartilage degeneration by intra-articular injection of heparan sulfate 6-O endosulfatase in a mouse osteoarthritis model. *Histol Histopathol* 32, 725–733. <https://doi.org/10.14670/HH-11-838>
- Otsuki, S., Taniguchi, N., Grogan, S.P., D’Lima, D., Kinoshita, M., Lotz, M., 2008. Expression of novel extracellular sulfatases Sulf-1 and Sulf-2 in normal and osteoarthritic articular cartilage. *Arthritis Res Ther* 10, R61. <https://doi.org/10.1186/ar2432>
- Ouyang, Y., Wu, C., Sun, X., Liu, J., Linhardt, R.J., Zhang, Z., 2016. Development of hydrophilic interaction chromatography with quadruple time-of-flight mass spectrometry for heparin and low molecular weight heparin disaccharide analysis. *Rapid Communications in Mass Spectrometry* 30, 277–284. <https://doi.org/10.1002/rcm.7437>
- Panigrahi, A., Benicky, J., Aljuhani, R., Mukherjee, P., Nováková, Z., Bařinka, C., Goldman, R., 2024. Galectin-3-Binding Protein Inhibits Extracellular Heparan 6-O-Endosulfatase Sulf-2. *Molecular & Cellular Proteomics* 23. <https://doi.org/10.1016/j.mcpro.2024.100793>
- Parker, R.B., Kohler, J.J., 2010. Regulation of intracellular signaling by extracellular glycan remodeling. *ACS Chem Biol* 5, 35–46. <https://doi.org/10.1021/cb9002514>
- Pempe, E.H., Burch, T.C., Law, C.J., Liu, J., 2012. Substrate specificity of 6-O-endosulfatase (Sulf-2) and its implications in synthesizing anticoagulant heparan sulfate. *Glycobiology* 22, 1353–62. <https://doi.org/10.1093/glycob/cws092>
- Perez, S., Makshakova, O., Angulo, J., Bedini, E., Bisio, A., de Paz, J.L., Fadda, E., Guerrini, M., Hricovini, Michal, Hricovini, Milos, Lisacek, F., Nieto, P.M., Pagel, K., Paiardi, G., Richter, R., Samsonov, S.A., Vivès, R.R., Nikitovic, D., Ricard Blum, S., 2023. Glycosaminoglycans: What Remains To Be Deciphered? *JACS Au* 3, 628–656. <https://doi.org/10.1021/jacsau.2c00569>
- Peterson, S.M., Iskenderian, A., Cook, L., Romashko, A., Tobin, K., Jones, M., Norton, A., Gómez-Yafal, A., Heartlein, M.W., Concino, M.F., Liaw, L., Martini, P.G., 2010. Human Sulfatase 2 inhibits in vivo tumor growth of MDA-MB-231 human breast cancer xenografts. *BMC Cancer* 10, 427. <https://doi.org/10.1186/1471-2407-10-427>
- Phillips, J.J., Huillard, E., Robinson, A.E., Ward, A., Lum, D.H., Polley, M.Y., Rosen, S.D., Rowitch, D.H., Werb, Z., 2012. Heparan sulfate sulfatase SULF2 regulates PDGFR α signaling and growth in human and mouse malignant glioma. *J Clin Invest* 122, 911–22. <https://doi.org/10.1172/JCI58215>
- Pichert, A., Schlorke, D., Franz, S., Arnhold, J., 2012. Functional aspects of the interaction between interleukin-8 and sulfated glycosaminoglycans. *Biomatter* 2, 142–148. <https://doi.org/10.4161/biom.21316>

- Poyer, S., Seffouh, I., Lopin-Bon, C., Jacquinet, J.-C., Neira, J.L., Salpin, J.-Y., Daniel, R., 2021. Discrimination of sulfated isomers of chondroitin sulfate disaccharides by HILIC-MS. *Anal Bioanal Chem* 413, 7107–7117. <https://doi.org/10.1007/s00216-021-03679-9>
- Ramsbottom, S.A., Maguire, R.J., Fellgett, S.W., Pownall, M.E., 2014. Sulf1 influences the Shh morphogen gradient during the dorsal ventral patterning of the neural tube in *Xenopus tropicalis*. *Developmental Biology* 391, 207–218. <https://doi.org/10.1016/j.ydbio.2014.04.010>
- Ratzka, A., Kalus, I., Moser, M., Dierks, T., Mundlos, S., Vortkamp, A., 2008. Redundant function of the heparan sulfate 6-O-endosulfatases Sulf1 and Sulf2 during skeletal development. *Dev Dyn* 237, 339–53. <https://doi.org/10.1002/dvdy.21423>
- Rauch, J.N., Chen, J.J., Sorum, A.W., Miller, G.M., Sharf, T., See, S.K., Hsieh-Wilson, L.C., Kampmann, M., Kosik, K.S., 2018. Tau Internalization is Regulated by 6-O Sulfation on Heparan Sulfate Proteoglycans (HSPGs). *Sci Rep* 8, 6382. <https://doi.org/10.1038/s41598-018-24904-z>
- Reily, C., Stewart, T.J., Renfrow, M.B., Novak, J., 2019. Glycosylation in health and disease. *Nat Rev Nephrol* 15, 346–366. <https://doi.org/10.1038/s41581-019-0129-4>
- Remacle, A.G., Shiryayev, S.A., Oh, E.-S., Cieplak, P., Srinivasan, A., Wei, G., Liddington, R.C., Ratnikov, B.I., Parent, A., Desjardins, R., Day, R., Smith, J.W., Lebl, M., Strongin, A.Y., 2008. Substrate Cleavage Analysis of Furin and Related Proprotein Convertases. *J Biol Chem* 283, 20897–20906. <https://doi.org/10.1074/jbc.M803762200>
- Reuillon, T., Alhasan, S.F., Beale, G.S., Bertoli, A., Brennan, A., Cano, C., Reeves, H.L., Newell, D.R., Golding, B.T., Miller, D.C., Griffin, R.J., 2016. Design and synthesis of biphenyl and biphenyl ether inhibitors of sulfatases. *Chem. Sci.* 7, 2821–2826. <https://doi.org/10.1039/C5SC03612G>
- Reznik, N., Fass, D., 2022. Disulfide bond formation and redox regulation in the Golgi apparatus. *FEBS Letters* 596, 2859–2872. <https://doi.org/10.1002/1873-3468.14510>
- Roberts, R.O., Kang, Y.N., Hu, C., Moser, C.D., Wang, S., Moore, M.J., Graham, R.P., Lai, J.P., Petersen, R.C., Roberts, L.R., 2017. Decreased Expression of Sulfatase 2 in the Brains of Alzheimer's Disease Patients: Implications for Regulation of Neuronal Cell Signaling. *J Alzheimers Dis Rep* 1, 115–124. <https://doi.org/10.3233/ADR-170028>
- Robertson, D.A., Callen, D.F., Baker, E.G., Morris, C.P., Hopwood, J.J., 1988. Chromosomal localization of the gene for human glucosamine-6-sulphatase to 12q14. *Hum Genet* 79, 175–178. <https://doi.org/10.1007/BF00280560>
- Robinson, P.J., Bulleid, N.J., 2020. Mechanisms of Disulfide Bond Formation in Nascent Polypeptides Entering the Secretory Pathway. *Cells* 9, 1994. <https://doi.org/10.3390/cells9091994>
- Rosen, S.D., Lemjabbar-Alaoui, H., 2010. Sulf-2: an extracellular modulator of cell signaling and a cancer target candidate. *Expert Opin Ther Targets* 14, 935–49. <https://doi.org/10.1517/14728222.2010.504718>
- Roy, D., Mondal, S., Khurana, A., Jung, D.B., Hoffmann, R., He, X., Kalogera, E., Dierks, T., Hammond, E., Dredge, K., Shridhar, V., 2017. Loss of HSulf-1: The Missing Link between Autophagy and Lipid Droplets in Ovarian Cancer. *Sci Rep* 7, 41977. <https://doi.org/10.1038/srep41977>
- Saad, O.M., Ebel, H., Uchimura, K., Rosen, S.D., Bertozzi, C.R., Leary, J.A., 2005. Compositional profiling of heparin/heparan sulfate using mass spectrometry: assay for specificity of a novel extracellular human endosulfatase. *Glycobiology* 15, 818–26. <https://doi.org/10.1093/glycob/cwi064>
- Sala-Newby, G.B., George, S.J., Bond, M., Dhoot, G.K., Newby, A.C., 2005. Regulation of vascular smooth muscle cell proliferation, migration and death by heparan sulfate 6-O-endosulfatase1. *FEBS Lett* 579, 6493–8. <https://doi.org/10.1016/j.febslet.2005.10.026>
- Schelwies, M., Brinson, D., Otsuki, S., Hong, Y., Lotz, M.K., Wong, C., Hanson, S.R., 2010. Glucosamine-6-sulfamate Analogues of Heparan Sulfate as Inhibitors of Endosulfatases. *ChemBioChem* 11, 2393–2397. <https://doi.org/10.1002/cbic.201000401>
- Schenk, H., Masseli, A., Schroder, P., Bolanos-Palmieri, P., Beese, M., Hegermann, J., Brasen, J.H., Haller, H., 2019. Sulfatases, in Particular Sulf1, Are Important for the Integrity of the Glomerular Filtration Barrier in Zebrafish. *Biomed Res Int* 2019, 4508048. <https://doi.org/10.1155/2019/4508048>

- Scott, H., Panin, V.M., 2014. N-glycosylation in Regulation of the Nervous System. *Adv Neurobiol* 9, 367–394. https://doi.org/10.1007/978-1-4939-1154-7_17
- Seffouh, A., El Masri, R., Makshakova, O., Gout, E., Hassoun, Z.E.O., Andrieu, J., Lortat-Jacob, H., Vivès, R.R., 2019. Expression and purification of recombinant extracellular sulfatase HSulf-2 allows deciphering of enzyme sub-domain coordinated role for the binding and 6-O-desulfation of heparan sulfate. *Cell. Mol. Life Sci.* 76, 1807–1819. <https://doi.org/10.1007/s00018-019-03027-2>
- Seffouh, A., Milz, F., Przybylski, C., Laguri, C., Oosterhof, A., Bourcier, S., Sadir, R., Dutkowski, E., Daniel, R., van Kuppevelt, T.H., Dierks, T., Lortat-Jacob, H., Vives, R.R., 2013. HSulf sulfatases catalyze processive and oriented 6-O-desulfation of heparan sulfate that differentially regulates fibroblast growth factor activity. *FASEB J* 27, 2431–9. <https://doi.org/10.1096/fj.12-226373>
- Seffouh, I., 2018. Analyse protéomique des endosulfatases humaines HSulfs, enzymes clés de la modulation de la sulfatation de l'héparane sulfate. PARIS-SACLAY.
- Seffouh, I., Bilong, M., Przybylski, C., El Omrani, N., Poyer, S., Lamour, G., Clément, M.-J., Boustany, R.-J., Gout, E., Gonnet, F., Vivès, R.R., Daniel, R., 2023. Structure and functional impact of glycosaminoglycan modification of HSulf-2 endosulfatase revealed by atomic force microscopy and mass spectrometry. *Sci Rep* 13, 22263. <https://doi.org/10.1038/s41598-023-49147-5>
- Seffouh, I., Przybylski, C., Seffouh, A., El Masri, R., Vives, R.R., Gonnet, F., Daniel, R., 2019. Mass spectrometry analysis of the human endosulfatase Hsulf-2. *Biochem Biophys Rep* 18, 100617. <https://doi.org/10.1016/j.bbrep.2019.01.010>
- Severmann, A.-C., Jochmann, K., Feller, K., Bachvarova, V., Piombo, V., Stange, R., Holzer, T., Brachvogel, B., Esko, J., Pap, T., Hoffmann, D., Vortkamp, A., 2020. An altered heparan sulfate structure in the articular cartilage protects against osteoarthritis. *Osteoarthritis Cartilage* 28, 977–987. <https://doi.org/10.1016/j.joca.2020.04.002>
- Shire, A., Lomberk, G., Lai, J.P., Zou, H., Tsuchiya, N., Aderca, I., Moser, C.D., Gulaid, K.H., Oseini, A., Hu, C., Warsame, O., Jenkins, R.B., Roberts, L.R., 2015. Restoration of epigenetically silenced SULF1 expression by 5-aza-2-deoxycytidine sensitizes hepatocellular carcinoma cells to chemotherapy-induced apoptosis. *Med Epigenet* 3, 1–18. <https://doi.org/10.1159/000375461>
- Sikora, A.-S., Hellec, C., Carpentier, M., Martinez, P., Delos, M., Denys, A., Allain, F., 2016. Tumour-necrosis factor- α induces heparan sulfate 6-O-endosulfatase 1 (Sulf-1) expression in fibroblasts. *The International Journal of Biochemistry & Cell Biology* 80, 57–65. <https://doi.org/10.1016/j.biocel.2016.09.021>
- Singer, Mark S., Phillips, J.J., Lemjabbar-Alaoui, H., Wang, Y.Q., Wu, J., Goldman, R., Rosen, S.D., 2015. SULF2, a heparan sulfate endosulfatase, is present in the blood of healthy individuals and increases in cirrhosis. *Clin Chim Acta* 0, 72–78. <https://doi.org/10.1016/j.cca.2014.10.038>
- Singer, M. S., Phillips, J.J., Lemjabbar-Alaoui, H., Wang, Y.Q., Wu, J., Goldman, R., Rosen, S.D., 2015. SULF2, a heparan sulfate endosulfatase, is present in the blood of healthy individuals and increases in cirrhosis. *Clin Chim Acta* 440, 72–8. <https://doi.org/10.1016/j.cca.2014.10.038>
- Sommerlade, H.J., Selmer, T., Ingendoh, A., Gieselmann, V., Von Figura, K., Neifer, K., Schmidt, B., 1994. Glycosylation and phosphorylation of arylsulfatase A. *Journal of Biological Chemistry* 269, 20977–20981. [https://doi.org/10.1016/S0021-9258\(17\)31917-8](https://doi.org/10.1016/S0021-9258(17)31917-8)
- Stam, M., Lelièvre, P., Hoebeke, M., Corre, E., Barbeyron, T., Michel, G., 2023. SulfAtlas, the sulfatase database: state of the art and new developments. *Nucleic Acids Research* 51, D647–D653. <https://doi.org/10.1093/nar/gkac977>
- Staples, G.O., Shi, X., Zaia, J., 2011. Glycomics Analysis of Mammalian Heparan Sulfates Modified by the Human Extracellular Sulfatase HSulf2. *PLoS ONE* 6, e16689. <https://doi.org/10.1371/journal.pone.0016689>
- Staub, J., Chien, J., Pan, Y., Qian, X., Narita, K., Aletti, G., Scheerer, M., Roberts, L.R., Molina, J., Shridhar, V., 2007. Epigenetic silencing of HSulf-1 in ovarian cancer: implications in chemoresistance. *Oncogene* 26, 4969–4978. <https://doi.org/10.1038/sj.onc.1210300>
- Steiner, D.F., 1998. The proprotein convertases. *Current Opinion in Chemical Biology* 2, 31–39. [https://doi.org/10.1016/S1367-5931\(98\)80033-1](https://doi.org/10.1016/S1367-5931(98)80033-1)

- Stewart, M.D., Sanderson, R.D., 2014. Heparan Sulfate in the Nucleus and its Control of Cellular Functions. *Matrix Biol* 35, 56–59. <https://doi.org/10.1016/j.matbio.2013.10.009>
- Sugaya, N., Habuchi, H., Nagai, N., Ashikari-Hada, S., Kimata, K., 2008. 6-*O*-Sulfation of Heparan Sulfate Differentially Regulates Various Fibroblast Growth Factor-dependent Signalings in Culture*. *Journal of Biological Chemistry* 283, 10366–10376. <https://doi.org/10.1074/jbc.M705948200>
- Szczepaniak, K., Bukala, A., Da Silva Neto, A.M., Ludwiczak, J., Dunin-Horkawicz, S., 2021. A library of coiled-coil domains: from regular bundles to peculiar twists. *Bioinformatics* 36, 5368–5376. <https://doi.org/10.1093/bioinformatics/btaa1041>
- Taghizadeh, E., Kalantar, S.M., Mahdian, R., Sheikhha, M.H., Farashahi-Yazd, E., Ghasemi, S., Shahbazi, Z., 2015. SULF 1 gene polymorphism, rs6990375 is in significant association with fetus failure in IVF technique. *Iran J Reprod Med* 13, 215–220.
- Takashima, Y., Keino-Masu, K., Yashiro, H., Hara, S., Suzuki, T., Van Kuppevelt, T.H., Masu, M., Nagata, M., 2016. Heparan sulfate 6- *O* -endosulfatases, Sulf1 and Sulf2, regulate glomerular integrity by modulating growth factor signaling. *American Journal of Physiology-Renal Physiology* 310, F395–F408. <https://doi.org/10.1152/ajprenal.00445.2015>
- Takemura, M., Nakato, H., 2017. *Drosophila* Sulf1 is required for the termination of intestinal stem cell division during regeneration. *J Cell Sci* 130, 332–343. <https://doi.org/10.1242/jcs.195305>
- Tang, R., Rosen, S.D., 2009. Functional consequences of the subdomain organization of the sulfs. *J Biol Chem* 284, 21505–14. <https://doi.org/10.1074/jbc.M109.028472>
- Tanzer, A., Amemiya, C.T., Kim, C., Stadler, P.F., 2005. Evolution of microRNAs located within *Hox* gene clusters. *J Exp Zool Pt B* 304B, 75–85. <https://doi.org/10.1002/jez.b.21021>
- Tao, Y., Han, T., Zhang, T., Sun, C., 2017. Sulfatase-2 promotes the growth and metastasis of colorectal cancer by activating Akt and Erk1/2 pathways. *Biomedicine & Pharmacotherapy* 89, 1370–1377. <https://doi.org/10.1016/j.biopha.2017.03.017>
- Terwilliger, T.C., Afonine, P.V., Liebschner, D., Croll, T.I., McCoy, A.J., Oeffner, R.D., Williams, C.J., Poon, B.K., Richardson, J.S., Read, R.J., Adams, P.D., 2023. Accelerating crystal structure determination with iterative *AlphaFold* prediction. *Acta Crystallogr D Struct Biol* 79, 234–244. <https://doi.org/10.1107/S205979832300102X>
- Tessema, M., Yingling, C.M., Thomas, C.L., Klinge, D.M., Bernauer, A.M., Liu, Y., Dacic, S., Siegfried, J.M., Dahlberg, S.E., Schiller, J.H., Belinsky, S.A., 2012. SULF2 methylation is prognostic for lung cancer survival and increases sensitivity to topoisomerase-I inhibitors via induction of ISG15. *Oncogene* 31, 4107–4116. <https://doi.org/10.1038/onc.2011.577>
- Thacker, B.E., Xu, D., Lawrence, R., Esko, J.D., 2014. Heparan sulfate 3-*O*-sulfation: A rare modification in search of a function. *Matrix Biology, Proteoglycan Biology* 35, 60–72. <https://doi.org/10.1016/j.matbio.2013.12.001>
- Thompson, N., Wakarchuk, W., 2022. O-glycosylation and its role in therapeutic proteins. *Biosci Rep* 42, BSR20220094. <https://doi.org/10.1042/BSR20220094>
- Timm, B.M., Follmar, J.L., Porell, R.N., Glass, K., Thacker, B.E., Glass, C.A., Godula, K., 2023. Human extracellular sulfatases use a dual mechanism for regulation of growth factor interactions with heparan sulfate proteoglycans. <https://doi.org/10.1101/2023.11.22.568358>
- Touahri, Y., Escalas, N., Benazeraf, B., Cochard, P., Danesin, C., Soula, C., 2012. Sulfatase 1 promotes the motor neuron-to-oligodendrocyte fate switch by activating Shh signaling in Olig2 progenitors of the embryonic ventral spinal cord. *J Neurosci* 32, 18018–34. <https://doi.org/10.1523/JNEUROSCI.3553-12.2012>
- Tran, T.H., Shi, X., Zaia, J., Ai, X., 2012. Heparan Sulfate 6-*O*-endosulfatases (Sulfs) Coordinate the Wnt Signaling Pathways to Regulate Myoblast Fusion during Skeletal Muscle Regeneration. *Journal of Biological Chemistry* 287, 32651–32664. <https://doi.org/10.1074/jbc.M112.353243>
- Tran, V.M., Wade, A., McKinney, A., Chen, K., Lindberg, O.R., Engler, J.R., Persson, A.I., Phillips, J.J., 2017. Heparan Sulfate Glycosaminoglycans in Glioblastoma Promote Tumor Invasion. *Molecular Cancer Research* 15, 1623–1633. <https://doi.org/10.1158/1541-7786.MCR-17-0352>

- Tsai, T.-T., Ho, N.Y.-J., Fang, H.-C., Lai, P.-L., Niu, C.-C., Chen, L.-H., Chen, W.-J., Pang, J.-H.S., 2015. Increased sulfatase 1 gene expression in degenerative intervertebral disc cells. *Journal of Orthopaedic Research* 33, 312–317. <https://doi.org/10.1002/jor.22766>
- Uchimura, K., Morimoto-Tomita, M., Bistrup, A., Li, J., Lyon, M., Gallagher, J., Werb, Z., Rosen, S.D., 2006. HSulf-2, an extracellular endoglucosamine-6-sulfatase, selectively mobilizes heparin-bound growth factors and chemokines: effects on VEGF, FGF-1, and SDF-1. *BMC Biochem* 7, 2. <https://doi.org/10.1186/1471-2091-7-2>
- Uhlén, M., Fagerberg, L., Hallström, B.M., Lindskog, C., Oksvold, P., Mardinoglu, A., Sivertsson, Å., Kampf, C., Sjöstedt, E., Asplund, A., Olsson, I., Edlund, K., Lundberg, E., Navani, S., Szigartyo, C.A.-K., Odeberg, J., Djureinovic, D., Takanen, J.O., Hober, S., Alm, T., Edqvist, P.-H., Berling, H., Tegel, H., Mulder, J., Rockberg, J., Nilsson, P., Schwenk, J.M., Hamsten, M., von Feilitzen, K., Forsberg, M., Persson, L., Johansson, F., Zwahlen, M., von Heijne, G., Nielsen, J., Pontén, F., 2015. Tissue-based map of the human proteome. *Science* 347, 1260419. <https://doi.org/10.1126/science.1260419>
- Varki, A., Cummings, R., Esko, J., Freeze, H., Hart, G., Marth, J., 1999. Proteoglycans and Glycosaminoglycans, in: *Essentials of Glycobiology*. Cold Spring Harbor Laboratory Press.
- Vicente, C.M., Lima, M.A., Yates, E.A., Nader, H.B., Toma, L., 2015. Enhanced Tumorigenic Potential of Colorectal Cancer Cells by Extracellular Sulfatases. *Molecular Cancer Research* 13, 510–523. <https://doi.org/10.1158/1541-7786.MCR-14-0372>
- Vitkup, D., Sander, C., Church, G.M., 2003. The amino-acid mutational spectrum of human genetic disease. *Genome Biol* 4, R72. <https://doi.org/10.1186/gb-2003-4-11-r72>
- Vives, R.R., Seffouh, A., Lortat-Jacob, H., 2014. Post-Synthetic Regulation of HS Structure: The Yin and Yang of the Sulfs in Cancer. *Front Oncol* 3, 331. <https://doi.org/10.3389/fonc.2013.00331>
- Viviano, B.L., Paine-Saunders, S., Gasiunas, N., Gallagher, J., Saunders, S., 2004. Domain-specific Modification of Heparan Sulfate by Qsulf1 Modulates the Binding of the Bone Morphogenetic Protein Antagonist Noggin. *Journal of Biological Chemistry* 279, 5604–5611. <https://doi.org/10.1074/jbc.M310691200>
- Waldow, A., Schmidt, B., Dierks, T., Von Bülow, R., Von Figura, K., 1999. Amino Acid Residues Forming the Active Site of Arylsulfatase A. *Journal of Biological Chemistry* 274, 12284–12288. <https://doi.org/10.1074/jbc.274.18.12284>
- Wang, C., Shang, C., Gai, X., Song, T., Han, S., Liu, Q., Zheng, X., 2021. Sulfatase 2-Induced Cancer-Associated Fibroblasts Promote Hepatocellular Carcinoma Progression via Inhibition of Apoptosis and Induction of Epithelial-to-Mesenchymal Transition. *Front. Cell Dev. Biol.* 9. <https://doi.org/10.3389/fcell.2021.631931>
- Wang, L., Xie, L., Wang, J., Shen, J., Liu, B., 2013. Correlation between the methylation of SULF2 and WRN promoter and the irinotecan chemosensitivity in gastric cancer. *BMC Gastroenterol* 13, 173. <https://doi.org/10.1186/1471-230X-13-173>
- Wang, T.-B., Li, Z.-F., Zhang, X.-J., Sun, C.-Y., Fei, H., Chen, Y.-T., Guo, C.-G., Zhao, D.-B., 2021. SULF2 Is a Prognostic Biomarker and Correlated with Tumor Associated Macrophages in Gastric Cancer. <https://doi.org/10.21203/rs.3.rs-1083793/v1>
- Wang, Y.H., Beck, C., 2015. Distinct patterns of endosulfatase gene expression during *Xenopus laevis* limb development and regeneration. *Regeneration (Oxf)* 2, 19–25. <https://doi.org/10.1002/reg2.27>
- Wiegmann, E.M., Westendorf, E., Kalus, I., Pringle, T.H., Lübke, T., Dierks, T., 2013. Arylsulfatase K, a Novel Lysosomal Sulfatase. *Journal of Biological Chemistry* 288, 30019–30028. <https://doi.org/10.1074/jbc.M113.499541>
- Winterbottom, E.F., Pownall, M.E., 2009. Complementary expression of HSPG 6-O-endosulfatases and 6-O-sulfotransferase in the hindbrain of *Xenopus laevis*. *Gene Expression Patterns* 9, 166–172. <https://doi.org/10.1016/j.gep.2008.11.003>
- Wojcinski, A., Nakato, H., Soula, C., Glise, B., 2011. DSulfatase-1 fine-tunes Hedgehog patterning activity through a novel regulatory feedback loop. *Dev Biol* 358, 168–80. <https://doi.org/10.1016/j.ydbio.2011.07.027>

- Woo, L.L., Purohit, A., Malini, B., Reed, M.J., Potter, B.V., 2000. Potent active site-directed inhibition of steroid sulphatase by tricyclic coumarin-based sulphamates. *Chemistry & Biology* 7, 773–791. [https://doi.org/10.1016/S1074-5521\(00\)00023-5](https://doi.org/10.1016/S1074-5521(00)00023-5)
- Wu, C., Zheng, M., Yang, Y., Gu, X., Yang, K., Li, M., Liu, Y., Zhang, Q., Zhang, P., Wang, Y., Wang, Q., Xu, Y., Zhou, Y., Zhang, Y., Chen, L., Li, H., 2020. Furin: A Potential Therapeutic Target for COVID-19. *iScience* 23, 101642. <https://doi.org/10.1016/j.isci.2020.101642>
- Xu, D., Esko, J.D., 2014. Demystifying Heparan Sulfate–Protein Interactions. *Annu. Rev. Biochem.* 83, 129–157. <https://doi.org/10.1146/annurev-biochem-060713-035314>
- Yang, M., Chen, W., Gupta, D., Mei, C., Yang, Y., Zhao, B., Qiu, L., Chen, J., 2024. Nanoparticle/Engineered Bacteria Based Triple-Strategy Delivery System for Enhanced Hepatocellular Carcinoma Cancer Therapy. *IJN* Volume 19, 3827–3846. <https://doi.org/10.2147/IJN.S453709>
- Yang, Y., Ahn, J., Edwards, N., Benicky, J., Rozeboom, A.M., Davidson, B., Karamboulas, C., Nixon, K.C.J., Ailles, L., Goldman, R., 2022. Extracellular heparan 6-O-endosulfatases SULF1 and SULF2 in HNSC and other malignancies (preprint). *Cancer Biology*. <https://doi.org/10.1101/2022.08.25.505356>
- Yang, Y., Ahn, J., Raghunathan, R., Kallakury, B.V., Davidson, B., Kennedy, Z.B., Zaia, J., Goldman, R., 2020. Expression of the Extracellular Sulfatase SULF2 Affects Survival of Head and Neck Squamous Cell Carcinoma Patients. *Front Oncol* 10, 582827. <https://doi.org/10.3389/fonc.2020.582827>
- Yang, Y.W., Jablons, D.M., Lemjabbar-Alaoui, H., 2021. Extracellular sulfatases as potential blood-based biomarkers for early detection of lung cancer. *Exp Lung Res* 47, 261–279. <https://doi.org/10.1080/01902148.2021.1885525>
- Yoon, S., Lee, E.J., Choi, J.H., Chung, T., Kim, D.Y., Im, J.Y., Bae, M.H., Kwon, J.H., Kim, H.H., Kim, H.C., Park, Y.N., Wang, H.J., Woo, H.G., 2018. Recapitulation of pharmacogenomic data reveals that invalidation of SULF2 enhance sorafenib susceptibility in liver cancer. *Oncogene* 37, 4443–4454. <https://doi.org/10.1038/s41388-018-0291-3>
- Yue, X., 2017. Epithelial Deletion of Sulf2 Exacerbates Bleomycin-Induced Lung Injury, Inflammation, and Mortality. *Am J Respir Cell Mol Biol* 57, 560–569. <https://doi.org/10.1165/rcmb.2016-0367OC>
- Yue, X., Li, X., Nguyen, H.T., Chin, D.R., Sullivan, D.E., Lasky, J.A., 2008. Transforming growth factor-beta1 induces heparan sulfate 6-O-endosulfatase 1 expression in vitro and in vivo. *J Biol Chem* 283, 20397–407. <https://doi.org/10.1074/jbc.M802850200>
- Yue, X., Lu, J., Auduong, L., Sides, M.D., Lasky, J.A., 2013. Overexpression of Sulf2 in idiopathic pulmonary fibrosis. *Glycobiology* 23, 709–719. <https://doi.org/10.1093/glycob/cwt010>
- Zahraei, M., Sheikha, M.H., Kalantar, S.M., Ghasemi, N., Jahaninejad, T., Rajabi, S., Mohammadpour, H., 2014. The association of arylendosulfatase 1 (SULF1) gene polymorphism with recurrent miscarriage. *J Assist Reprod Genet* 31, 157–161. <https://doi.org/10.1007/s10815-013-0150-7>
- Zeng, F., Liu, Y., Ouyang, Q., Sun, Z., Zhang, K., Li, X., Liu, Y., 2021. Rs3802278 in 3'-UTR of SULF1 associated with platinum resistance and survival in Chinese epithelial ovarian cancer patients. *J Chemother* 33, 564–569. <https://doi.org/10.1080/1120009X.2021.1913702>
- Zhang, H., Newman, D.R., Bonner, J.C., Sannes, P.L., 2012. Over-expression of human endosulfatase-1 exacerbates cadmium-induced injury to transformed human lung cells in vitro. *Toxicol Appl Pharmacol* 265, 27–42. <https://doi.org/10.1016/j.taap.2012.09.008>
- Zhang, S., Condac, E., Qiu, H., Jiang, J., Gutierrez-Sanchez, G., Bergmann, C., Handel, T., Wang, L., 2012. Heparin-induced leukocytosis requires 6-O-sulfation and is caused by blockade of selectin- and CXCL12 protein-mediated leukocyte trafficking in mice. *J Biol Chem* 287, 5542–5553. <https://doi.org/10.1074/jbc.M111.314716>
- Zhao, W., Allen, S., Dhoot, G.K., 2007. FGF mediated Sulf1 regulation. *FEBS Letters* 581, 4960–4964. <https://doi.org/10.1016/j.febslet.2007.09.033>
- Zheng, X., Gai, X., Han, S., Moser, C.D., Hu, C., Shire, A.M., Floyd, R.A., Roberts, L.R., 2013. The human sulfatase 2 inhibitor 2,4-disulfonylphenyl-tert-butylnitron (OKN-007) has an antitumor

- effect in hepatocellular carcinoma mediated via suppression of TGFB1/SMAD2 and Hedgehog/GLI1 signaling. *Genes Chromosomes Cancer* 52, 225–36. <https://doi.org/10.1002/gcc.22022>
- Zhu, C., He, L., Zhou, X., Nie, X., Gu, Y., 2016. Sulfatase 2 promotes breast cancer progression through regulating some tumor-related factors. *Oncol Rep* 35, 1318–28. <https://doi.org/10.3892/or.2015.4525>

Titre : Caractérisation structurale et fonctionnelle des endosulfatases humaines HSulfs, enzymes clés de l'édition de l'héparane sulfate

Mots clés : Endosulfatases, Héparane sulfate, Spectrométrie de masse, 6-O-désulfatation, Oligosaccharides sulfatés

Résumé : Les endosulfatases humaines HSulf-1 et HSulf-2 catalysent la 6-O-désulfatation de l'héparane sulfate (HS), un composant majeur de la matrice extracellulaire, essentiel à la communication cellulaire. La modification des motifs de sulfatation de l'HS par HSulfs module ses propriétés d'interaction. Bien qu'ayant des activités enzymatiques similaires *in vitro*, les HSulfs présentent *in vivo* une dualité fonctionnelle, notamment dans le cancer où HSulf-1 est généralement anti-oncogénique et HSulf-2 pro-oncogénique. Ce travail vise à caractériser les propriétés structurales et fonctionnelles des HSulfs pour comprendre le lien entre leurs caractéristiques structurales uniques et leur impact fonctionnel. En combinant approches analytiques (chromatographie, électrophorèse, spectrométrie de masse) et techniques d'imagerie (photométrie de masse, microscopie à force atomique), nous nous sommes focalisés sur trois aspects principaux : (1) les éléments structuraux influençant l'oligomérisation de HSulf-2, en particulier sa chaîne de GAG (CS/DS) et son domaine hydrophile (HD), (2) les caractéristiques fonctionnelles de l'activité endosulfatase des HSulfs, notamment leur spécificité de substrat, via le développement d'un nouveau test évaluant leur réactivité envers des séquences oligosaccharidiques spécifiques et (3) l'évaluation d'oligosaccharides fonctionnalisés par des sulfamates comme inhibiteurs. Les résultats obtenus apportent de nouvelles perspectives quant aux relations structure-fonction des HSulfs et leur ciblage thérapeutique.

Title: Structural and functional characterization of the human endosulfatases HSulfs, key editing enzymes of heparan sulfate

Keywords: Endosulfatases, Heparan sulfate, Mass Spectrometry, 6-O-desulfation, Sulfated oligosaccharides

Abstract: Human endosulfatases HSulf-1 and HSulf-2 catalyze the 6-O-desulfation of the polysaccharide heparan sulfate (HS), a key cellular component used by cells as an external communication tool. By editing the sulfation patterns of HS, HSulfs regulate its biomolecular interaction properties. Despite their similar enzymatic activities *in vitro*, HSulfs often display form-dependent discrepancies *in vivo*, particularly in cancer, where HSulf-1 generally demonstrates anti-oncogenic properties while HSulf-2 shows pro-oncogenic effects. This work aims to characterize the structural and functional properties of HSulfs to understand the link between their unique structural characteristics and functional involvement. Using complementary analytical approaches, including chromatography, electrophoresis, mass spectrometry, and single-molecule Imaging techniques, we investigated three main aspects: (1) the structural elements influencing HSulf-2 oligomerization, with particular emphasis on its CS/DS GAG chain and hydrophilic domain (HD), (2) the functional characteristics of HSulf endosulfatase activity, particularly substrate specificity, using a novel assay to assess HSulfs' reactivity towards specific oligosaccharide sequences and (3) the evaluation of sulfamate-modified oligosaccharides as potential specific inhibitors of HSulf activity. The results obtained provide new insights into our understanding of HSulf structure-function relationships and contribute to the growing knowledge base for potential therapeutic approaches targeting these enzymes.